TRANSIENT REFLECTIVITY RESPONSE OF LASER MIRRORS TO ELECTRON BEAM IRRADIATION

by

Kevin A. Stroh

B.S., Kansas State University, 1984

A MASTER'S THESIS

submitted in partial fulfillment of the

requirements for the degree

MASTER OF SCIENCE

Department of Nuclear Engineering

KANSAS STATE UNIVERSITY
Manhattan, Kansas

1987

Approved by:

Hermann Domnert

Major Professor

TABLE OF CONTENTS

LIST OF FIGURES

1. Introduction

Since the advent of the Strategic Defense Initiative (SDI), questions have appeared on reliability of key components exposed to radiation fields. Regardless whether the radiation fields originate from cosmic-ray background, enemy attack, or from nuclear reactions in the system, the SDI system components and laser mirrors must retain integrity and reliability in order to function within design parameters. In addition, mirror radiation damage could be an important problem in nuclear-pumped lasers, free-electron lasers and inertial-confinement fusion laser systems. The goal of the work was to assess the radiation effects on the mirrors as a function of dose and dose rate.

Another purpose of the research was to determine the transient reflectivity response of laser mirrors when the mirrors were exposed to a variety of currents and charges. The researchers looked for statistically significant deviations from the pre-irradiation mirror reflectivity.

The scope of the work is limited to high energy and flux-density electrons to simulate both an electron field and the secondary effects from a gamma-ray field. The high energy and flux-density electron fields were generated using an electron linear accelerator (LINAC).

Three different types of laser mirrors were used in the experiments. All of the mirrors were produced by coating a fused-silica substrate (5 cm diameter, 1 cm thick circular

cylinder). Coatings over the substrate were either a thin layer of aluminum, a thicker layer of silver on top of a copper layer, or multiple layers of Al_2O_3+SiO_2 dielectric material.

Previous work on radiation damage to laser mirrors has addressed long-term and transient damage and damage mechanisms. Although the ultimate question on radiation damage may be answered for the steady-state case, knowledge of mirror transient behavior and annealing processes is not completely researched (17).

Transient radiation damage studies of various materials have been conducted by several authors. However, the specific questions regarding radiation damage to laser mirrors, their coatings and substrates is poorly understood. Although some comparisons to previous work are outlined in the review of literature chapter, no other papers directly cover the type of work summarized in this thesis.

2. Review of Literature

Transient radiation damage has been investigated for many materials and forms of radiation. Of the available papers, the most useful include transient studies on fiber optics, dielectric electronics, and laser mirrors with a silicon-dioxide substrate. Unfortunately, the number of papers discussing the transient effects for the materials of interest represent a small fraction of the works covering transient radiation damage. The number of useful papers is further reduced when the time interval of the observed transient, type of radiation and irradiated material are considered.

Papers cited in the review section were found through an extensive search of DOE and DOD unclassified documents and the INSPEC data base. The reports used in section 2.1 are a subset of the wealth of material available from studying transient effects on optical fibers and electronic equipment. Conversely, the material in section 2.2 represents the bulk of information available on transient properties of mirrors. In all papers reporting transient behavior, the transient absorption was based on changes in transmittance, not reflectance.

2.1 Transient Radiation Effects on Optical Fibers and Electronic Equipment

Because relatively few papers address transient radiation damage to laser mirrors, the review of literature was expanded to cover transients in fiber-optic cables and electronics. Most of the papers dealing with transient effects of radiation on ceramic

electronics resulted from underground nuclear-weapons testing. The papers covering transient effects on electronics provide good theoretical bases for understanding the effects of nuclear-weapon radiation on ceramic or glass optical components (18) (19) (21). The information from weapons tests is useful for the research described in this thesis because the radiation fluences incident on the mirror during operation would be of the same magnitude of those present in a weapons test (4).

The goal of the fiber-optic research was to determine the effects of wavelength, fluence, and fiber history on the transmission of the fiber. The same effects are important in the study of laser mirror transients. A study on the effects of ultraviolet radiation on fused-silica optical fibers showed a "...sharp, quasiexponential transmission decay immediately upon exposure to 248 nm excimer pulses." The transmission was observed to drop in the fused-silica fibers as a result of irradiation with a KrF excimer beam at 248 nm. Furthermore, the fibers took between two to three weeks to return to 10% of their original pre-irradiation transmissions after irradiation at 1 Hz to 25 Hz with 15 ns pulses of laser light having a fluence of a few mJ/cm^2. The transient effects of the ultraviolet radiation on the fused-silica fiber-optic cable became more apparent as the KrF excimer laser pulse repetition rate was reduced (20). Most importantly, transient absorption was observed in the silicon-dioxide cable at 248 nm.

A study by Hopkins et. al. detected transient behavior in several fibers of various construction when the fibers were exposed to 22 MeV electrons in 40 ns to 50 ns pulses from the EG&G electron linear accelerator (LINAC). Although the total charge in each pulse was around 9 nC, enough electrons were present to cause a significant transient radiation effect in the nanosecond time region.

Hopkins also stated the energies required to displace a silicon or oxygen atom creating a color center are 260 keV and 160 keV, respectively. However, the number of silicon and oxygen displacements were small in comparison to the number of free electrons present from irradiation. Hopkins stated both free electrons and color centers were responsible for most of the reduced transmission (15). Although the fibers were not constructed of silicon dioxide exclusively, similar transient effects would be expected for silicon dioxide fibers exposed to electron pulses.

The effects of intense radiation on optical fibers in short times, less than 100 ns, were studied by Lyons, et. al. (16). Lyons reported some success in describing the transient light attenuation of optical fibers given doses on the order of 1 Mrad, using a recombination model.

2.2 Transient Radiation Effects on Laser Mirrors

A paper by Brannon et. al. is one of very few sources of information on the effects of reactor radiation on the optical

properties of laser mirrors. According to Brannon, induced absorption from radiation can be removed by annealing. Furthermore, the induced absorption depends on the total ionization dose instead of displacements from neutron irradiation. The results of Brannon verified earlier work by Compton and Arnold confirming the ionizing radiation plays a significant role in radiation damage to fused silica for most situations. However, the utility of the results of Brannon are limited because the transients effects were sought on the microsecond time scale, not the nanosecond scale, and the radiation included gamma-rays and neutrons (17) (22).

In other closely related work, Mace and Gill observed transient visible absorption in fused silica at 514 nm when irradiated with 200 ns pulses of electrons. Mace and Gill observed no visible transient effect on aluminum-coated or dielectric mirrors at 514 nm (23).

In another study using 7940 fused silica, Siegel and Grissom observed transient absorption at 210 nm when irradiating samples with 50 ns pulses of electrons. No absorption was seen at wavelengths above 300 nm (24) (25).

Finally, Brannon notes the transient absorption coefficient at 257 nm for 7940 fused silica exposed to reactor radiation is smaller than the coefficients for MgF_2, BaF_2, or sapphire. The latter materials were all considered possible substrate materials. "This implies that 7940 fused silica is the best choice of materials for

reactor-pumped lasers that operate at a wavelength near 257 nm" (17). In the case of the KrF laser operating at 248 nm, the fused-silica substrate is expected to exhibit a measurable transient response to electron irradiation. However, the expected transient response would be less than transients observed for the other substrate materials mentioned above.

3. Laser Mirrors

3.1 Laser Mirror Types and Construction

Three mirror types were used in the experiments, all having a fused-silica substrate. Coatings were either a thin layer of aluminum, a layer of silver on top of a layer of copper or dielectric multilayers of Al_2O_3 and SiO_2. All mirrors were right circular cylinders 5.0 cm in diameter and 1.0 cm thick. The mirrors used in the experiments, their coatings and identification numbers are listed in Table 3.1.

Table 3.1 The construction of the metal-coated mirrors (MCM) and dielectric-multilayered mirrors (DMM) used in the transient radiation effects study.

Mirror Identification	MCM or DMM	Coating Thickness (nm)		
		Aluminum	Copper	Silver
1L	MCM	---	100	190
2L	MCM	---	100	200
6L	MCM	200	---	---
7L	MCM	200	---	---
12	DMM	---	---	---
13	DMM	---	---	---
14	DMM	---	---	---
26	DMM	---	---	---

3.1.1 Dielectric-multilayer Mirror Construction

The dielectric-multilayer mirrors were designed for a KrF eximer laser operating at 248 nm. The mirror coatings from the fused-silica substrate to the atmosphere are given by:

$$S[(HL)^{24}H(L)^{2}]AIR \qquad (3.1)$$

where S ≡ Fused-silica substrate,

H ≡ High refractive-index material, (Al_2O_3),

L ≡ Low refractive-index material, (SiO_2),

and AIR ≡ Surrounding air medium.

That is, the fused-silica substrate is followed by twenty-four layers of (HL), one layer of H and finally a double layer of L. The quarter-wavelength design thicknesses and refractive indices for the dielectric mirror layers and substrate are givien in Table 3.2.

Table 3.2 The refractive indices and design thicknesses for the quarter-wavelength coatings and substrate of the dielectric-multilayer mirrors for the KrF eximer laser.

Layer or Substrate	Refractive Index	Design Thickness (nm)
Fused Silica	1.50	1.0 E+07
H (Al_2O_3)	1.66	37.3

L (SiO_2)	1.46	42.5
L^2 [1]	1.46	84.9

3.1.2 Metal-coated Mirror Construction

The mirror coatings from the fused-silica substrate to the atmosphere for the aluminum-coated mirrors are given by:

$$S[Al]AIR \tag{3.2}$$

where S ≡ Fused-silica substrate,

and Al ≡ Aluminum coating.

Similarly, for the copper-and-silver-coated mirrors, the following formula applies:

$$S[CuAg]AIR \tag{3.3}$$

where S ≡ Fused-silica substrate,

Cu ≡ Copper coating,

and Ag ≡ Silver coating.

---

[1] The final half-wavelength layer L^2 serves to protect the mirror from environmental threats, e.g., corrosive excimer-laser gases.

As a short-hand notation the copper-and-silver-coated mirrors are called CuAg mirrors. The short-hand notation does not imply the copper and silver are bound chemically. The design thicknesses and refractive indices for the substrate and coatings for the metal-coated mirrors are given in Table 3.3.

Table 3.3 The design thicknesses and refractive indices for the substrate and coatings of the metal-coated mirrors. The optical properties for the evaporated metal coatings are taken from Ref. 26.

Layer or Substrate	Wavelength (nm)	Refractive Index	Extinction Coefficient	Design Thickness (nm)
Fused Silica	248	1.50	---	1.0 E+07
Aluminum	260	0.19	2.85	200
Copper	200	0.94	1.51	100
Silver	260	1.45	1.35	200

3.2 Mirror Optical Characteristics

Optical properties of interest in the experiment were limited to pre-irradiation reflectivities and transient reflectivities at near-normal incidence. As the reader may verify by checking the

experiment geometry in Fig. 4.2, the transient transmission could not be obtained.[2] The pre-irradiation reflectivity for the metal-coated and dielectric mirrors was measured using a CARY 2300 spectrophotometer at the Air Force Weapons Laboratory, Kirtland Air Force Base. The complete set of pre-irradiation mirror reflectivities is found in Appendix D. Except when stated elsewhere, all reflectivities were measured with the incident light source ten degrees off normal.

A companion work on the permanent effects of electron beam irradiation of laser mirrors was carried out by Scronce (1). The mirrors used by Scronce were of the same design as the mirrors used in the transient study, summarized here.

3.2.1 Dielectric Mirror Reflectivities and Transmissions

A theoretical model, developed by Scronce, for the dielectric-multilayer mirrors, produced analytical reflectivities comparable to the experimentally obtained reflectivities. By accounting for variable indices of refraction and source light angle of incidence, Scronce was able to to match the thoeretical and experimentally

---

[2] No transient transmission measurements were made because the mirrors were placed immediately in front of the LINAC beam port window. The mirror placement immediately in front of the beam window was necessary to insure the mirrors were exposed to the maximum dose and dose rate. Placing the mirrors further from the beam port window would have reduced the dose and dose rate at the irradiation spot because of beam divergence.

determined peak reflectivities for the dielectric-multilayer mirrors to within 1.6% at half maximum. However, the off-peak interference patterns did not match at the relative maxima and minima, suggesting the need for further refinements in the theoretical model (1).

Pre-irradiation theoretical reflectivities for various angles of spectrophotometer light source incidence and the experimentally measured reflectivity for a typical dielectric-multilayer mirror are shown in Fig. 3.1. Although the reader may be able to identify slight variations between the experimentally measured reflectivity in Fig. 3.1 and the reflectivity curve for other dielectric mirrors, the variations are believed to be insignificant with respect to the theoretical model from Scronce (1).

The general expression describing conservation of energy for light incident upon a surface is given by Eq. (3.4),

$$1 = R + (T + A) \tag{3.4}$$

where $T \equiv$ Transmission,

$R \equiv$ Reflectivity,

and $A \equiv$ Absorption.

Because the experimental design allows for measurement of mirror reflectivity only, the transmission and absorption terms are shown as the combined term (T + A).

The dielectric mirror transmission can be estimated by solving Eq. (3.4) for (T + A) given the reflectivity, or found by

experimentally measuring the transmission in a spectrophotometer. No significant differences were noticed in comparing the measured transmission to the transmission found using Eq. 3.4 for the dielectric mirrors used in the steady-state study. Thus, pre-irradiation transmissions of the mirrors in Table 3.1 can be found by using Eq. 3.4. The transmissions found using Eq. 3.4 are accurate to within a few percent of the experimentally-measured transmissions for the dielectric mirrors.

3.2.2 Metal-coated Mirror Reflectivities and Transmissions

Typical pre-irradiation reflectivities for the two types of metal-coated mirrors are shown in Fig. 3.2 and 3.3. The mirror reflectivities were determined spectrophotometrically using the CARY 2300's double-bounce technique described in section 4.1.1.

Theoretical reflectivities for the metal-coated mirrors can be derived given the refractive indices for the coatings as a function of wavelength. Hecht and Zajac state the reflectance of a metal plate is given by Eq. (3.5):

$$R(\lambda)=\{(n_e(\lambda)-1)/(n_c(\lambda)+1)\}*\{(n_c(\lambda)-1)/(n_c(\lambda)+1)\}^{*} \quad (3.5)$$

where

$R \equiv$ Reflectivity of the metal mirror,

$n_c \equiv$ Complex index of refraction $= n_R - in_I$,

n_R and $n_I \equiv$ Real numbers,

$\lambda \equiv$ Wavelength,

and

$i \equiv$ Square root of -1.

Equation (3.5) is constrained to the simplest case of normal incidence and an index of refraction of unity for the medium of incident light. Although empirical relations for the complex index of refraction are available, comparisons of the metal-coated mirror reflectivities will be based on Fig 3.4, 3.5 and 3.6 taken from Hecht and Zajac (2)(3).

Figures 3.4, 3.5 and 3.6 show the spectral reflectance at normal incidence for metal film coatings of silver, aluminum and copper (2). The reader will notice many similarities in comparing the typical aluminum-coated mirror of Fig. 3.2 to the aluminum-coated mirror of Fig. 3.4.

Also, by comparing Fig. 3.3 to Fig. 3.5 and 3.6, the reader will notice the thickness of the silver on the copper- and silver-coated mirrors accounts for most of the reflectivity. The silver is the dominant reflecting medium while the copper acts as an adhesive between the fused-silica substrate and silver layer. According to H.J. Donnert, the mirror manufacturers found the silver layer would not adhere to the fused-silica substrate without an interface material, like copper, to join both materials (4). Because the silver layer dominates, the copper and silver-coated mirrors can be approximated by a single-layered silver mirror, without concern for the optical properties of the copper underlayer.

Although the technique used in section 3.2.1 can accurately predict the pre-irradiation transmission for the dielectric mirrors,

no similar technique is available to predict the the transmission for the metal-coated mirrors because the metal coatings have non-zero absorption.

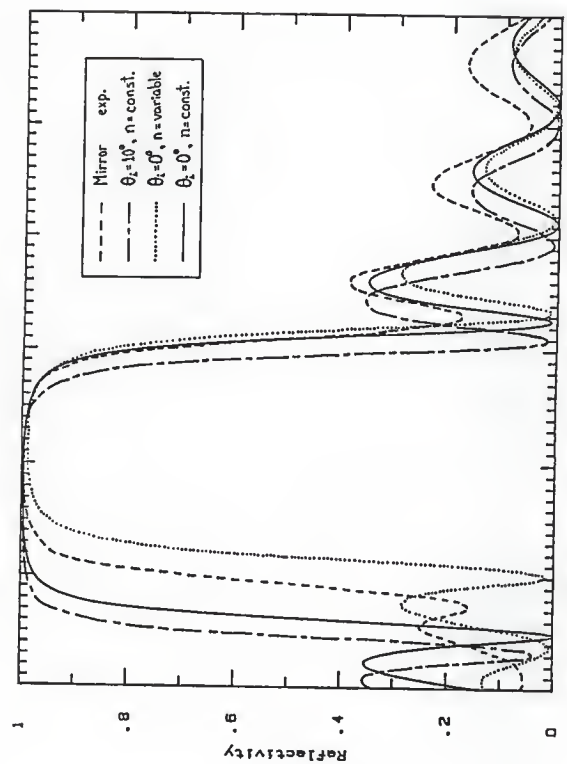

Fig. 3.1 Theoretical and measured reflectances for a typical dielectric mirror. The theoretical model results include variable angles of incidence, and indices of refraction. (1)

Fig. 3.2 The spectral reflectance at 10 degrees incidence for metal-coated mirror 6L.

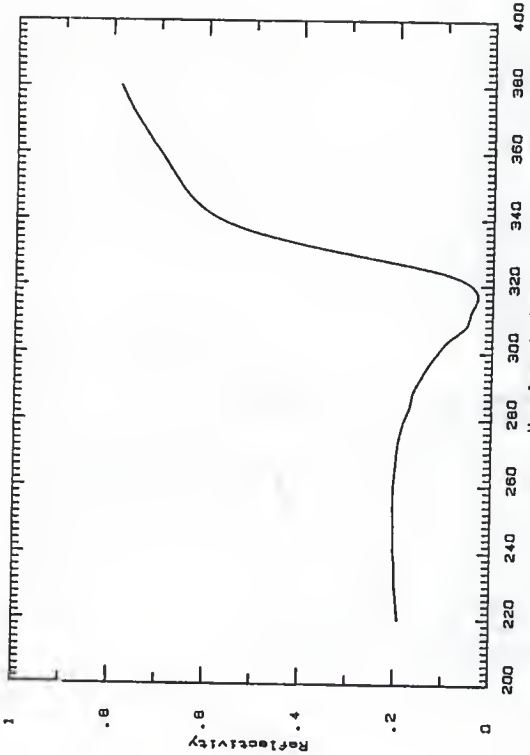

Fig. 3.3 The spectral reflectance at 10 degrees incidence for metal-coated mirror 2L.

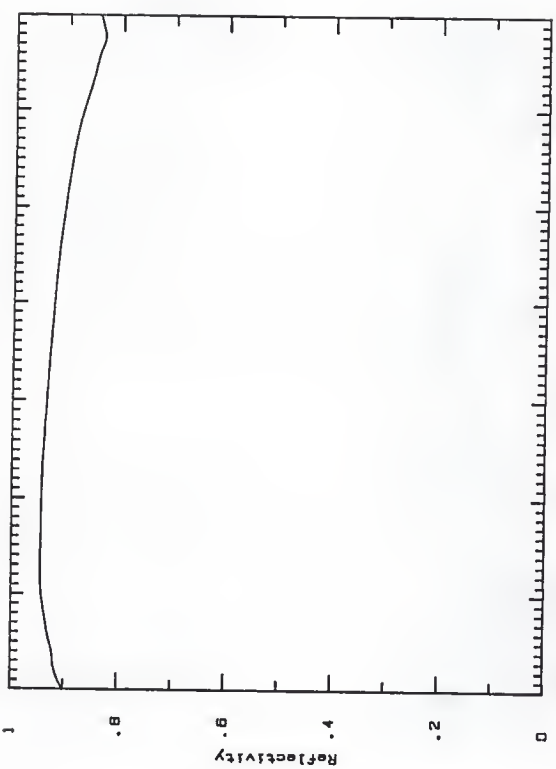

Fig. 3.4 The spectral reflectance at normal incidence for an evaporated film of aluminum. (2)

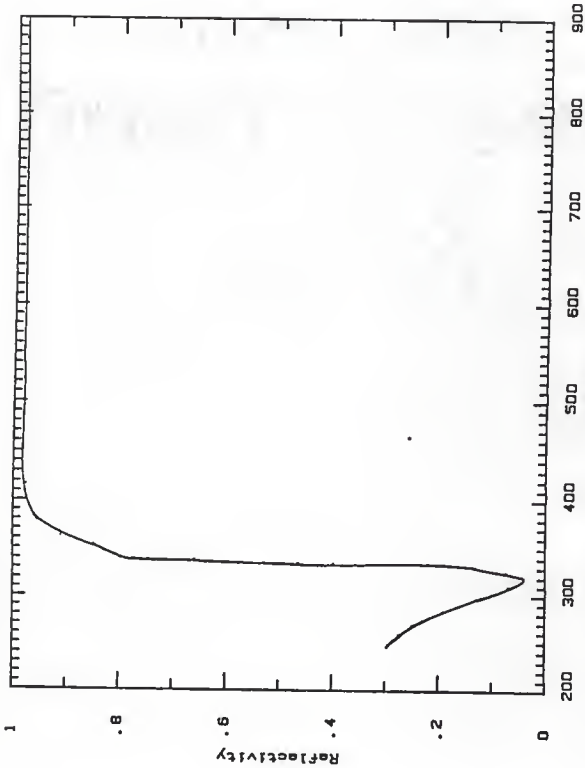

Fig. 3.5 The spectral reflectance at normal incidence for an evaporated film of silver. (2)

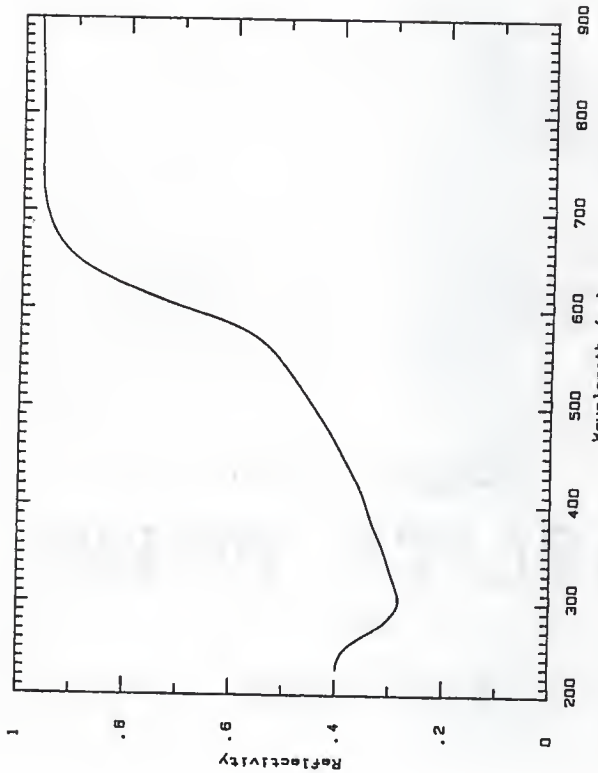

Fig. 3.6 The spectral reflectance at normal incidence for an evaporated film of copper. (2)

4. Experimental Methods and Materials

Before any mirrors could be irradiated, pre-irradiation mirror reflectivity had to be measured. Then the mirrors could be exposed to radiation from the electron linear accelerator, LINAC, and tested for transient radiation damage or statistically significant deviations from the pre-irradiation reflectivity.

4.1 Determining the Pre-irradiation Mirror Reflectivity

For each mirror the square of the reflectivity was measured using a CARY 2300 spectrophotometer at the Air Force Weapons Laboratory, Kirtland Air Force Base. The CARY 2300 can perform three basic measurements: reflectivity squared, transmission, and optical density. The CARY 2300 is incapable of measuring the reflectivity of a sample directly because the spectrophotometer source light bounces off the sample twice before being measured in a photo-multiplier tube (PMT).

4.1.1 Operations of the CARY 2300 Spectrophotometer

Before measuring the reflectivity of a sample mirror, the mirror is placed in the spectrophotometer sample chamber and on the optics plate shown in Fig. 4.1. Once the mirror face is aligned on the optics plate in the chamber, the CARY 2300 spectrophotometer uses one of to three lamps to generate the light incident on the sample mirror. The lamps cover the infrared and near-infrared

(tungsten), visible (quartz-iodide), and ultraviolet (hydrogen) wavelength regions with the quartz-iodide lamp overlapping wavelengths in the infrared and ultraviolet regions. The CARY 2300 varies the size of an aperture depending on the lamp intensity so the light intensity incident on the sample mirror remains roughly constant for a given wavelength.

In measuring the square of the mirror reflectivity, the CARY 2300 uses a double-bounce technique. In the double-bounce technique the source light hits one mirror location approximately 10 degrees off the mirror normal. Then, the reflected light coming from the sample mirror is reflected back to the sample mirror to a second location but still at 10 degrees off normal. Finally, the light coming from the second reflection off the sample mirror is collected in the photomultiplier tube of the CARY 2300.

Mirror reflectivity could be found by taking the square root of the PMT signal before the signal is recorded on the spectrophotometer strip-chart. But, because the strip-chart curves needed to be digitized for input to a personal computer regardless of original data form, no circuit to take the square root of the PMT signal was installed. Instead, each reflectivity-squared curve, i.e. the unaltered PMT signal recorded on the strip-chart, was digitized by eye and converted to a reflectivity curve using the HP 9816 personal computer.

Initial reflectivity measurements on all mirrors were conducted between 200 and 900 nm at the slowest strip-chart speed. The

initial measurements showed no absorption centers, so chart speed was increased for subsequent measurements. After determining the mirrors had no absorption centers, the reflectivity spectrum was recorded only in the region of interest between 200 nm and 371 nm for both the dielectric mirrors and for the metal-coated mirrors. The complete set of pre-irradiation reflectivities for all mirrors is found in Appendix D.

4.2 Mirror Irradiation

All mirrors were irradiated using an electron linear accelerator at the EG&G Irradiator Facility, Goleta, California. Due to the complexity of performing a single irradiation and the details behind preparing the LINAC for an irradiation, only the basic steps in irradiating a mirror will be covered. Thus, the specific accelerator settings required for each electron beam pulse will not be discussed because the accelerator settings were solely under the control of the EG&G employees.[3] However, the beam alignment and energy, mirror placement and optics arrangement were controlled by the researchers and will be discussed.

---

[3]Note, additional preparation was needed for installation of a water cooling system for the LINAC beam port on the longer pulses and higher current irradiations. The water cooling system was installed to prevent the beam port window from melting during the long pulse and high current irradiations.

All mirrors, except dielectric mirror 26, were irradiated with one single pulse of electrons from the LINAC. Mirror 26 was exposed to multiple irradiations because of its use in optics alignment.

4.2.1 Preparing for Mirror Irradiation

Before any mirrors could be irradiated, the experiment's optical components needed to be set up and properly aligned. The aligned optical components and the supporting electronic equipment, shown in Fig. 4.2, are identified in Table 4.1:

Table 4.1 A list of the optical components of Fig. 4.2, their manufacturers and serial numbers.

Equipment Name	Manufacturer	ID/Serial Number
Video Camera model C1000 type 18	Hamamatsu Tu Co. Ltd.	38027479
Temporal Disperser model C1370-01	Hamamatsu Tu Co. Ltd.	83038034
High Voltage Power Supply model C1307	Hamamatsu Tu Co. Ltd.	83038034
Monochromator cat. no. 82-498	Jarrell Ash, Div. of Fisher Scientific Co.	728427
U.V. Flash Lamp	Chelsea Instruments Ltd.	L59109
Trigger Input to Flash Lamp	Chelsea Instruments Ltd.	127
Camera Power Supply C1000	Hamamatsu Tu Co. Ltd.	83027479
Polyprocessor Frame Image Analysis System	Hamamatsu Tu Co. Ltd.	8303003

2 Inch Cylindrical Optics Holder	Ealing	
Quartz Condensing Lens f= 0.2 m	Ealing	
Pulsed Xenon Light Source Model 3021	Chelsea Instruments Ltd.	FX108AU
Keyboard & Monitor	Hamamatsu Tu Co. Ltd.	8303003

The equipment on the optical table (see Fig. 4.2) was aligned in two steps. First, with a sample mirror mounted in the optics holder, the xenon flash lamp was fired manually until the flash passed through a condensing lens, off a pellicle mirror and formed a spot on the sample mirror roughly 1.6 cm in diameter. Next, the xenon flash lamp was fired manually until the streak camera detector, i.e. the video camera, output was maximized. The light signal received at the streak camera originated at the xenon lamp, had passed through two condensing lenses and an aperture and reflected once off the sample mirror and twice off the pellicle mirror. The relative output for the pulsed xenon light source is shown in Fig. 4.3.

After aligning the equipment on the optical table, the spot the xenon flash lamp hit the sample mirror had to be aligned with the LINAC electron beam spot, also about 1.6 cm in diameter. The electron beam alignment was accomplished using a HeNe laser and a piece of aluminum foil covered with a phosphor.

In a previous set of experiments, dielectric mirror 26 was used as a target for beam alignment. Thus, dielectric mirror 26 was chosen again for alignment of the beam for the transient experiments. With mirror 26 in the optics holder, the xenon lamp was fired until the light from the xenon lamp was centered on the HeNe laser beam. Next a phosphor-coated aluminum sheet was placed over the beam port window of the LINAC. By firing the LINAC and adjusting the beam with a series of electromagnets, the LINAC beam and the laser beam were aligned based on the location of the glowing beam spot on the phosphor-coated aluminum sheet. After turning the accelerator off, mirror 26 was removed and replaced with a pristine sample mirror, coated side facing the pellicle mirror. Finally, before the pristine mirror could be irradiated, an edge of the mirror was marked with a pencil or pen to align the mirror with a similar line on the optics holder. Alignment of the mirror in the optics holder was necessary for post-irradiation steady-state studies for Scronce (1).

Periodically after beam alignment and just prior to the irradiation of a mirror at a unique dose and dose rate, radiochromic film was attached to the surface of mirror 26 to check beam shape, intensity, and strength. With mirror 26 in the optics holder, the mirror and the radiochromic film were exposed to a series of beam pulses. Then, the radiochromic film was developed by the EG&G personnel, yielding an average pulse shape, strength, and intensity. If the pulse shape strength or intensity did not check with their

expected shape or values, appropriate adjustments were made to the LINAC by the controller. A sample output of the radiochromic dosimetry is shown in Fig. 4.4.

4.2.2 Beam Shots with Block-in and Block-out

With the mirror alignment completed and beam shape, strength and intensity confirmed, the pristine mirror in the optics holder of Fig. 4.2 was irradiated with a beam of electrons. Mirror irradiation consisted of two LINAC shots, one with a large copper block in the path of the electron beam (block-in) and the other shot with the copper block out of the path of the electron beam (block-out).

The block-in shots allowed the researchers to estimate the amount of noise associated with each electron pulse. With the block-in, none of the electron beam made its way through the copper block to the mirror. Thus, the signal received at the detector and recorded on magnetic tape was a combination of noise, xenon spectrum, condensing lens transmissions and mirror reflectivities.

The block-out pulse did the actual irradiation of the mirror i.e. with no copper block to absorb the electron beam, the beam hit the mirror. For mirrors irradiated once, the beam hit the mirror in position A (see Fig. 4.5). However, mirrors irradiated twice were shot in position A, then rotated in the optics holder to irradiate position B. The signal received at the detector for the block-out shots was a combination of noise, xenon spectrum, mirror

reflectivities, lens transmissions and the transient reflectivity effects of the electron beam pulse.

4.2.3 Beam Characteristics

The mean energy of the electrons leaving the LINAC beam port window was 16.5 MeV. The electron beam was focused to irradiate a circular area about 1.6 cm in diameter. The beam was Gaussian in shape and could be approximated by a square wave in pulse length. For confirmation of the beam shape profile, see Fig. 4.4. A sample black-and-white photograph showing a typical beam pulse shape, pulse length, and net current for the block-out irradiation of dielectric mirror 14 is shown in Fig. 4.6.

4.3 Data Recording

For each block-out and block-in shot, the monochromator repeatedly scanned through a preset window of wavelengths while the video camera recorded during a preset time interval determined by the temporal disperser. In most cases, the time window began before the electron pulse initiated. For example, for dielectric mirror 13 irradiated in position A, the time window included data values recorded 30 ns before the beam hit the mirror to 313 ns after beam initiation. In the figures of Appendix A, all times are reported with respect to the pulse initiation. Thus, for dielectric mirror 13 irradiated in position A, the time intervals reported begin at -30 ns and end at 313 ns.

The data collected at the streak camera detector were made of 471 scanlines each with 512 channel values. Each channel value corresponds to a specific time while each scanline corresponds to a wavelength. Time and wavelength calibrations will be taken up in the following section. A sample of data from the block-out file of dielectric mirror 14 irradiated in position A is shown in Table 4.2.

The light intensity versus wavelength and time data were collected at the streak camera detector and sent to EG&G's VAX-11 Computer for analysis. Once in the computer memory, the data were analyzed on the Hamamatsu monitor and dumped to magnetic tape. For the studies mentioned in the thesis, the data were recorded in binary format on the VAX tape, read from the VAX tape at Kansas State University and restored on a tape compatible with the KSU computer system. The program used to strip the binary data from EG&G's VAX tape is listed in Appendix B.

In addition to the data on magnetic tape, color pictures representing the data stored on magnetic tape were taken by the EG&G personnel. The color levels on the pictures represent the varying light intensities seen at the streak camera detector versus time and wavelength. A sample color photograph for the block-out irradiation of dielectric mirror 14 is shown in Fig. 4.6. A complete set of color photographs can be found in Appendix E.

Table 4.2 Sample data from scanline number 10 for the block out irradiation of mirror 14.

Scanline Number 10

82	98	103	99	78	97	77	93	97	88	105	104	100	96	84	76
79	86	66	84	110	101	93	83	85	66	79	75	87	80	77	93
93	88	83	87	88	83	92	78	85	97	102	84	92	98	82	90
101	87	88	94	77	89	102	82	85	77	83	82	83	79	87	75
66	70	79	80	71	77	80	67	67	72	76	72	99	93	86	82
84	84	79	77	81	97	91	66	68	88	60	95	111	86	78	75
68	69	83	87	77	72	69	75	66	85	65	83	88	78	70	63
84	78	81	84	84	69	76	89	96	80	81	83	75	83	66	78
77	76	75	51	95	81	83	56	63	74	73	77	66	82	56	62
75	63	69	59	66	62	68	48	73	66	71	66	76	63	73	64
78	68	76	71	75	74	66	61	50	55	83	62	72	58	68	45
68	59	69	92	79	69	79	54	79	69	72	67	78	68	67	60
67	75	75	60	50	52	71	75	69	49	41	50	45	54	51	47
71	65	61	70	62	62	73	62	45	61	73	77	56	73	58	62
62	50	58	68	61	62	49	53	55	57	66	64	71	58	69	64
55	63	62	68	61	63	58	51	68	60	53	56	44	54	76	77
52	55	50	62	62	61	63	64	61	57	60	59	64	60	66	60
62	37	51	55	44	57	52	68	64	71	45	40	65	64	63	60
60	58	63	67	62	48	64	61	60	60	60	70	54	44	60	59
42	61	51	42	66	59	67	66	71	43	51	40	73	64	56	53
52	56	71	72	49	55	64	66	48	59	57	61	59	67	84	66
70	70	55	81	69	69	53	66	55	41	72	84	67	70	63	76
56	67	68	61	73	57	70	67	76	65	63	61	64	72	60	74
89	70	55	62	46	67	07	78	83	85	68	64	58	71	58	75
49	62	64	54	59	69	69	78	76	71	77	05	74	86	86	92
84	85	71	71	84	79	66	73	72	77	63	68	72	91	104	93
91	77	70	83	91	88	95	75	77	86	98	65	05	75	92	84
80	78	81	61	85	88	89	102	127	116	81	83	95	99	02	93
90	92	83	99	90	94	95	05	106	121	97	100	05	04	92	116
102	86	99	90	116	117	119	118	114	120	107	137	144	135	131	140
117	139	125	108	93	98	122	132	130	126	125	113	104	105	91	117
127	119	110	128	106	127	122	107	117	115	113	85	112	116	115	106

4.4 Time and Wavelength Calibrations

4.4.1 Time Calibration

Time calibration of the block-out and block-in data files was based on the time interval settings of each irradiation. Table 4.3 lists the time interval data were recorded for each block-out and block-in shot for the mirrors in Table 3.1.

Table 4.3 The block-out and block-in time intervals for each mirror of Table 3.1 and the block-out pulse length and mean current. The time interval defines the start and end of data recording.

Mirror Number	Irradiation Position	Time Interval (ns) Start	End	Block-out Pulse Length (ns)	Block-out Mean Current (A)
1L	A	-40.0	88.0	20.0	5.0
2L	A	-160	183	200	0.225
2L	B	-50.0	293	200	0.225
6L	A	-40.0	88.0	20.0	5.0
7L	A	-30.0	313	500	0.225
7L	B	250	593	500	0.225
12	A	-30.0	313	500	0.225
12	B	250	593	500	0.225
13	A	-160	183	200	0.225
13	B	-50.0	293	200	0.225

14	A	-40.0 to 88.0	20.0	5.0
26	A	-30.0 to 313	500	0.225

To find the time, in ns, corresponding to a channel for any of the 512 channels in a block-in or block-out data file, Eq. 4.1 was used.

$$t(CH) = t_w * (CH - 1) / 511 + t_o \qquad (4.1)$$

where $t \equiv$ The time from the initiation of the electron beam pulse, (ns),

$t_w \equiv$ The time interval of Table 4.3, (ns),

$CH \equiv$ Channel number (integer from 1 to 512),

and $t_o \equiv$ The starting time in the time interval of Table 4.3, (ns).

For example, for mirror 1L, the time corresponding to channel 40 is found by using Eq. 4.1:

Given: t_w from Table 4.3 is 88.0-(40.0) or 128 ns, the time interval for the irradiation,

and t_o from Table 4.3 is -40.0 ns, the starting time in the time interval.

Substituting values,

$$t(40) = 128 \text{ ns} * (40-1)/511 + (-40.0 \text{ ns})$$

yields t(40) = -30.2 ns, i.e. 30.2 ns before the electron pulse hit the sample mirror. Similarly, at channel 161, t(161) equals 0.33 ns, roughly the start of the electron beam hitting the mirror. Channel 241 corresponds to 20.1 ns after the beam initiated firing on the mirror and also marks the end of the electron beam pulse for mirror 1L. Finally, channel 512 marks the end of data recording, 88.0 ns after the initiation of the electron beam.

4.4.2 Wavelength Calibration

The wavelength calibration found using a mercury lamp spectrum and a least-squares fit is given in Eq. 4.2:

$$\lambda(SC) = -0.361 \text{ nm} * SC + 375.1 \text{ nm} \qquad (4.2)$$

where $\lambda \equiv$ Wavelength, (nm),

and SC ≡ Scanline number (integer from 10 to 480).

For the 480 scanlines per data file, the wavelength range spans from 201 nm to 371 nm. Equation 4.2 is a linear least-squares fit based on the known wavelengths of the mercury lamp spectrum and corresponding scanline numbers read off the Hamamatsu monitor.

Unfortunately, a check of the wavelength calibration given by Eq. 4.2 was impossible due to a recording error on the VAX magnetic tape. The researchers hoped to check the initial calibration based on the values read from the monitor by using the mercury lamp spectrum recorded in the same format as the irradiation data. However, an error in recording occurred, thus leaving the

researchers with the calibration in Eq. 4.2. The loss of the mercury spectrum was not catastrophic because the researchers recorded the necessary information to perform the calibration in a separate log. The difference between the two calibrations was expected to be insignificant.

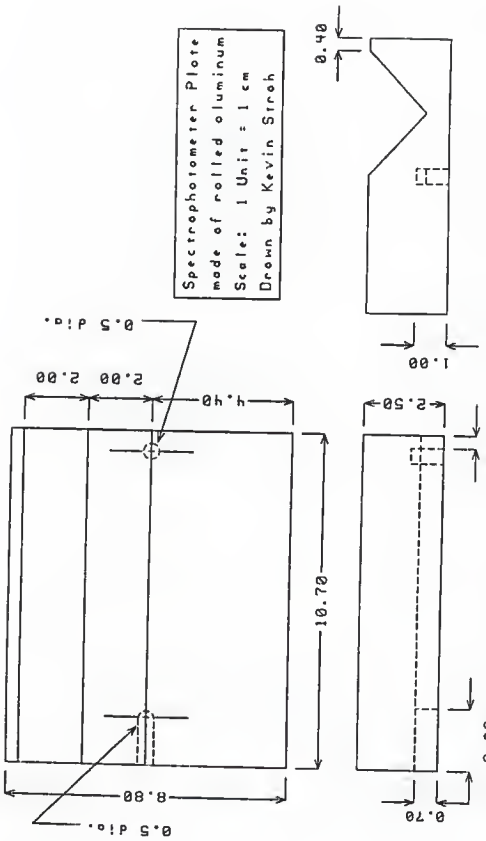

Fig. 4.1 The optics plate used to hold the mirrors for the pre-irradiation reflectivity measurements. The mirror sat in the V-notch of the plate with the coated side of the mirror in the plane of the right-side view.

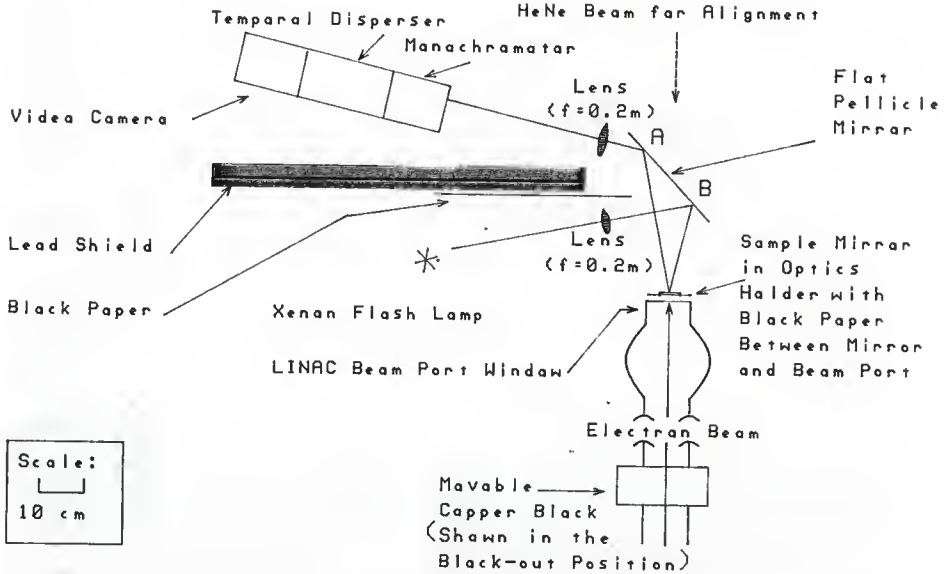

Fig. 4.2 The experimental optics set-up. Note, the spots on the pellicle mirror, A and B, are outside the diverging electron beam. The coated side of the sample mirror faces the pellicle mirror.

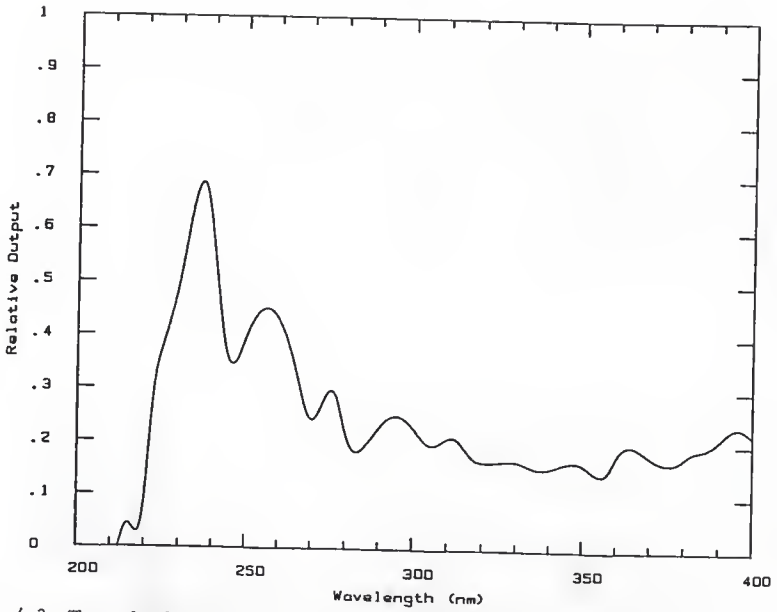

Fig. 4.3 The pulsed Xenon light source relative output versus wavelength. (5)

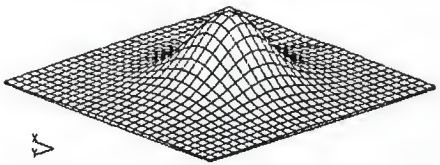

20 ns pulse, 5 A, 20 pulses, 601 x 11 nm filter
Lamp set to 3.60 V, Peak dose = 2.10 MRad,
Total integrated dose = 0.56 MRad cm^2
FWHM = 4.1 mm, Centered at X = -37.5 mm

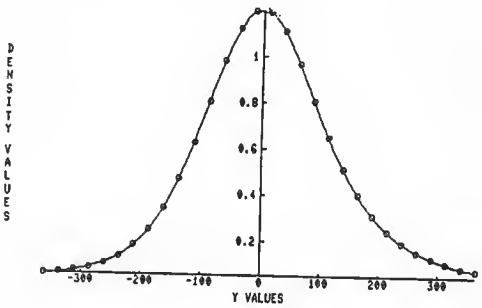

Fig. 4.4 Sample radiochromic dosimetry output for metal-coated mirror 6L. The radiochromic film was shot 20 times with the beam used to irradiate mirror 6L.

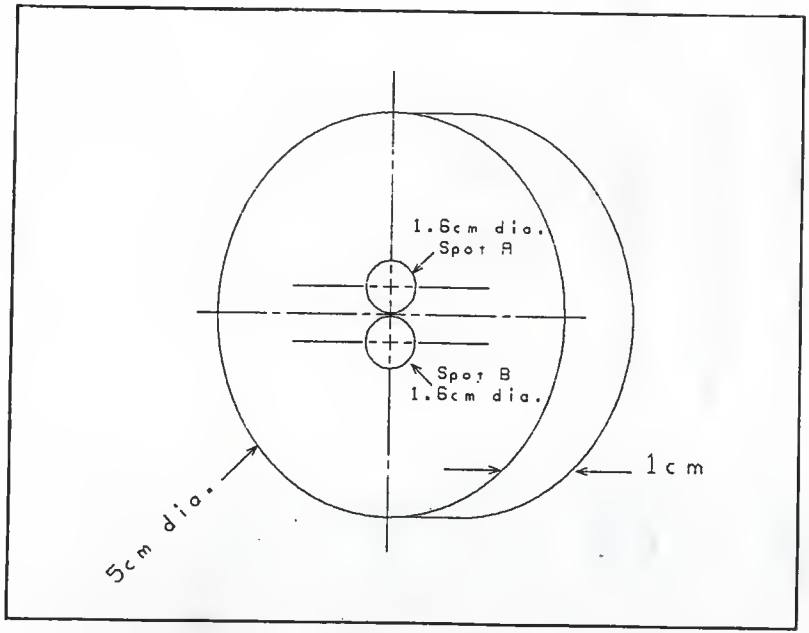

Fig. 4.5 Isometric view of a typical laser mirror used in the experiments. The figure details mirror dimensions and location and size of the beam spot positions A and B.

(a)

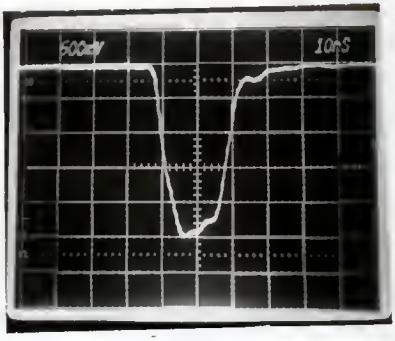

(b)

Fig. 4.6 Sample color photographs of raw data (a) and beam profile (b) for the electron irradiation of dielectric mirror 14. The color levels identify the light intensity level at the camera detector.

5. Theory of the Experiment and Data Analysis

The purpose of this section is to detail the theory and data analysis directly related to the design of the experiment. The optical theory is used in interpreting the light intensity seen at the streak camera detector, while the theory on data analysis is developed to provide transient mirror reflectivity.

5.1 Theory of Experimental Optics Arrangement

The theory of the experiment is based on the optics design shown in Fig. 4.2. From Fig. 4.2, the signal light intensity versus wavelength and time seen at the streak camera for a block-in pulse, i.e. a beam shot where the electron beam does not irradiate the mirror but is stopped in a copper block, is given by Eq. 5.1.

$$I_{SCDi}(\lambda,t) = I_{FL}(\lambda,t) * T_{L1}(\lambda,t) * T_{L2}(\lambda,t) * R_{PM}(\lambda,t) * R_{P}(\lambda,t)^2 * L(\lambda,t) \quad (5.1)$$

where I_{SCDi} ≡ Signal light intensity seen at the streak camera detector for the block-in irradiation,

I_{FL} ≡ Xenon light intensity leaving the xenon flash lamp,

T_{L1} ≡ Transmission for the condensing lens in line with the xenon flash lamp and pellicle mirror,

T_{L2} ≡ Transmission for the condensing lens in line with the pellicle mirror and streak camera detector,

R_{PM} ≡ The pristine sample mirror reflectivity,

R_P ≡ The pellicle mirror reflectivity,

L ≡ A factor estimating the fractional loss of light from the xenon flash lamp due to geometry and other mechanisms, $0 \leq L \leq 1$,

t ≡ Time,

and λ ≡ Wavelength.

Similarly, for a block-out irradiation, i.e. an irradiation where the electron beam is incident on the mirror, the signal light intensity seen at the streak camera detector is given by Eq. 5.2.

$$I_{SCDo}(\lambda,t) = I_{FL}(\lambda,t) * T_{L1}(\lambda,t) * T_{L2}(\lambda,t) * R_{IM}(\lambda,t) * R_{P}^{2}(\lambda,t) * L(\lambda,t) \quad (5.2)$$

where I_{SCDo} ≡ Signal light intensity seen at the streak camera detector for the block-out irradiation,

R_{IM} The sample mirror reflectivity under irradiation from the electron beam,

and all previous definitions for the other variables hold. Color photographs, representing the digitized data of the block-in and block-out shots, are presented in Appendix E.

5.1.1 Simplification of Theory

Although Eq. 5.1 and 5.2 are exact, their utility is questionable because the functional form of many of the variables is

unknown, e.g. the analytical form of $T(\lambda,t)$. To utilize the
L1
equations to their full potential, several simplifications are used to obtain the signal ratio. (See Section 5.2 for the definition of the signal ratio.)

First, the optical properties of the critical spots on the pellicle mirror and the condensing lenses did not change as a result of the block-in or block-out shots because neither were exposed to the LINAC electron beam. The pellicle mirror and condensing lens placement were partly based on electron beam divergence. The EG&G personnel determined the electron beam divergence using an electron transport code. Based on the transport code results, the condensing lenses and critical reflecting spots on the pellicle mirror were placed out of the diverging electron beam path. The critical reflecting spots on the pellicle mirror are labled A and B in Fig. 4.2. Because the condensing lenses and critical spots on the pellicle mirror are not affected by the electron beam, their optical properties were not altered from the irradiation.[5]

---

[5]Note, the pellicle mirror was exposed to the electron beam during block-out irradiation but not at the critical points shown in Fig. 4.2. Using the electron range techniques described in Faw et. al., the residual range of the 15 MeV electrons used in the experiments is easily calculated (7). For 15 MeV electrons, an approximate value of electron range in the mirror's fused-silica substrate is 7.5 g/cm^2 (8)(9). Assuming negligible effects from mirror coatings and using tabulated densities of dry air and fused silica of 0.0012 g/cm^3 and 2.16 g/cm^3 respectively, the residual range of a 15 MeV electron incident on a 1 cm thick fused-silica substrate is calculated to be 5.34 g/cm^2 (10). That is, the 15 MeV electrons incident on the mirrors have enough energy remaining after leaving the mirror to travel about 4500 cm in dry air. Thus, the electron

Secondly, the xenon lamp intensity did vary, but not dramatically, from block-in to block-out shots. According to the bulb manufacturer, Chelsea, "...there is a shot-to-shot fluctuation on lamp output of up to some 1% peak to peak", resulting from arc discharging starting at a slightly different place on the end electrodes (5). According to Moore, Davis and Coplan the spectral output of the xenon bulb varies slightly during the flash and exhibits the spectral features of the fill gas, xenon, for the flash energy used in the experiment (6). By designing the experiment to measure the relative change in reflectivity, the ratio of data values represented by the signal ratios is devoid of any dependence possible light intensity fluctuations of the xenon lamp. Even if the shot-to-shot fluctuations were significant, the signal ratios described in Section 5.2 would account for the variation with the normalization function $A(\lambda)$.

5.2 Data Analysis

The transient reflectivity for the mirror was assumed to be of the form of Eq. 5.3:

$$R_T(\lambda,t) = R_{SS}(\lambda) * f(\lambda,t) \qquad (5.3)$$

---

beam hit and possibly interacted with the pellicle mirror. The electron range technique was confirmed at the EG&G Irradiator Facility by the LINAC operators using an electron transport code.

where R_T ≡ Transient mirror reflectivity,

R_{SS} ≡ Pre-irradiation mirror reflectivity,

and f ≡ Function describing the relation between the pre-irradiation and transient reflectivities also called the transient signal response function. $f(\lambda,t)$ is calculated from the block-in and block-out data files as shown in section 5.2.1.

If the transient response of the laser mirrors was desired for a specific time and wavelength inclusive in the data files, the block-in and block-out data files could have been consulted. Alternatively, the color pictures showing the streak camera signal light intensity versus time and wavelength could have been used.[6] However, neither analysis technique is very useful. The error from using individual observations at a given time and wavelength is largely due to the presence of auto-correlated error.[7] Secondly, the photograph technique is too crude to produce quantitative results.

---

[6]See Fig. 4.6 for a sample color photograph detailing the time and wavelength dependence of the block-out signal light intensity for dielectric mirror 14.

[7]The error for a given data point is called auto-correlated if dependent on the error or value of previous data. Almost every signal-ratio plot in Appendix A demonstrates auto-correlation with respect to the Fourier transform curve, the model of the signal-ratio data. If the error were random, one would expect nearly the same number of signal-ratio data points randomly distributed above and below the Fourier curve. However, the signal-ratio data do not fall randomly above or below the Fourier curve, thus suggesting auto-correlation.

Bearing in mind the statistical problems associated with analyzing signal light intensities for single data points, the researcher's main concerns became the general trends of the transient signal response function over discrete pre-determined time intervals. The block-out and block-in data files were integrated over pre-determined time intervals and used to calculate the average behavior of the transient signal response function. Then, the average transient mirror reflectivity was calculated based on the behavior of the transient signal response function for the same time interval.

The time integration of Eq. 5.3 was warranted for a second reason, error analysis. Although the transient reflectivity is hidden in the noise of the block-in and block-out data files, too much auto-correlated noise is present to confidently predict transient reflectivity behavior. By integrating over pre-determined time intervals, the transient signal response function for a single wavelength and time is lost, but the average behavior of $f(\lambda,t)$ in the time region is now known. In addition, the error for the time integrated region is usually smaller than the error associated with a single time and wavelength observation. See section 5.3 for details on error analysis.

To obtain the estimate for the transient reflectivity, during a defined time interval, the steady-state reflectivity was multiplied by the averaged value of the transient signal response function also integrated over the same time interval, as stated in Eq. 5.4:

$$R_{T}(\lambda, t_1 \rightarrow t_2) = R_{SS}(\lambda) * f(\lambda, t_1 \rightarrow t_2) \qquad (5.4)$$

where $R_{T}(\lambda, t_1 \rightarrow t_2)$ ≡ The average transient reflectivity for time region $t_1 \rightarrow t_2$.

$f(\lambda, t_1 \rightarrow t_2)$ ≡ The average transient signal response function for time region $t_1 \rightarrow t_2$, also called the signal ratio for the time region,

and t_1 & t_2 ≡ Time limits of the pre-determined time regions defined in Table 5.1, ($t_1 < t_2$).

5.2.1 Determining $f(\lambda,t)$ and $f(\lambda, t_1 \rightarrow t_2)$

Notice $f(\lambda,t)$ could be found by taking the ratio of block-in and block-out signal data as stated in Eq. 5.5.

$$f(\lambda,t) = I_{SCDo}(\lambda,t) \;/\; I_{SCDi}(\lambda,t) \;/\; A(\lambda) \qquad (5.5)$$

where $A(\lambda)$ is defined as

$$A(\lambda) = \int_{t=t_s}^{t=t_e} I_{SCDo}(\lambda),t)\; dt \;/\; \int_{t=t_s}^{t=t_e} I_{SCDi}(\lambda),t)\; dt \qquad (5.6)$$

where t_s ≡ The starting time, t_1, in region number one of Table 5.1,

t_e ≡ The ending time, t_2 , in region number one of Table 5.1.

and all other variables are defined from previous equations. For example, for dielectric mirror 14, t_s and t_e are −40.0 ns and 0.0 ns, respectively.

Now Eqs. 5.5 and 5.6 can be simplified,

$$f(\lambda,t) = C2(\lambda) * R_{IM}(\lambda,t) \,/\, (C1(\lambda) * R_{PM}(\lambda,t) * A(\lambda)) \quad (5.7)$$

$$A(\lambda,t) = \int_{t=t_s}^{t=t_e} R_{PM}(\lambda,t)\, dt \;/\; \int_{t=t_s}^{t=t_e} R_{IM}(\lambda,t)\, dt * C3(\lambda) \quad (5.8)$$

respectively, where $C1(\lambda)$, $C2(\lambda)$, and $C3(\lambda)$ are constants with respect to time resulting from applying simplifications of section 5.1.1 to Eq. 5.5 and 5.6. Furthermore, $C3(\lambda) = C2(\lambda)/C1(\lambda)$. Note, $C1(\lambda)$, $C2(\lambda)$ and $C3(\lambda)$ cancel after substitution of Eq. 5.8 into Eq. 5.7 leaving a ratio of transient and pre-irradiation mirror reflectivity integrals.

For a given wavelength, $A(\lambda)$ is the ratio of the integrals of block-out and block-in reflectivities before the electron beam has hit the mirror. The need for the function $A(\lambda)$ is twofold: First, without $A(\lambda)$, Eq. 5.5 could yield artificially high or low values of $f(\lambda,t)$ depending on the measured signal light intensities. Secondly, no difference in mirror reflectivities is expected before the electron beam hits the mirror. That is, the signal light intensity, measured at the streak camera detector, before the beam hits the mirror should be the same for block-out and block-in

irradiations. $A(\lambda)$ affects $f(\lambda,t)$ by accounting for any differences in the measured signal light intensities from a block-out to a block-in irradiation occuring before the beam has hit the mirror.

Also, $A(\lambda)$ accounts for any differences in the xenon lamp intensity between block-out and block-in shots. Although the second simplification of section 5.1.1 is reasonable, the light emitted from the xenon flash lamp could unexplainably vary between block-in and block-out shots. $A(\lambda)$ is a normalizing factor used to match the pre-irradiation and transient signals, contained in the block-in and block-out files, respectively, in the time region prior to the time the beam hits the mirror.

To find $f(\lambda, t_1 \rightarrow t_2)$ from $f(\lambda,t)$, integrate Eq. 5.7 over the time region $t_1 \rightarrow t_2$. Namely,

$$f(\lambda, t_1 \rightarrow t_2) = \begin{cases} \int_{t=t_1}^{t=t_2} f(\lambda,t)\ dt & t_1 \leq t \leq t_2 \\ 0 & \text{otherwise.} \end{cases} \qquad (5.9)$$

Now, substituting Eq. 5.7 and 5.8 into 5.9 yields the signal ratio for $t_1 \leq t \leq t_2$.

$$f(\lambda, t_1 \rightarrow t_2) = \int_{t=t_1}^{t=t_2} R(\lambda,t)_{IM}\ dt \ / \left[\int_{t=t_1}^{t=t_2} R(\lambda,t)_{PM}\ dt \right.$$

$$\left. * \int_{t_s}^{t_e} R(\lambda,t)_{IM}\ dt \ / \int_{t_s}^{t_e} R(\lambda,t)_{PM}\ dt \right] \qquad (5.10)$$

A complete set of signal ratios is contained in Appendix A. Note, the ordinate axis label identifies the signal ratio as I1(out)*I2(in)/(I1(in)*I2(out)). The I1 and I2 labels are short-hand notation for the integrals of the signal light intensity terms in Eq. 5.10. In the expression, I1 and I2 cover the different time regions defined in Table 5.1, with I2 always defined as region one. The (out) and (in) designations differentiate between the block-out and block-in beam shots. From left to right, the integrals in Eq. 5.10 are I1(out), I1(in), I2(out) and I2(in).

In addition to the signal ratios, two sets of error bars and the inverse of a fast-Fourier transform of the signal-ratio data are plotted. The significance of the error bars is outlined in the error analysis section, section 5.3, while the necessity of the fast-Fourier transform analysis is covered in section 5.2.3.

5.2.2 Time Integration

To calculate the signal ratio, $f(\lambda, t_1 \rightarrow t_2)$, the block-in and block-out data files were integrated with respect to time over defined time regions. In the preliminary analysis of the block-out and block-in data, the effects of noise on the data were obvious and pronounced. To reduce the effects of noise on the transient data, Eq. 5.3 was integrated over the time regions listed in Table 5.1.

Three numerical integration techniques were tried for integrating the block-in and block-out data until the best technique was determined. The three methods used for numerical integration were the Romberg, trapezoidal and simple-summation techniques. After finding the optimal integration technique, trapezoidal integration, all subsequent integrations were carried out using the optimal technique. A discussion on the integration techniques and their accuracies is found in reference 12. A listing of the computer programs used to perform the numerical integrations is found in Appendix B.[8]

---

[8] Although the Romberg integration technique promises to yield the best estimate for the tightly-packed spiked data, the additional computer effort and cost did not warrant the added accuracy. In fact, the maximum relative error, in comparing the simple-summation technique with the Romberg technique, computed using

$$\text{Error} = \frac{/\ \text{Romberg Estimate} - \text{Simple-Summation Estimate}\ /}{\text{Romberg Estimate}}$$

was 0.005. Thus, even the crudest estimator of the integral, the simple-summation technique, gave nearly identical results compared with the Romberg estimate. The differences between the Romberg and trapezoidal estimates were negligible.

All three techniques provided nearly identical estimates for the total integral over all times for the block-in and block-out data. Thus, because the techniques were nearly identical and the trapezoid technique differs from the simple-summation technique only at endpoint evaluation, the trapezoidal technique was chosen the best integral estimator.

Table 5.1 Time regions used for the time integration of the block-out and block-in shots. The times t_1 and t_2 represent the start and end of the time region, respectively. Also listed in the table are the mirrors numbers, with corresponding irradiation positions, having that time region division type.

Mirror Number	Irradiation Position	Time Region Division Type	Region Number	Time Region t_1 (ns)		t_2 (ns)
14	A	I	1	-40.0	to	0.0
1L	A		2	0.0	to	5.0
6L	A		3	5.0	to	10.0
			4	10.0	to	15.0
			5	15.0	to	20.0
			6	20.0	to	25.0
			7	25.0	to	41.3
			8	41.3	to	57.5
			9	57.5	to	73.8
			10	73.8	to	88.0
12	A	II	1	-30.0	to	0.0
26	A		2	0.0	to	37.0
7L	A		3	37.0	to	70.5
			4	70.5	to	104
			5	104	to	138
			6	138	to	171
			7	171	to	205
			8	205	to	238
			9	238	to	272
			10	272	to	313

12	B	III[9]	1	-30.0	to 0.0
7L	B		2	250	to 284
			3	284	to 317
			4	317	to 351
			5	351	to 384
			6	384	to 418
			7	418	to 451
			8	451	to 485
			9	485	to 518
			10	518	to 552
			11	552	to 593
13	A	IV	1	-160	to 0.8
2L	A		2	0.8	to 20.9
			3	20.9	to 41.0
			4	41.0	to 61.1
			5	61.1	to 81.2
			6	81.2	to 101
			7	101	to 121
			8	121	to 142
			9	142	to 162
			10	162	to 183
13	B	V	1	-50.0	to 0.25
2L	B		2	0.25	to 33.8
			3	33.8	to 67.3
			4	67.3	to 101
			5	101	to 134
			6	134	to 168
			7	168	to 201
			8	201	to 235
			9	235	to 268
			10	268	to 293

[9]For time region III, the region number one files are the same as region one files for the position A shots of the same mirror. For example, for mirror 7L, position B, the region one files used in Eq. 5.10 are the same files used for mirror 7L, position A.

5.2.3 Fast-Fourier Transform Analysis of the Signal Ratios

Before Eq. 5.4 could be used to predict the transient behavior of the laser mirrors, the noise in the signal ratios needed to be lessened or removed. According to Aubanel and Oldham the signal-ratio data could be smoothed using moving-average, least-squares or Fourier-transform techniques (11). Both the least-squares and Fourier methods were tried for noise reduction. This researcher found the least-squares method was ineffective in predicting a statistically significant fit to the signal-ratio data, even up to tenth degree polynomials.[10] Instead, the smoothed signal-ratio curves from the Fourier transform provided a better prediction of the transient signal ratios of Eq. 5.4.

The Fourier-transform technique used the filter function, f_k, suggested by Reference 11, to remove high frequency noise. Namely,

$$f_k = \begin{cases} 1 - (k/E)^2 & k = 1,2,3,\ldots E-1 \\ 0 & k = E,E+1,\ldots N-1 \end{cases} \qquad (5.11)$$

---

[10] Because the least-squares method was ineffective, the details of the technique are not included. The least-squares method used to analyze the signal-ratio data sought polynomial fits up to the tenth degree. In order for a given polynomial model to be judged the best fit for a given model, the t-test statistics for highest order parameter in the next two polynomial models needed to be insignificant at the 95% confidence level. Polynomial models were used exclusively in the least-squares analyses.

where

$$E = \begin{cases} (N-1)/2 & \text{when N is odd} \\ N/2 & \text{when N is even} \end{cases}$$

and k ranges from zero to the number of data values, N, minus one. f_k is a commonly used digital filter function used to remove high frequency noise found in the recording of electronic data.

The smaller the value chosen for E, the more denuded of high frequencies the signal-ratio data became. Figures 5.1 to 5.6 illustrate the effects of varying E on the signal-ratio data of dielectric mirror 14, irradiated in position A, during time region seven.

5.2.3.1 Determining the Optimum E-value for the Fourier Transform

In choosing the best value of E for a particular Fourier transform of a signal ratio, an F-test was performed comparing the variances about the transform curve for E = 2 and E = 3. If the F-ratio was greater than 1.164, the critical F-statistic for 470 degrees of freedom in the numerator and denominator, the E = 2 model was rejected.[11] If E = 2 was rejected, the F-ratio would be

[11]The critical F statistic for 470 degrees of freedom in the numerator and denominator was calculated using SAS, a statistical programming language, and confirmed using an International Math and Science Library routine named MDGAM. All statistics, unless otherwise stated are at the 95% confidence level.

re-calculated for the E = 3 model. Then, if the F-ratio is less than the critical F-statistic, the E = 3 model would be accepted.

For example, in Fig. 5.1, the original signal-ratio data and Fourier transform with E=2 are plotted. Similarly, in Fig. 5.2, the original signal-ratio data and the Fourier transform with E=3 are plotted. The variances of the original signal data about the E=2 and E=3 Fourier transforms are 89.1 and 76.8 respectively.[12] The variances correspond to an F-statistic of 1.159, i.e. insignificant with respect to the critical statistic of 1.164. Thus, the E=3 model is not significantly different than the E=2 model and the E=2 model is accepted.

---

[12]The variance about the Fourier transform curves are calculated in the same manner as the mean square of residuals is found in least-squares analysis. That is,

$$\sigma^2 = \frac{\sum_{i=1}^{n} (f_i(\lambda, t_1 \rightarrow t_2) - \mu_i(\lambda, t_1 \rightarrow t_2))^2}{N - 1}$$

where $f_i(\lambda, t_1 \rightarrow t_2)$ is the signal ratio at λ_i.

$\mu_i(\lambda, t_1 \rightarrow t_2)$ is the Fourier estimate of the signal ratio at λ_i.

σ^2 is the estimate for the population variance,

and i=1 to N data values. (N = 471 for the signal-ratio files.)

For all but one signal ratio, the E=2 Fourier transform was accepted. Finally, the Fourier transform curves were substituted for the signal-ratio term in Eq. 5.4 and used to calculate the transient reflectivity for the laser mirrors. The transient mirror reflectivities are found in Appendix C. Sample transient reflectivity curves for each mirror type are found in Fig. 5.15 to Fig. 5.17.

5.3 Error Analysis

Error analysis will be broken into three sections: error on pre-irradiation reflectivity measurements, error on the signal ratios and error on the transient reflectivities.

5.3.1 Error from Pre-irradiation Reflectivity Measurements

A source of error, not taken into account in the final transient reflectivity curves, partly resulted from the digitizing of the CARY 2300 strip-chart output. When the data from the strip-chart needed analysis and digitization, no mechanical or computer digitizer was available for use. Thus, the strip chart curves were digitized by hand, i.e. numerical values were assigned to points on the strip-chart curve using the naked eye. Next, the digitized points were fed into the HP 9816 computer before being plotted.

An estimate of 4% relative error was made for the error resulting from using the plotting program, manual digitization of

the strip-chart data, and the CARY 2300. The error estimate is based on the thickness of the line plotted on the strip-chart, the effects of the natural cubic spline routine in the HP plotting program, and the performance of the CARY 2300 spectrophotometer.

Once plotted, the pre-irradiation reflectivity curves were assumed invariable, i.e., no error bars were assigned to the pre-irradiation reflectivity curves. Instead, the reflectivity curves were treated as constants in the propagation of error from the signal-ratio files. Treatment of the curves as constants is allowable considering the magnitude of the error resulting from the signal-ratio data.

5.3.2 Error on Signal Ratio Data

5.3.2.1 Mean-Square-Residual Technique

Two techniques were used to assign error to the signal-ratio data. In the first technique, the population mean square residual, MSRES, is calculated using Eq. 5.12:

$$MSRES = SSRES \;/\; (N - df) \qquad (5.12)$$

where

$$SSRES = \sum_{i=1}^{N} \left(f_i(\lambda, t_1 \rightarrow t_2) - \mu_i\ (\lambda, t_1 \rightarrow t_2)\right)^2,$$

the sum of squares due to residual,

N = The number of data points in the signal-ratio file (=471),

df = The degrees of freedom associated with the fast-Fourier transform,

$f_i(\lambda, t_1 \rightarrow t_2)$ = The signal ratio at λ_i.

and $\mu_i(\lambda_1, t \rightarrow t_2)$ = The fast-Fourier transform estimate at λ_i.

The definition for the MSRES is taken from least-squares theory and poses a problem for evaluation using the Fourier analysis. In least-squares analyses μ_i would be defined as the predicted value at λ_i during $t_1 \rightarrow t_2$. However, because the least-squares technique failed to supply fits to the signal-ratio data, μ_i was re-defined as stated above. The difficulty in evaluating Eq. 5.12 arises in assigning the proper degrees of freedom, df, in the denominator. In the least-squares method, the form of the regression function and its associated degrees of freedom are known, while for the Fourier technique neither are known.

A general rule-of-thumb allows for the estimation of the degrees of freedom associated with a given curve. Stated in equation form,

$$df \simeq L + 1$$

where L is defined as the number of times the second derivative of the curve changes sign when evaluated in the defined range of data. Furthermore, the number of sign changes can be approximated by the number of bends in the curve. Of course the use of the rule should be limited to estimating the degrees of freedom (14).

For most of the signal-ratio Fourier curves, the number of bends do not exceed six. Thus, the denominator of Eq. 5.12 would vary from 465 to 470 depending on the individual Fourier-transform curves. To standardize the error computation, Eq. 5.12 was simplified to

$$MSRES \simeq SSRES \; / \; 470 \qquad (5.13)$$

because the effect of varying the degrees of freedom was minimal in comparison to the size of the SSRES and N.

The population estimate of the standard deviation, the square root of the mean square residual, was calculated and used to form one set of error bars on the signal-ratio plots. Because no repeated measurements were made, the standard deviation, based on the total population of data, is an acceptable standard deviation for each signal-ratio data value. For the signal-ratio plots in Appendix A, an approximate 95% confidence interval about the Fourier-transform line, based on the MSRES error estimate, is represented by the dash-dot lines. The dash-dot lines are plus-or-minus two times the square root of the mean-square-residual error estimate.

5.3.2.2 Moving-Mean-Square-Residual Technique

The other set of error bars on the signal-ratio plots resulted from developing a moving-mean-square-residual technique, MMSRES.

The MMSRES defines a MSRES for a data point inside a window of data points, instead of the whole population (13).

To calculate the MMSRES for a data point in the signal-ratio file, MMSRES, begin by numbering the 470 signal-ratio data points from 1 to 470, e.g.:

1 2 3 ... i-1 i i+1 ... 468 469 470

Next, define a half-window size, NN, about the data point i and look at the window defined by i and NN.

i-NN i-NN+2 ... i-1 i i+1 ... i+NN-2 i+NN

i-NN-1 i+NN-1

In the window defined by NN and i, there are 2(NN) + 1 data points. The moving mean square residual for data point i is defined in Eq. 5.14:

$$MMSRES_I = \frac{\sum^{NN} (f_j(\lambda, t_1 \rightarrow t_2) - \mu_j(\lambda, t_1 \rightarrow t_2))^2}{2 * NN} \qquad (5.14)$$

where the summation is taken over the full-window region, 2(NN) + 1 data points.

In evaluating the moving mean square residual for i-NN < 1 or i+NN>N, the window size is adjusted to account for the loss of data

values on the shortened side. For example, with NN=50 and i=1, the summation over nearest neighbors covers data points 1 to 51. For i=2, the summation covers data points 1 to 52 and so on until the window reaches its full size at i=51. Similarly, when calculating the MMSRES for i=425, the summation over nearest neighbors covers points 375 to 470. Written another way,

$$\text{MMSRES}_i \frac{\sum_{j=1}^{i+NN} (f_j(\lambda, t_1 \rightarrow t_2) - \mu_j(\lambda, t_1 \rightarrow t_2))^2}{i + NN - 1}$$

$$\text{for } i<NN \qquad (5.15)$$

and

$$\text{MMSRES}_i = \frac{\sum_{j=i-NN}^{N(=470)} (f_j(\lambda, t_1 \rightarrow t_2) - \mu_j(\lambda, t_1 \rightarrow t_2))^2}{i + NN - 1}$$

$$\text{for } i > 470-NN \qquad (5.16)$$

Finally, to obtain the estimate of one standard deviation about data point i, the square root of the MMSRES_i is taken.

The advantage of using the MMSRES technique lies in the shape of the signal-ratio plots. The reader should notice from the signal-ratio plot in Fig. 5.14 the MSRES technique was very crude in estimating error in the upper wavelength region of the plot. The crudeness stems from accounting for the whole population variation

even though the variation about the Fourier-transform line for a window of data points could be smaller. That is, the variance is not constant within the signal-ratio data from low to high wavelengths.

To understand the effects of window size on the value of the error assigned to each signal-ratio data value, one must compare various window sizes. For example, Fig. 5.7 shows the signal-ratio data and Fourier-transform line for metal-coated mirror 2L, irradiated in position A, with the block-out. Also shown on the graph is a plot of the Fourier-transform line plus or minus two times the square root of the MMSRES with a half-window size, NN, of 5. Although, with NN=5, the MMSRES technique seems to adequately describe the error in the upper wavelength region, the first derivative of the error associated with the lower wavelengths is discontinuous.[13] Conversely, in Fig. 5.13 with NN=150, the MMSRES technique adequately describes the lower wavelength error, while the error for the upper wavelength signal ratios is overestimated. Thus, an intermediate half-window size of fifty was found to be the optimum size. The MMSRES technique adequately described the error throughout all wavelengths with NN=50. The effect on the MMSRES for various NN is seen in Fig. 5.7 to 5.13.

---

[13]The first derivative of the error is expected to be continuous because it describes a real system.

In comparing the error estimates from the two techniques, MMSRES and MSRES, the MMSRES technique tends to give smaller error bands when the magnitude of the signal ratio dampens out. The researcher believes the MMSRES describes the error for the signal ratio of Fig. 5.14 better than the MSRES. Although, the MMSRES technique yields larger error bars in the lower wavelengths than the MSRES, the increase is not significantly different.

Finally, an approximate 95% confidence interval about the Fourier-transform curve, based on the MMSRES variance estimate, is plotted with a triple-dash on the signal-ratio plots of Appendix A. The triple-dash curves are the Fourier curve estimate at data point λ_i plus-or-minus two times the square root of the MMSRES variance at point λ_i. The MMSRES technique for estimating error was used in the propagation of error to find the transient reflectivities. All errors assigned to the transient reflectivities result from the MMSRES technique.

5.3.3 Error on the Transient Reflectivities

As stated earlier in section 5.3.1, the pre-irradiation, reflectivity is assumed constant and error free with respect to error propagation. Using standard error propagation techniques, the error associated with the transient reflectivity equals the product of the transient reflectivity and two times the square root of the moving mean square residual at a given wavelength. That is, the

error bars around any transient reflectivity are found using Eq. 5.17.

$$R_T(\lambda, t_1 \rightarrow t_2) \pm R_{SS}(\lambda) * 2(\text{MMSRES}\ (\lambda, t_1 \rightarrow t_2))^{0.5} \qquad (5.17)$$

Because the MMSRES values for a signal-ratio file are not continuous, a natural cubic spline program was used to evaluate the pre-irradiation reflectivity at the same wavelengths as the MMSRES. The transient reflectivity plots in Appendix C show the transient reflectivity curves and the associated error based on the MMSRES technique, and Eq. 5.4 and 5.17. In addition, the pre-irradiation reflectivity is also shown on each plot of Appendix C. The MMSRES technique error bars represent an approximate 95% confidence interval about the transient reflectivity.

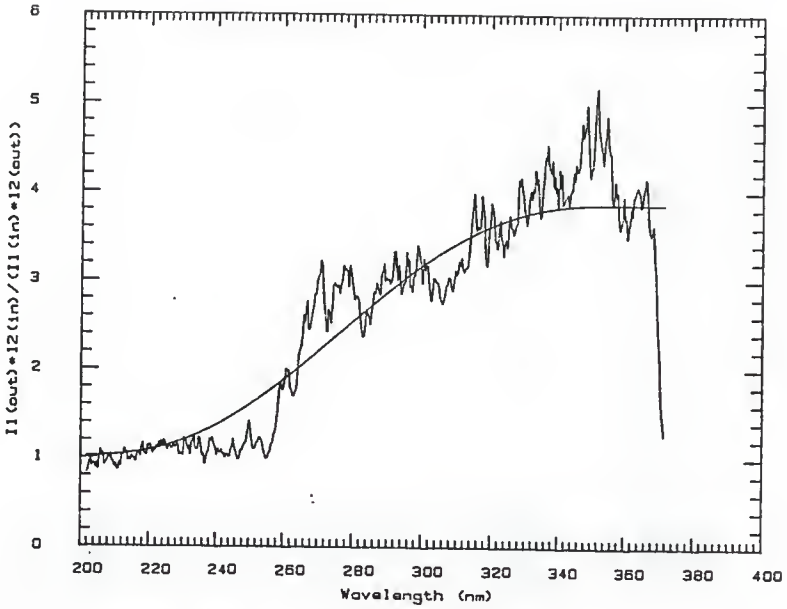

Fig. 5.1 The signal ratio and Fourier curve, with E=2, for dielectric mirror 14. I1 is defined during 25 to 41.3 ns.

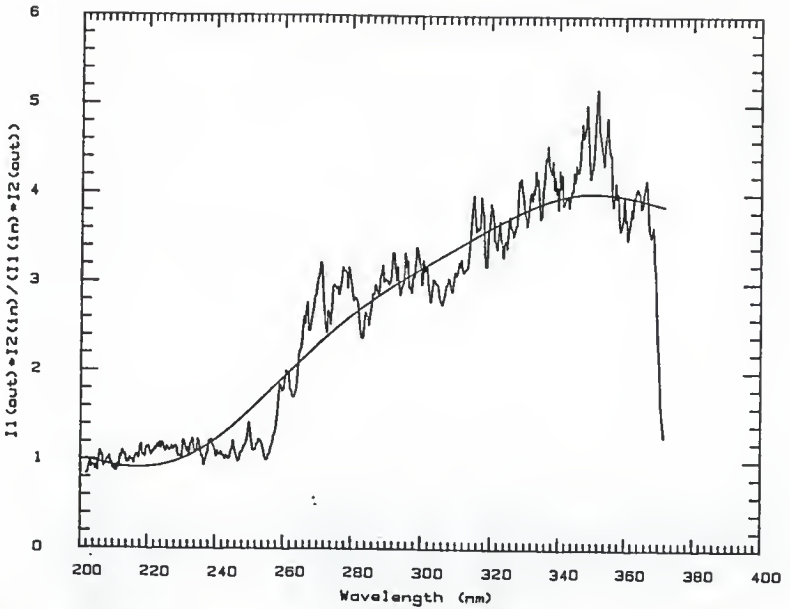

Fig. 5.2 The signal ratio and Fourier curve, with E=3, for dielectric mirror 14. I1 is defined during 25 to 41.3 ns.

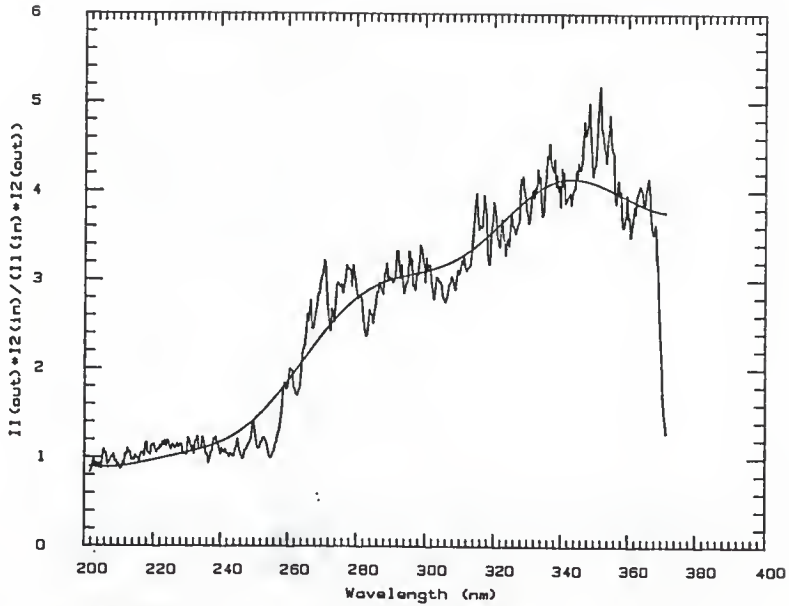

Fig. 5.3 The signal ratio and Fourier curve, with E=4, for dielectric mirror 14. I1 is defined during 25 to 41.3 ns.

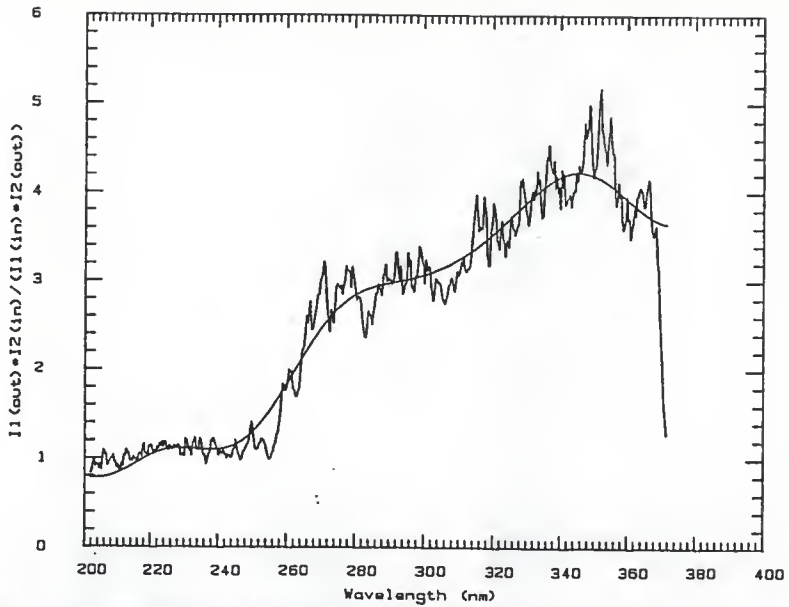

Fig. 5.4 The signal ratio and Fourier curve, with E=5, for dielectric mirror 14. I1 is defined during 25 to 41.3 ns.

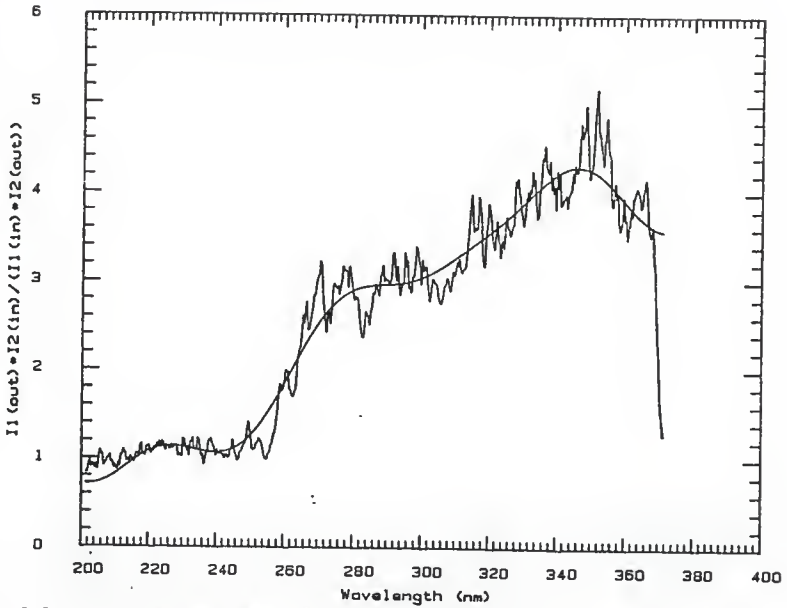

Fig. 5.5 The signal ratio and Fourier curve, with E=6, for dielectric mirror 14. I1 is defined during 25 to 41.3 ns.

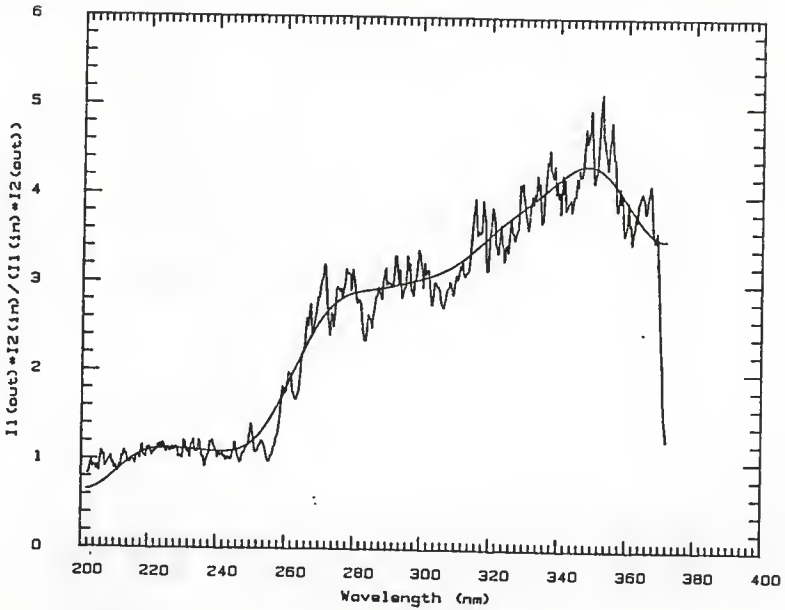

Fig. 5.6 The signal ratio and Fourier curve, with E=7, for dielectric mirror 14. I1 is defined during 25 to 41.3 ns.

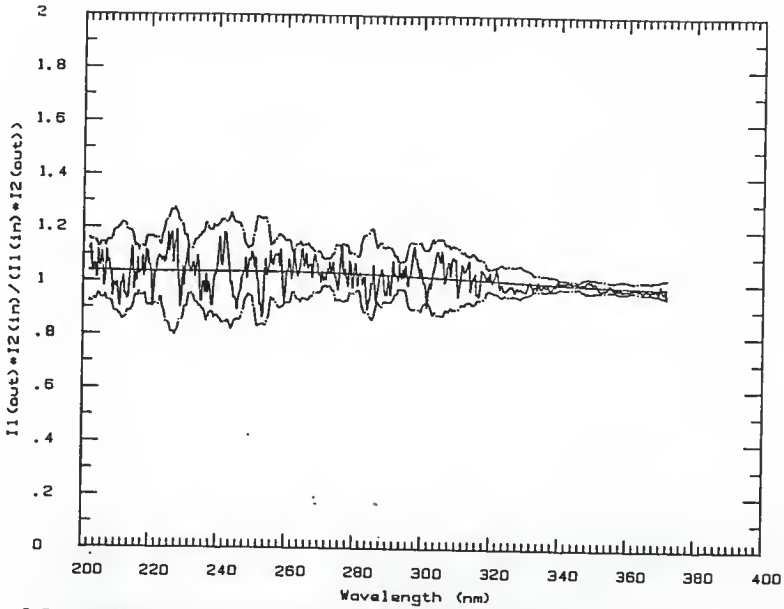

Fig. 5.7 The signal ratio and Fourier curve (solid lines) and Fourier curve +/- $2*(\text{MMSRES})^{\frac{1}{2}}$ error estimate (dash-dot lines) for metal-coated mirror 2L, irradiated in position A. The MMSRES estimate is based on a half-window size of 5. I1 is defined during 61.1 to 81.2 ns.

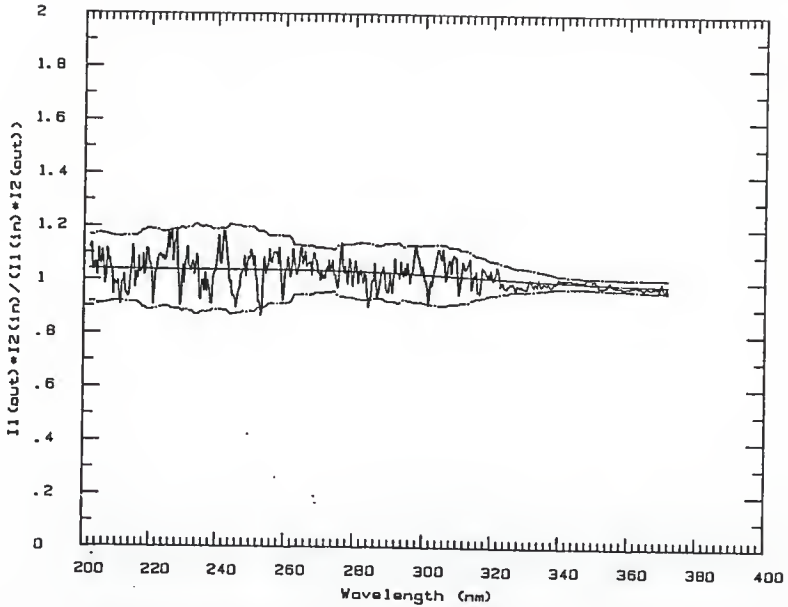

Fig. 5.8 The signal ratio and Fourier curve (solid lines) and Fourier curve +/- $2*(\text{MMSRES})^{\frac{1}{2}}$ error estimate (dash-dot lines) for metal-coated mirror 2L, irradiated in position A. The MMSRES estimate is based on a half-window size of 25. I1 is defined during 61.1 to 81.2 ns.

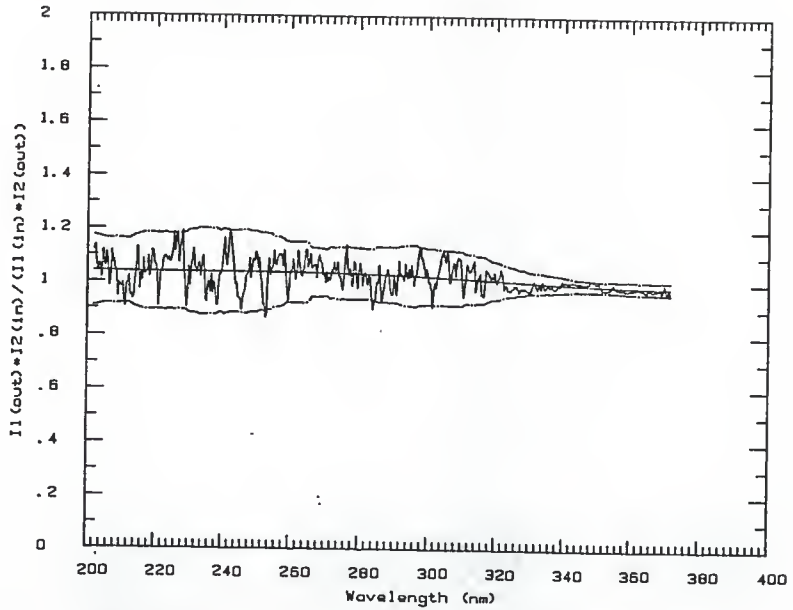

Fig. 5.9 The signal ratio and Fourier curve (solid lines) and Fourier curve +/- $2*(\text{MMSRES})^{\frac{1}{2}}$ error estimate (dash-dot lines) for metal-coated mirror 2L, irradiated in position A. The MMSRES estimate is based on a half-window size of 35. I1 is defined during 61.1 to 81.2 ns.

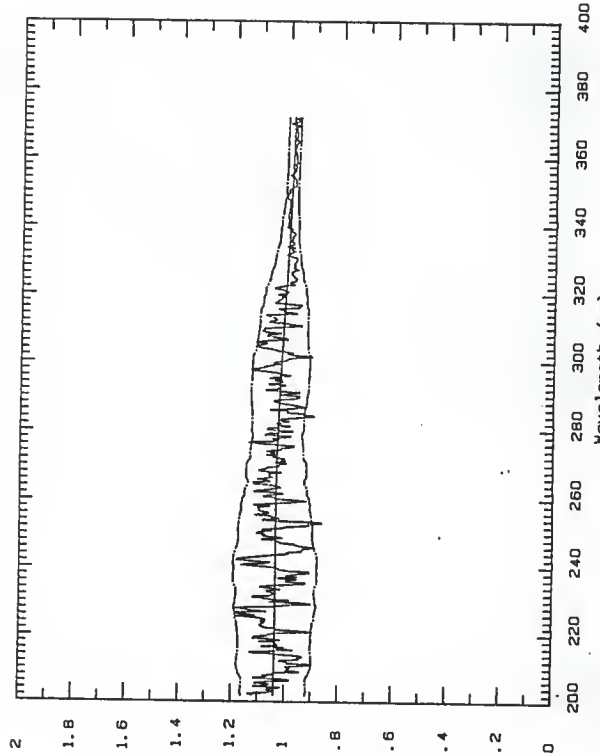

Fig. 5.10 The signal ratio and Fourier curve (solid lines) and Fourier curve +/- $2*(MMSRES)^{\frac{1}{2}}$ error estimate (dash-dot lines) for metal-coated mirror 2L, irradiated in position A. The MMSRES estimate is based on a half-window size of 50. I1 is defined during 61.1 to 81.2 ns.

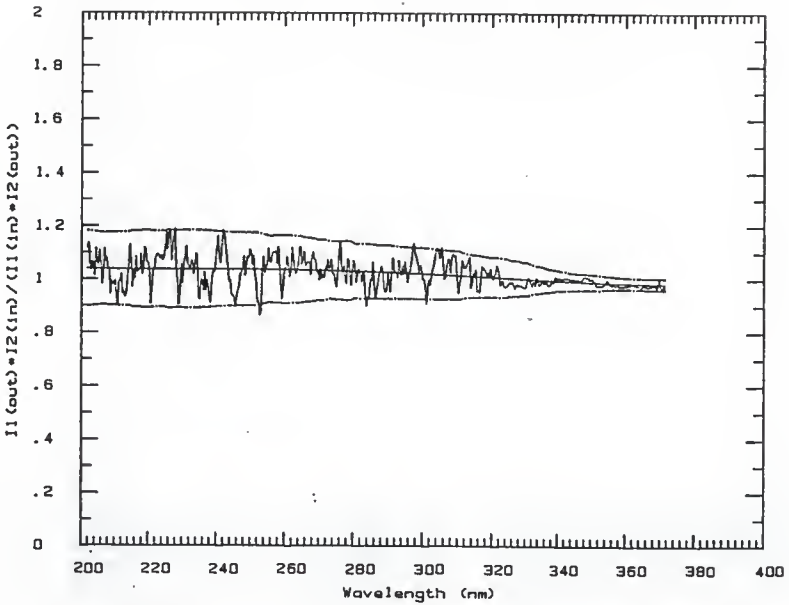

Fig. 5.11 The signal ratio and Fourier curve (solid lines) and Fourier curve +/- $2*(\text{MMSRES})^{\frac{1}{2}}$ error estimate (dash-dot lines) for metal-coated mirror 2L, irradiated in position A. The MMSRES estimate is based on a half-window size of 75. I1 is defined during 61.1 to 81.2 ns.

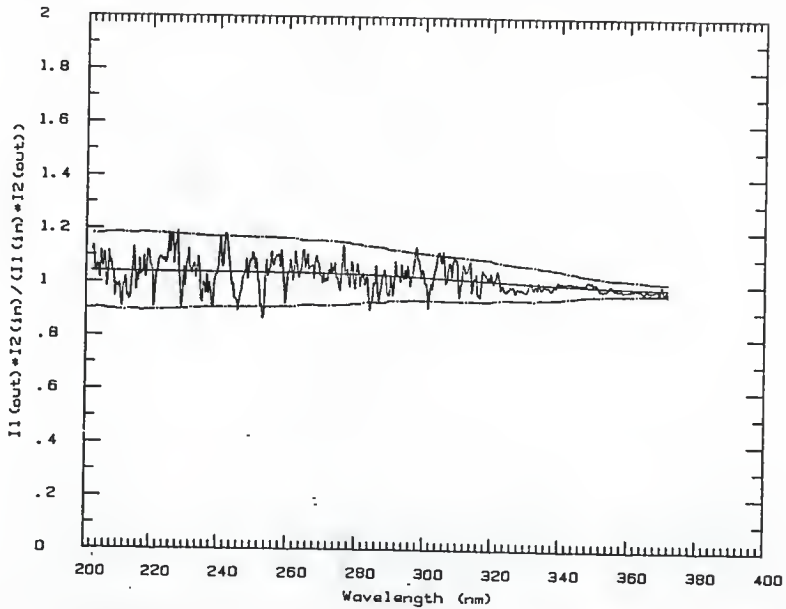

Fig. 5.12 The signal ratio and Fourier curve (solid lines) and Fourier curve +/- $2*(\text{MMSRES})^{\frac{1}{2}}$ error estimate (dash-dot lines) for metal-coated mirror 2L, irradiated in position A. The MMSRES estimate is based on a half-window size of 100. I1 is defined during 61.1 to 81.2 ns.

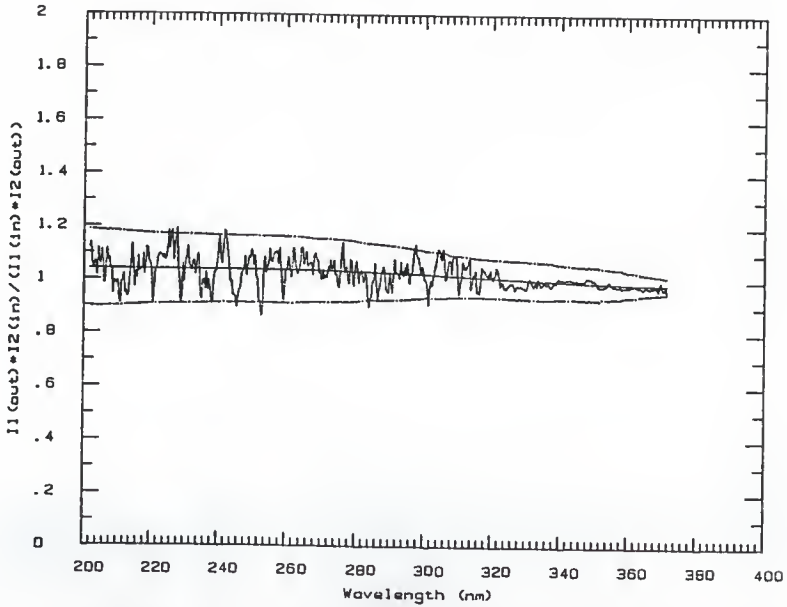

Fig. 5.13 The signal ratio and Fourier curve (solid lines) and Fourier curve +/- $2*(MMSRES)^{\frac{1}{2}}$ error estimate (dash-dot lines) for metal-coated mirror 2L, irradiated in position A. The MMSRES estimate is based on a half-window size of 150. I1 is defined during 61.1 to 81.2 ns.

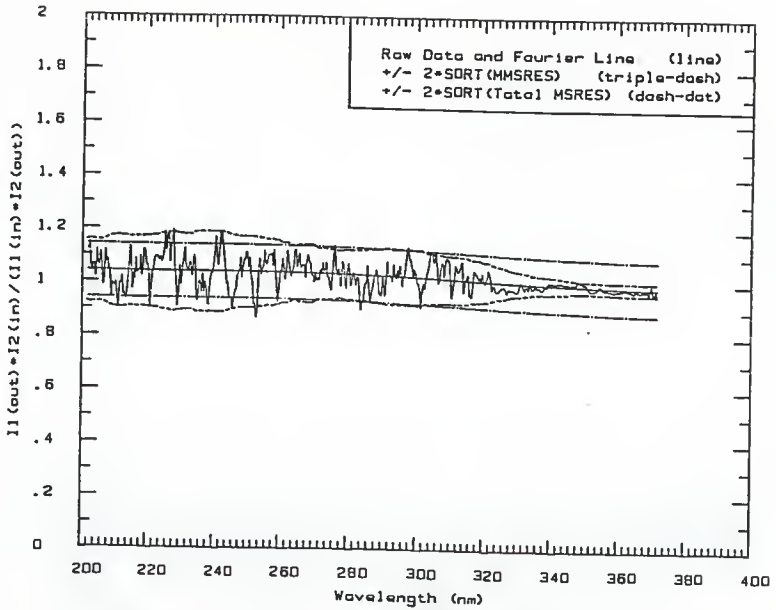

Fig. 5.14 A comparison of the MSRES and MMSRES error estimates for the metal-coated mirror 2L, irradiated in position A. The MMSRES estimate is based on the optimal half-window size, 50.

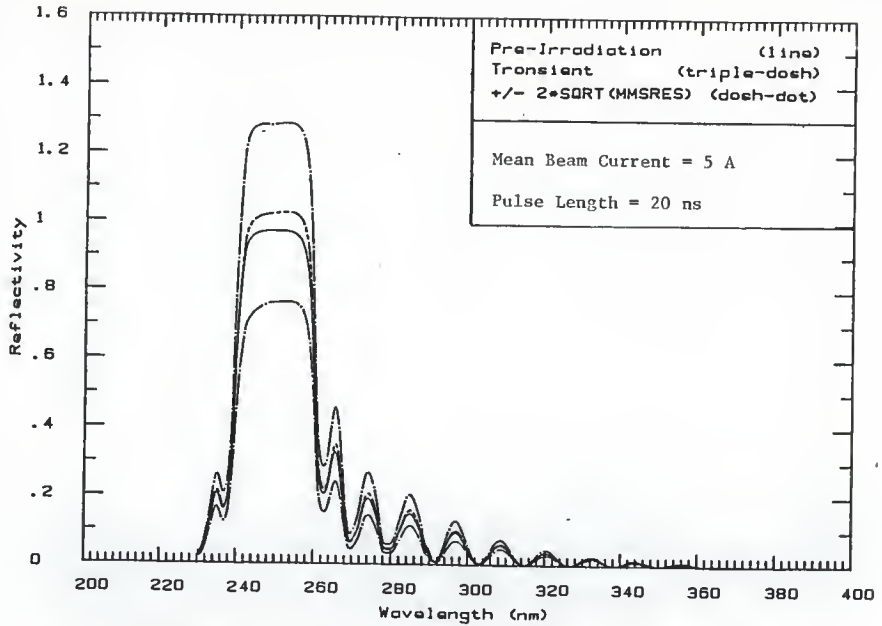

Fig. 5.15 The pre-irradiation reflectivity compared to the transient reflectivity based on the signal ratio in Fig. 1a for dielectric mirror 14.

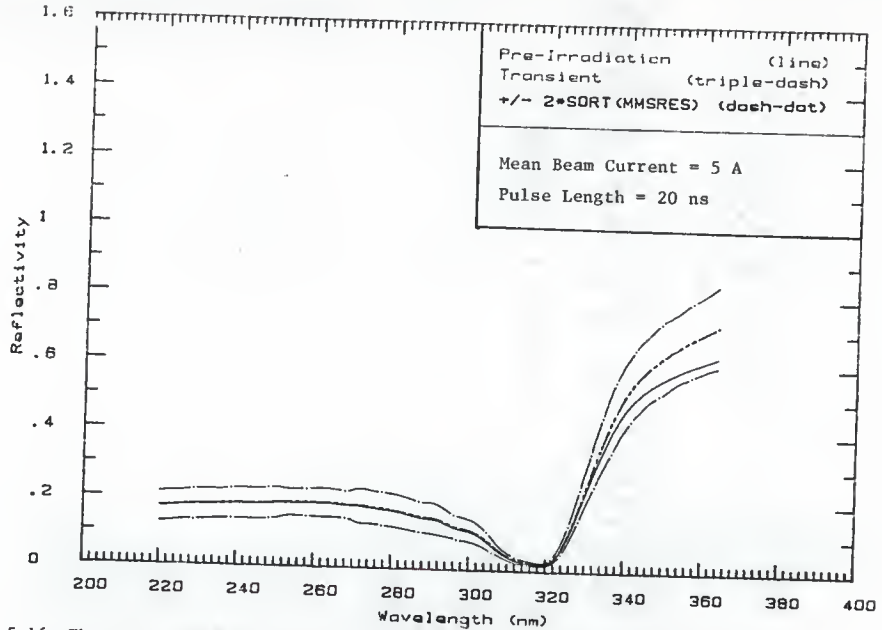

Fig. 5.16 The pre-irradiation reflectivity compared to the transient reflectivity based on the signal ratio in Fig. 7a for metal-coated mirror 1L.

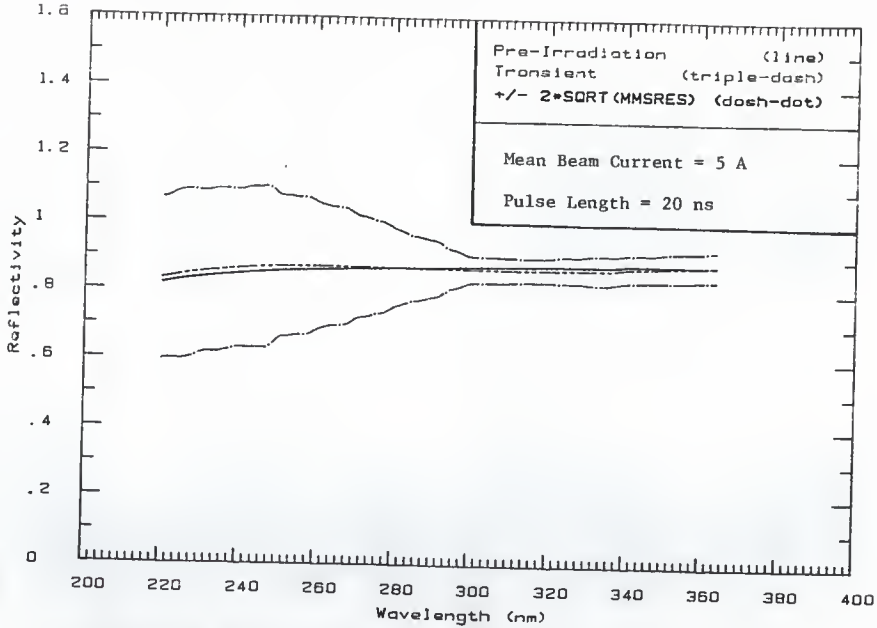

Fig. 5.17 The pre-irradiation reflectivity compared to the transient reflectivity based on the signal ratio in Fig. 10a for metal-coated mirror 6L.

6. Results

The results of the experiment are broken into two categories: the results based on the signal ratios, and the transient reflectivity results. Note, for all irradiations, the energy of the incident electrons in the beam was about 16.5 MeV.

6.1 Results from the Signal Ratios

As mentioned before, the complete set of signal-ratio plots for the time intervals defined in Table 5.1 are listed in Appendix A. The main results to be drawn from the plots of the signal-ratio files are the regions where the signal ratio deviates significantly from unity.

Significant deviation occurs when the Fourier transform curve plus or minus two times the square root of the MMSRES error estimate falls outside of a signal ratio equal to unity. Ideally, for no transient effect, the signal ratio equals one. Listed in Table 6.1 are the wavelength regions the signal ratio has statistically significantly deviated from unity for each mirror.

Table 6.1 Time and wavelength regions of statistically significant deviations from unity of the Fourier transform of the measured signal ratio plus or minus two times the square root of the MMSRES. The time region numbers and division types corresponding to the statistically significant time regions are defined in Tables 5.1 and 5.2, respectively. The irradiation positions are defined in Fig. 4.5. Also listed under the mirror number is the pulse length, τ and mean current, $\bar{I}$ of the electron beam in the block-out irradiation.

		Statistically Significant		
Mirror Number	Irradiation Position	Region Number	Time Region (ns)	Wavelength Region (nm)
1L	A	3	5.0 to 10.0	343 to 371
τ = 20 ns	$\bar{I}$ = 5 A			
2L	A		None	None
τ = 200 ns	$\bar{I}$ = 225 mA			
2L	B		None	None
τ = 200 ns	$\bar{I}$ = 225 mA			
6L	A		None	None
τ = 20 ns	$\bar{I}$ = 5 A			
7L	A	2	0.0 to 37.0	342 to 371
		3	37.0 to 70.5	332 to 371
		4	70.5 to 104	328 to 371
		5	104 to 138	330 to 362
		6	138 to 171	314 to 371
		7	171 to 205	None
		8	205 to 238	346 to 371
τ = 500 ns	$\bar{I}$ = 225 mA			

7L	B	3	284 to 317	324 to 371
		4	317 to 351	316 to 371
		5	351 to 384	300 to 352
		6	384 to 418	278 to 350
		7	418 to 451	298 to 346
		8	451 to 485	288 to 350
		9	485 to 518	276 to 350
		10	518 to 552	280 to 371
		11	552 to 593	280 to 344

τ = 500 ns $\bar{I}$ = 225 mA

12	A	4	70.5 to 104	261 to 371
		5	104 to 138	279 to 371
		6	138 to 171	274 to 360
		7	171 to 205	264 to 371
		8	205 to 238	271 to 371
		9	238 to 272	263 to 371
		10	272 to 313	256 to 371

τ = 500 ns $\bar{I}$ = 225 mA

12	B	2	250 to 284	266 to 371
		3	284 to 317	254 to 371
		4	317 to 351	254 to 371
		5	351 to 384	248 to 371
		6	384 to 418	256 to 371
		7	418 to 451	248 to 371
		8	451 to 485	236 to 371
		9	485 to 518	246 to 371
		10	518 to 552	242 to 371
		11	552 to 593	259 to 371

τ = 500 ns $\bar{I}$ = 225 mA

13	A	5	61.1 to 81.2	291 to 359
		6	81.2 to 101	274 to 371
		7	101 to 121	278 to 371
		8	121 to 142	272 to 371
		9	142 to 162	270 to 371
		10	162 to 183	274 to 371

τ = 200 ns $\bar{I}$ = 225 mA

13	B	4	67.3 to 101	286 to 359
		5	101 to 134	284 to 371
		6	134 to 168	286 to 366
		7	168 to 201	None
		8	201 to 235	270 to 371[13]
		9	235 to 268	276 to 371[1]
		10	268 to 293	276 to 371[1]
τ = 200 ns	$\bar{I}$ = 225 mA			
14	A	6	20.0 to 25.0	282 to 371
		7	25.0 to 41.3	262 to 371
		8	41.3 to 57.5	250 to 371
τ = 20 ns	$\bar{I}$ = 5 A			
26	A	8	205 to 238	280 to 371
		9	238 to 272	266 to 371
		10	272 to 313	257 to 371
τ = 500 ns	$\bar{I}$ = 225 mA			

The statistically significant wavelength and time regions define the times and wavelengths of significant transient response from the mirror. With the exception of the noted time and wavelength regions of dielectric mirror 13 irradiated in position B, all of the significant regions mark increases in the signal ratio. For example, the measured signal-ratio curve deviated significantly

[13]For dielectric mirror 13, irradiated in position B, the Fourier curve plus or minus two times the square root of the MMSRES was statistically significant and less than unity. For all other statistically significant wavelength regions, the transient signal was greater than unity.

above unity during the time region 20 ns to 25 ns in wavelengths 282 nm to 371 nm for dielectric mirror 14, irradiated in position A. The interpretation of the statistically significant deviations from a unity signal ratio is taken up in the conclusions section.

6.2 Transient Reflectivity Results

In interpreting the transient reflectivity curves in Appendix C, note the statistically significant deviation regions listed in Table 6.1 are the same regions found by inspecting the transient reflectivity curves. The regions of significant deviation of transient reflectivity from the pre-irradiation reflectivity match with the Table 6.1 regions because the pre-irradiation reflectivity of Eq. 5.4 is assumed error free.

As stated earlier, by assuming the pre-irradiation reflectivity in Eq. 5.4 is a function of wavelength without an assigned error resulting from computer analyses, digitization, or spectrophotometer performance, the reflectivity can be treated as a constant in the propagation of error in the equation. Thus, the signal-ratio curves could be viewed as transient reflectivities with pre-irradiation reflectivities of unity for all wavelengths. The pre-irradiation reflectivity, if lacking an error estimate, does not affect the predicted transient reflectivity or associated error bars. Thus, the regions of statistically significant deviation of transient reflectivity from the pre-irradiation reflectivity match the regions of Table 6.1.

For example, for dielectric mirror 14, the signal ratio deviated from unity significantly in time regions 6, 7, and 8. The estimate of the transient reflectivity deviated in the same time regions and corresponding wavelengths as the signal ratio. Thus, the reader need only look at the signal-ratio plots to know the time region and wavelengths of any statistically significant deviation. However, if an estimate of the magnitude of the change in reflectivity is desired, the reader should consult the transient reflectivity curves.

7. Conclusions and Recommendations

The effects of radiation on the mirrors will be discussed according to mirror variety because each mirror type exhibitied statistically significant transient response. The conclusions are based on the available data and should not be treated as the absolute answer to whether transient radiation damage occurs without substantiating studies.

7.1 Conclusions on the Dielectric-multilayered Mirrors

According to H.J. Donnert, the significant transient response demonstrated by the dielectric mirrors could be due to the mirrors taking on the properties of a metal-coated mirror (4). Prior to irradiation, the electrons present on the dielectric mirror reflecting surface were primarily occupied in the covalent bonds of the coating materials. The mirror behaved like a ceramic, meaning the conduction band was sparsely populated. According to the hypothesis, upon irradiation, the high-energy electrons from the beam gave the dielectric material a populated conduction band similar to a metal. For a short time, less than 400 ns to 500 ns, the mirror would exhibit the reflecting properties of a metal-coated mirror because of an increase in electrons in the conduction band. The hypothesis suggests the dielectric mirror behaves like a metal-coated mirror by displaying a non-zero conductivity and a complex index of refraction. Verification of the hypothesis might

be found in using a complex index of refraction for the dielectric mirrors in the theoretical model of Scronce (1).

The temporary metallic behavior explained the measured increase in the intensity of the reflected light. At lower wavelengths, where the reflectivity of the pristine dielectric mirror was close to unity, the light intensity could have increased due to the de-excitation of the electrons deposited on the mirror surface or the secondary electrons created by electron bombardment. Note, no statistically significant deviations resulted in a transient reflectivity greater than unity.

The measured light intensity increased for the upper wavelengths for two reasons. First, the light intensity probably increased from the induced metallic properties. As the dielectric mirror behaved like a metal mirror, the reflectivity for the upper wavelengths was characterized by a metal more than the dielectric. Because the reflectivity was small for the dielectric mirror the induced metallic reflectivity represented an increase in the signal light intensity. Also, the same process of electron de-excitation probably contributed to the increase in measured signal light intensity.

Statistically significant deviations from the pre-irradiation reflectivity were observed for all of the dielectric-multilayered mirrors. From a practical standpoint, the transient behavior appeared as an increase in mirror reflectivity for all mirrors except dielectric mirror 13, irradiated in position B. This

researcher does not claim an actual increase in reflectivity occurred because the transient measurements are not absolute. However, the researcher does claim the signal light intensity increased under irradiation at the wavelengths listed in Table 6.1.

For dielectric mirror 13, irradiated in position B, the statistically significant decrease in signal light intensity is not completely understood. Because no other dielectric mirror exhibited similar behavior, one is tempted to dismiss the unsubstantiated observation. However, possibilities of defective mirror construction, improper alignment, or rapid de-excitation of the electrons emitting in the upper wavelengths could explain the transient behavior.

7.2 Conclusions on the CuAg-coated Mirrors

The CuAg-coated mirrors exhibited the least amount of transient response. In only one time region for mirror 1L, the transient reflectivity deviated significantly from the pre-irradiation reflectivity. This researcher views the CuAg-coated mirrors the least likely to exhibit transient radiation damage.

Although the electron beam may have affected the CuAg mirrors, the effects were masked by the beam strength with respect to the number of conduction electrons on the mirror surface. The number of electrons in the beam was on the order of 10E+11 to 10E+12, compared to about 10E+19 present in the conduction band of the mirror coatings. By accounting for beam electrons not interacting at the

surface of the mirror or passing through the mirror, the magnitude of the beam electrons interacting at the coating surface is further reduced.

Thus, the number of electrons interacting with the metal coating was much less than the number of conduction electrons. The increase in electron density would not change the reflecting surface properties from the pre-irradiation metallic characteristics. That is, the pre-irradiation reflectivity was based on the properties of a metal reflector. The presence of more electrons resulting from irradiation only enhances the pre-irradiation metallic reflectivity behavior.

7.3 Conclusions on the Al-coated mirrors

At first, the same reasoning used in concluding the CuAg-coated mirrors were unaffected by the electron beam would seem to apply for the Al-coated mirrors. Aluminum-coated mirror 6L seemed to confirm the 10E+12 electrons present in the beam did not significantly affect the 10E+18 valence electrons in the irradiated beam spot or the 10E+19 valence electrons on a pure aluminum mirror surface. The lack of transient response indicated the electron beam did not effect mirror 6L significantly.

However, aluminum-coated mirror 7L displayed significant transient response in both position A and B. In comparing current, beam pulse length and number of electrons incident on the mirror, one would expect significant transient behavior to occur with mirror

6L before mirror 7L, i.e. the dose-rate, and total dose of electrons was greater for mirror 6L than mirror 7L.

One theory suggests the surrounding atmosphere played an important role in determining the transient response of the mirrors. By allowing exposure of the aluminum-coated mirrors to the atmosphere, the aluminum metal was oxidized. Thus, instead of having a pure aluminum reflecting surface, the reflecting surface of the mirror became a composite of metallic aluminum and aluminum oxide. Because some of the valence electrons of the pure aluminum would be occupied in covalent bonds with oxygen, the number of conduction band electrons would be reduced. As the density of aluminum oxide molecules at the reflecting surface increased, the mirror reflectivity would change from metallic to dielectric in behavior. The theory suggests significant oxidization of the aluminum mirror surface has occured and the mirror now behaves as a dielectric mirror.

7.4 Recommendations for Future Work

In order to confirm the conclusions stated above and to improve on the experimental results, the following are recommended:

1. Repeat the experiments using identically constructed mirrors and dose and dose rates to confirm, statistically, mirror transient behavior.

2. Perform periodic reflectivity measurements on pristine mirrors stored in either an oxidizing or inert atmospheres to detect changes in mirror reflectivity subject to storage. Mirror degradation with exposure to various

atmospheres contributed to reflectivity changes in a related work by Ferrel (26).

3. Verify experimentally the normalization factor $A(\lambda)$ to be time independent by studying the transient behavior of the xenon lamp output.

4. Re-design the experiment to measure transient transmission and to confirm when the mirrors no longer statistically deviate from pre-irradiation behavior.

To measure transient transmission, modifications of the existing LINAC facility would be necessary to compensate for electron beam divergence. In order to insert the required detectors behind the mirror to measure transient transmission, the mirror would have to be moved farther away from the beam port window. To maintain the same dose and dose rate of electrons, the electron beam divergence would have to be controlled, possibly with another series of electromagnets.

ACKNOWLEDGEMENTS

The author thanks the Air Force Systems Command, the Air Force Office of Scientific Research, and Universal Energy Systems, Inc. for providing the opportunity to spend an enriching summer at the Frank J. Seiler Research Laboratory, USAF Academy, Colorado Springs, CO. Additional thanks go to the members of the Lasers and Aerospace Mechanics Directorate, in particular Majors Albert Alexander and Terry Deaton, for aiding in the research. The author acknowledges the support from Mr. Charles Bowles and Lt. Col. Jack Fannin for their help in using the VAX-11 computer system.

The author thanks the employees of EG&G in Goeleta, CA, for their assistance in using their electron LINAC facility: Paul A. Zagarino, Stephen S. Lutz, Steven G. Iverson, Steven A. Jones, Ron Sturges, and Paul E. Nash.

The author gratefully acknowledges the support and patience of Mr. Roger Gurke of the Department of Physics, Dr. John Boyer of Statistics and the entire staff of the Department of Nuclear Engineering: Dr. N.D. Eckhoff, Dr. H.J. Donnert, Dr. R.E. Faw, Dr. J.K. Shultis, Dr. J.F. Merklin and Dr. G.G. Simons. Without their help and guidance, the study would have been exceedingly more difficult.

My fellow graduate students, Mr. Mark A. Ferrel, Mr. Gary W. Scronce and Mr. W. Gu are thanked for their support and efforts instrumental to the completion of the study.

Next, the author thanks Ms. Connie Schmidt for her help in preparing the thesis.

A special thanks goes to Dr. Hermann Donnert for introducing the area of research to the author and his guidance throughout the graduate school program.

Finally, I thank my wife Stephanie and my parents for their encouragement and support throughout my graduate studies.

References

1. G. W. Scronce, "Effects of Nuclear Radiation on the Optical Properties of Al_2O_3+SiO_2 Mirrors in the Ultraviolet Region", M.S. Thesis, 1986 (unpublished).

2. E. Hect and A. Zajac, Optics, 4th ed. (Addison-Wesley, Don Mills, Ontario, Canada), 1979, p. 88.

3. H. Anders, Thin Films in Optics, translated by J. N. Davidson, (Focal Press Limited, English Edition), 1967.

4. H. J. Donnert, Kansas State University, (private communication).

5. "Pulsed Xenon Light Source Type 3021", Chelsea Instruments Limited, (London), (unpublished).

6. J. H. Moore, C. C. Davis and M. A. Coplan, Building Scientific Apparatus, (Addison-Wesley, Reading, Massachusetts) 1983, pp. 191-194.

7. R. E. Faw, A. B. Chilton and J. K. Shultis, Principles of Radiation Shielding, (Prentice-Hall, Englewood Cliffs, New Jersey), 1984, pp. 67-74.

8. L. Katz and A. S. Penfold, Rev. Mod. Phys. 24, 28 1952.

9. M. J. Berger and S. M. Seltzer, "Tables of Energy Losses and Ranges of Electrons and Positrons", N.A.S.A., 1964.

10. CRC Handbook of Chemistry and Physics, 58th ed. (CRC Press, Cleveland, Ohio), 1978, p. B-155.

11. E. E. Aubanel and K. B. Oldham, "Fourier Smoothing", BYTE Feb. 1985, pp. 207-218.

12. R. W. Hornbeck, Numerical Methods, (Prentice-Hall, Englewood Cliffs, New Jersey), 1975.

13. J. Boyer, Kansas State University, (private communications).

14. J. Boyer, Regression and Correlation, Kansas State University, 1985, (unpublished).

15. A. A. Hopkins, R. E. Kelly, L. D. Looney and P. B. Lyons, "Transient Attenuation in Optical Fibers", presented at the SPIE annual technical symposium, San Diego, California, 1984.

16. P. B. Lyons, L. D. Looney and J. W. Ogle, "Radiation-Induced Transient Attenuation of PCS Fiber", presented at PHOTON '83 international conference on optical fibers and their applications, Paris, France, 1983.

17. P. J. Brannon, R. W. Morris, and J. B. Gerardo, "Nuclear-radiation-induced absorption in optical materials", presented at the SPIE Southwest Conference on Optics, 1985.

18. V. R. Honnold, C. C. Berggren, R. R. Emmert and G. D. Thomas, "An Investigation of Basis Mechanisms of Transient High Energy Radiation Effects in Insulators and Semiconductors", (Hughes Aircraft Co., Fullerton, California), 1964.

19. D. Neamen, W. Shedd and B. Buchanan, "Effects of Ionizing Radiation on Dielectrically Isolated Junction Field Effect Transistors", IEEE Trans. on Nucl. Sci., vol. 19 n. 6 1972, pp. 400-405.

20. E. A. Nevis, "Alteration of the transmission characteristics of fused silica optical fibers by pulsed ultraviolet radiation", SPIE vol. 540 Southwest Conference on Optics, 1985.

21. F. A. Frankovosky and M. Shatzkes, "Study of Effect of High-Intensity Pulsed Nuclear Radiation on Electronic Parts and Materials", (IBM Federal Systems Division, Owego, New York), 1966.

22. W. D. Compton and G. W. Arnold, Discuss. Faraday Soc. vol 31, 130, 1961.

23. P. M. Mace and D. H. Gill, IEEE Trans. on Nucl. Sci. NS-14, 6, p. 62, 1967.

24. G. H. Sigel, Jr. and D. L. Grisson, Bull. Am. Ceram. Soc. vol. 48, p447, 1969.

25. D. L. Grisson, G. H. Sigel, Jr., Bull. Am. Phys. Soc. vol. 13, p. 1474.

26. M. A. Ferrel, "The Effects of Radiation on the Optical Characteristics of (SiO_2+ZrO_2 on Si Substrate) Mirrors", M.S. Thesis, Kansas State University, 1986 (unpublished).

27. American Institute of Physics Handbook, 3rd ed., American Institute of Physics, (McGraw-Hill, Inc.), 1972, p. 6-124, 6-134, 6-149.

Appendix A: The Signal-ratio Plots

Figures 1a to 1i, the signal ratio plots for dielectric mirror number 14, irradiated in position A. For the block-out irradiation, the beam current (mean) was 5 A and the pulse length was 20 ns.

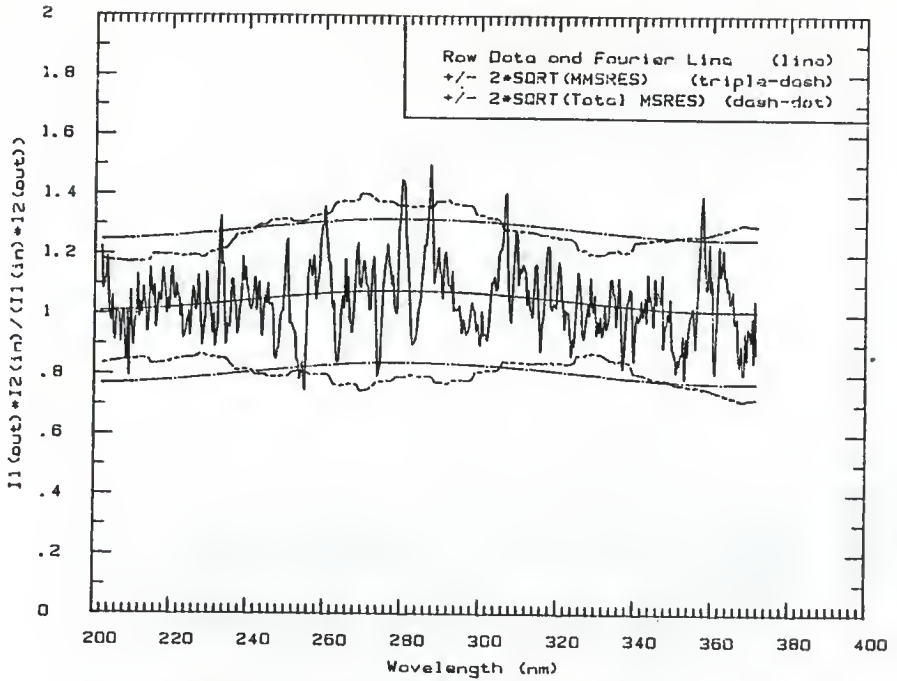

Fig. 1o Signal ratio for I1 defined in 0.0-5.0 ns time region and I2 defined during -40-0 ns region for dielectric mirror 14.

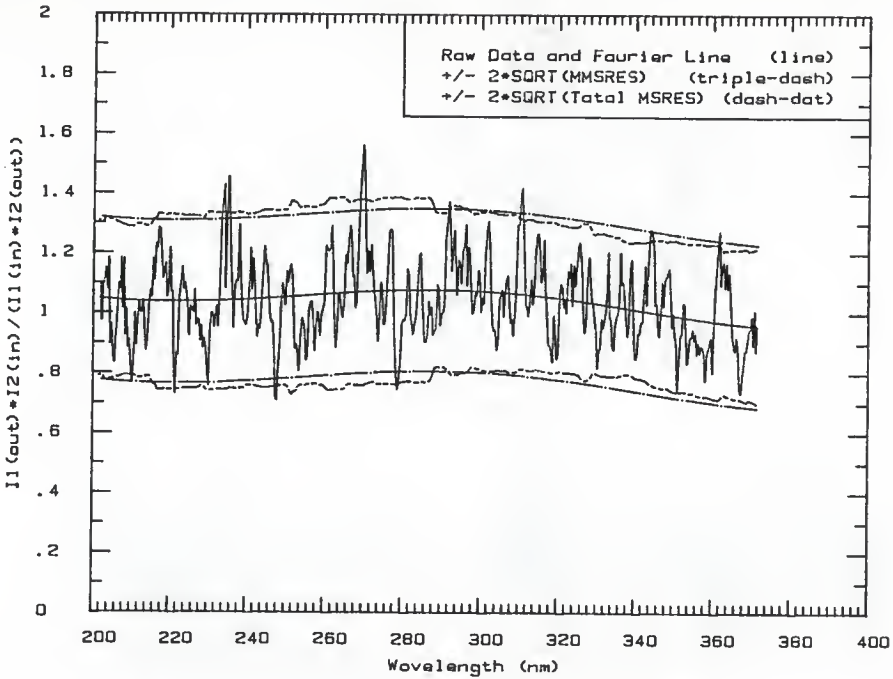

Fig. 1b Signal ratio for I1 defined in 5.0-10.0 ns time region and I2 defined during -40-0 ns region for dielectric mirror 14.

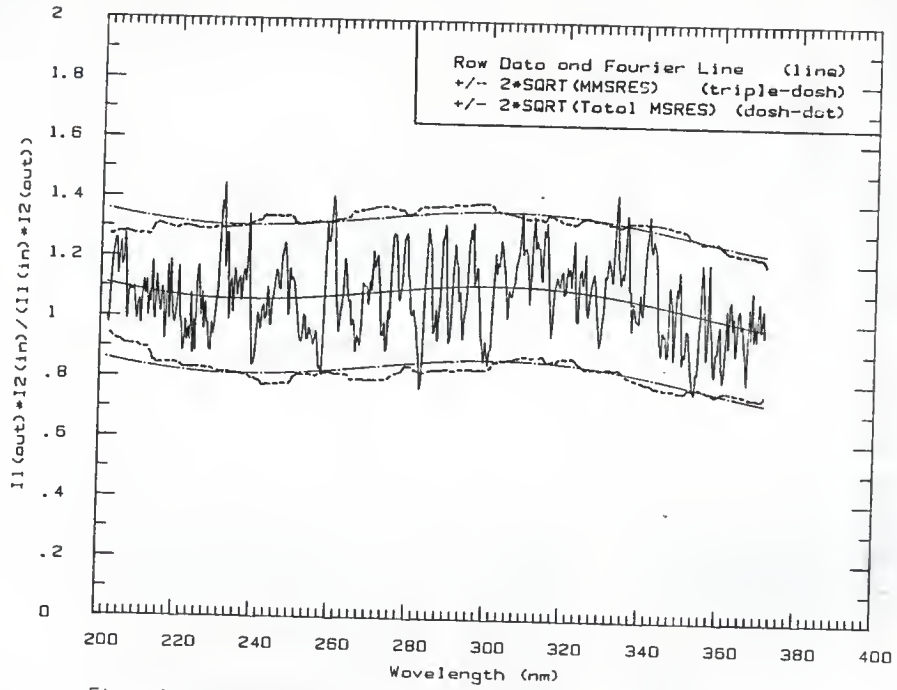

Fig. 1c Signal ratio for I1 defined in 10.0-15.0 ns time region and I2 defined during -40-0 ns region for dielectric mirror 14.

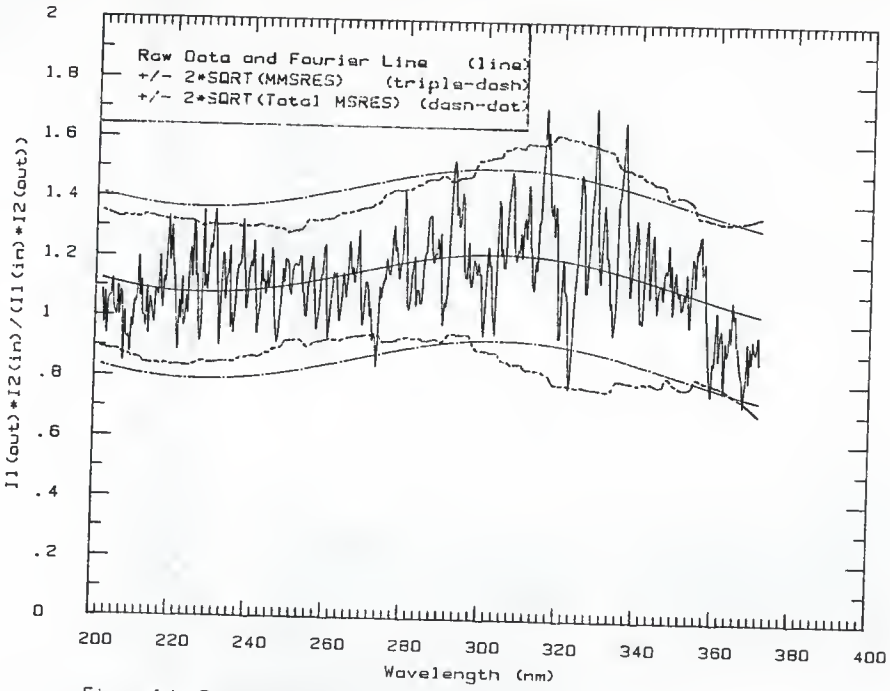

Fig. 1d Signal ratio for I1 defined in 15.0-20.0 ns time region and I2 defined during -40-0 ns region for dielectric mirror 14.

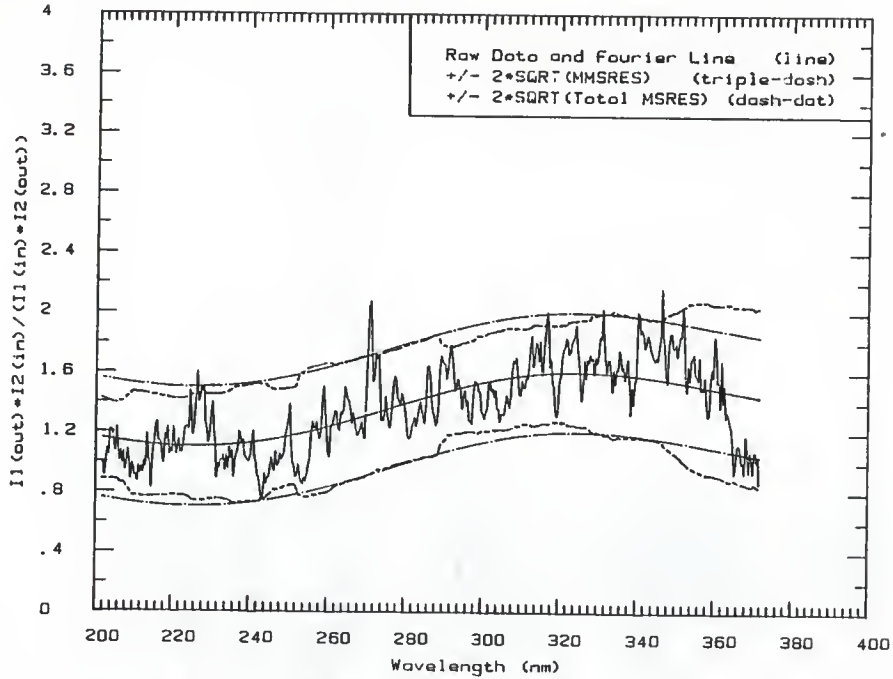

Fig. 1e Signal ratio for I1 defined in 20.0-25.0 ns time region and I2 defined during -40-0 ns region for dielectric mirror 14.

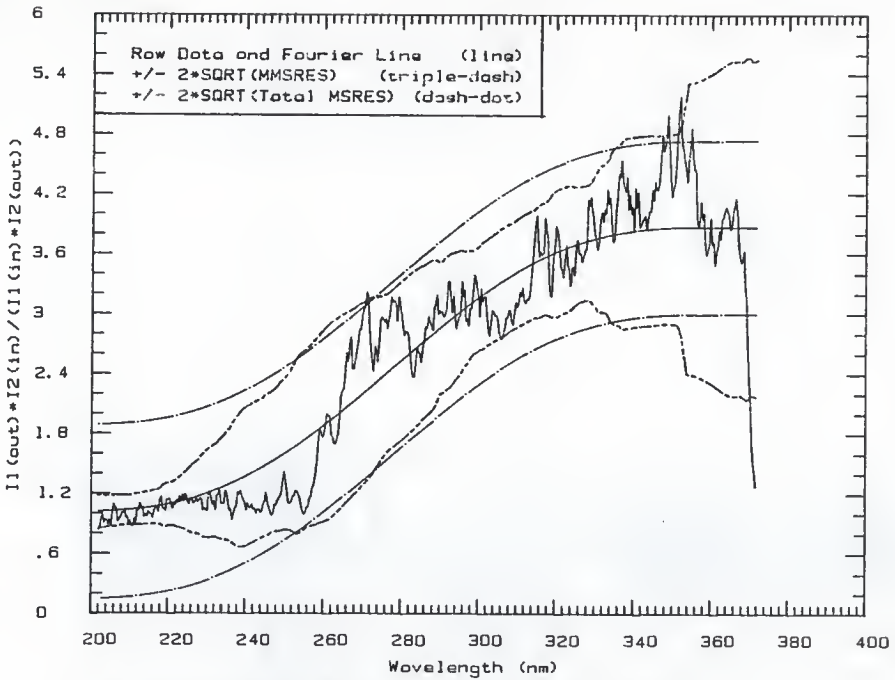

Fig. 1f Signal ratio for I1 defined in 25.0-41.3 ns time region and I2 defined during -40-0 ns region for dielectric mirror 14.

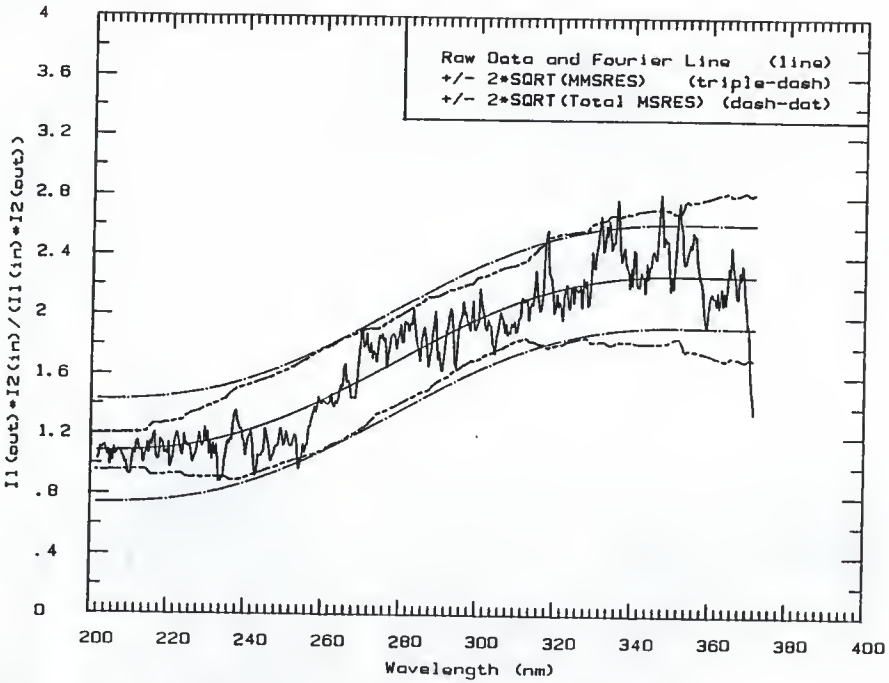

Fig. 1g Signal ratio for I1 defined in 41.3-57.5 ns time region and I2 defined during -40-0 ns region for dielectric mirror 14.

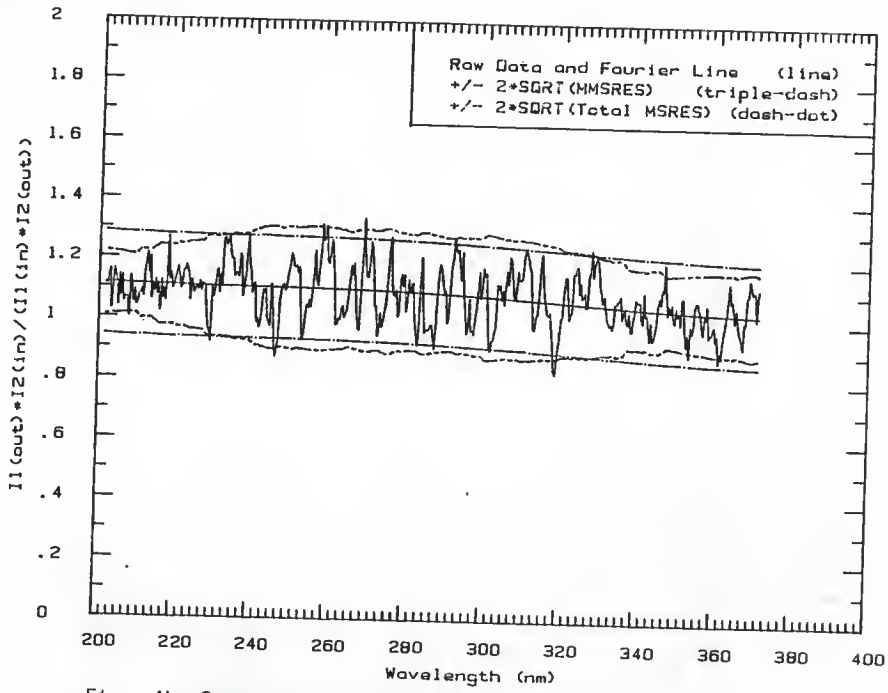

Fig. 1h Signal ratio for I1 defined in 57.5-73.8 ns time region and I2 defined during -40-0 ns region for dielectric mirror 14.

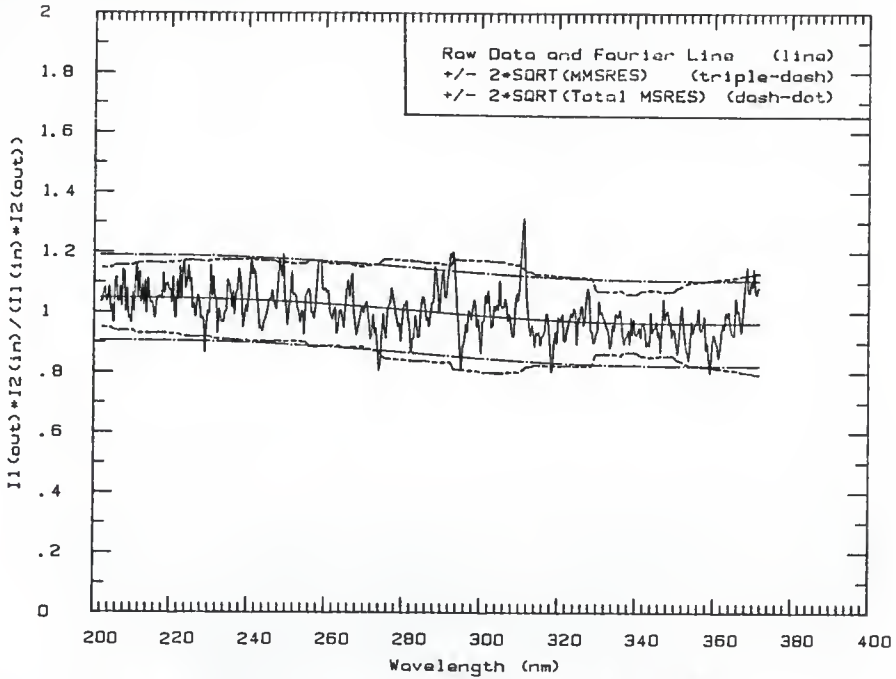

Fig. 11 Signal ratio for I1 defined in 73.8-88.0 ns time region and I2 defined during -40-0 ns region for dielectric mirror 14.

Figures 2a to 2i, the signal-ratio plots for dielectric mirror 12, irradiated in position A. For the block-out irradiation, the mean beam current was 225 mA and the pulse length was 500 ns.

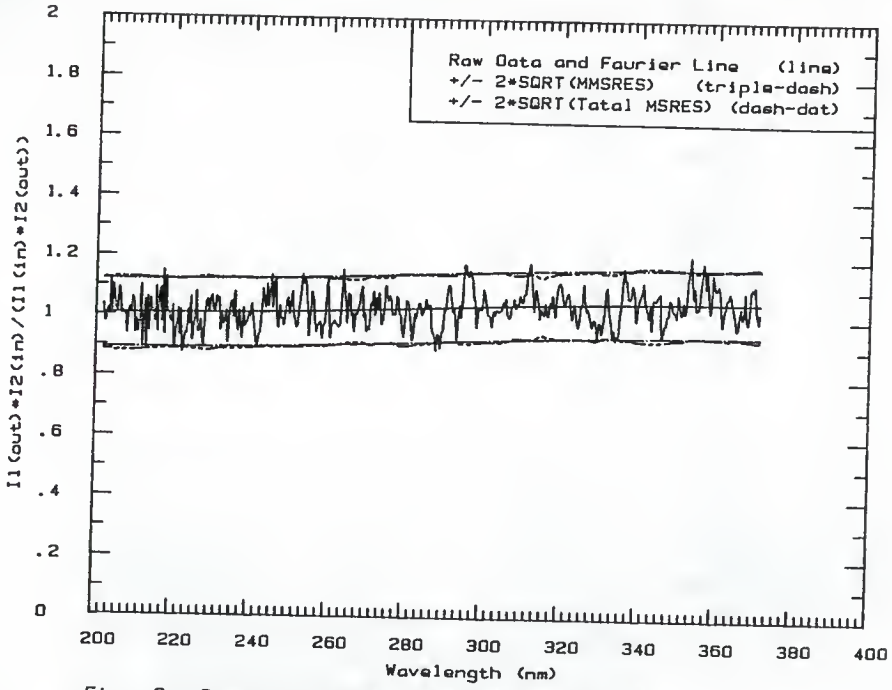

Fig. 2a Signal ratio for I1 defined in 0-37 ns time region and I2 defined during -30-0 ns region for dielectric mirror I2, irradiated in position A.

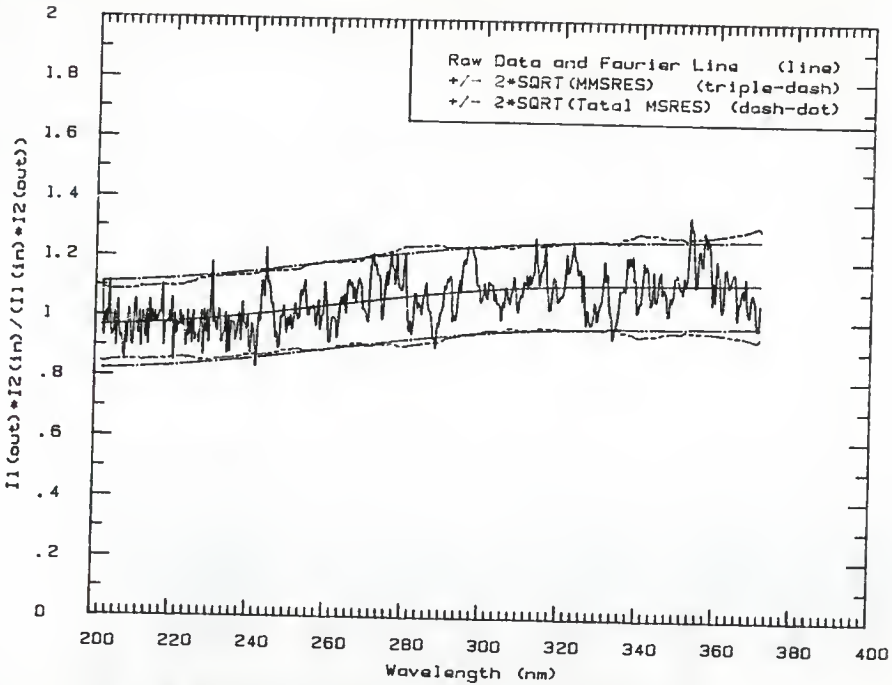

Fig. 2b Signal ratio for I1 defined in 37.0-70.5 ns time region and I2 defined during -30-0 ns region for dielectric mirror I2, irradiated in position A.

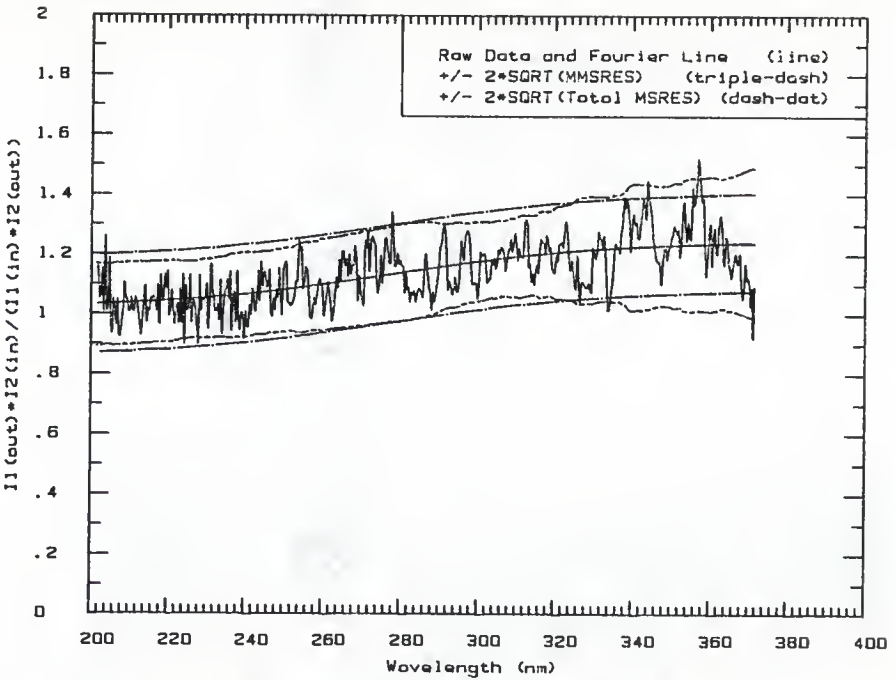

Fig. 2c Signal ratio for I1 defined in 70.5-104 ns time region and I2 defined during -30-0 ns region for dielectric mirror 12, irradiated in position A.

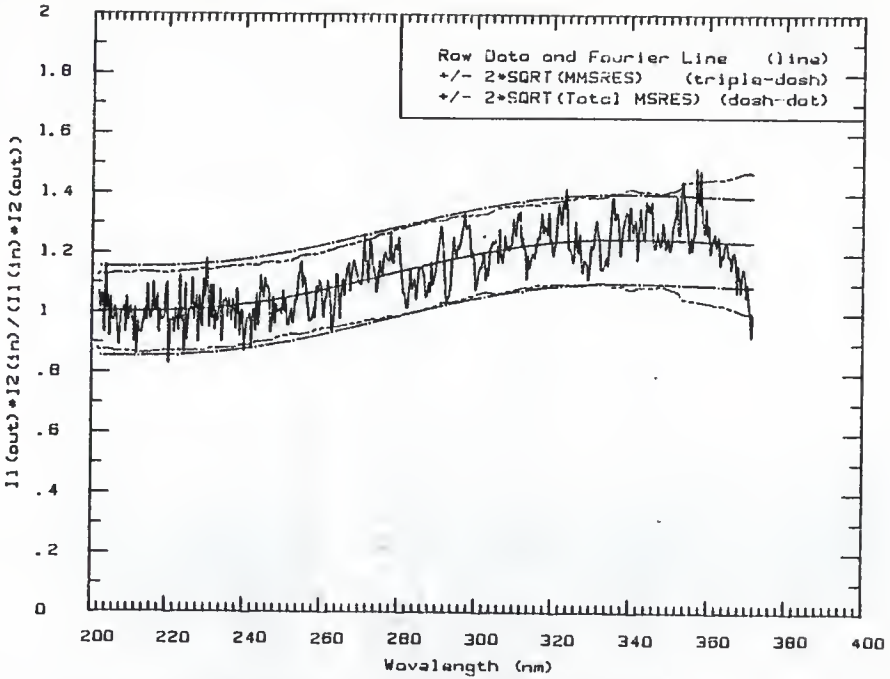

Fig. 2d Signal ratio for I1 defined in 104-138 ns time region and I2 defined during -30-0 ns region for dielectric mirror 12, irradiated in position A.

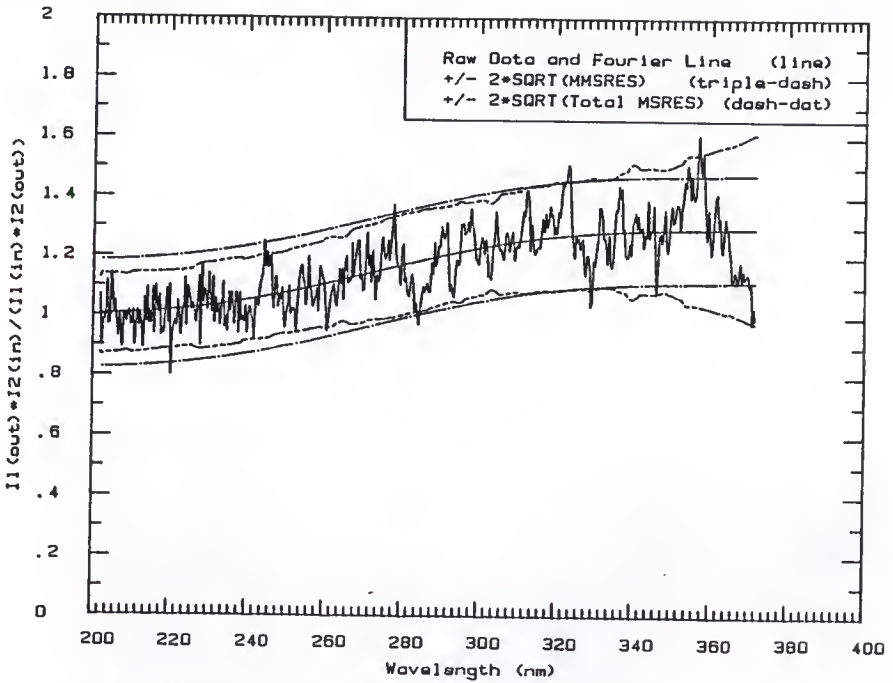

Fig. 2e Signal ratio for I1 defined in 138-171 ns time region and I2 defined during -30-0 ns region for dielectric mirror 12, irradiated in position A.

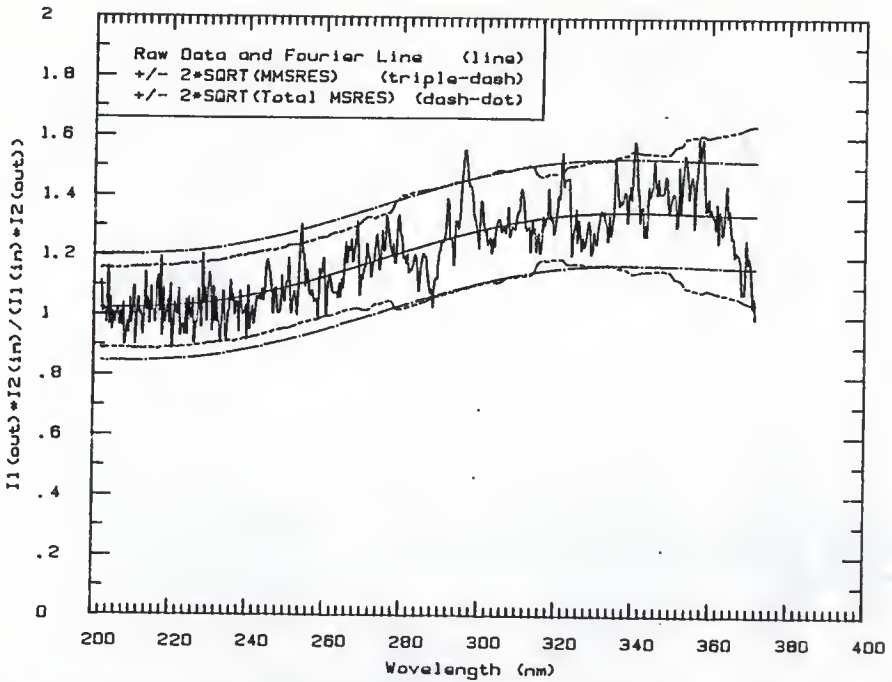

Fig. 2f Signal ratio for I1 defined in 171-205 ns time region and I2 defined during -30-0 ns region for dielectric mirror 12, irradiated in position A.

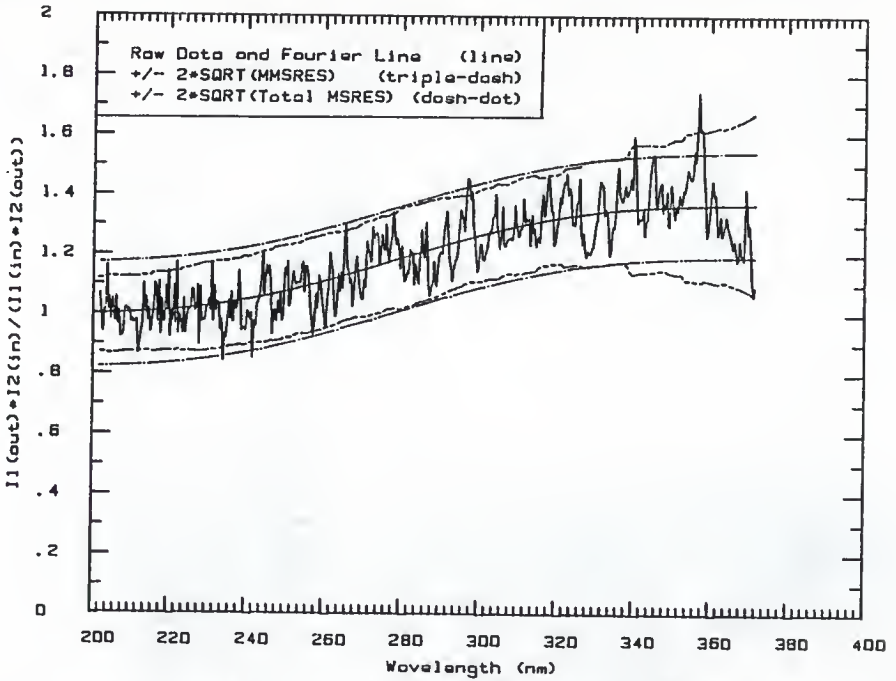

Fig. 2g Signal ratio for I1 defined in 205-238 ns time region and I2 defined during -30-0 ns region for dielectric mirror 12, irradiated in position A.

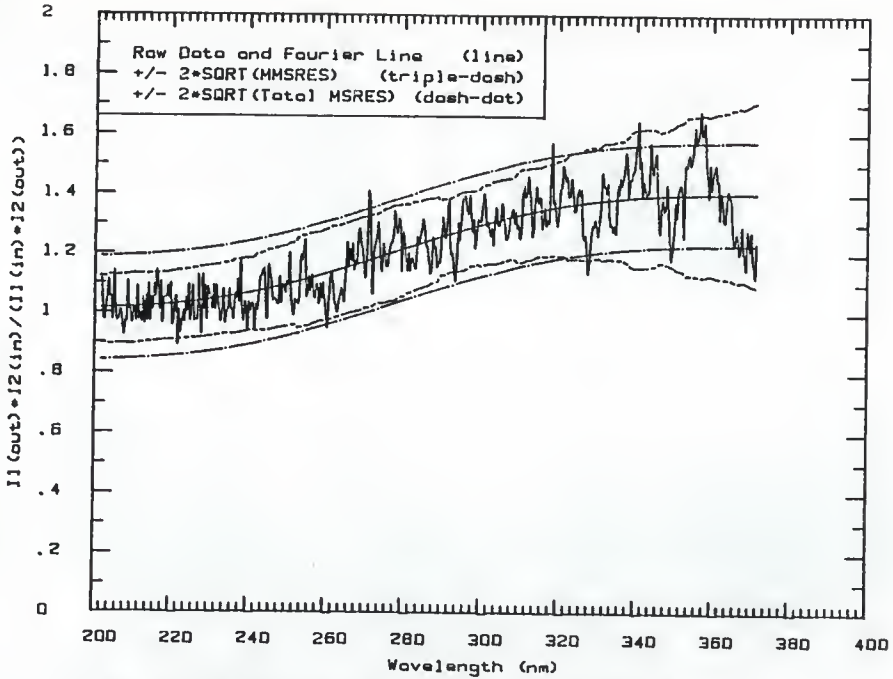

Fig. 2h Signal ratio for I1 defined in 238-272 ns time region and I2 defined during -30-0 ns region for dielectric mirror I2, irradiated in position A.

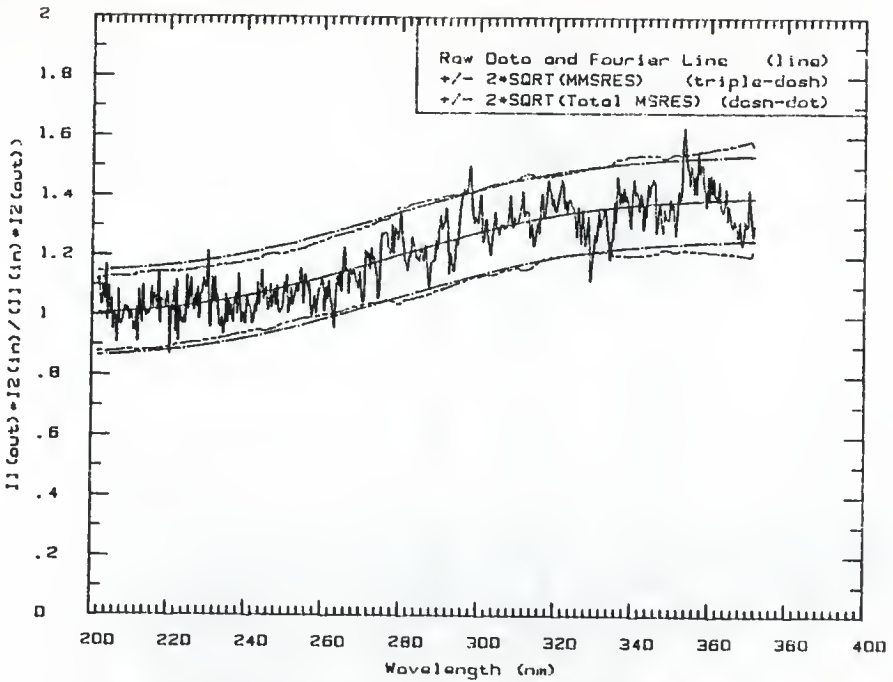

Fig. 21 Signal ratio for I1 defined in 272-313 ns time region and I2 defined during -30-0 ns region for dielectric mirror 12, irradiated in position A.

Figures 3a to 3j, the signal-ratio plots for dielectric mirror 12, irradiated in position B. The block-out irradiation had a mean beam current of 225 mA and a pulse length of 500 ns.

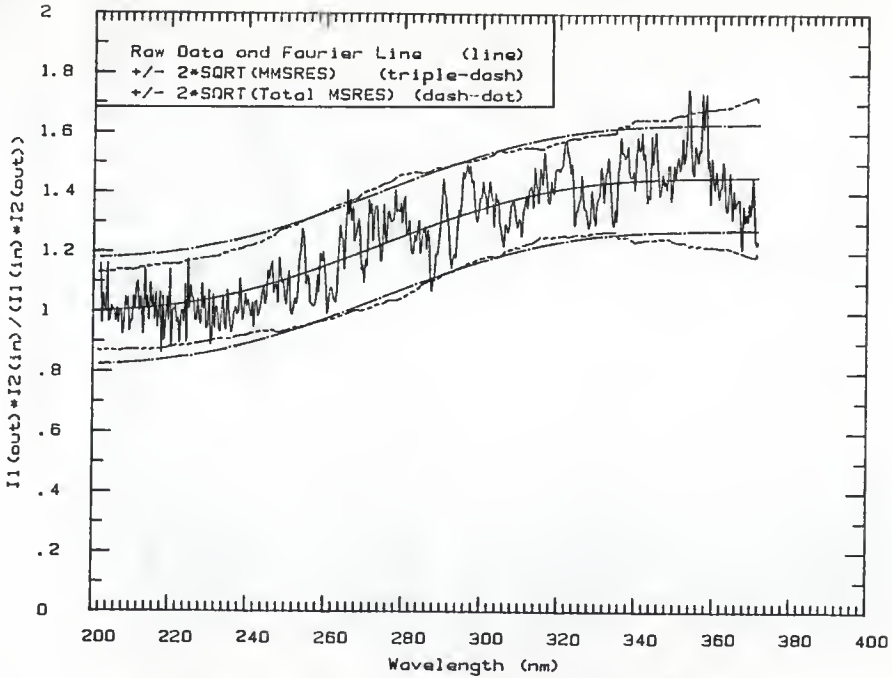

Fig. 3a Signal ratio for I1 defined in 250-284 ns time region and I2 defined during -30-0 ns region for dielectric mirror 12, irradiated in position B.

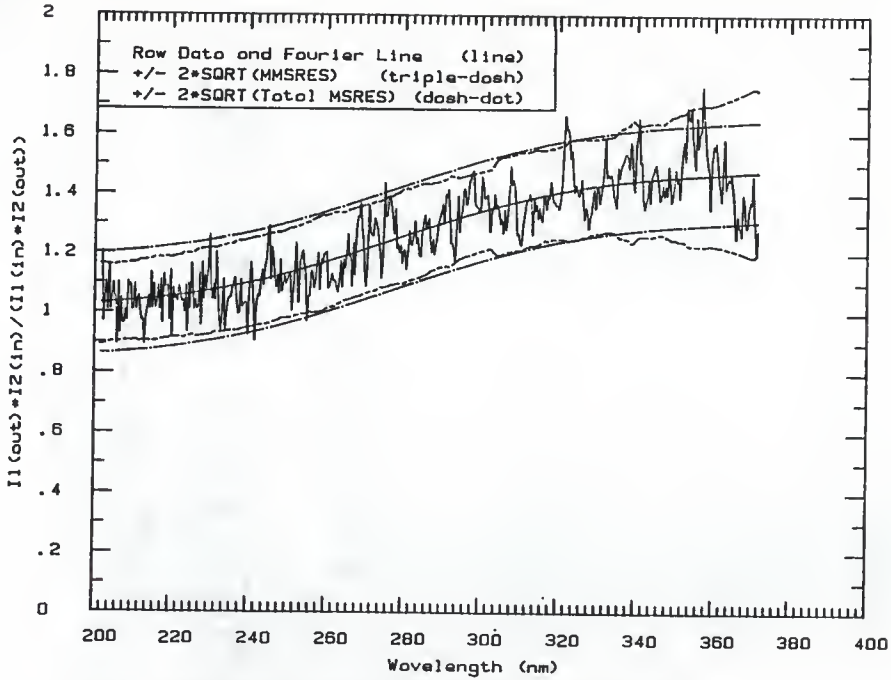

Fig. 3b Signal ratio for I1 defined in 284-317 ns time region and I2 defined during -30-0 ns region for dielectric mirror 12, irradiated in position B.

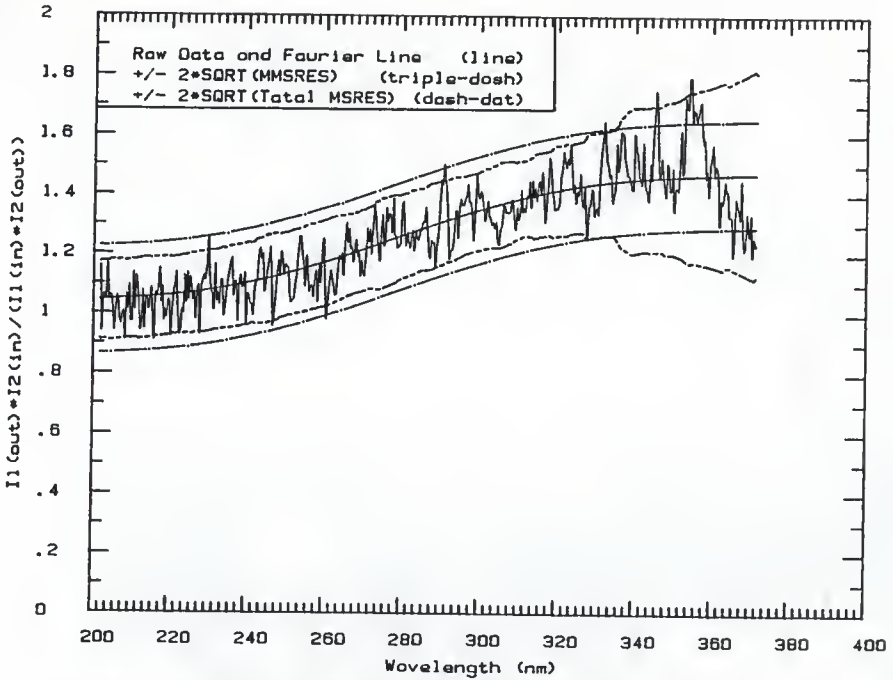

Fig. 3c Signal ratio for I1 defined in 317-351 ns time region and I2 defined during -30-0 ns region for dielectric mirror 12, irradiated in position B.

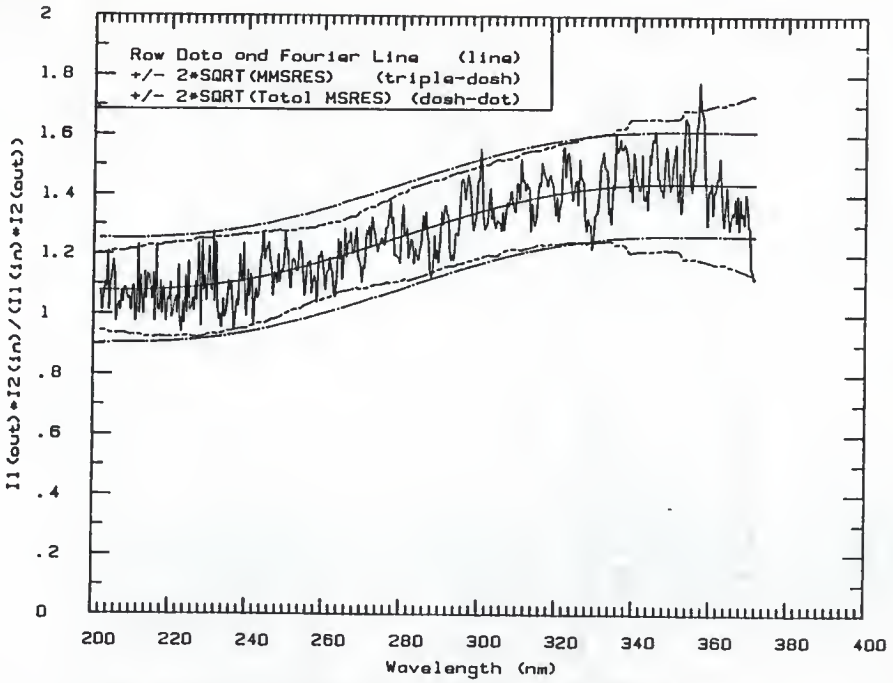

Fig. 3d Signal ratio for I1 defined in 351-384 ns time region and I2 defined during -30-0 ns region for dielectric mirror 12, irradiated in position 8.

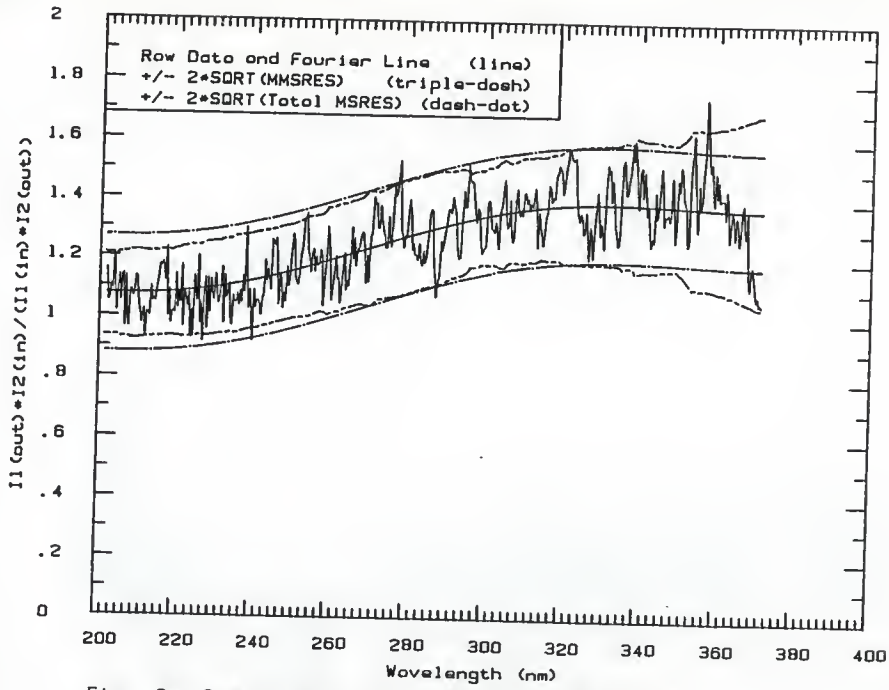

Fig. 3e Signal ratio for I1 defined in 384-418 ns time region and I2 defined during -30-0 ns region for dielectric mirror 12, irradiated in position B.

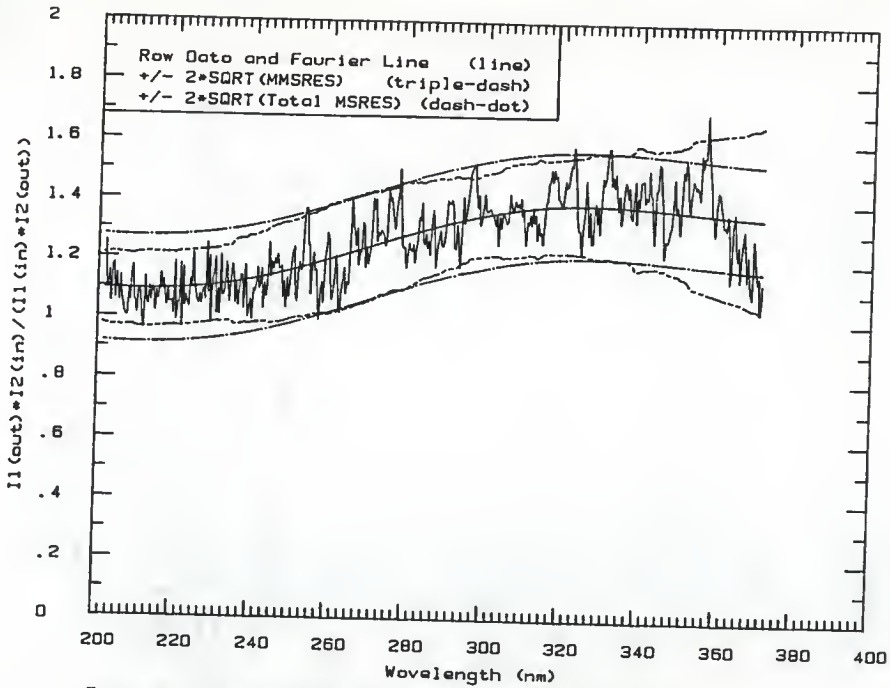

Fig. 3f Signal ratio for I1 defined in 418-451 ns time region and I2 defined during -30-0 ns region for dielectric mirror 12, irradiated in position B.

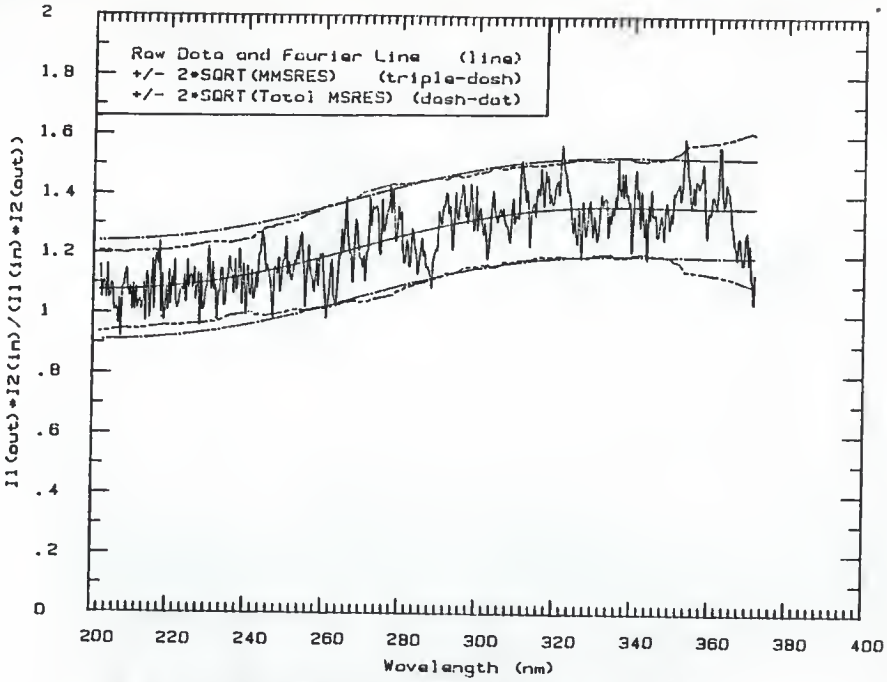

Fig. 3g Signal ratio for I1 defined in 451-485 ns time region and I2 defined during -30-0 ns region for dielectric mirror 12, irradiated in position B.

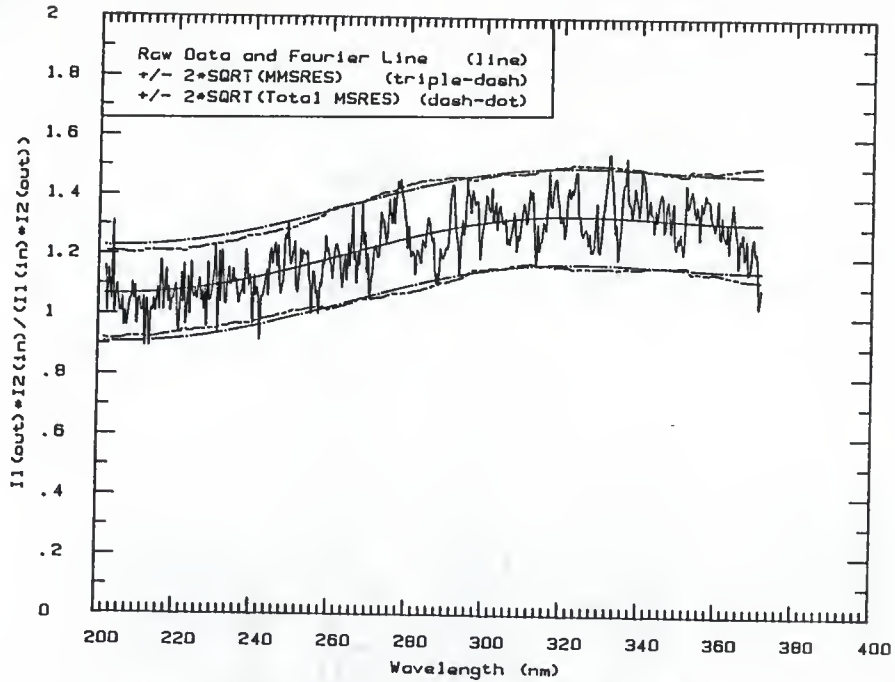

Fig. 3h Signal ratio for I1 defined in 485-518 ns time region and I2 defined during -30-0 ns region for dielectric mirror 12, irradiated in position B.

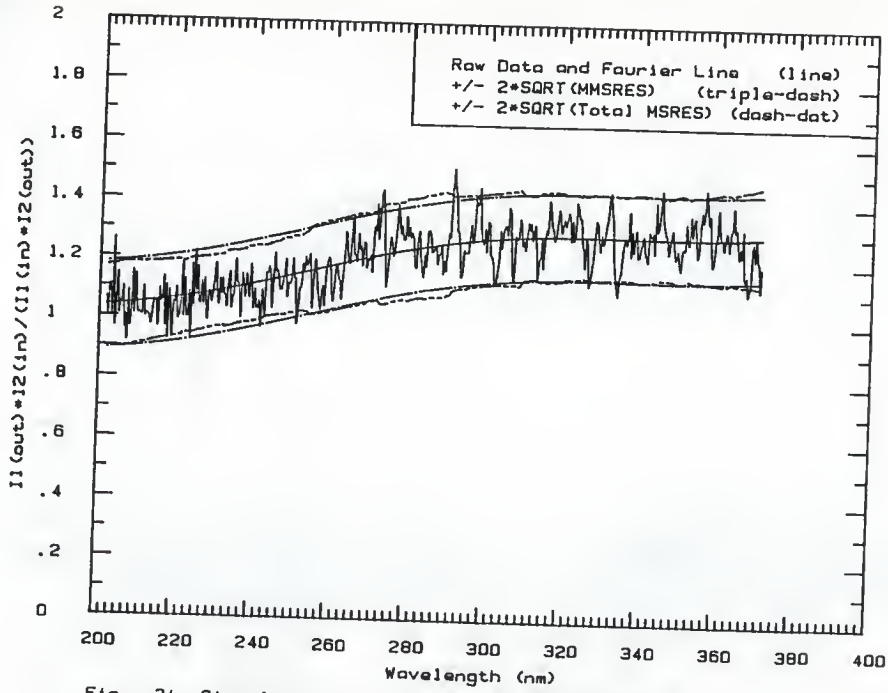

Fig. 3i Signal ratio for I1 defined in 518-552 ns time region and I2 defined during -30-0 ns region for dielectric mirror 12, irradiated in position B.

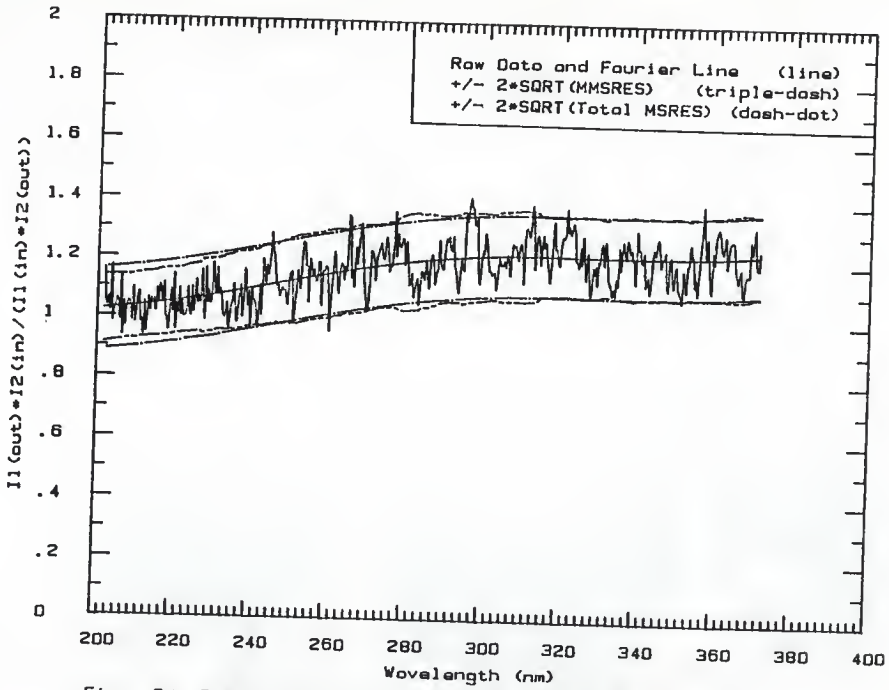

Fig. 3j Signal ratio for I1 defined in 552-593 ns time region and I2 defined during -30-0 ns region for dielectric mirror 12, irradiated in position B.

Figures 4a to 4i, the signal-ratio plots for dielectric mirror 13, irradiated in position A. For the block-out irradiation, the mean beam current was 225 mA and the pulse length was 200 ns.

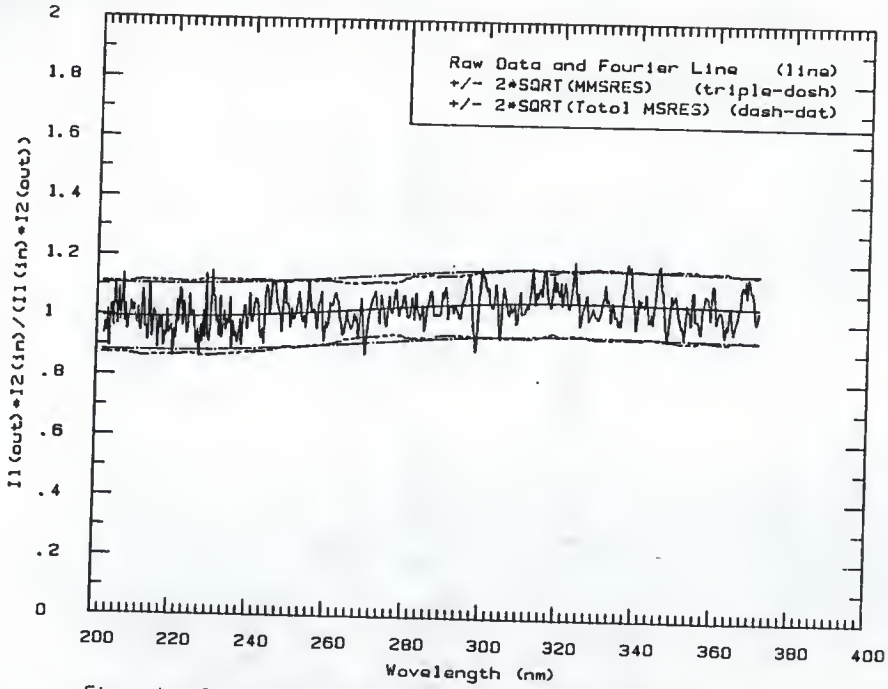

Fig. 4o Signal ratio for I1 defined in 0.8-20.9 ns time region and I2 defined during -160-0.8 ns region for dielectric mirror 13, irradiated in position A.

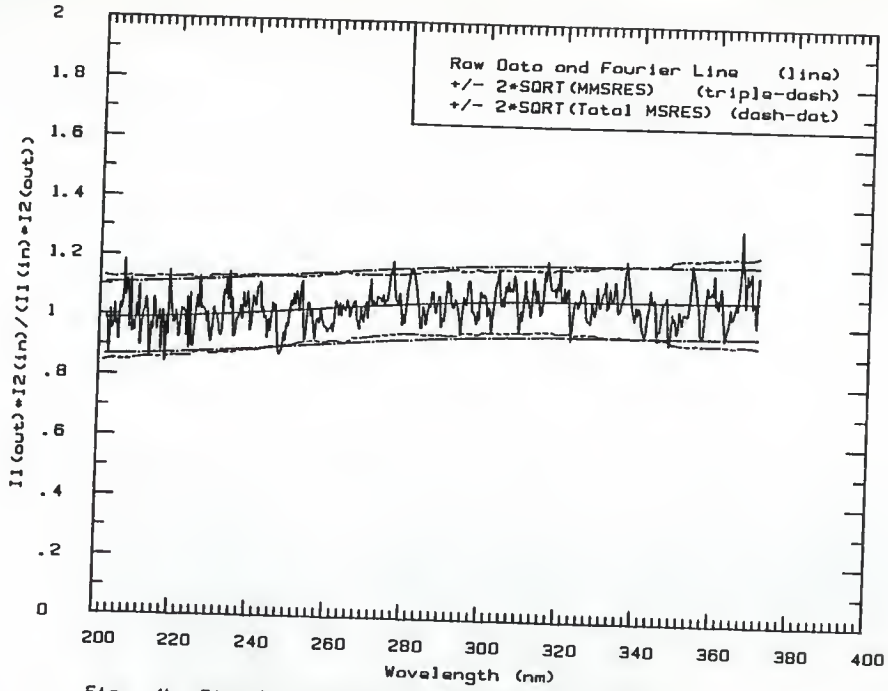

Fig. 4b Signal ratio for I1 defined in 20.9-41.0 ns time region and I2 defined during -160-0.8 ns region for dielectric mirror 13, irradiated in position A.

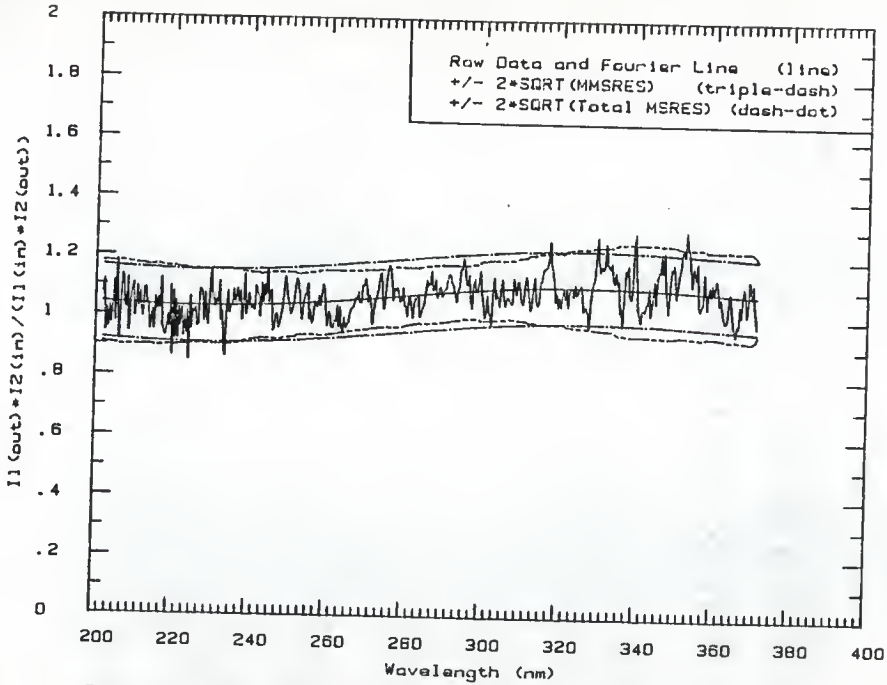

Fig. 4c Signal ratio for I1 defined in 41.0-61.1 ns time region and I2 defined during -160-0.8 ns region for dielectric mirror 13, irradiated in position A.

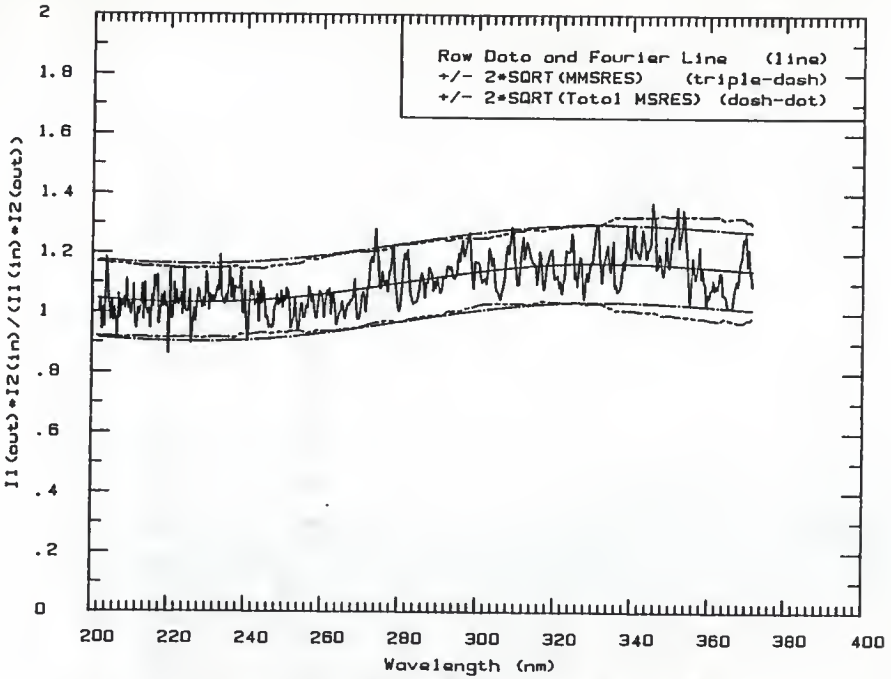

Fig. 4d Signal ratio for I1 defined in 61.1-81.2 ns time region and I2 defined during -160-0.8 ns region for dielectric mirror 13, irradiated in position A.

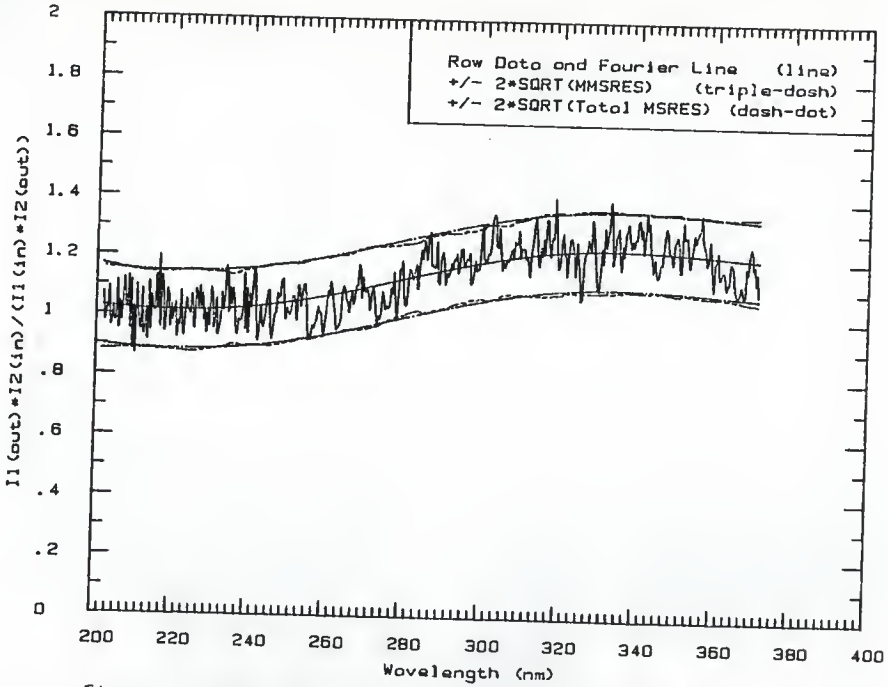

Fig. 4a Signal ratio for I1 defined in 81.2-101 ns time region and I2 defined during -160-0.8 ns region for dielectric mirror 13, irradiated in position A.

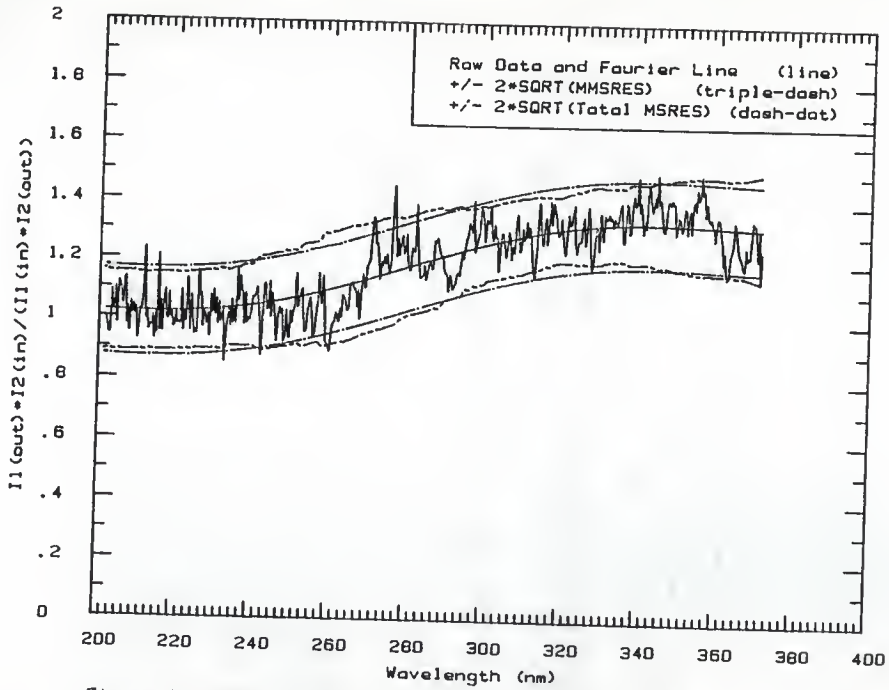

Fig. 4f Signal ratio for I1 defined in 101-121 ns ns time region and I2 defined during -160-0.8 ns for dielectric mirror 13, irradiated in position A.

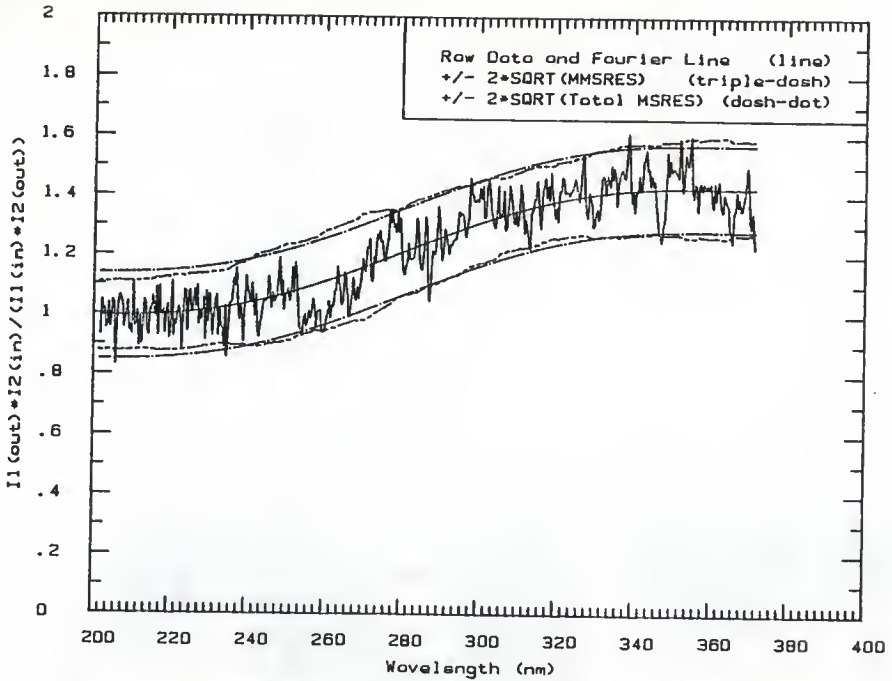

Fig. 4g Signal ratio for I1 defined in 121-142 ns time region and I2 defined during -160-0.8 ns for dielectric mirror 13. irradiated in position A.

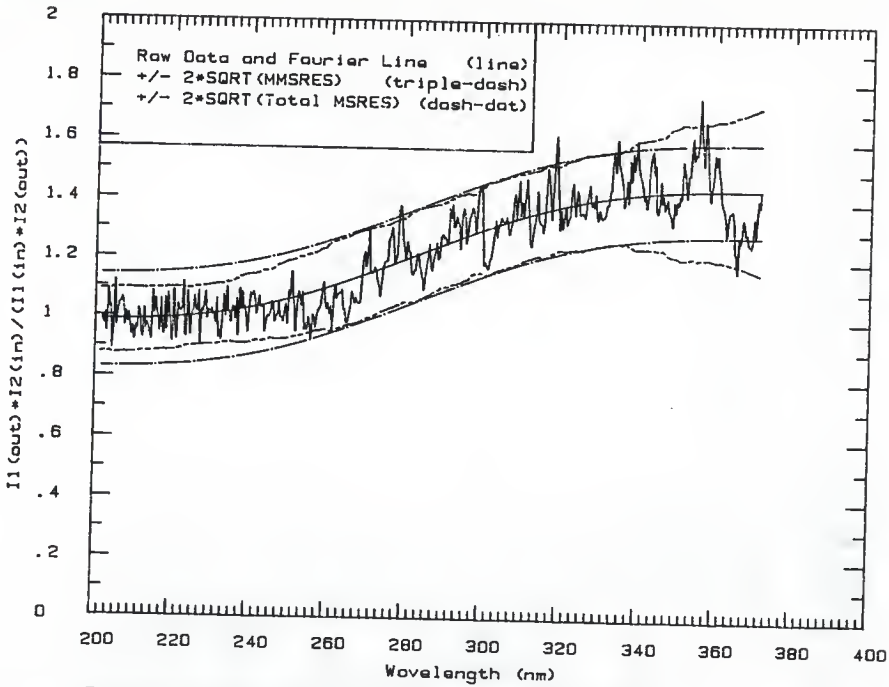

Fig. 4h Signal ratio for I1 defined in 142-162 ns time region and I2 defined during -160-0.8 ns for dielectric mirror 13, irradiated in position A.

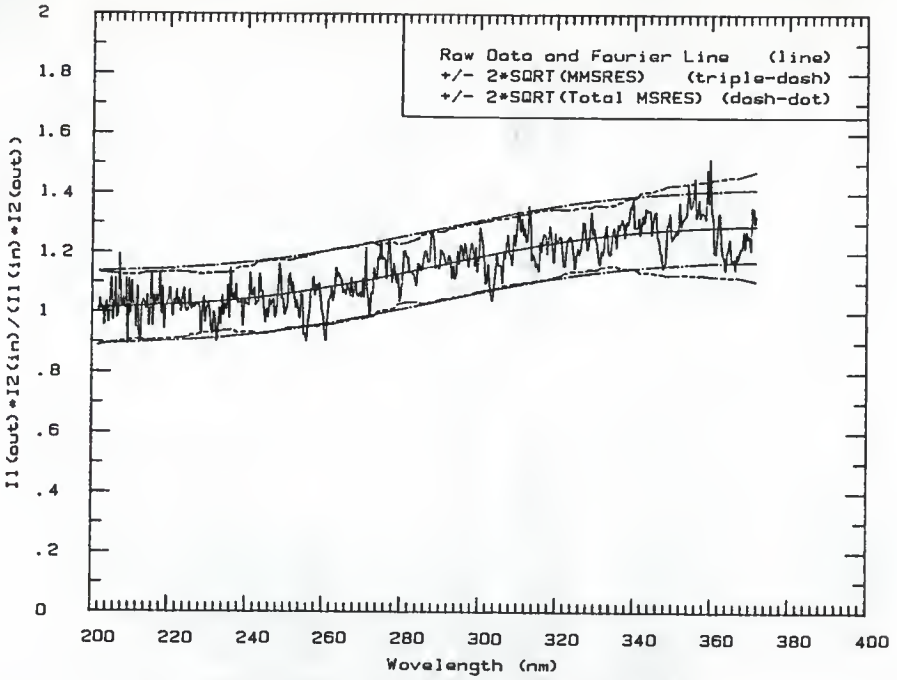

Fig. 4i Signal ratio for I1 defined in 162-183 ns time region and I2 defined during -160-0.8 ns region for dielectric mirror 13, irradiated in position A.

Figures 5a to 5i, the signal-ratio plots for dielectric mirror 13, irradiated in position B. For the block-out irradiation, the mean beam current was 225 mA and the pulse length was 200 ns.

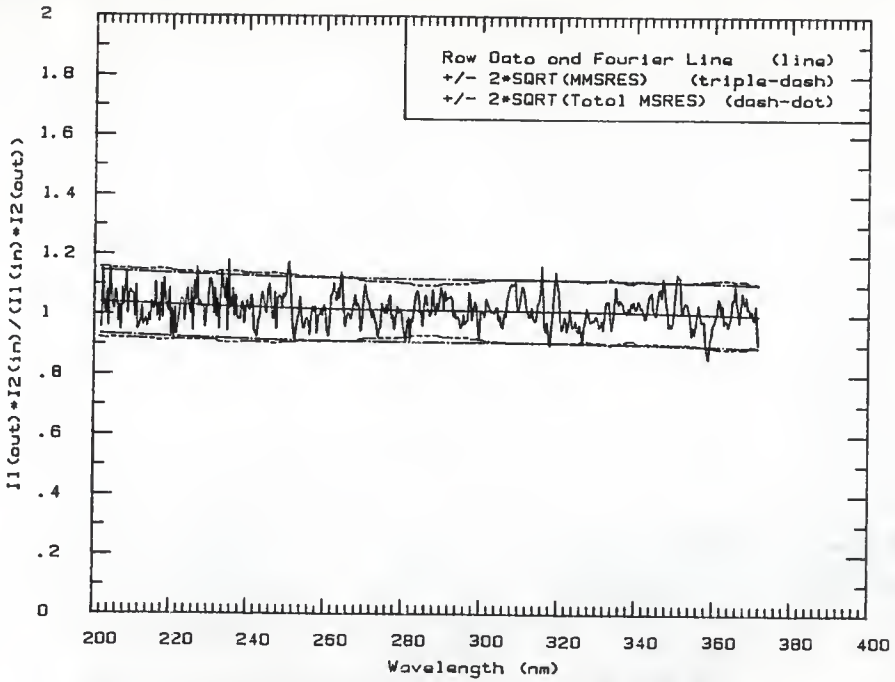

Fig. 5a Signal ratio for I1 defined in 0.25-33.8 ns time region and I2 defined during -50-0.25 ns region for dielectric mirror 13, irradiated in position 8.

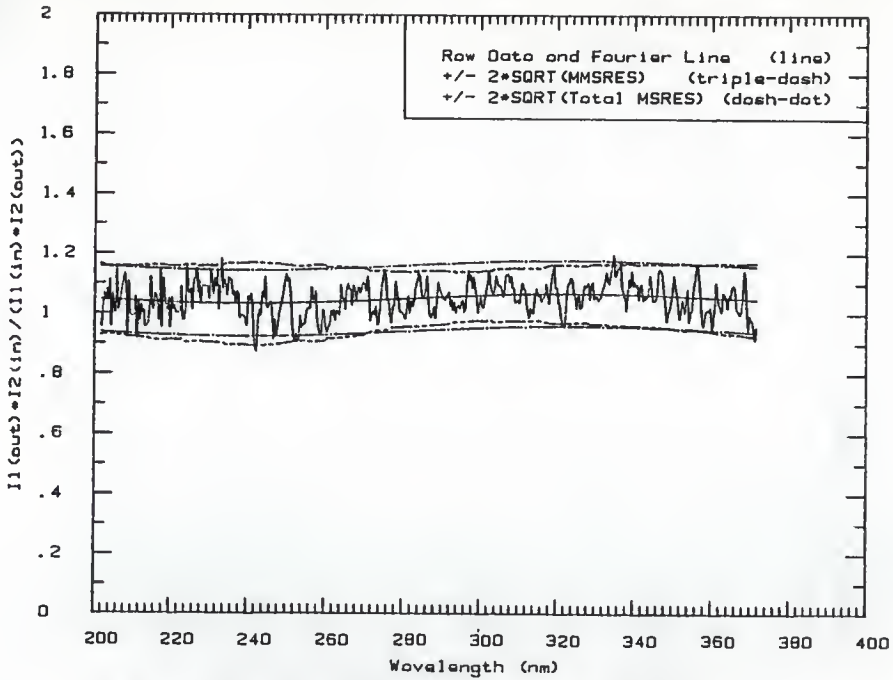

Fig. 5b Signal ratio for I1 defined in 33.8-67.3 ns time region and I2 defined during -50-0.25 ns for dielectric mirror 13, irradiated in position 8.

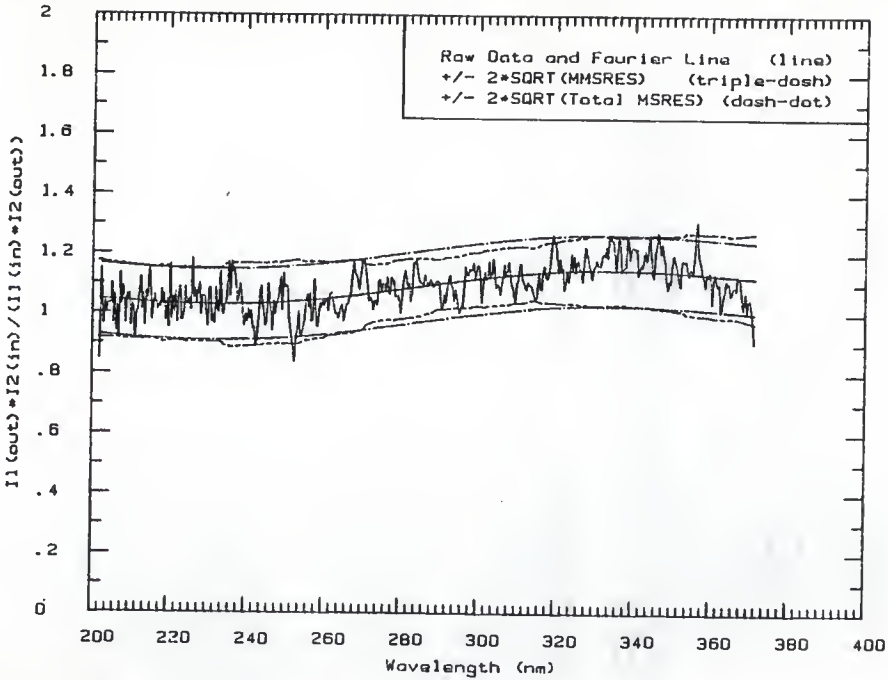

Fig. 5c Signal ratio for I1 defined in 67.3-101 ns time region and I2 defined during -50-0.25 ns for dielectric mirror 13, irradiated in position 8.

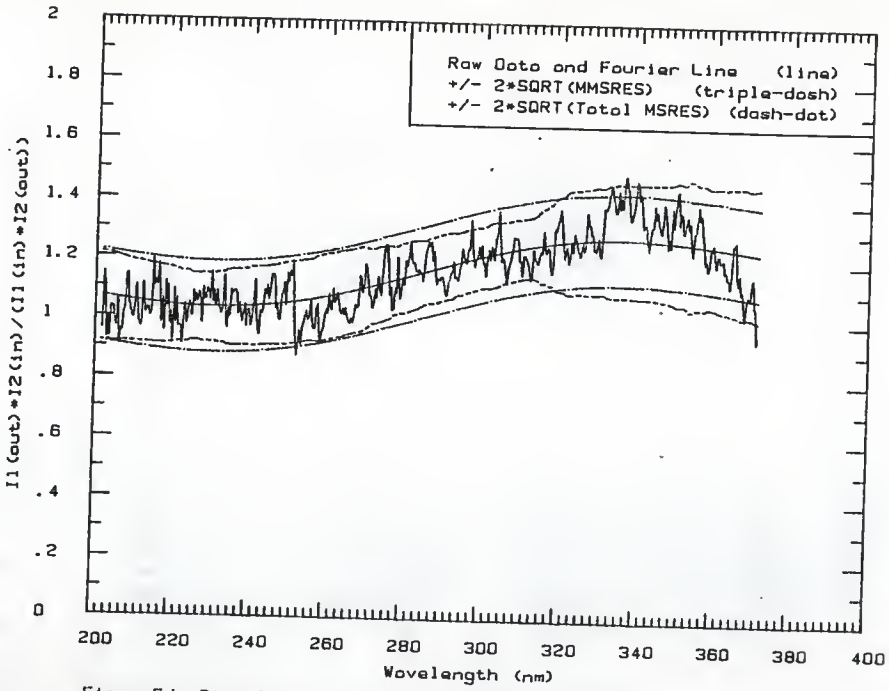

Fig. 5d Signal ratio for I1 defined in 101-134 ns time region and I2 defined during -50-0.25 ns for dielectric mirror 13, irradiated in position 8.

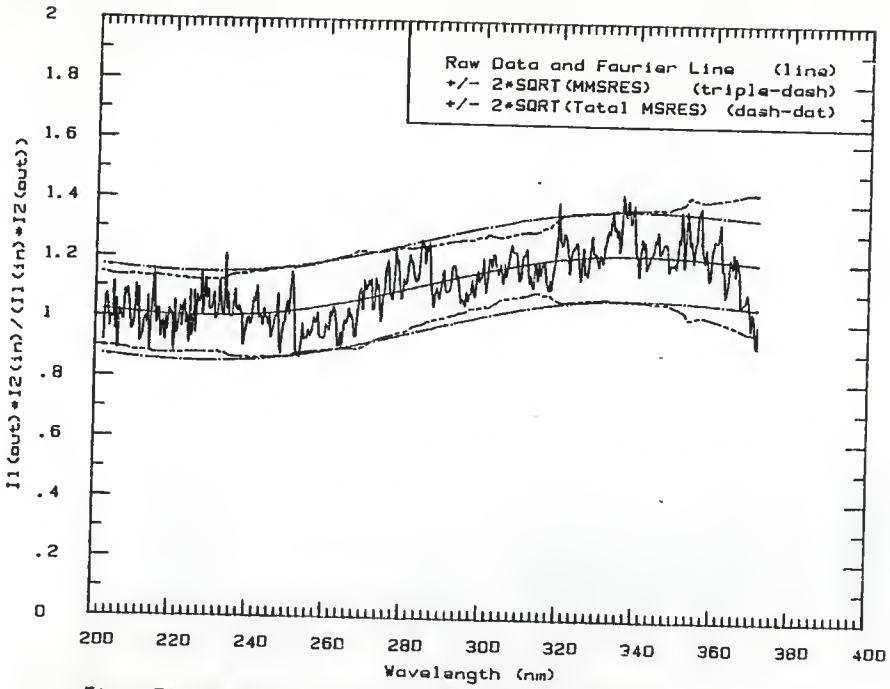

Fig. 5a Signal ratio for I1 defined in 134-168 ns time region and I2 defined during -50-0.25 ns for dielectric mirror 13, irradiated in position 8.

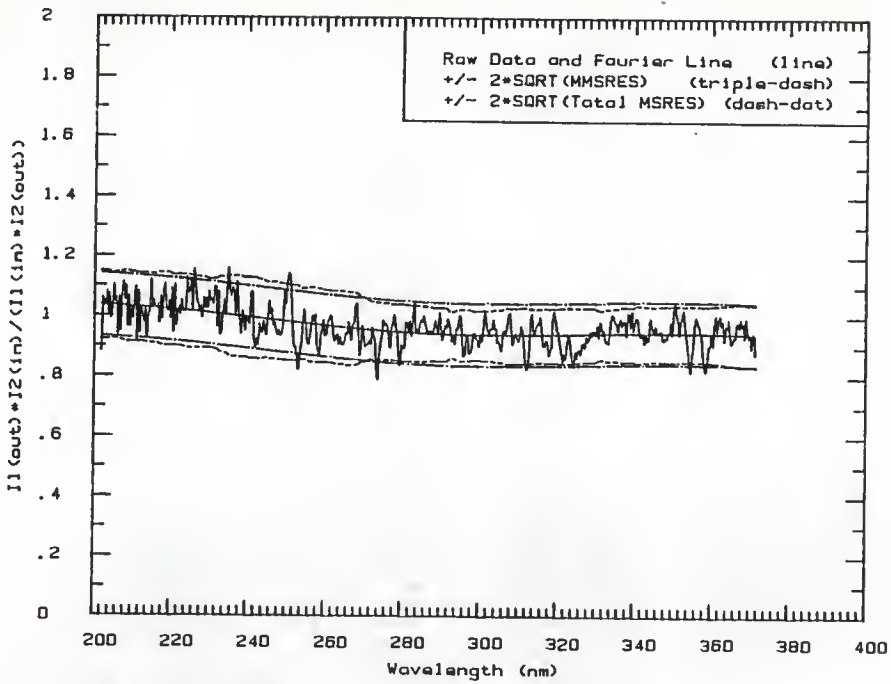

Fig. 5f Signal ratio for I1 defined in 168-201 ns time region and I2 defined during -50-0.25 ns for dielectric mirror 13, irradiated in position 8.

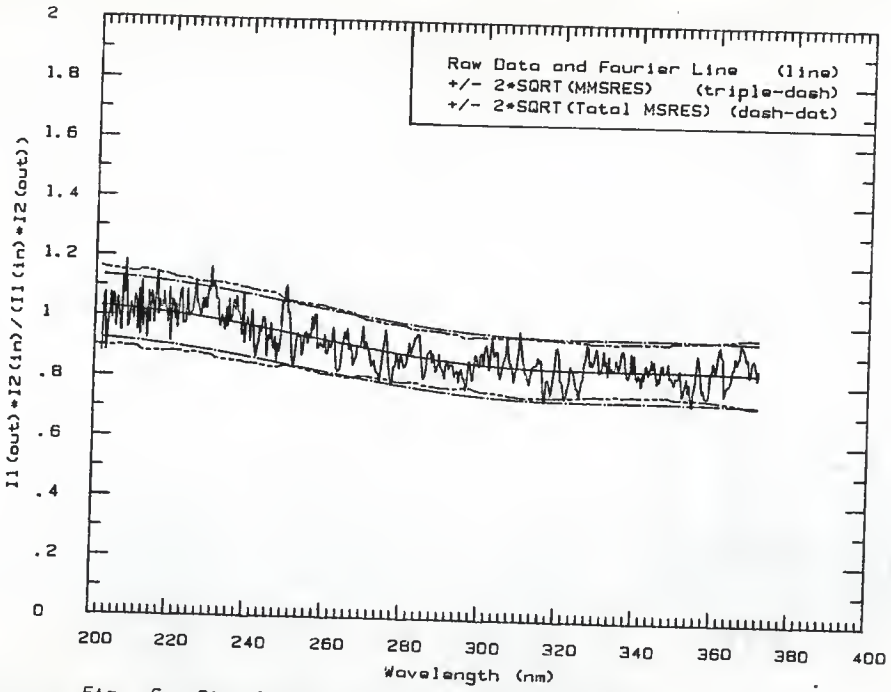

Fig. Sg Signal ratio for I1 defined in 201-235 ns time region and I2 defined during -S0-0.25 ns for dielectric mirror 13, irradiated in position 8.

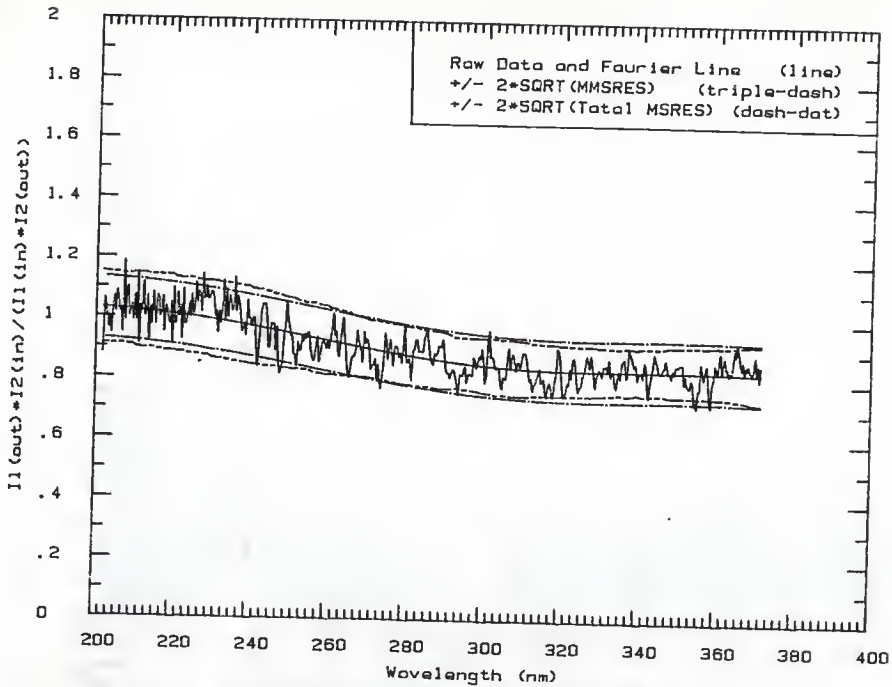

Fig. 5h Signal ratio for I1 defined in 235-268 ns time region and I2 defined during -50-0.25 ns region for dielectric mirror 13, irradiated in position 8.

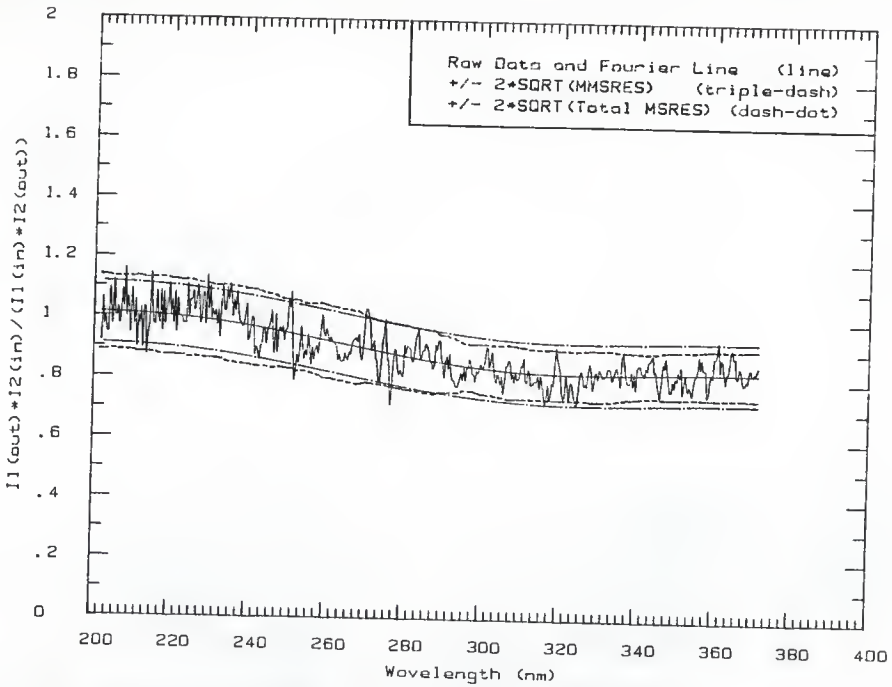

Fig. 5i Signal ratio for I1 defined in **268-293 ns** time region and I2 defined during -50-0.25 ns region for dielectric mirror 13, irradiated in positon B.

Figures 6a to 6i, the signal-ratio plots for dielectric mirror number 26, irradiated in position A. For the block-out irradiation, the mean beam current was 225 mA and the pulse length was 500 ns.

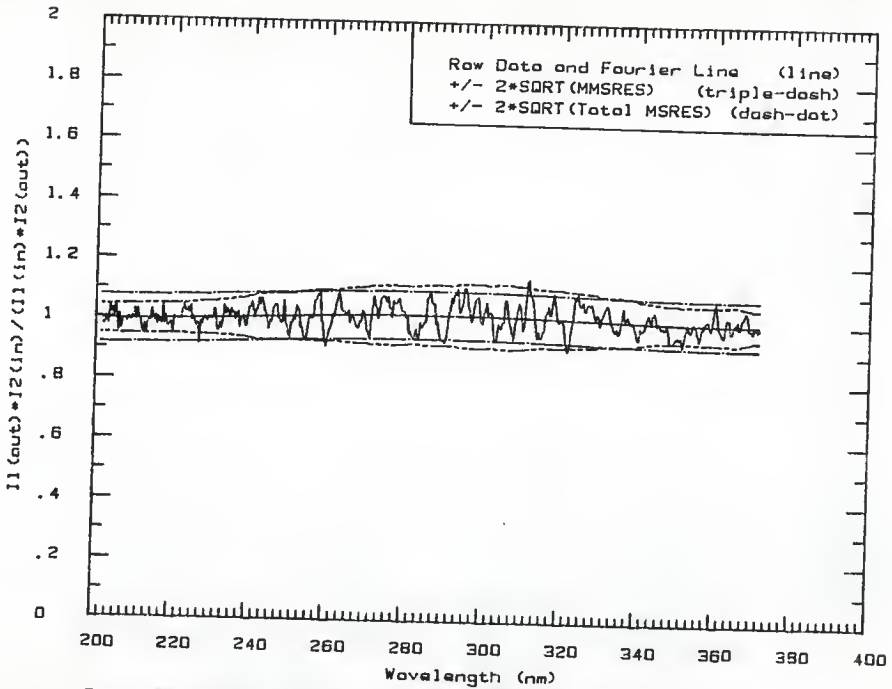

Fig. 6a Signal ratio for I1 defined for 0-37 ns time region and I2 defined during -30-0 ns region for dielectric mirror 26.

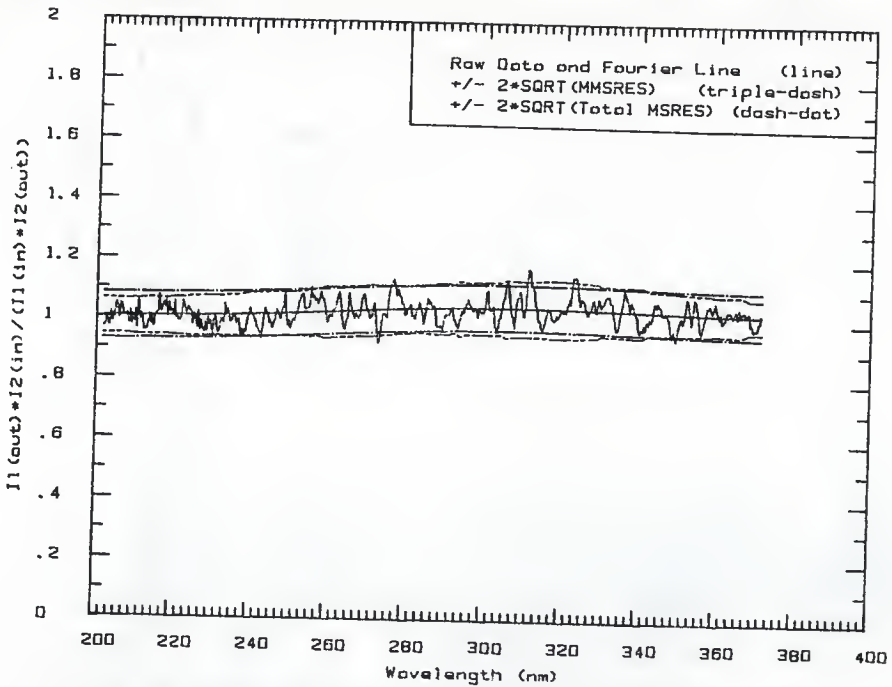

Fig. 6b Signal ratio for I1 defined for 37-70.5 ns time region and I2 defined during -30-0 ns region for dielectric mirror 26.

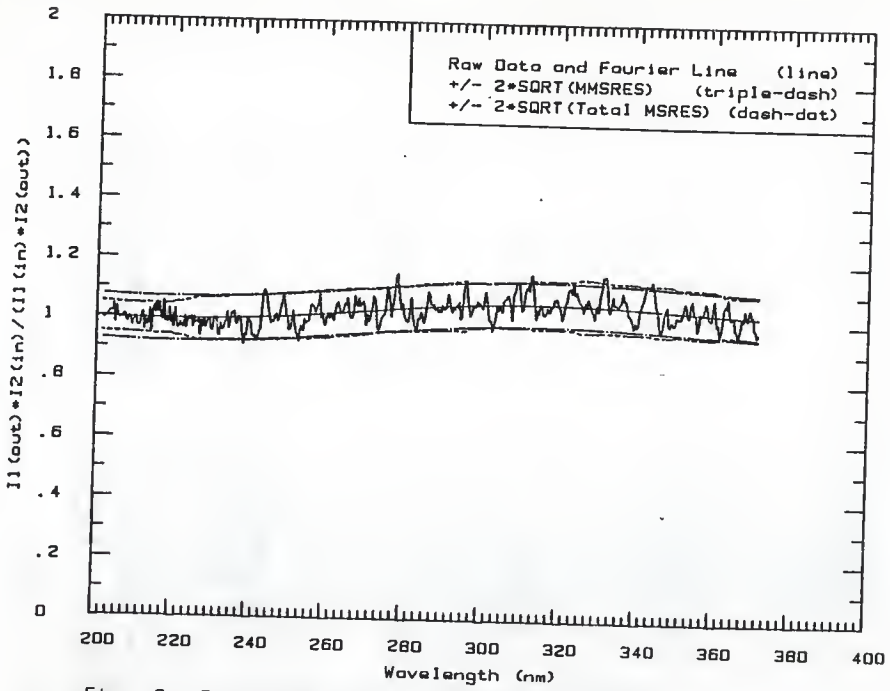

Fig. 6c Signal ratio for I1 defined for 70.5-104 ns time region and I2 defined during -30-0 ns region for dielectric mirror 26.

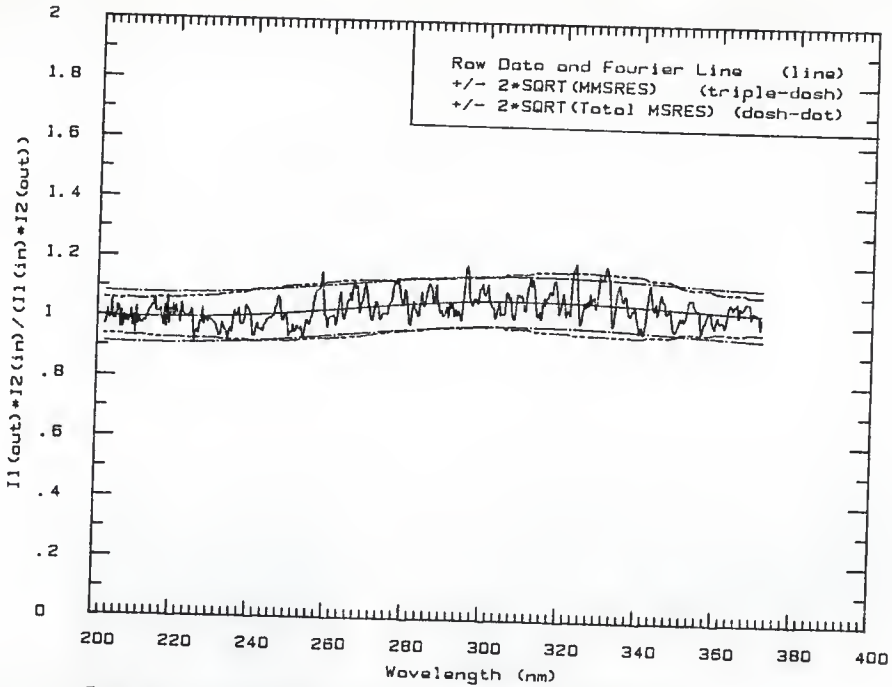

Fig. 6d Signal ratio for I1 defined for 104-138 ns time region and I2 defined during -30-0 ns region for dielectric mirror 26.

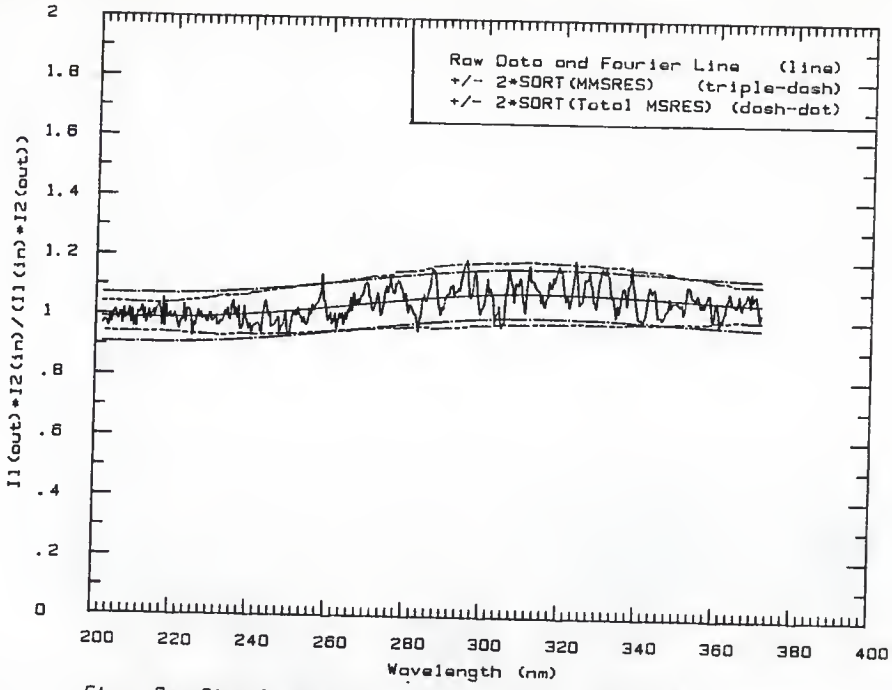

Fig. 6e Signal ratio for I1 defined for 138-171 ns time region and I2 defined during -30-0 ns region for dielectric mirror 26.

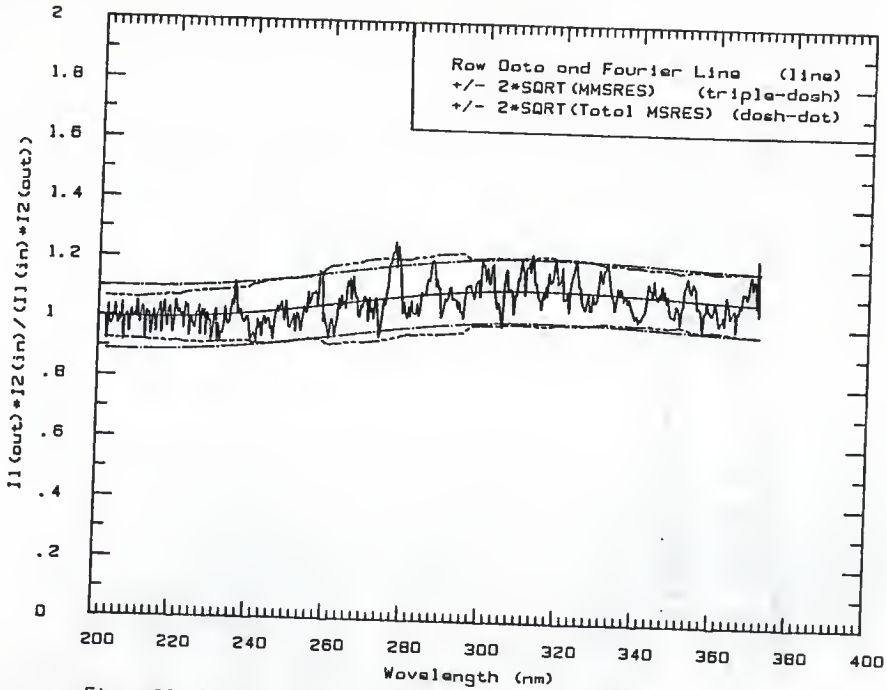

Fig. 6f Signal ratio for I1 defined for 171-205 ns time region and I2 defined during -30-0 ns region for dielectric mirror 20.

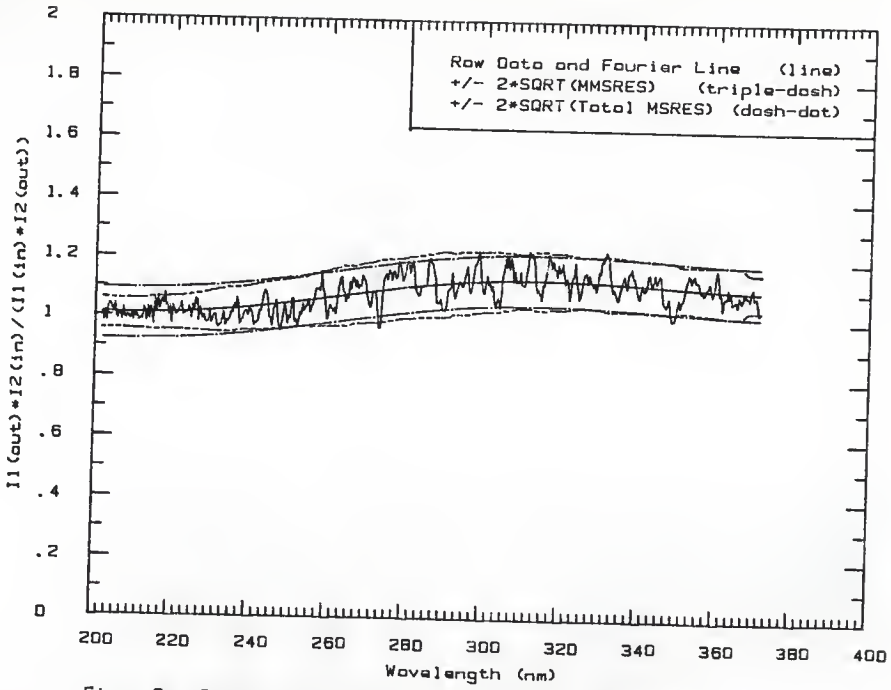

Fig. 6g Signal ratio for I1 defined for 205-238 ns time region and I2 defined during -30-0 ns region for dielectric mirror 26.

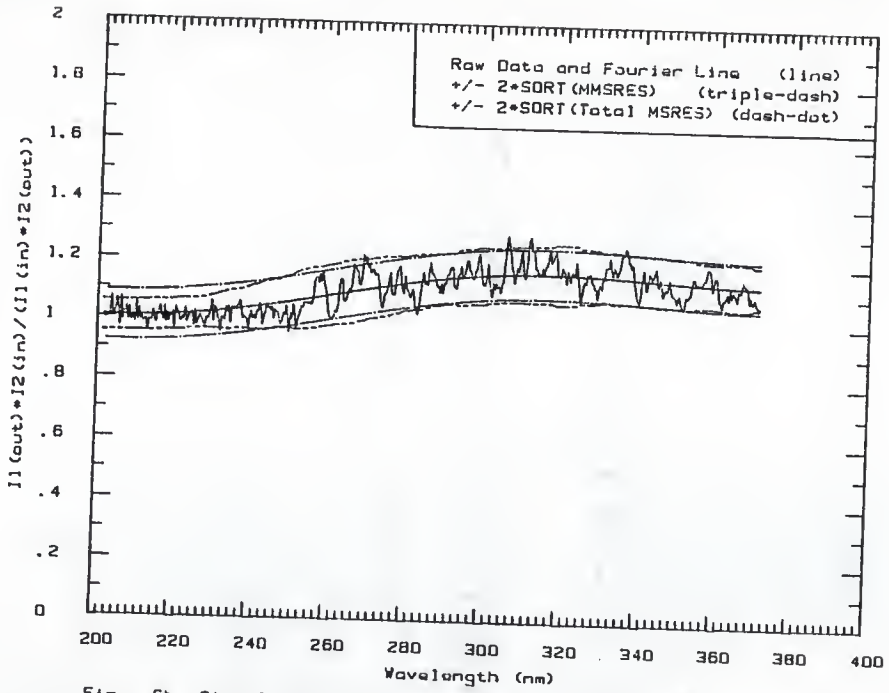

Fig. 6h Signal ratio for I1 defined for 238-272 ns time region and I2 defined during -30-0 ns region for dielectric mirror 26.

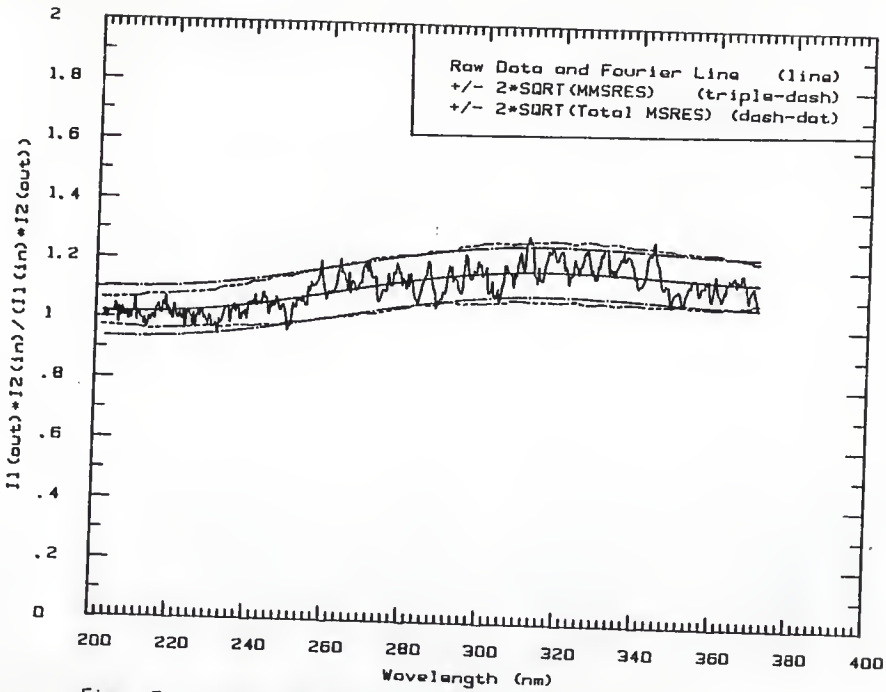

Fig. 6i Signal ratio for I1 defined for 272-313 ns time region and I2 defined during -30-0 ns region for dielectric mirror 26.

Figures 7a to 7i, the signal-ratio plots for metal-coated mirror 1L, irradiated in position A. For the block-out irradiation the mean current was 5 A and the pulse length was 20 ns.

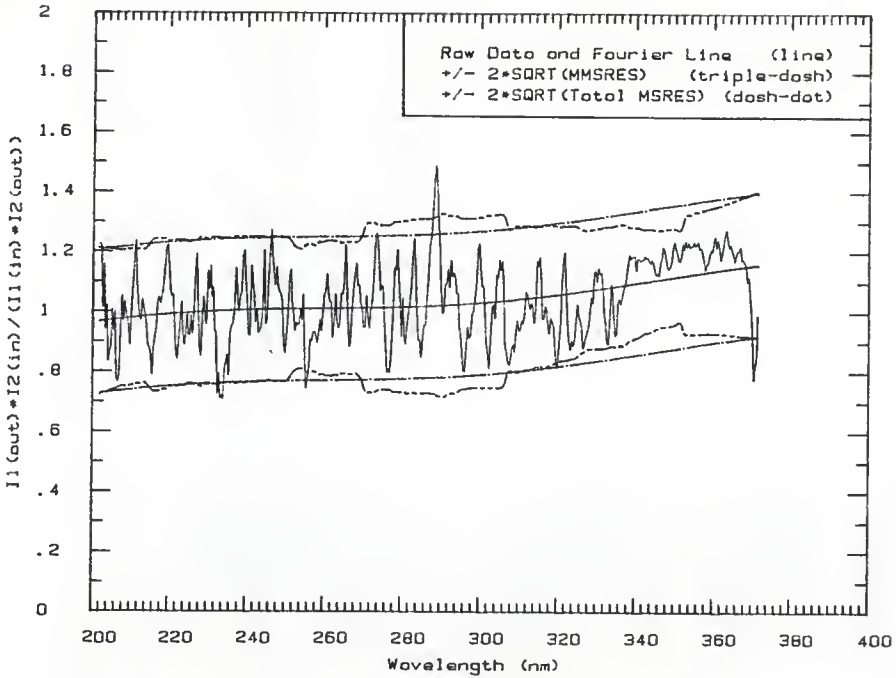

Fig. 7o Signal ratio for I1 defined in 0.0-5.0 ns time region and I2 defined during -40-0 ns region for metal-coated mirror 1L.

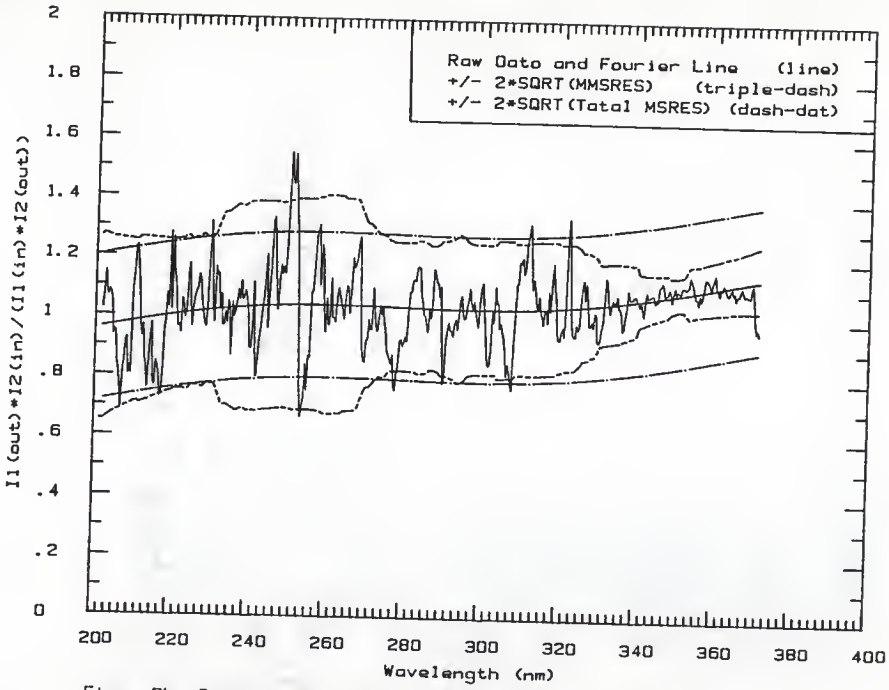

Fig. 7b Signal ratio for I1 defined in 5.0-10.0 ns time region and I2 defined during -40-0 ns region for metal-coated mirror 1L.

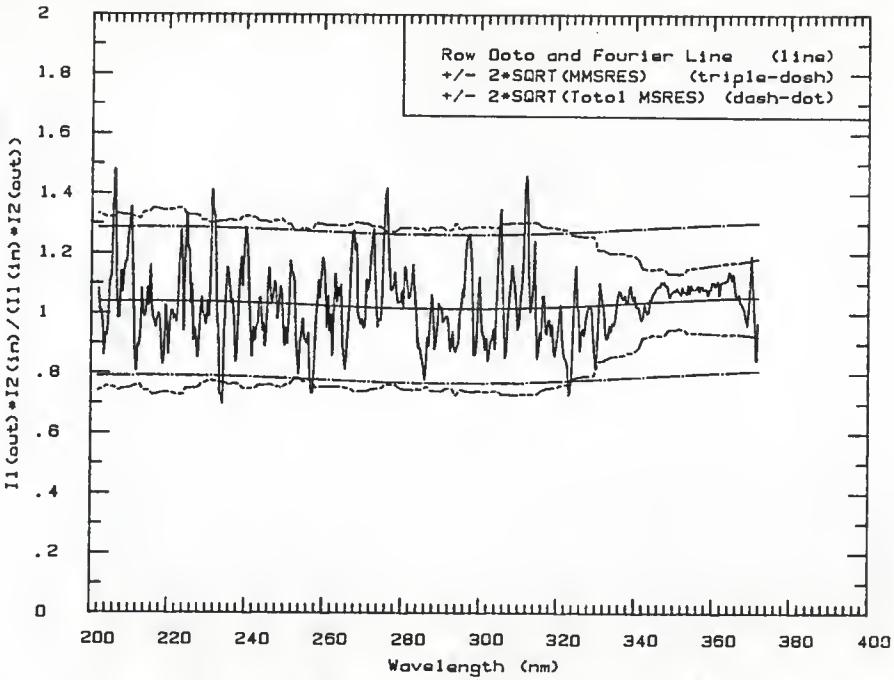

Fig. 7c Signal ratio for I1 defined in 10.0-15.0 ns time region and I2 defined during -40-0 ns region for metal-coated mirror 1L.

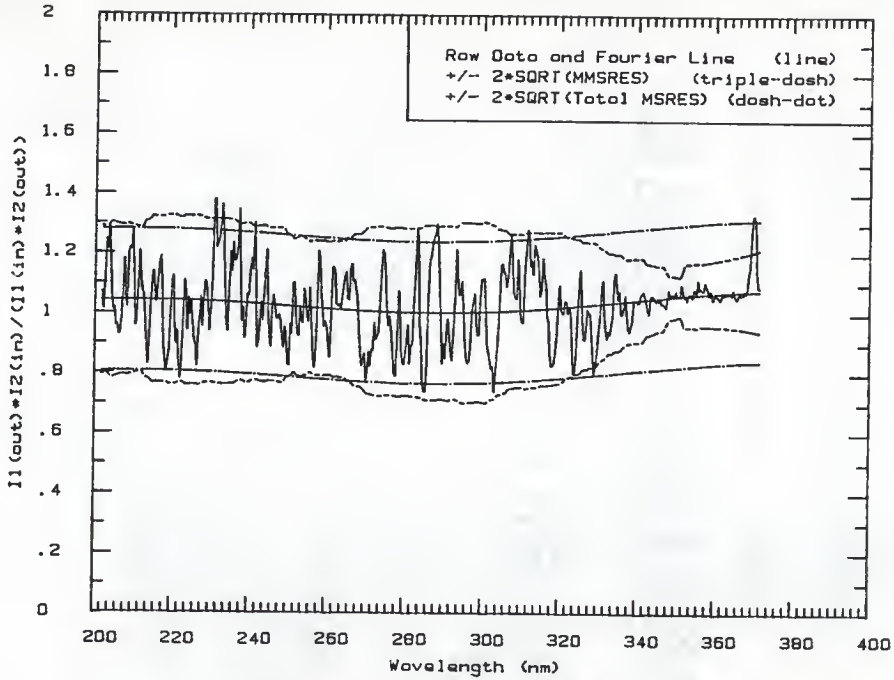

Fig. 7d Signal ratio for I1 defined in 15.0-20.0 ns time region and I2 defined during -40-0 ns region for metal-coated mirror 1L.

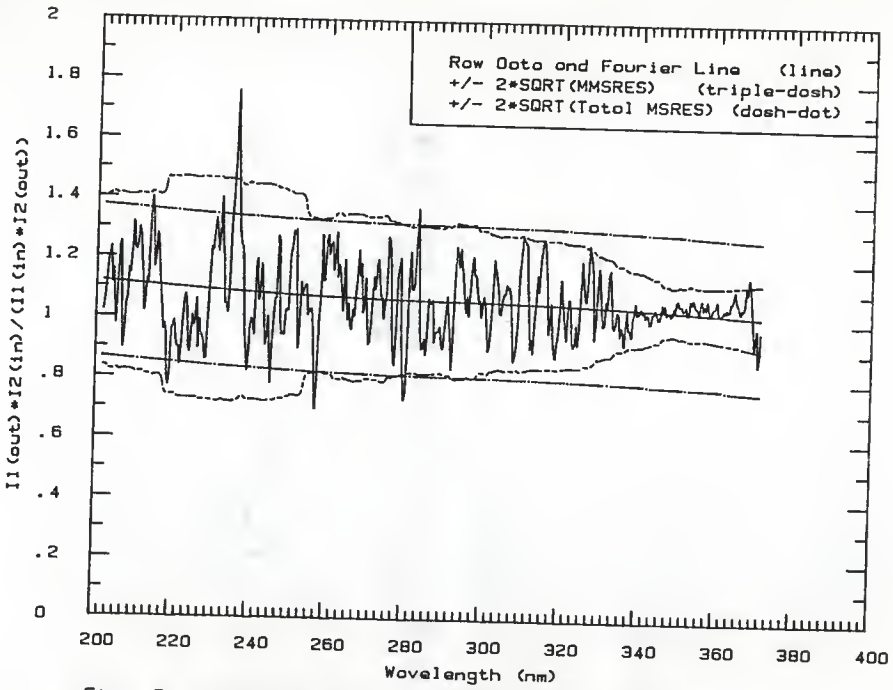

Fig. 7e Signal ratio for I1 defined in 20.0-25.0 ns time region and I2 defined during -40-0 ns region for metal-coated mirror 1L.

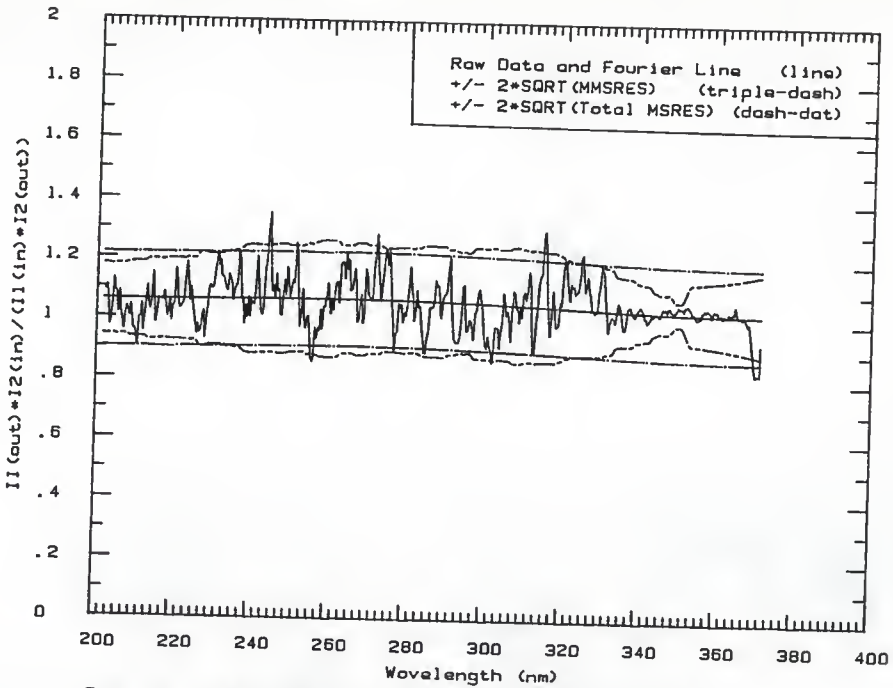

Fig. 7f Signal ratio for I1 defined in 25.0-41.3 ns time region and I2 defined during -40-0 ns region for metal-coated mirror 1L.

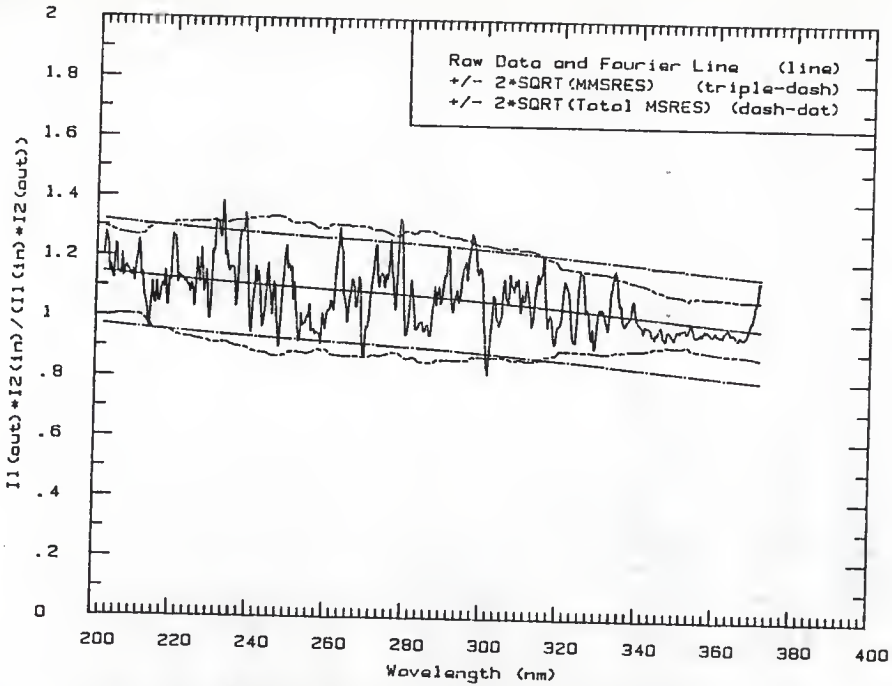

Fig. 7g Signal ratio for I1 defined in 41.3-57.5 ns time region and I2 defined during -40-0 ns region for metal-coated mirror 1L.

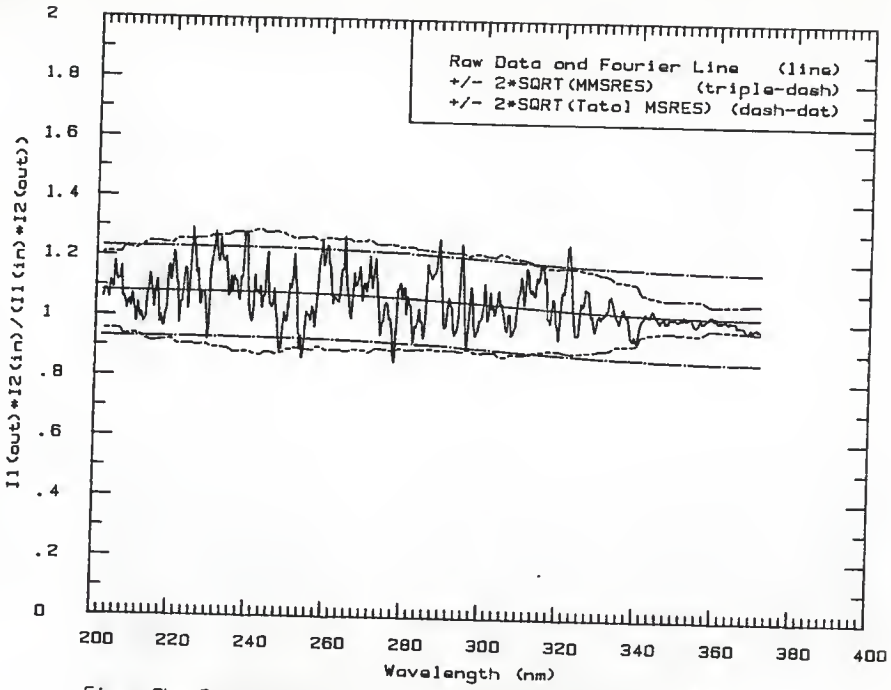

Fig. 7h Signal ratio for I1 defined in 57.5-73.8 ns time region and I2 defined during -40-0 ns region for metal-coated mirror 1L.

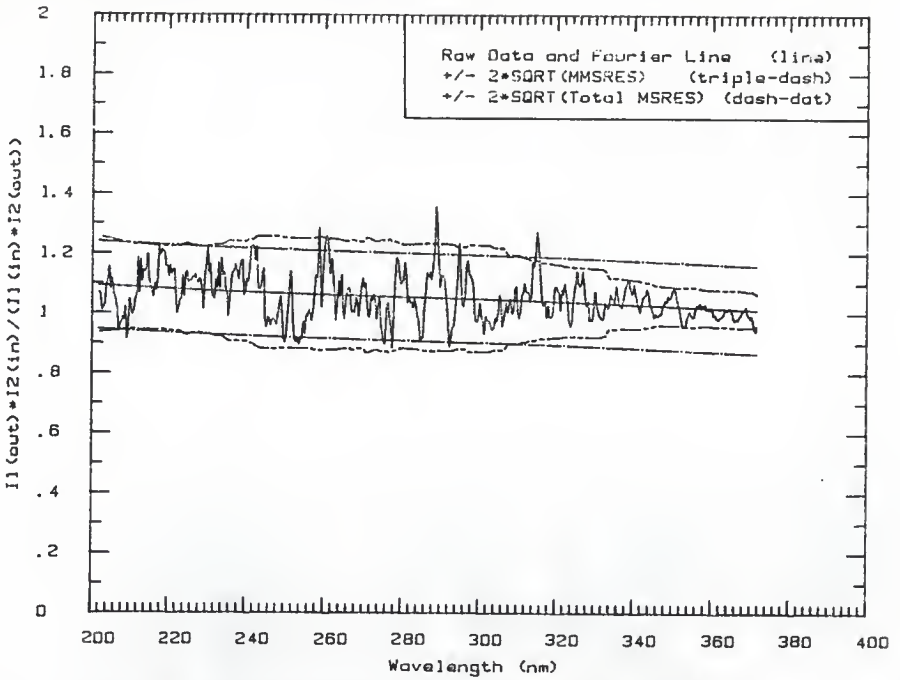

Fig. 7i Signal ratio for I1 defined in 73.8-88.0 ns time region and I2 defined during -40-0 ns region for metal-coated mirror 1L.

Figures 8a to 8i, the signal-ratio plots for metal-coated mirror 2L, irradiated in position A. For the block-out irradiation, the mean current was 225 mA and the pulse length was 200 ns.

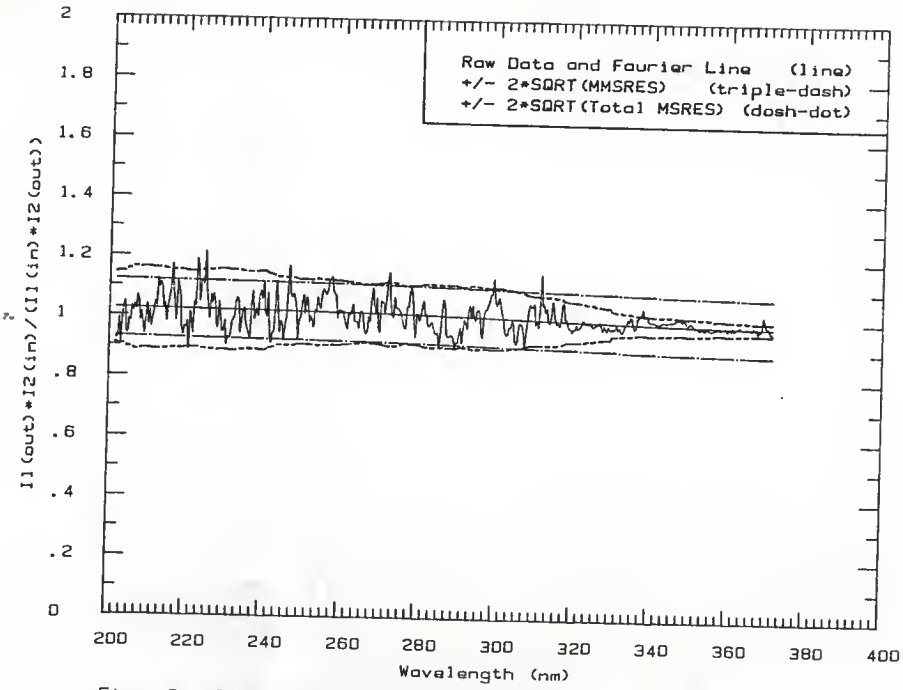

Fig. 8a Signal ratio for I1 defined in 0.8-20.9 ns time region and I2 defined during -160-0.8 ns region for metal-coated mirror 2L, irradiated in position A.

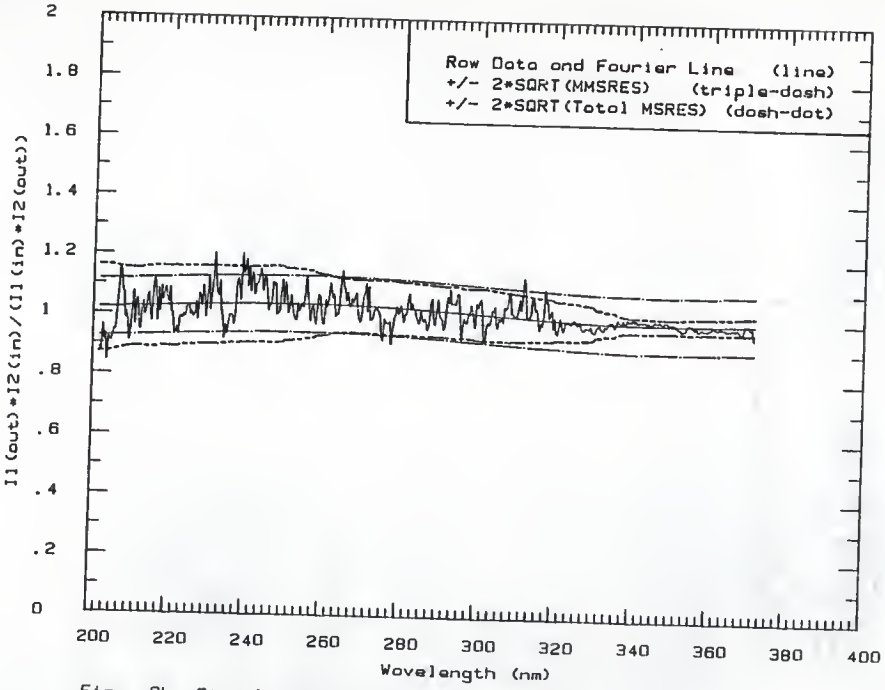

Fig. 8b Signal ratio for I1 defined in 20.9-41.0 ns time region and I2 defined during -160-0.8 ns region for metal-coated mirror 2L. irradiated in position A.

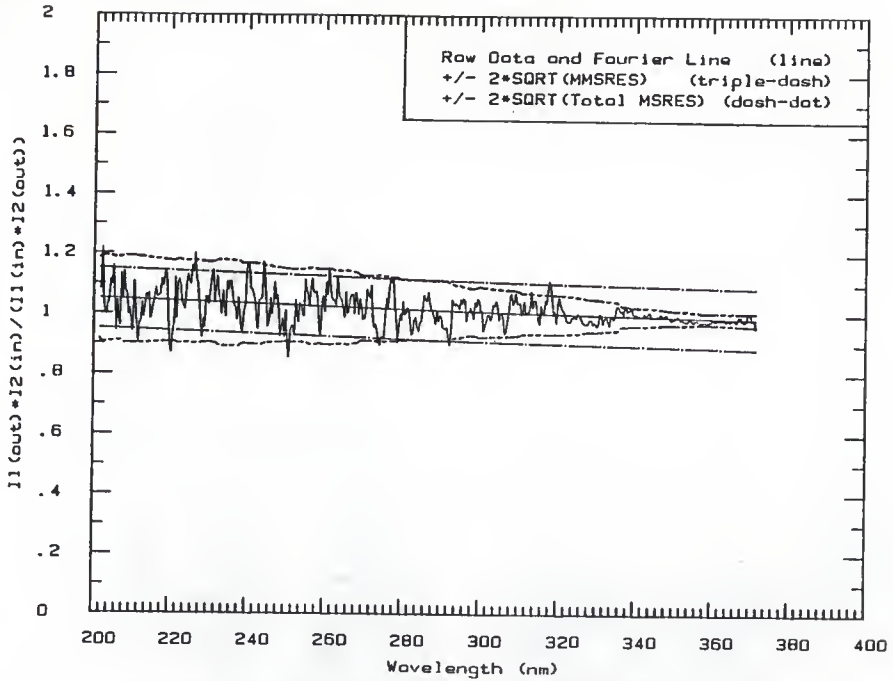

Fig. 8c Signal ratio for I1 defined in 41.0-61.1 ns time region and I2 defined during -160-0.8 ns region for metal-coated mirror 2L, irradiated in position A.

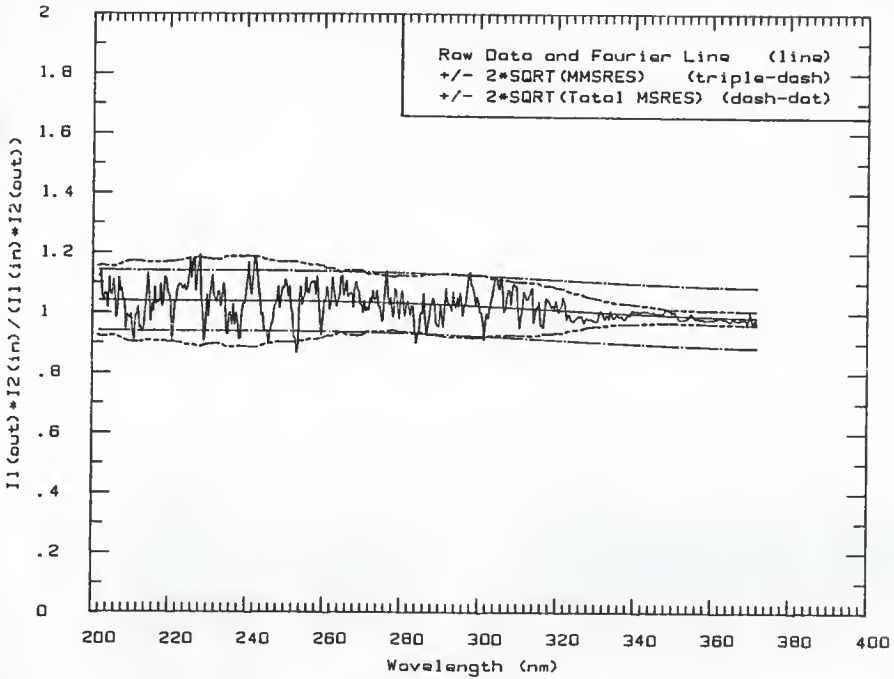

Fig. 8d Signal ratio for I1 defined in 61.1-81.2 ns time region and I2 defined during -160-0.8 ns region for metal-coated mirror 2L, irradiated in postion A.

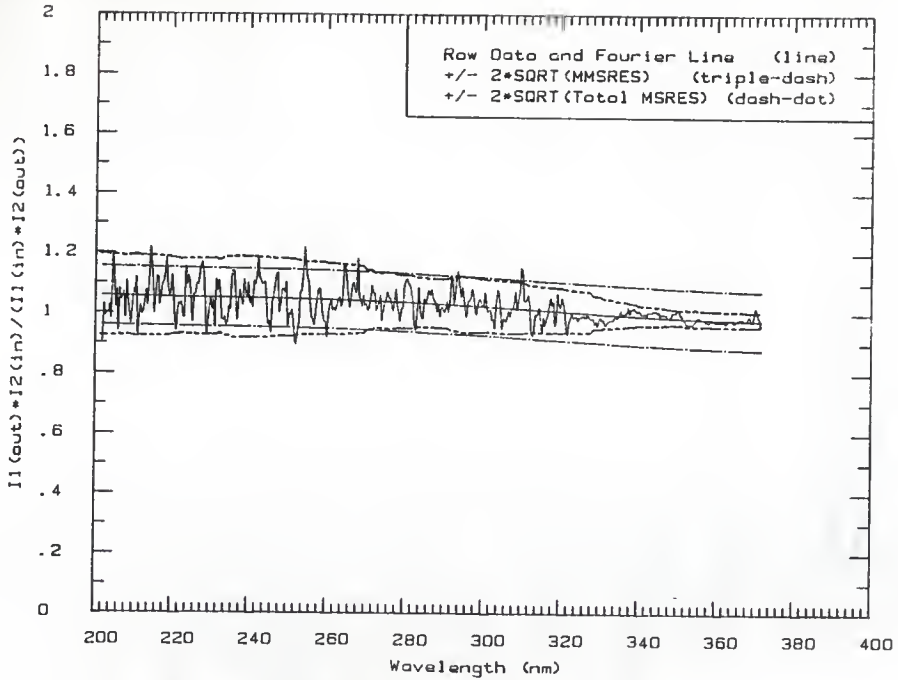

Fig. 8e Signal ratio for I1 defined in 81.2-101 ns time region and I2 defined during -160-0.8 ns region for metal-coated mirror 2L, irradiated in position A.

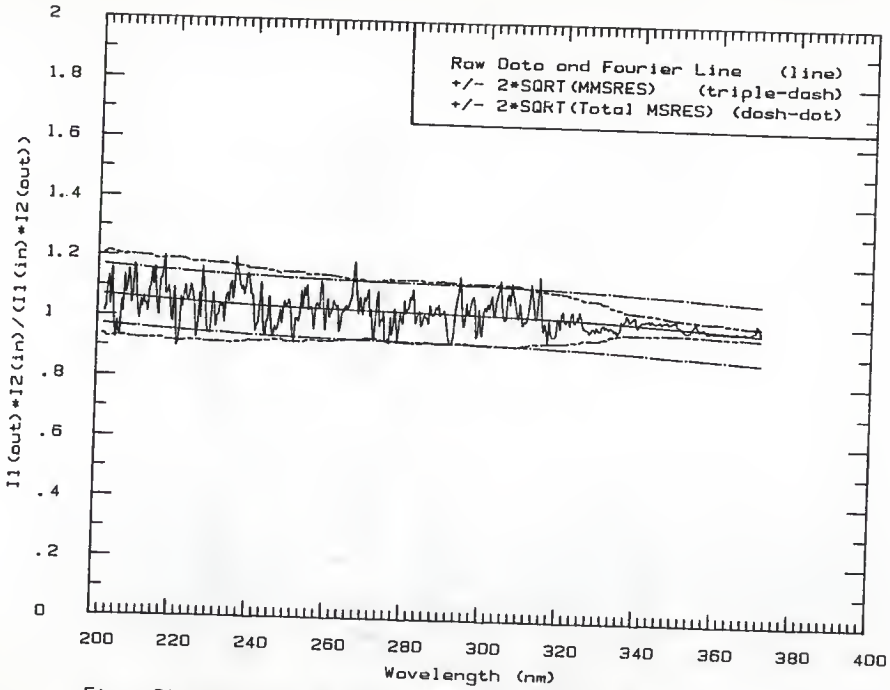

Fig. 8f Signal ratio for I1 defined in 101-121 ns time region and I2 defined during -160-0.8 ns for metal-coated mirror 2L, irradiated in position A.

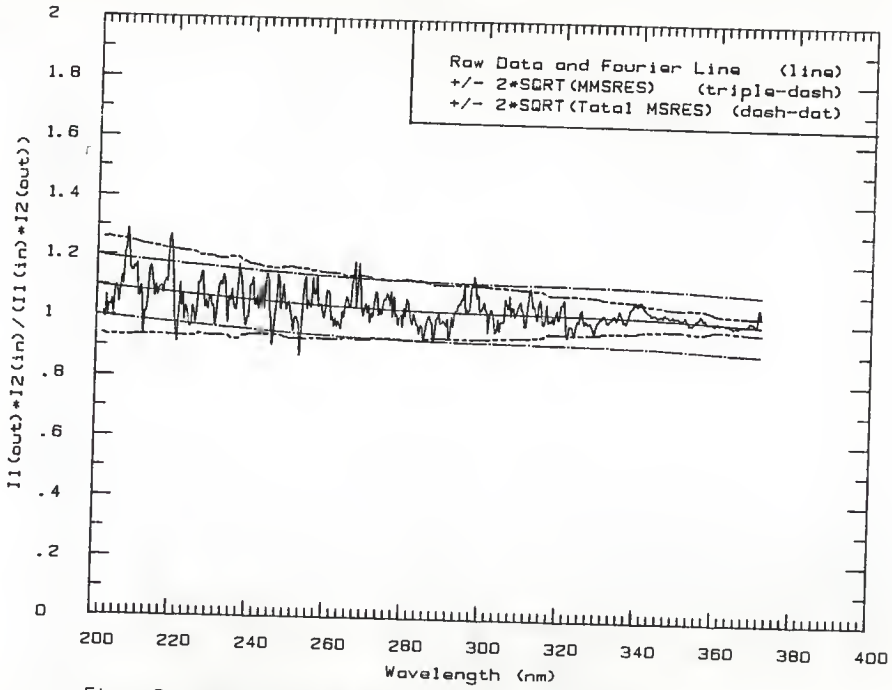

Fig. 8g Signal ratio for I1 defined in 121-142 ns time region and I2 defined during -160-0.8 ns for metal-coated mirror 2L, irradiated in position A.

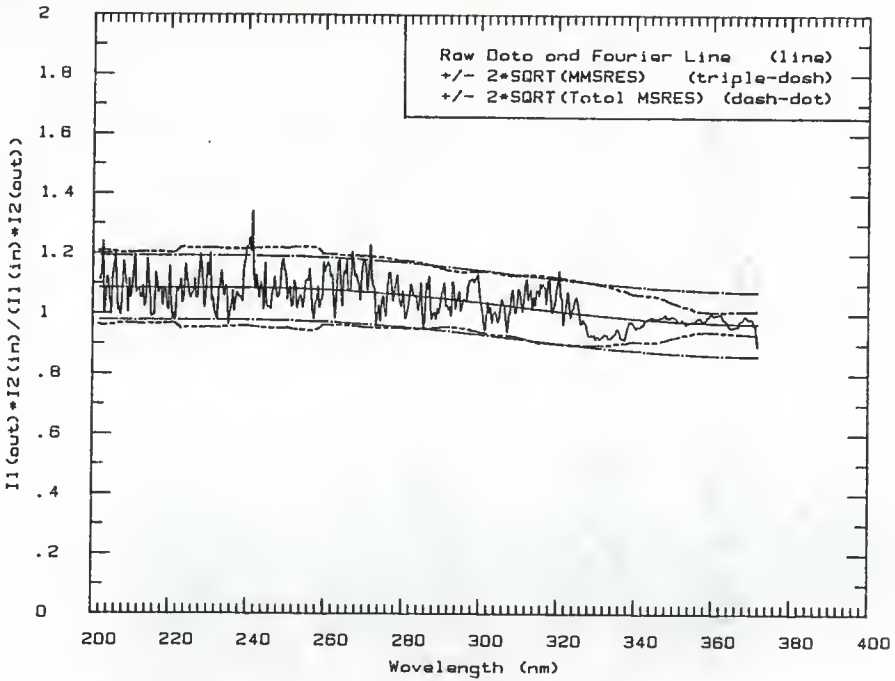

Fig. 8h Signal ratio for I1 defined in 142-162 ns time region and I2 defined during -160-0.8 ns for metal-coated mirror 2L, irradiated in position A.

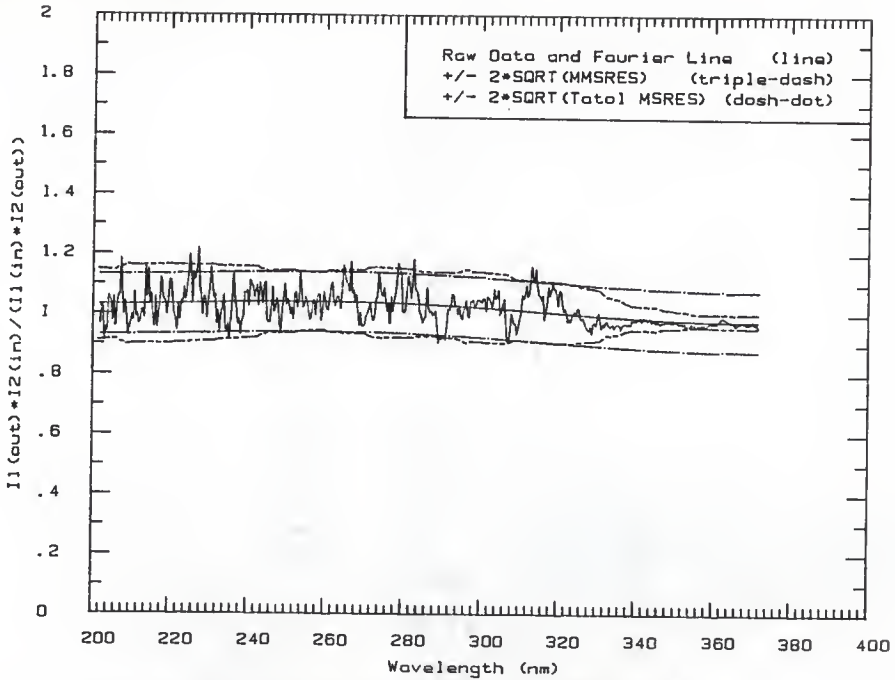

Fig. 81 Signal ratio for I1 defined in I62-183 ns time region and I2 defined during -160-0.8 ns region for metal-coated mirror 2L, irradiated in position A.

Figures 9a to 9i, the signal-ratio plots for metal-coated mirror 2L, irradiated in position B. For the block-out irradiation, the mean beam current was 225 mA, and the pulse length was 200 ns.

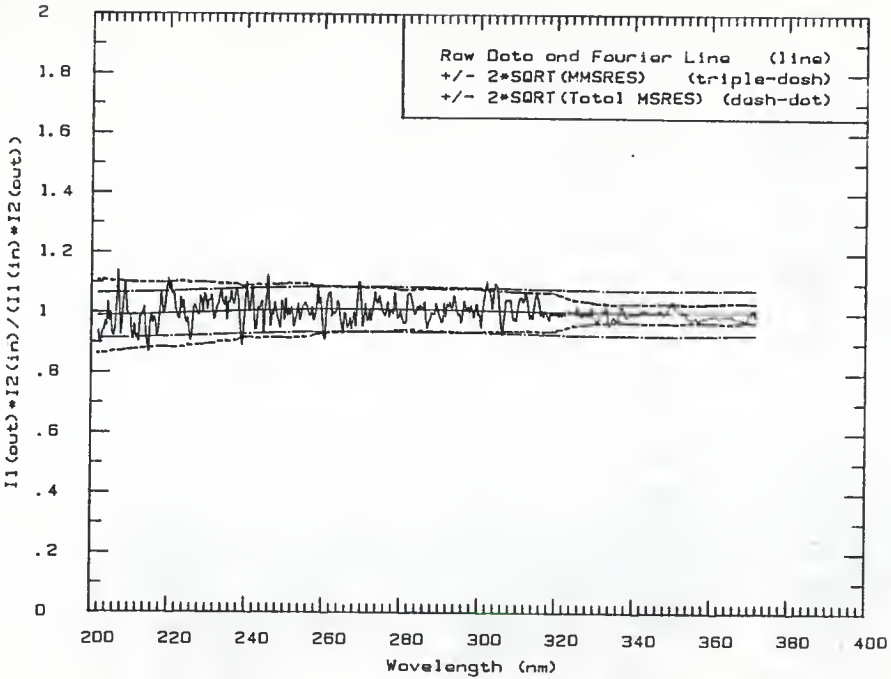

Fig. 9a Signal ratio for I1 defined in 0.25-33.8 ns time region and I2 defined during -50-0.25 ns region for metal-coated mirror 2L. irradiated in position 8.

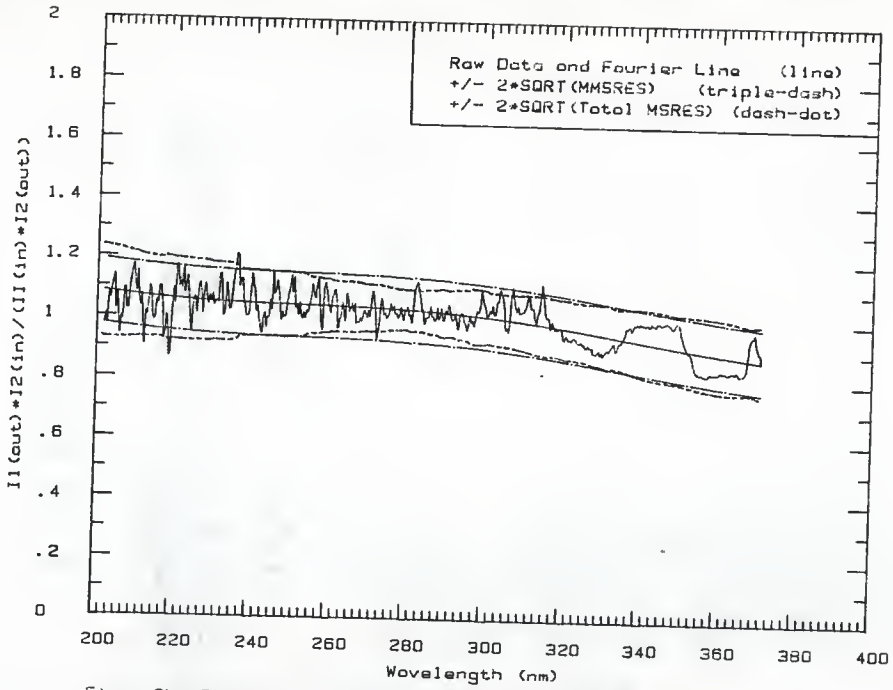

Fig. 9b Signal ratio for I1 defined in 33.8-67.3 ns time region and I2 defined during -50-0.25 ns for metal-coated mirror 2L, irradiated in position B.

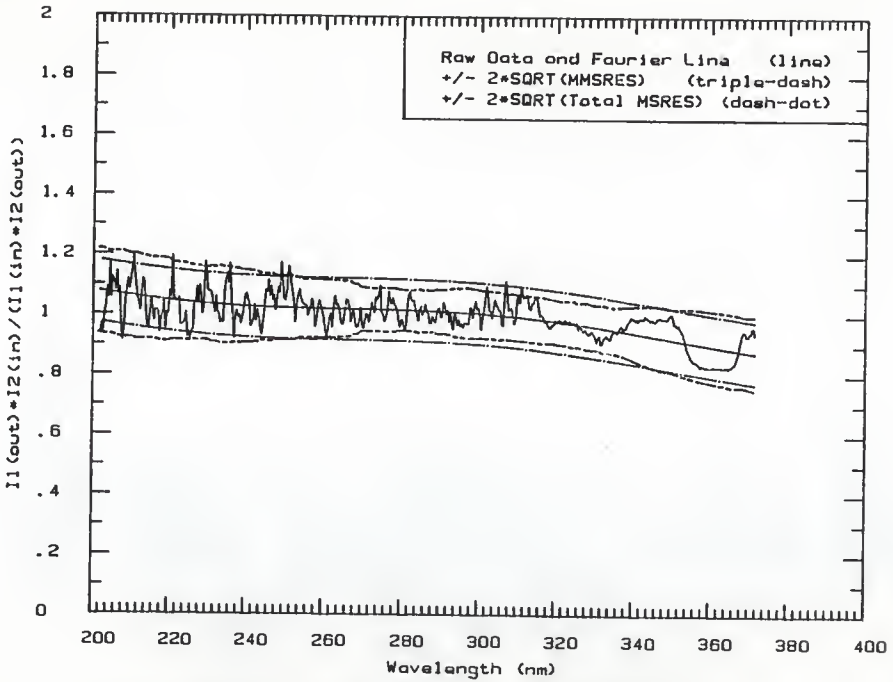

Fig. 9c Signal ratio for I1 defined in 67.3-101 ns time region and I2 defined during -50-0.25 ns for metal-coated mirror 2L, irradiated in position 8.

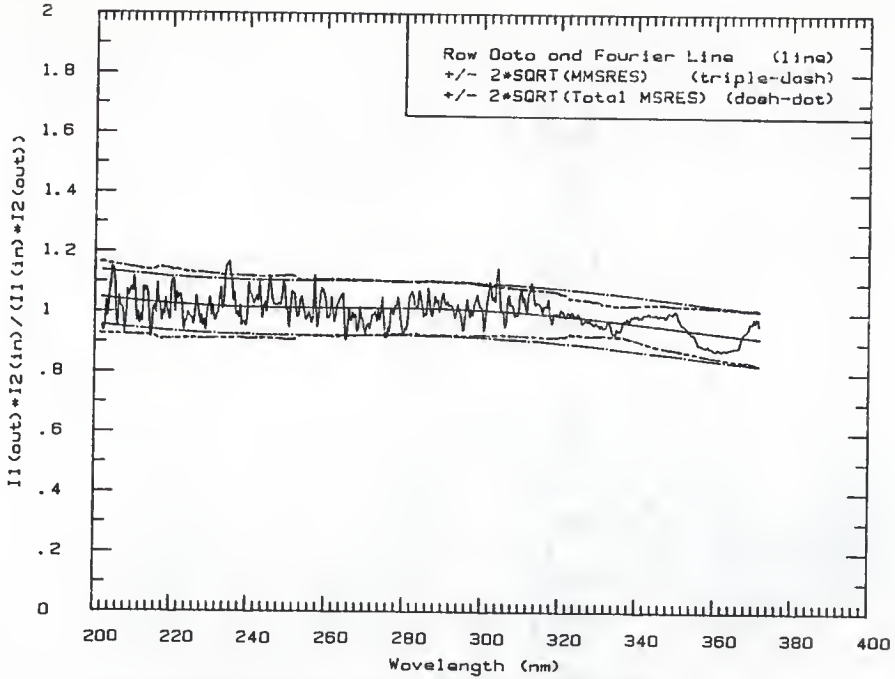

Fig. 9d Signal ratio for I1 defined in 101-134 ns time region and I2 defined during -50-0.25 ns for metal-coated mirror 2L, irradiated in position B.

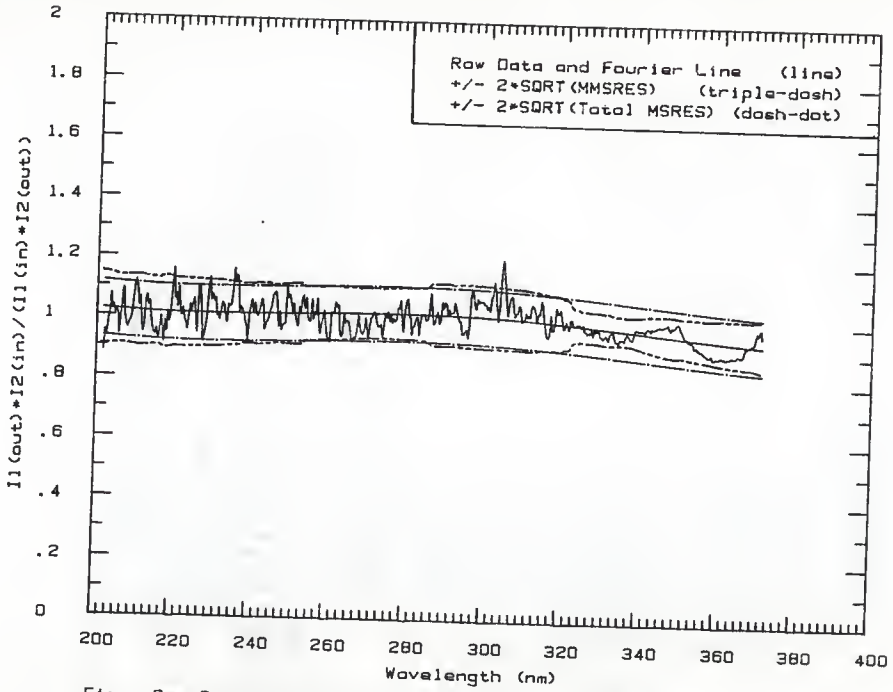

Fig. 9e Signal ratio for I1 defined in 134-168 ns time region and I2 defined during -50-0.25 ns for metal-coated mirror 2L. irradiated in position 8.

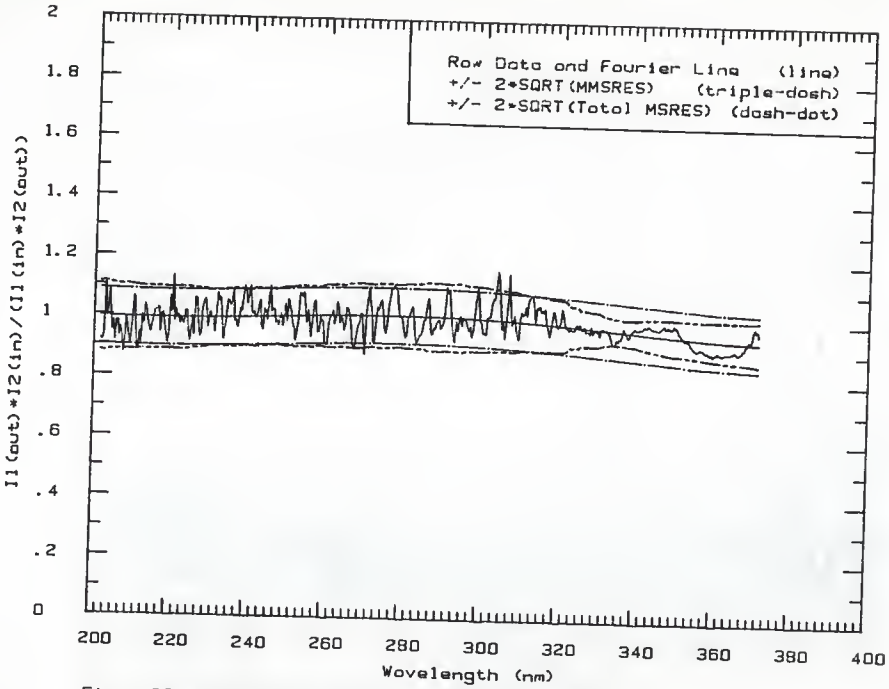

Fig. 9f Signal ratio for I1 defined in 164-201 ns time region and I2 defined during -50-0.25 ns for metal-coated mirror 2L, irradiated in position 8.

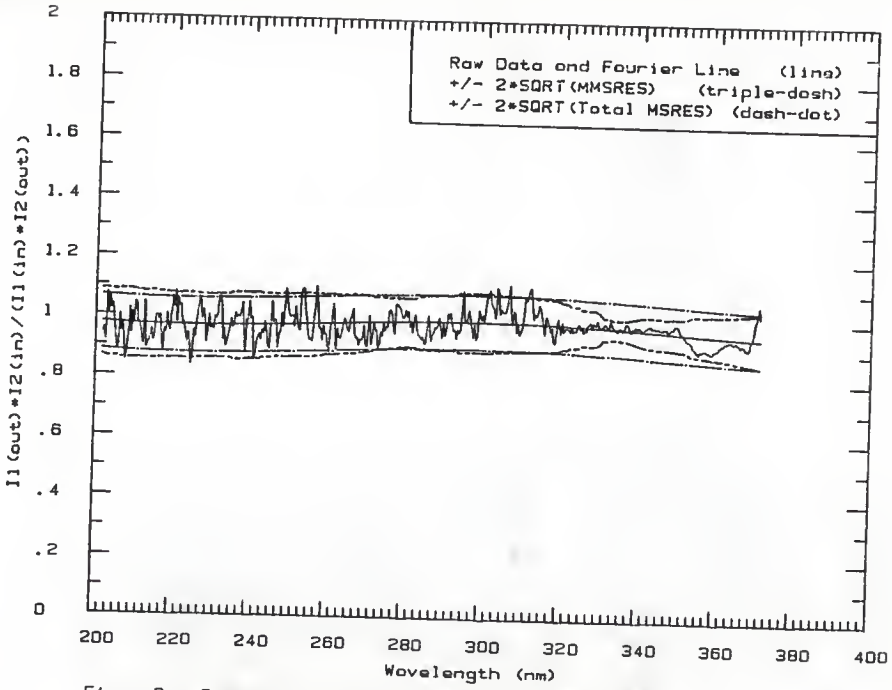

Fig. 9g Signal ratio for I1 defined in 201-235 ns time region and I2 defined during -50-0.25 ns for metal-coated mirror 2L, irradiated in position 8.

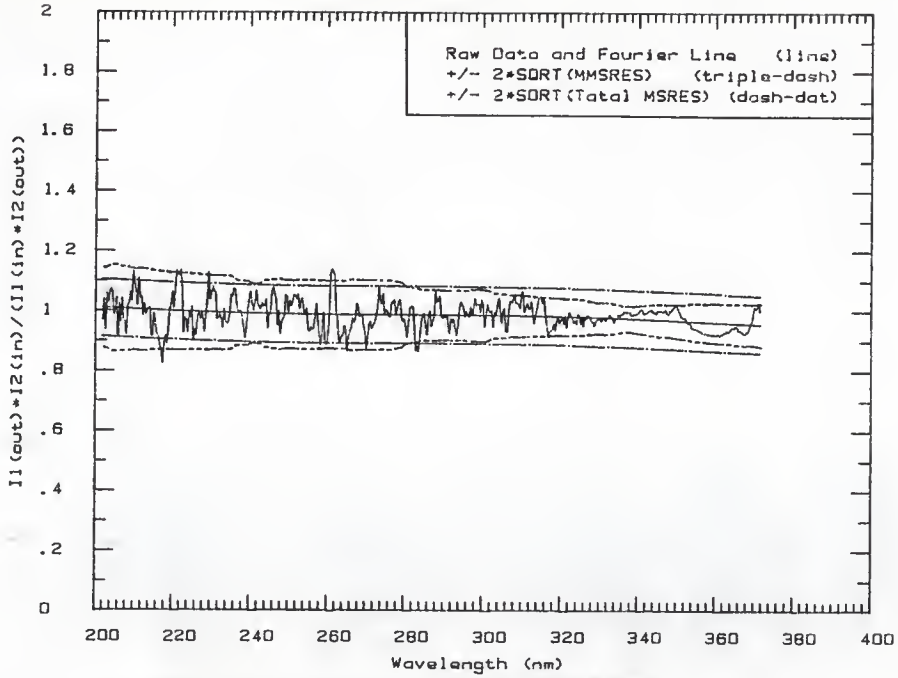

Fig. 9h Signal ratio for I1 defined in 235-268 ns time region and I2 defined during -50-0.25 ns for metal-coated mirror 2L, irradiated in position B.

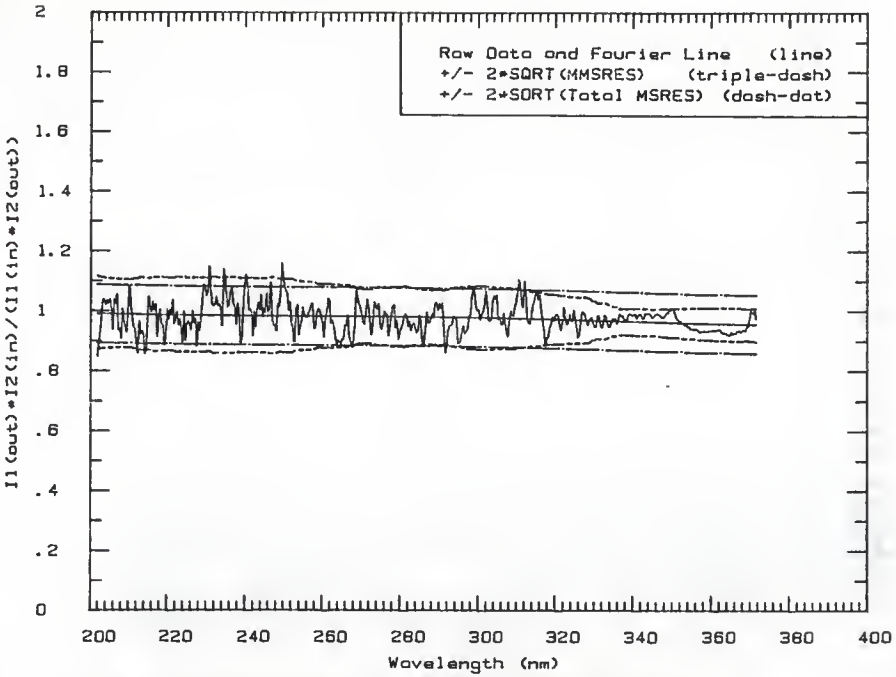

Fig. 9i Signal ratio for I1 defined in 268-293 ns time region and I2 defined during -50-0.25 ns region for metal-coated mirror 2L, irradiated in position 8.

Figures 10a to 10i, the signal-ratio plots for metal-coated mirror 6L, irradiated in position A. For the block-out irradiation, the mean beam current was 5 A and the pulse length was 20 ns.

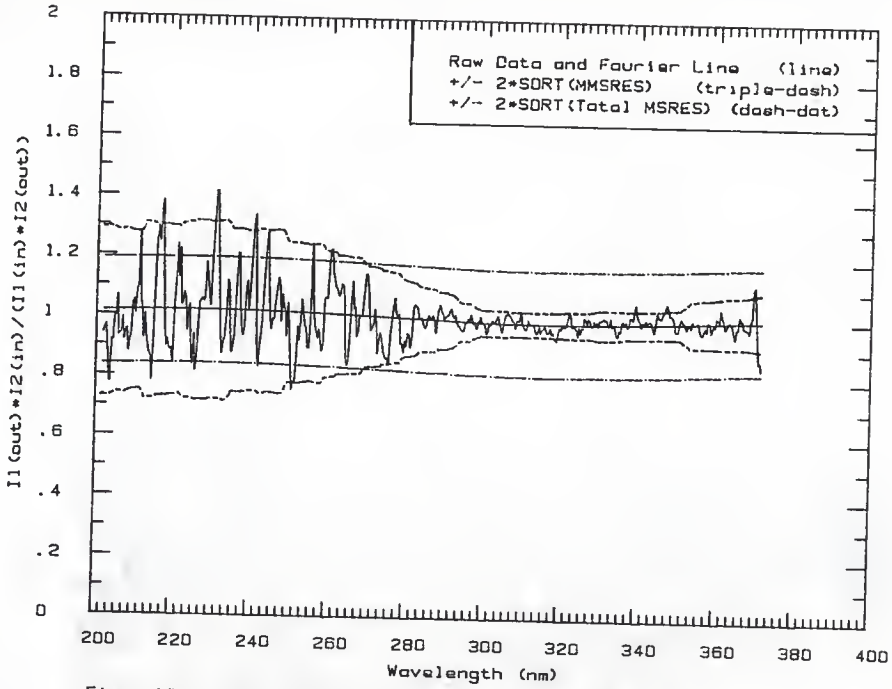

Fig. 10a Signal ratio for I1 defined in 0.0-5.0 ns time region and I2 defined during -40-0 ns region for metal-coated mirror 6L.

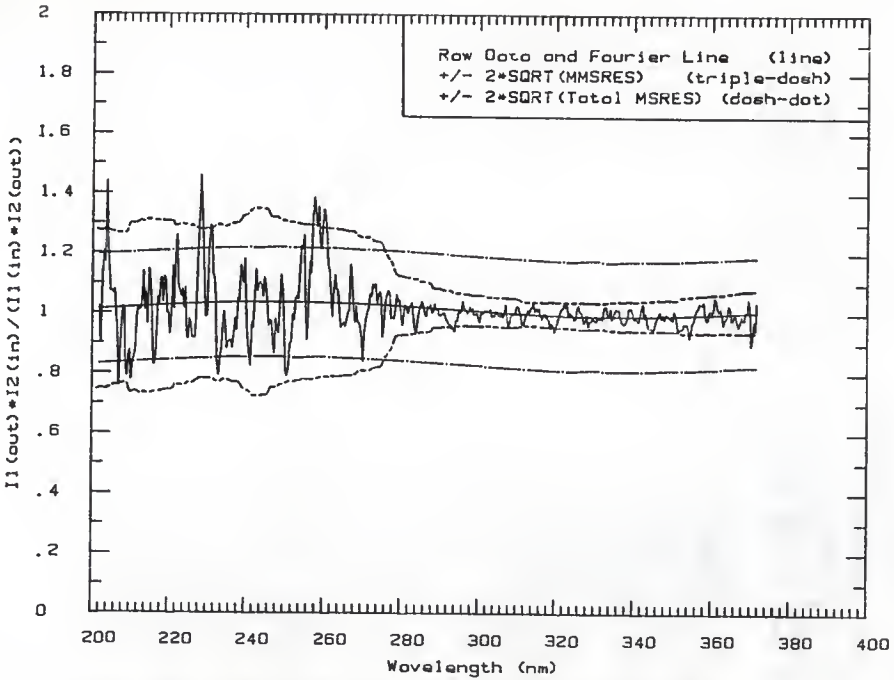

Fig. 10b Signol rotio for I1 defined in 5.0-10.0 ns time region ond I2 defined during -40-0 ns region for metol-cooted mirror 6L.

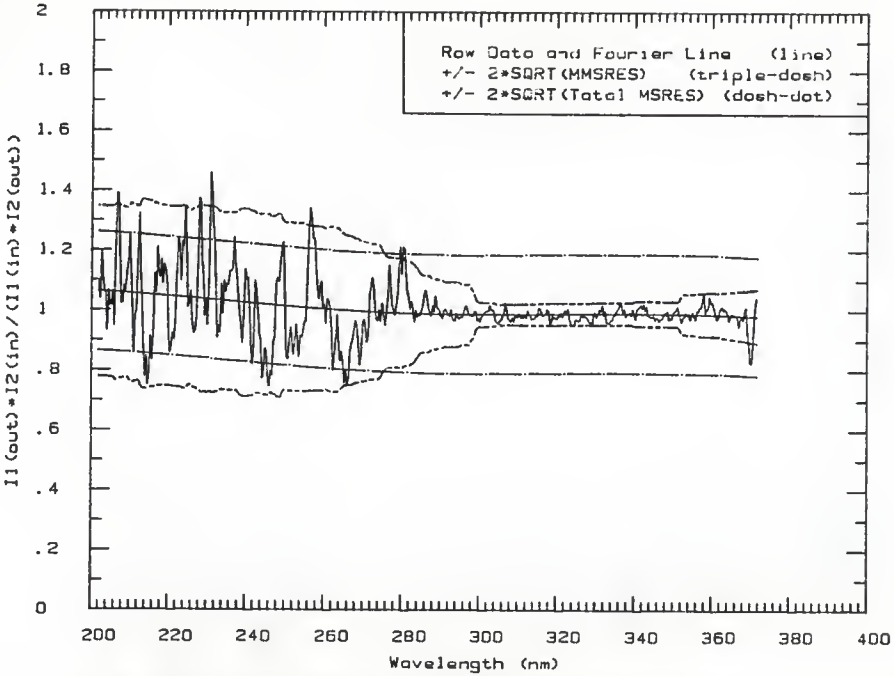

Fig. 10c Signal ratio for I1 defined in 10.0-15.0 ns time region and I2 defined during -40-0 ns region for metal-coated mirror 6L.

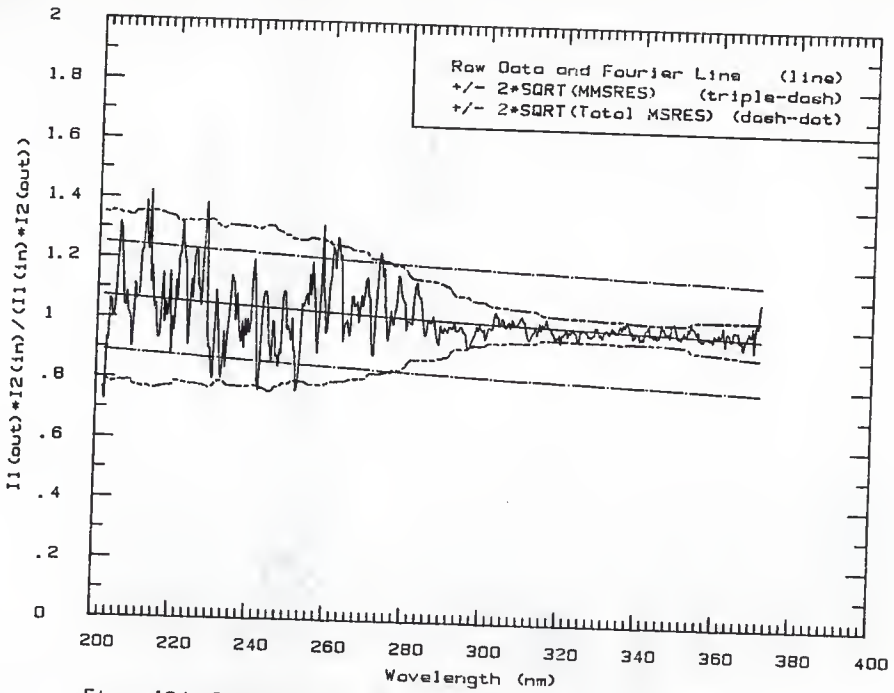

Fig. 10d Signal ratio for I1 defined in 15.0-20.0 ns time region and I2 defined during -40-0 ns region for metal-coated mirror 6L.

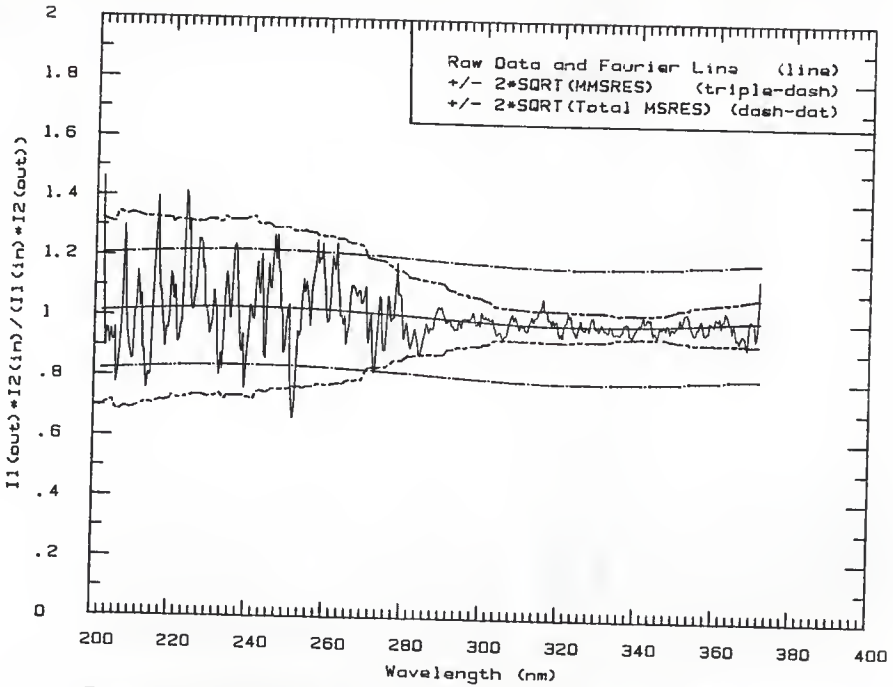

Fig. 10a Signal ratio for I1 defined in 20.0-25.0 ns time region and I2 defined during -40-0 ns region for metal-coated mirror 6L.

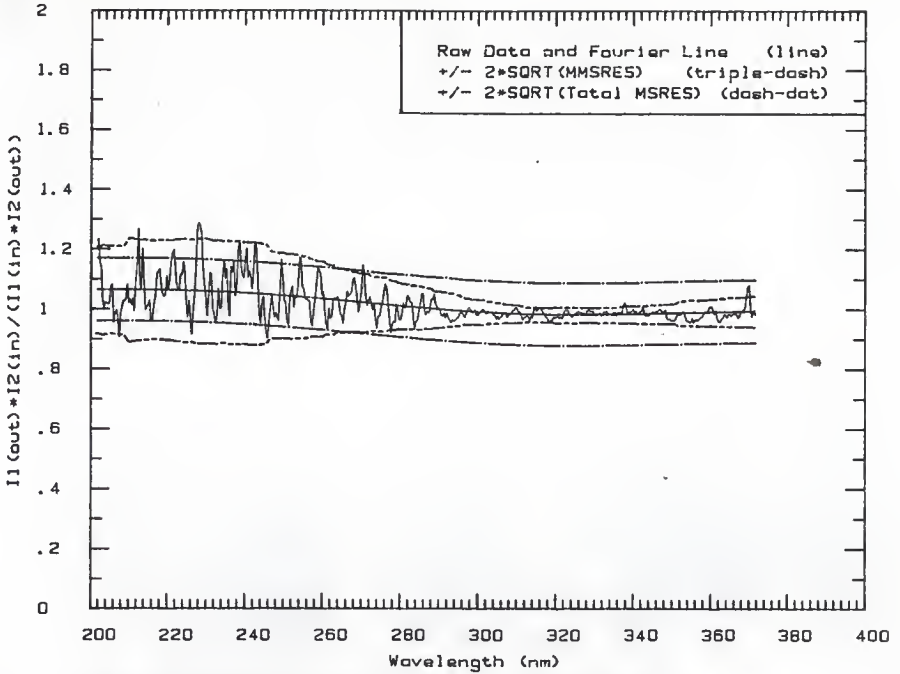

Fig. 10f Signal ratio for I1 defined in 25.0-41.3 ns ns time region and I2 defined during -40-0 ns for metal-coated mirror 6L.

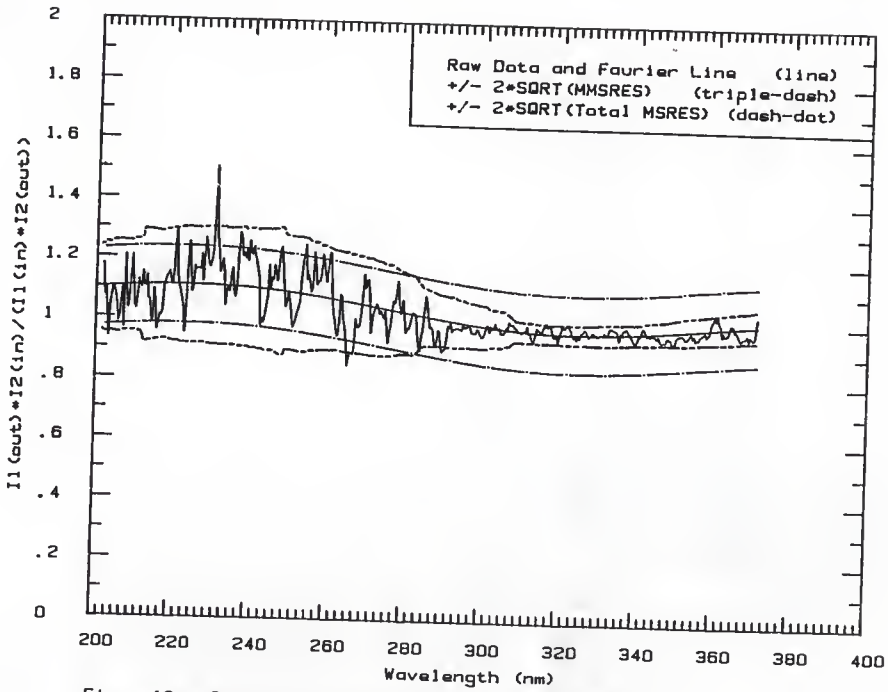

Fig. 10g Signal ratio for I1 defined in 41.3-57.5 ns time region and I2 defined during -40-0 ns for metal-coated mirror 6L.

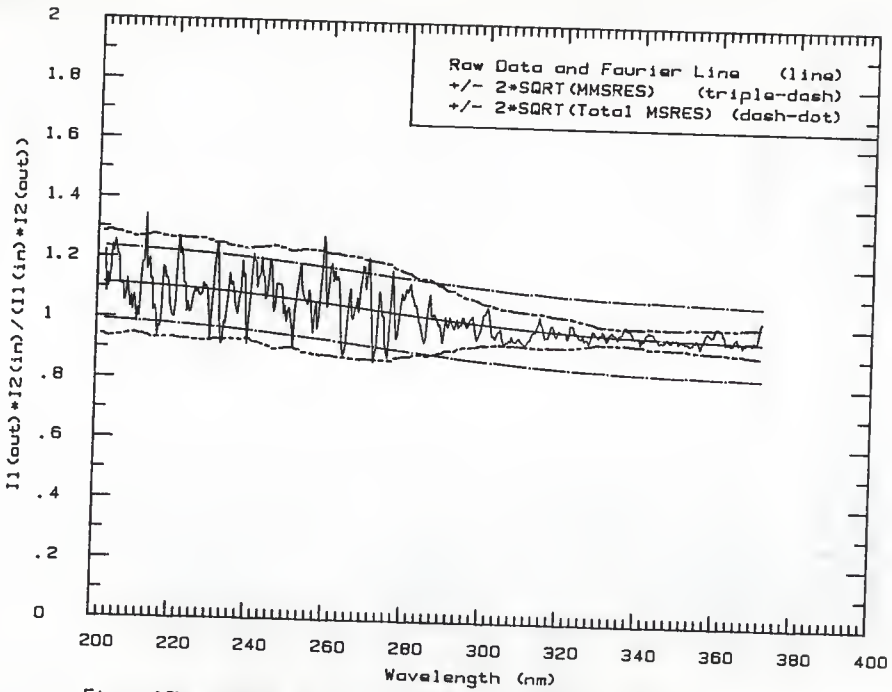

Fig. 10h Signal ratio for I1 defined in 57.5-73.8 ns time region and I2 defined during -40-0 ns for metal-coated mirror 6L.

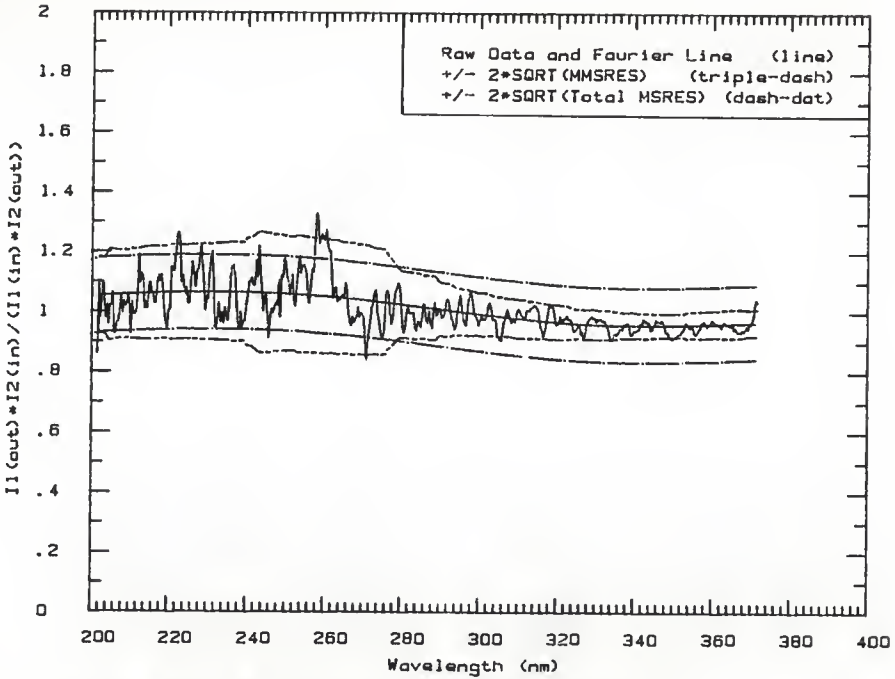

Fig. 10i Signal ratio for I1 defined in 73.8-88.0 ns time region and I2 defined during -40-0 ns for metal-coated mirror 6L.

Figures 11a to 11i, the signal-ratio plots for metal-coated mirror 7L, irradiated in position A. For the block-out irradiation, the mean beam current was 225 mA and the pulse length was 500 ns.

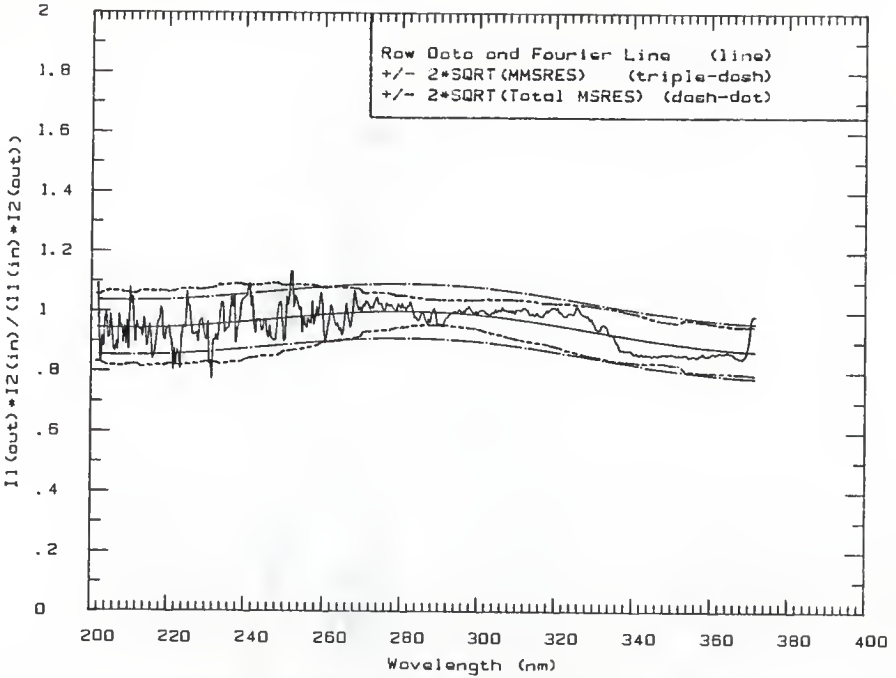

Fig. 11o Signal ratio for I1 defined in 0-37 ns time region and I2 defined during -30-0 ns region for metal-coated mirror 7L, irradiated in position A.

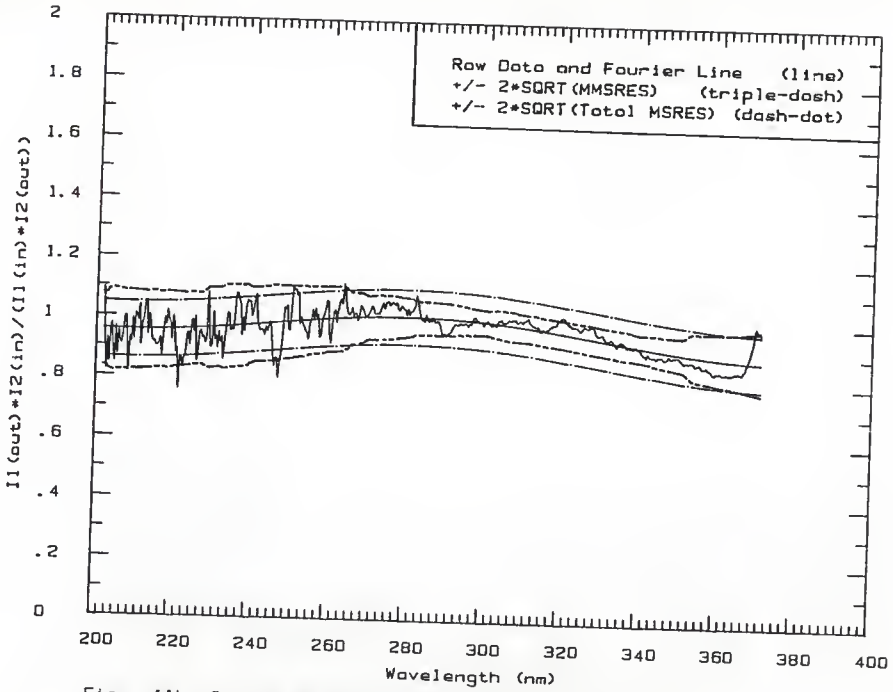

Fig. 11b Signal ratio for I1 defined in 37-70.5 ns time region and I2 defined during -30-0 ns region for metal-coated mirror 7L, irradiated in position A.

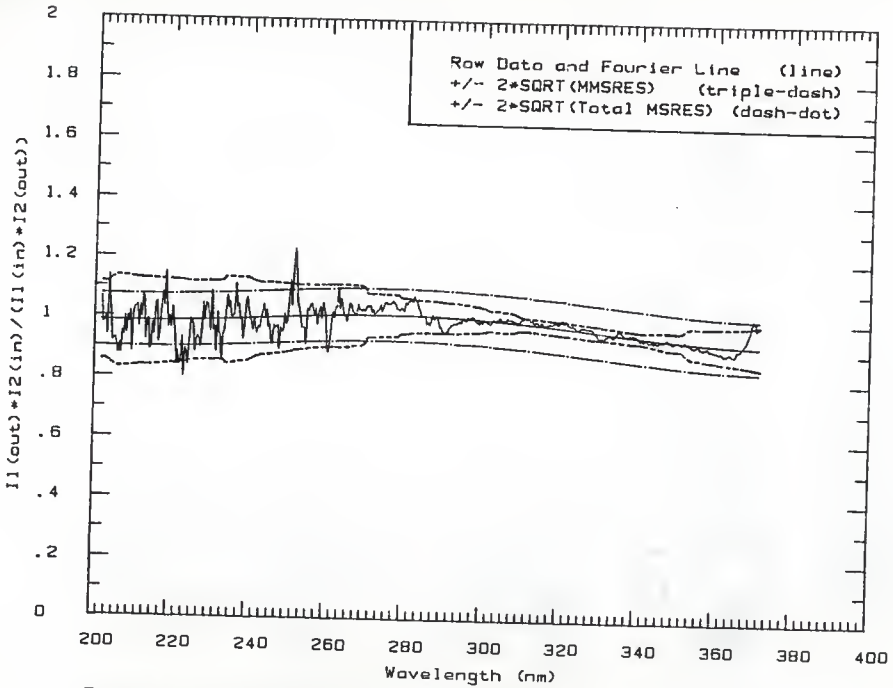

Fig. 11c Signal ratio for I1 defined in 70.5-104 ns time region and I2 defined during -30-0 ns region for metal-coated mirror 7L. irradiated in position A.

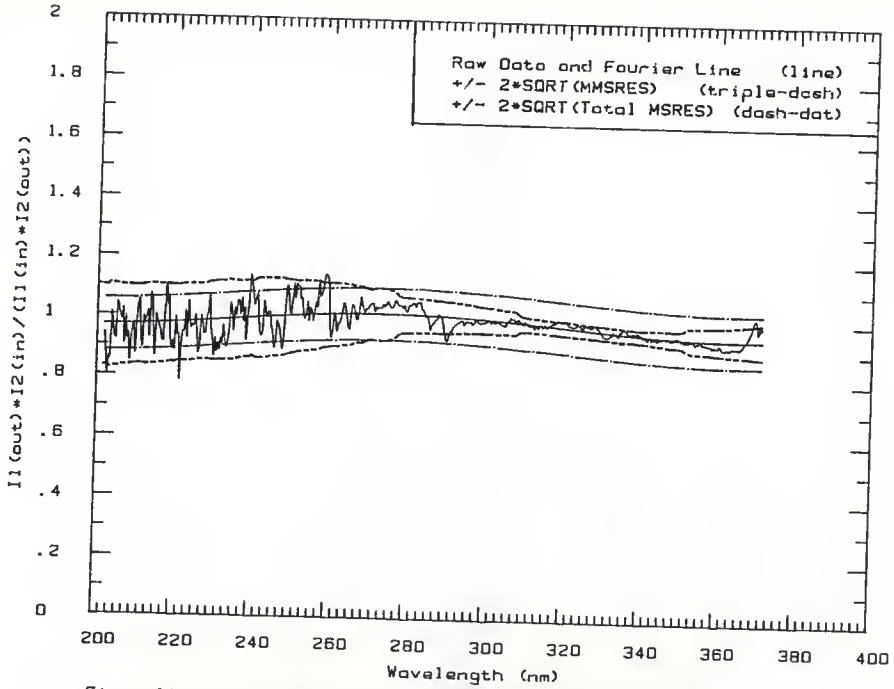

Fig. 11d Signal ratio for I1 defined in 104-138 ns time region and I2 defined during -30-0 ns region for metal-coated mirror 7L, irradiated in position A.

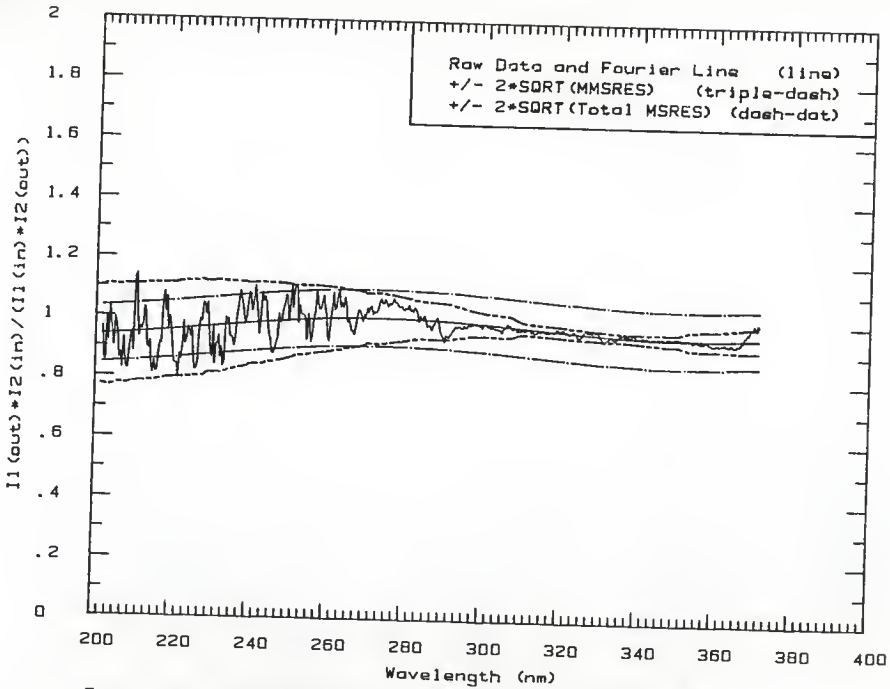

Fig. 11e Signal ratio for I1 defined in 138-171 ns time region and I2 defined during -30-0 ns region for metal-coated mirror 7L, irradiated in position A.

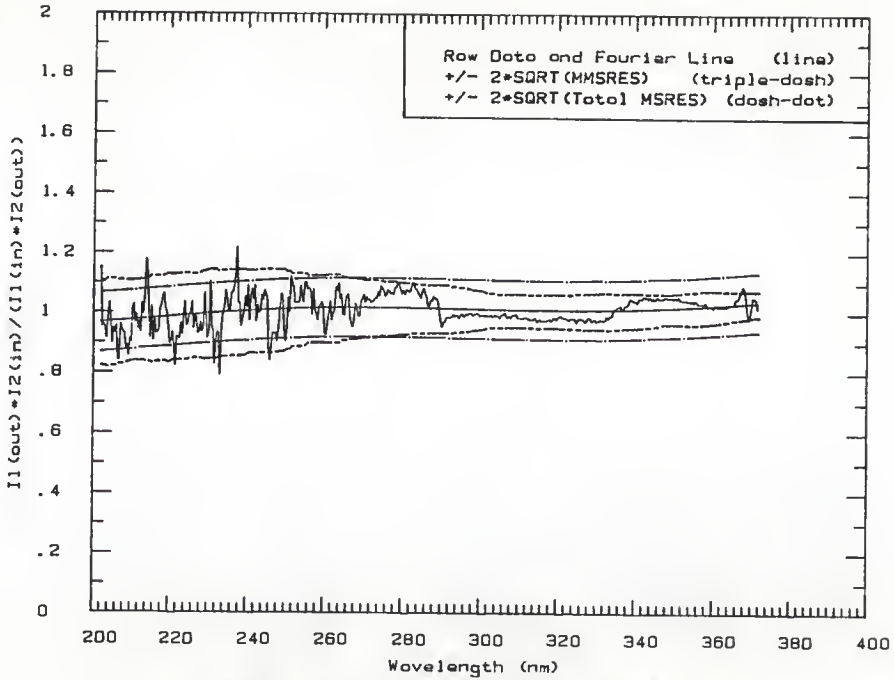

Fig. 11f Signal ratio for I1 defined in 171-205 ns time region and I2 defined during -30-0 ns region for metal-coated mirror 7L, irradiated in position A.

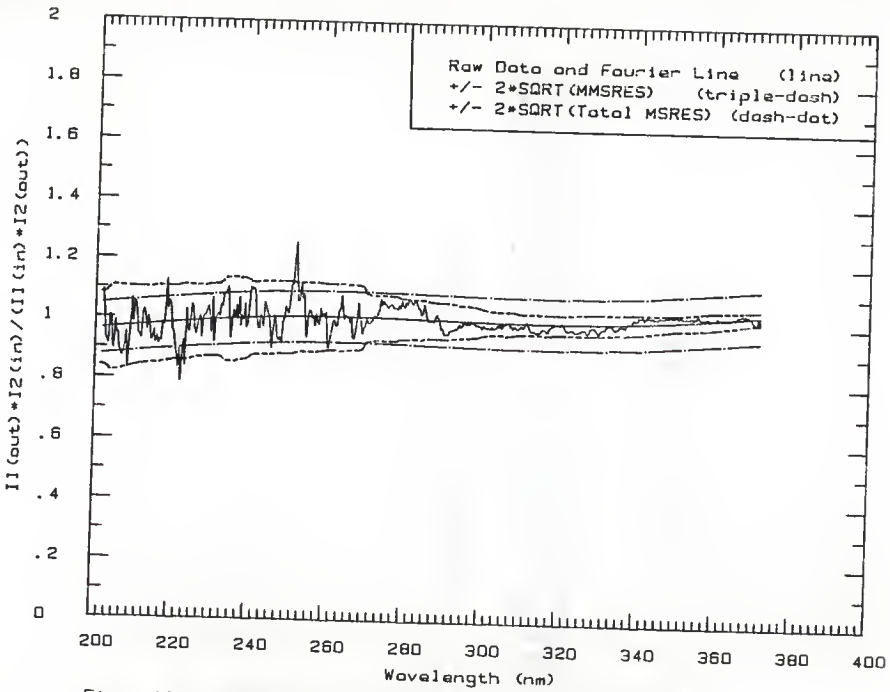

Fig. 11g Signal ratio for I1 defined in 205-238 ns time region and I2 defined during -30-0 ns region for metal-coated mirror 7L, irradiated in position A.

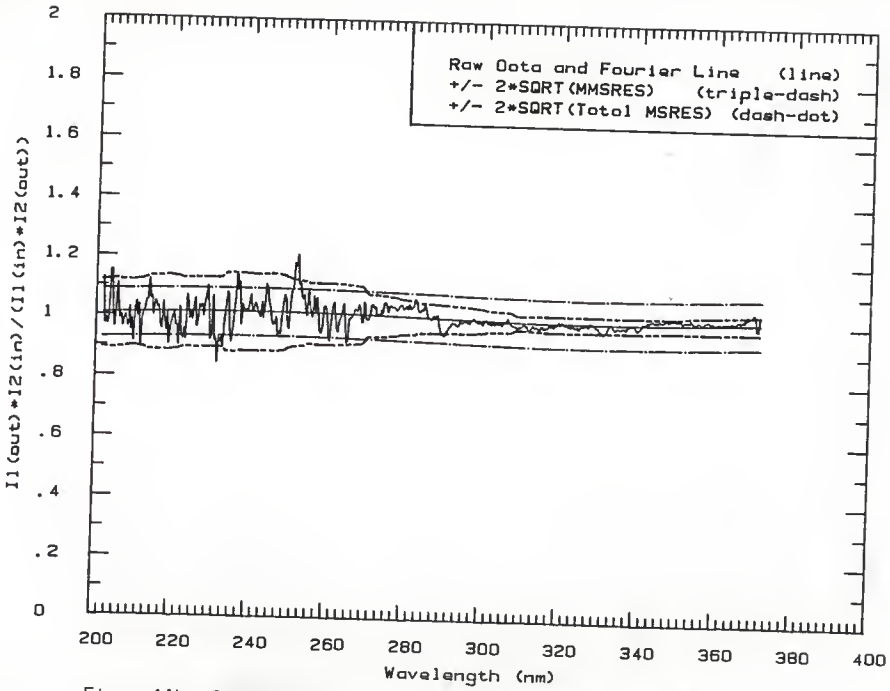

Fig. 11h Signal ratio for I1 defined in 238-272 ns time region and I2 defined during -30-0 ns region for metal-coated mirror 7L. irradiated in position A.

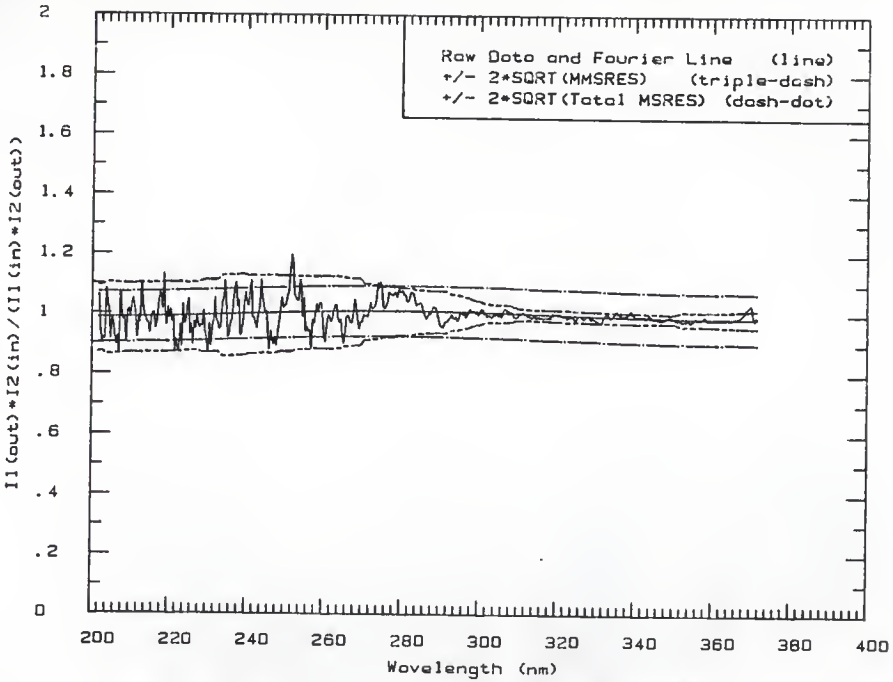

Fig. 11i Signal ratio for I1 defined in 272-313 ns time region and I2 defined during -30-0 ns region for metal-coated mirror 7L, irradiated in position A.

Figures 12a to 12j, the signal-ratio plots for metal-coated mirror 7L, irradiated in position B. The mean beam current for the block out-irradiation was 225 mA while the pulse length was 500 ns.

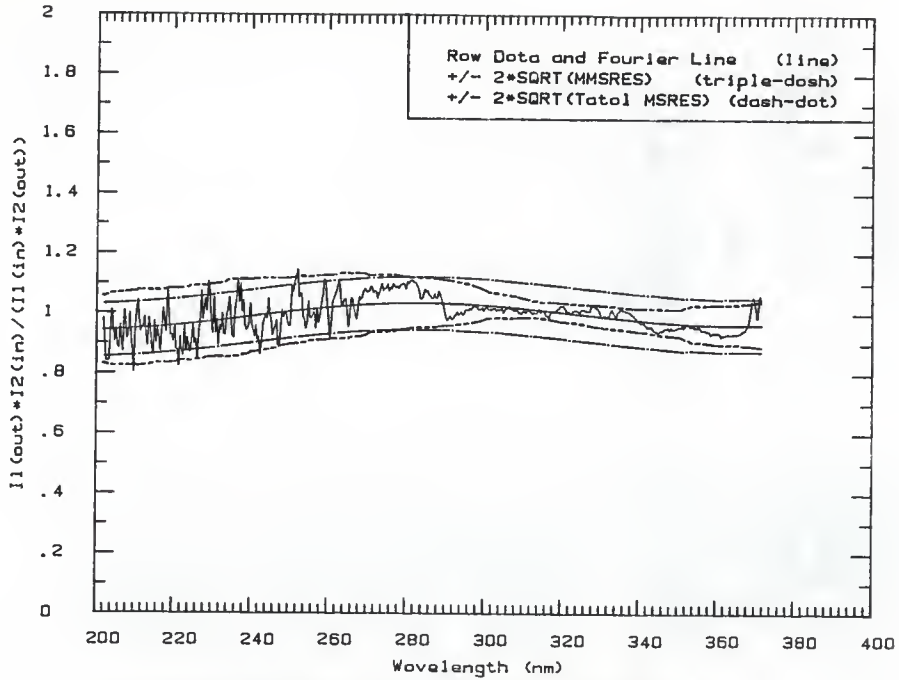

Fig. 12o Signal ratio for I1 defined in 250-284 ns time region and I2 defined during -30-0 ns region for metal-coated mirror 7L, irradiated in position 8.

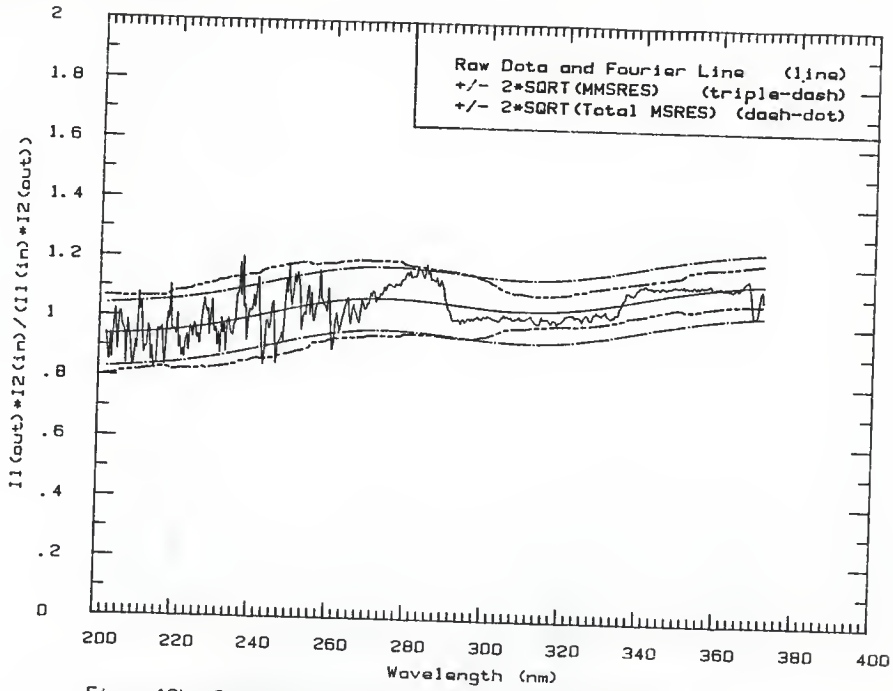

Fig. 12b Signal ratio for I1 defined in 284-317 ns time region and I2 defined during -30-0 ns region for metal-coated mirror 7L, irradiated in position 8.

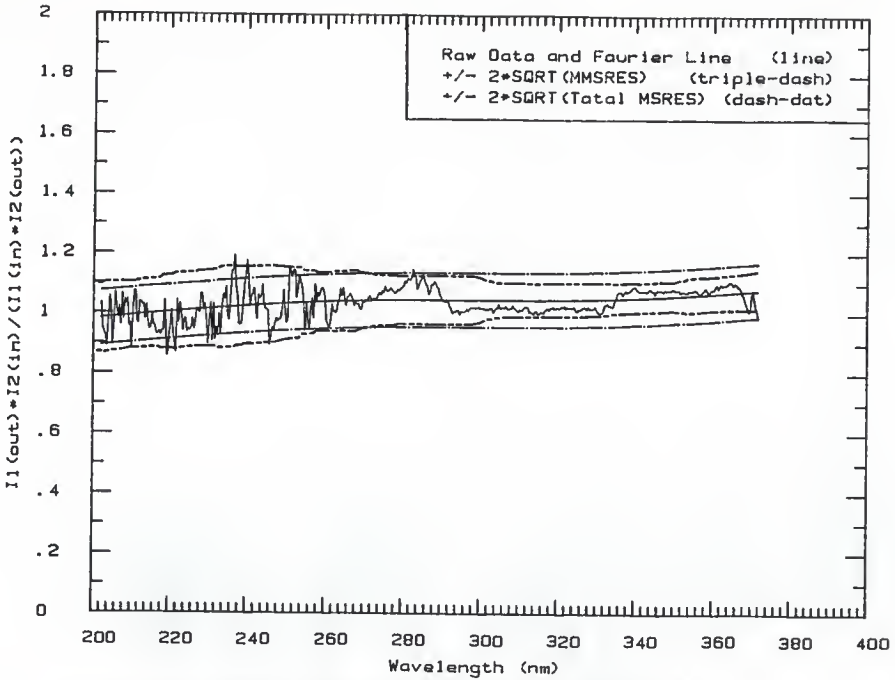

Fig. 12c Signal ratio for I1 defined in 317-351 ns time region and I2 defined during -30-0 ns region for metal-coated mirror 7L. irradiated in position 8.

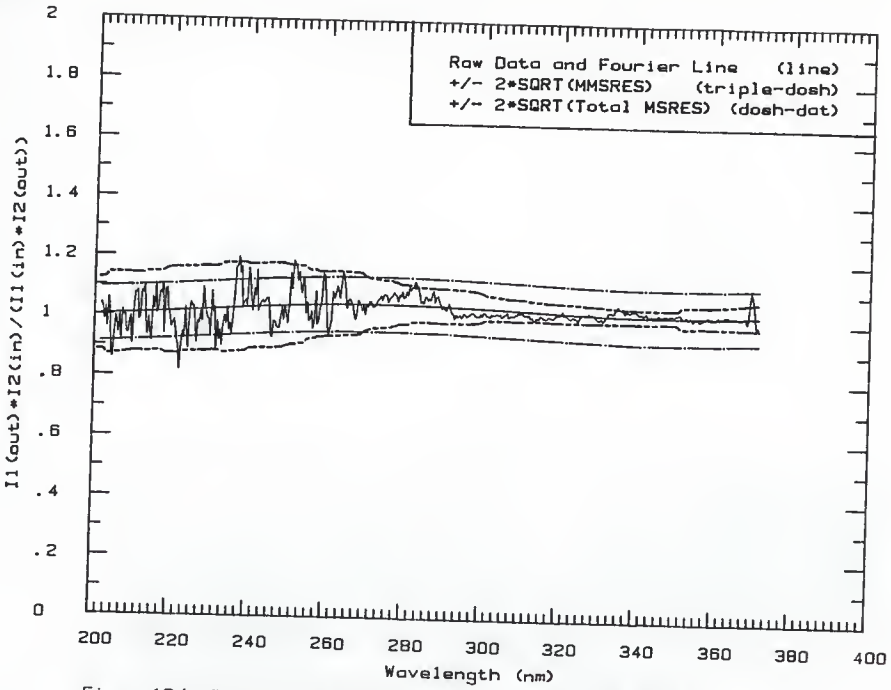

Fig. 12d Signal ratio for I1 defined in 351-384 ns time region and I2 defined during -30-0 ns region for metal-coated mirror 7L, irradiated in position 8.

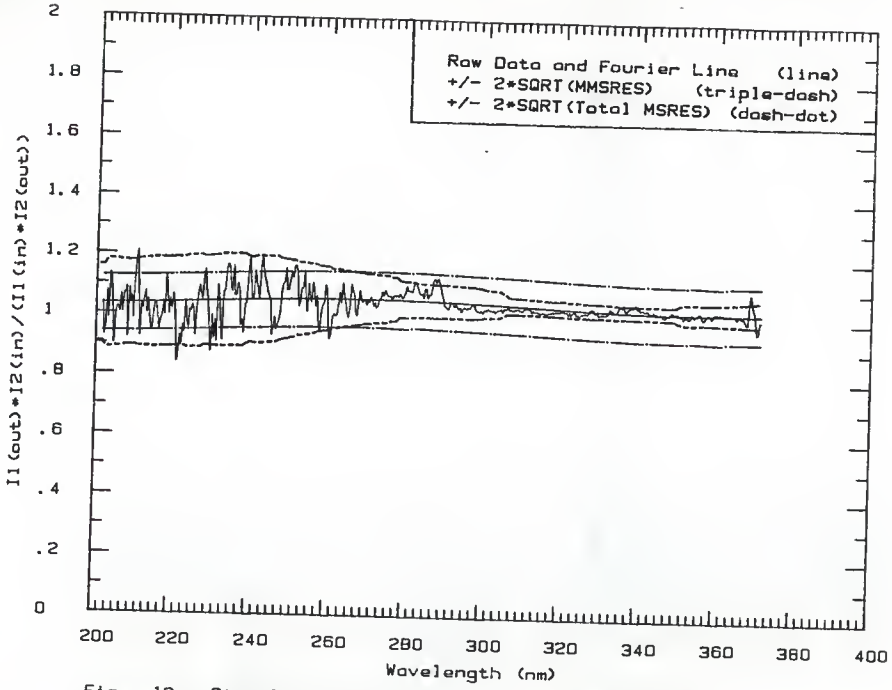

Fig. 12e Signal ratio for I1 defined in 384-418 ns time region and I2 defined during -30-0 ns region for metal-coated mirror 7L, irradiated in position B.

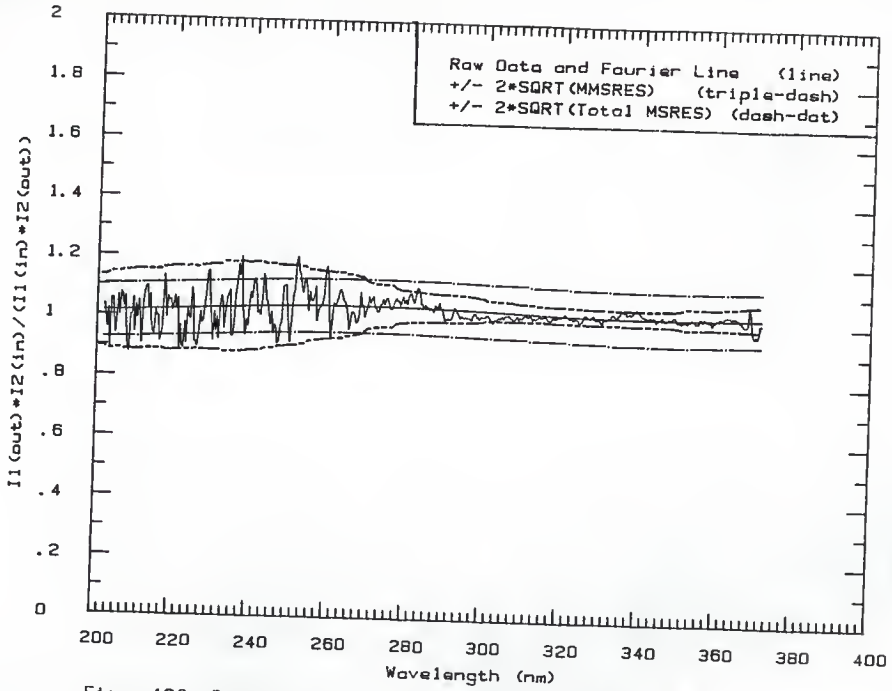

Fig. 12f Signal ratio for I1 defined in 418-451 ns time region and I2 defined during -30-0 ns region for metal-coated mirror 7L, irradiated in position 8.

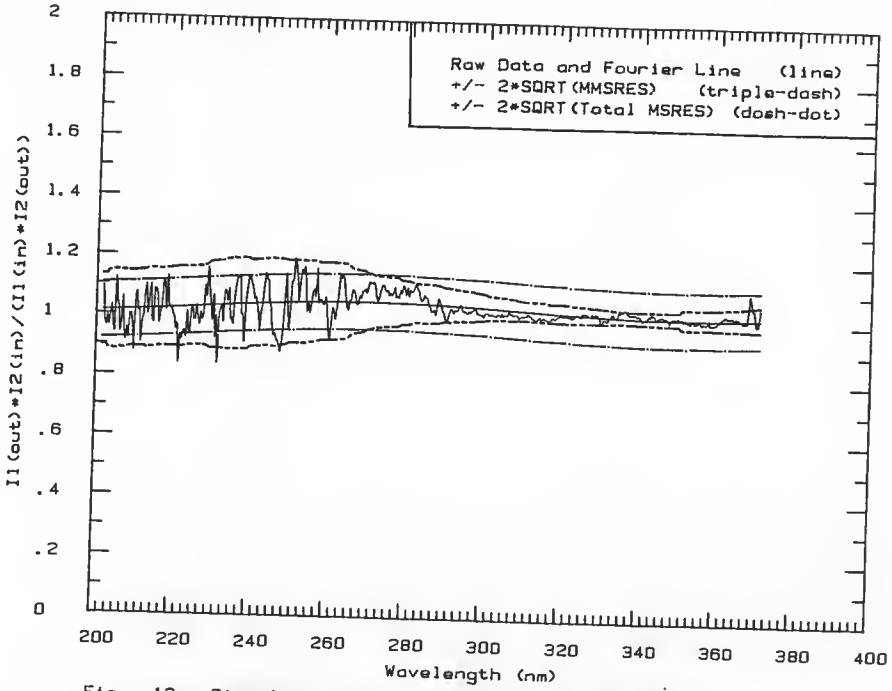

Fig. 12g Signal ratio for I1 defined in 451-485 ns time region and I2 defined during -30-0 ns region for metal-coated mirror 7L, irradiated in position 8.

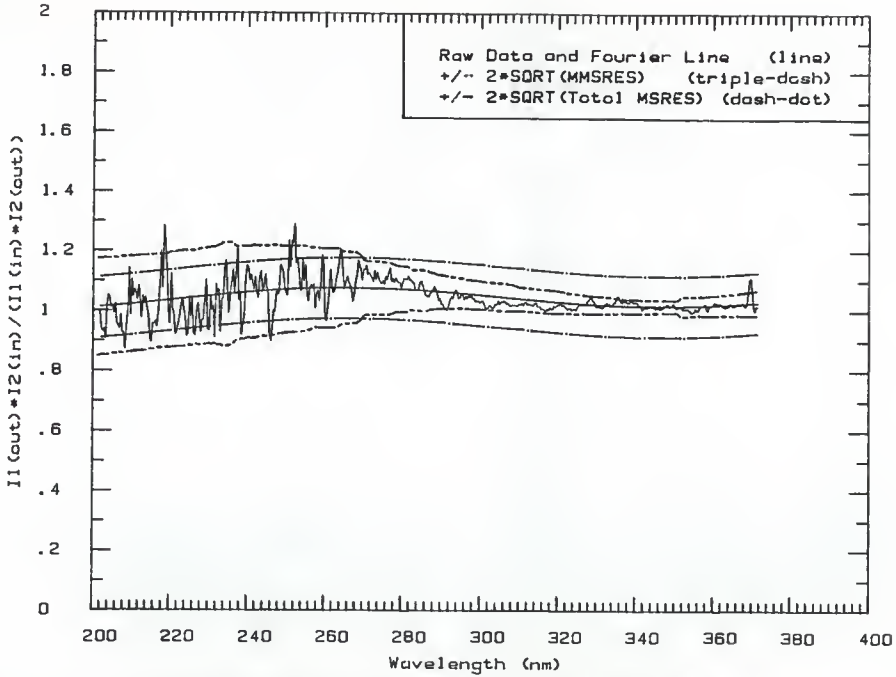

Fig. 12h Signal ratio for I1 defined in 485-518 ns time region and I2 defined during -30-0 ns region for metal-coated mirror 7L, irradiated in position 8.

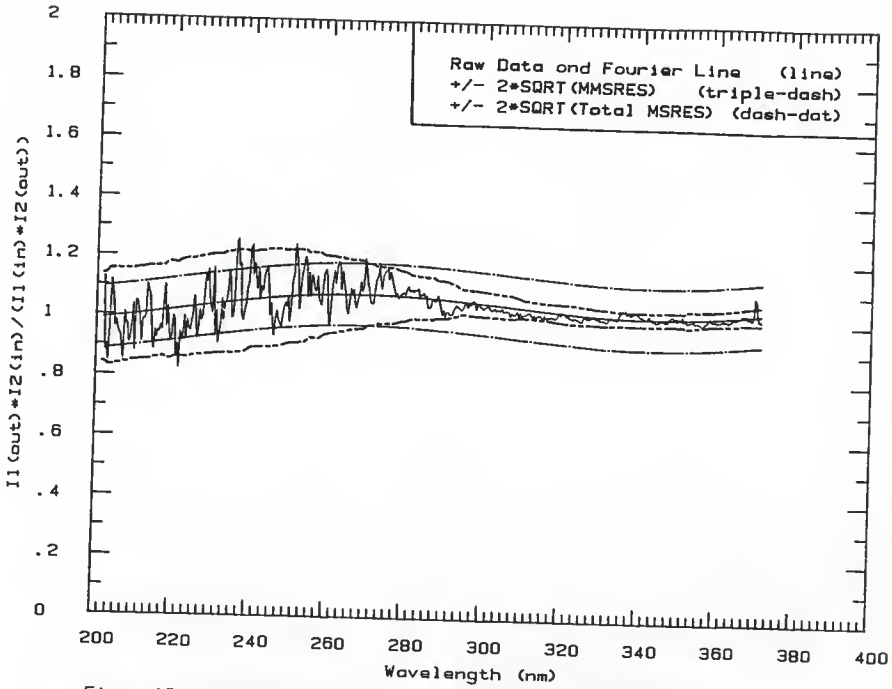

Fig. 12i Signal ratio for I1 defined in 518-552 ns time region and I2 defined during -30-0 ns region for metal-coated mirror 7L, irradiated in position B.

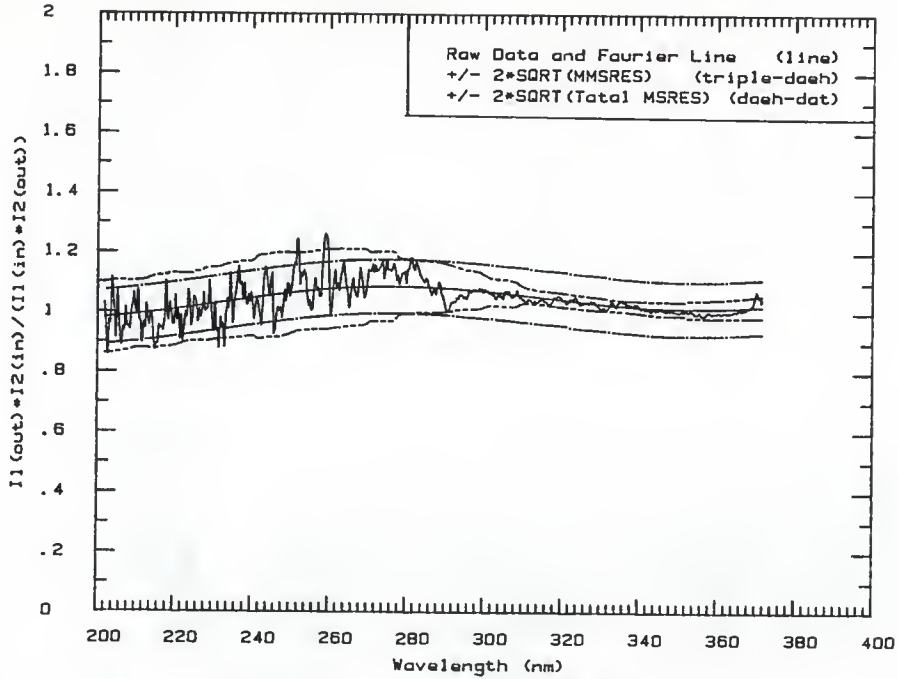

Fig. 12j Signal ratio for I1 defined in 552-593 ns time region and I2 defined during -30-0 ns region for metal-coated mirror 7L, irradiated in position 8.

Appendix B: Programs used in data analysis

Program "BINTOASCII" used to convert binary data into ASCII format for the KSU Mainframe.

```
      PROGRAM BINTOASCII                ! Convert binary direct access files
!+
! VERSION:       1-001
!
! FACILITY:      Standalone Program
!
! ABSTRACT:      This program is used to convert 944 block binary direct
!                access Streak Camera data files to ASCII form.
!
! ENVIRONMENT:   User Mode
!
! AUTHOR:        Mark Probert, EG&G Energy Measurements, 130 Robin Hill Road,
!                Goleta, CA 93117                  CREATION DATE: 27-May-1986
!-

!++
! FUNCTIONAL DESCRIPTION:
!
!               Convert 944 block Streak Camera binary files to ascii.
!               The program should be installed as a VMS foreign command:
!
!                       $ BINTOASCII :== $disk:[directory]BINTOASCII.EXE
!
!               The only input needed on the command line is the name of
!               a binary file, eg. $ BINTOASCII LPA304.0AT .  An output
!               file with the same filename but an extension of *.TXT*
!               will be used.
!
!
!               Streak Camera video image
!
!                    IXS                                          IXE
!                     |                                           |
!                     ---------------------------------------------
!                     |      |      |      |      |      |      |
!                     | scan | scan |      | scan | scan | scan | scan
!                     | line | line |      | line | line | line | line
!                     |      |      |      |      |      |      |
!                  t  |      |      | scan |      |      |      |
!                  i  |      |      | line |      |      |      |
!                  m  |      |      |      |      |      |      |
!                  e  |      |      | scan - 612 integer*2 binary nos.
!                     |      |      |      |      |      |      |
!                     V      |      |      |      |      |      |
!                     |      |      |      |      |      |      |
!                     V      V      V      V      V      V      V
!                     ---------------------------------------------
!                            <--------- wave length ---------
!
!
```

```
!
!           A Streak Camera image is a  digitized video frame consisting
!           of 512 by 512 pixels. 512 pixels in the time direction
!           form a scanline.  Each scanline is at a constant wavelength.
!
!           A scanline is stored as 512 integer*2 binary values.  Since
!           each record in the data file contains 512 bytes and we are
!           using integer*2 data, it takes two records to make up a
!           complete scanline.
!
!           These particular Streak Camera files have 944 512-byte
!           binary records. The first two records contain information
!           about the image and the last 942 records contain pairs of
!           records.  The first record contains 2 data items.  The
!           first two bytes contain the integer*2 variable IXS and the
!           second two bytes contain the integer*2 variable IXE.  These
!           variables tell the the range of scanlines saved from the
!           Streak Camera image, i.e. IXS is the scan number of the first
!           scanline in the file, and IXE is the last.  These numbers
!           needed because a full image need not be saved into a data
!           file.  The rest of the first record is garbage, and so is
!           all of the second record in the file.
!
!           Note that the polaroid images included with this package
!           have rotated the image pi/2 radians counter-clockwise.
!--

      IMPLICIT INTEGER (A-Z)

C     Variable Declarations
      INTEGER*2       BUFFER(256)
      INTEGER*2       IXS, IXE
      CHARACTER*132   INFILE, OUTFILE

C     Function Declarations
      LOGICAL*4 IS_ODD

      EQUIVALENCE(IXS,BUFFER(1))
      EQUIVALENCE(IXE,BUFFER(2))

C     Open the Input File
      STATUS = LIB$GET_FOREIGN(INFILE,,LEN,)
      OPEN (1,NAME=INFILE(1:LEN),TYPE='OLD',ACCESS='DIRECT',
     1       RECORDSIZE=128,ERR=9900)

C     Open the Output File
      I = INDEX(INFILE,' ')
      OUTFILE = INFILE(1:I)//'.TXT'
      OPEN (2,FILE=OUTFILE,TYPE='NEW',CARRIAGECONTROL='LIST')

C     Read the image frame information
      READ(1'1) BUFFER
      WRITE(2,1000) IXS,IXE
      LINE_NUMBER = IXS
      READ(1'2) BUFFER                    ! Garbage
1000  FORMAT(2I10)

C     Read the scanlines
      DO I = 3,944
          IF(IS_ODD(I) .EQ. .TRUE.) THEN        ! Do this every other record
              WRITE (2,1010) CHAR(12)           ! Put a form-feed in file
              WRITE (2,1020) LINE_NUMBER        ! Let'em know which line we are on
```

```
            LINE_NUMBER = LINE_NUMBER+1
        END IF
        READ(1'I) BUFFER
        DO J = 1,256,16
            WRITE(2,1030) (BUFFER(K),K=J,J+15)
        END DO
    END DO

1010    FORMAT(A1)
1020    FORMAT('Scanline Number ',I3)
1030    FORMAT(16I5)

        CLOSE (2)
        CLOSE (1)

        GO TO 9999

9900    TYPE 9910, INFILE(1:LEN)
9910    FORMAT ('The file ',A<LEN>,' could not be opened.')

9999    CONTINUE
        END

        FUNCTION IS_ODD(INT_VAL)
!++
!       Determine if INT_VAL is an odd number
!--
        IMPLICIT INTEGER (A-Z)
        I = INT_VAL/2
        IF ((INT_VAL - I*2) .EQ. 1) THEN
            IS_ODD = .TRUE.
        ELSE
            IS_ODD = .FALSE.
        END IF
        RETURN
        END
```

```
Scanline Number  10
  82   98  103   89   70   87   77   03   87   88  105  104  100   96   64   76
  79   86   66   84  110  101   93   03   05   66   70   75   87   90   77   03
  03   80   93   87   00   83   02   70   85   97  102   84   02   80   82   00
 101   87   88   94   77   89  102   82   05   77   83   02   03   79   87   75
  66   70   79   80   71   77   00   07   67   72   76   72   99   93   66   82
  84   84   70   77   81   87   81   66   68   88   80   05  111   66   78   75
  60   69   03   87   77   72   69   75   66   85   65   03   80   76   70   63
  84   78   81   64   04   69   76   09   06   00   01   03   75   03   68   70
  77   76   75   51   95   01   83   66   63   74   73   77   66   62   56   62
  75   63   69   59   56   62   50   48   73   66   71   66   76   63   73   64
  70   60   76   71   75   74   60   61   60   65   03   62   72   50   68   45
  68   59   69   87   79   60   79   64   79   69   72   67   70   60   67   80
  67   75   75   60   60   52   71   75   59   40   41   50   45   54   51   47
  71   65   61   70   62   62   73   62   45   61   73   77   56   73   58   62
  62   50   58   60   61   62   49   53   55   57   66   64   71   58   69   64
  55   63   62   50   61   63   60   61   60   60   53   56   44   54   76   77
  62   55   50   62   62   61   63   64   51   67   60   69   64   60   66   60
  62   37   51   50   44   57   62   60   64   71   45   40   65   64   63   80
  60   58   63   67   62   40   64   61   60   60   60   70   54   44   60   59
  42   61   51   42   66   59   67   66   71   43   51   40   73   64   56   53
  52   56   71   72   49   65   64   66   49   58   57   61   59   87   64   66
  70   70   55   81   60   69   53   66   55   41   72   04   67   70   63   76
  56   67   68   61   73   57   70   67   76   65   03   61   64   72   60   74
  89   70   55   62   46   67   07   78   03   05   68   64   58   71   50   75
  49   62   64   54   58   69   69   78   76   71   77   85   74   66   06   02
  84   85   71   71   04   79   66   73   72   77   63   68   72   01  104   03
  91   77   70   83   01   08   95   75   77   00   08   65   85   75   92   04
  80   78   81   61   05   80   89  102  127  116   01   83   95   89   82   03
  90   02   83   99   90   84   95   95  106  121   97  100   85   84   82  116
 102   86   99   98  116  117  119  118  114  120  107  137  144  135  131  140
 117  139  125  108   03   98  122  132  130  128  125  113  104  105   91  117
 127  119  110  128  106  127  122  107  117  115  113   85  112  116  115  106
```

Sample output of BINTOASCII

Program "INOUT" used to compare the simple-summation, trapezoidal, and Romberg integration techniques.

```
C*****************************************************************
*
C     THIS PROGRAM CALCULATES THE TOTAL INTEGRAL, OVER ALL TIMES, OF
C THE SIGNAL LIGHT INTENSITIES.  THE PROGRAM CALCULATES THE INTEGRAL
C OVER THE STARTING AND ENDING TIMES DEFINED IN TABLE 4.3 FOR EACH
C DATA FILE.  THE PROGRAM IS EXECUTED FROM AN EXEC PROGRAM.
C
C     THE PROGRAM USES THREE TECHNIQUES TO NUMERICALLY ESTIMATE THE
C VALUE OF THE TOTAL TIME INTEGRAL, THE SIMPLE-SUMMATION,
C TRAPEZOIDAL, AND ROMBERG TECHNIQUES.  EACH TECHNIQUE IS DEFINED IN
C REFERENCE 12.
C NOTE THE ROMBERG TECHNIQUE DIVIDES THE FILE INTO FOURTHS SO THE
C REQUIRED SPACING NEVER EXCEEDS THE SPACING AVAILABLE.
C*****************************************************************
C
C SET VARIABLES TO DOUBLE PRECISION
C AND DEFINE THE INPUT AND OUTPUT FILES (FN=4 AND 6 RESPECTIVELY)
C
      REAL*8 T(8,8,4),X1(16,32),TRAP(8,8),X(512),SUM,TOTAL,REL,LAMDA
      INTEGER START,FINI,I,J,K,L,M,II,KK,FN
      CHARACTER*30 STRING
      FN=4
C
C READ THE STARTING AND ENDING SCANLINE NUMBERS FOR THE INTEGRATION
C FOR TOTAL INTEGRATION OVER ALL TIMES, START=1 AND FINI=470.
C
200   READ(FN,110)START,FINI
C
C PRINT TO THE OUTPUT FILE THE HEADERS AND STARTING AND FINISHING
C SCANLINE NUMBERS.
C
      WRITE(6,150)START,FINI
      WRITE(6,170)
      WRITE(6,170)
      WRITE(6,160)
      WRITE(6,170)
C
C READ IN THE SIGNAL LIGHT INTENSITY DATA INTO ARRAY X(I)
C NEXT CALCULATE THE SIMPLE-SUMMATION INTEGRAL ESTIMATE BY SUMMING
C OVER ALL X(I).
C
      KK=0
      DO 100 II=START,FINI
      TOTAL=0.0D0
      READ(FN,130)STRING
      READ(FN,130)STRING
         DO 1 I=1,32
1        READ(FN,120)(X1(J,I),J=1,16)
      DO 6  J=1,16
         DO 5 I=1,32
```

```
          M=(I-1)*16+J
          X(M)=X1(J,I)
5         TOTAL=TOTAL+X(M)
6       CONTINUE
C
C INITIALIZE TRAPEZOIDAL AND ROMBERG ESTIMATES TO ZERO  (T AND TRAP)
C
        DO 30 I=1,8
           DO 20 J=1,8
              DO 10 K=1,4
                 T(I,J,K)=0.0D0
10               TRAP(I,J)=0.0D0
20            CONTINUE
30         CONTINUE
C
C CALCULATE THE ROMBERG ESTIMATE OF THE ENDPOINT CONTRIBUTION OF
C EACH OF THE FOUR REGIONS.
C
        T(1,1,1)=64.0D0*X(128)
        T(1,1,2)=64.0D0*(X(128)+X(256))
        T(1,1,3)=64.0D0*(X(256)+X(384))
        T(1,1,4)=64.0D0*(X(384)+X(512))
C
C CALCULATE THE COLUMN ESTIMATES FOR THE ROMBERG TECHNIQUE AND THE
C TRAPEZOIDAL ESTIMATE
C
        DO 50 J=2,8
           DO 40 K=1,4
              I=J-1
40            T(1,J,K)=(T(1,1,K)+SUM(X,J,K)*128.0D0)/(2.0D0**(J-1))
50         CONTINUE
        DO 70 J=1,8
           DO 60 K=1,4
60            TRAP(1,J)=T(1,J,K)+TRAP(1,J)
70      CONTINUE
        DO 80 L=2,8
80         CALL ROMBER(TRAP,L)
C
C CALCULATE RELATIVE ERROR BASED ON SUMMATION AND ROMBERG INTEGRALS
C AND PERFORM WAVELENGTH CALIBRATION BEFORE PRINTING RESULTS
C
        REL=100.0D0*DABS(TRAP(8,1)-TOTAL)/TRAP(8,1)
        LAMDA=-0.361D0*(II)+375.108D0
        WRITE(6,175)LAMDA,TOTAL,II,TRAP(8,1),REL
        IF(II.LT.179)WRITE(7,180)LAMDA,TRAP(8,1)/1.0D04
        IF(II.GT.170.AND.II.LT.340)WRITE(8,180)LAMDA,TRAP(8,1)/1.0D04
        IF(II.GT.330)WRITE(9,180)LAMDA,TRAP(8,1)/1.0D04
        IF(KK.NE.5)GOTO90
        WRITE(6,170)
        KK=0
```

```
90    KK=KK+1
100   CONTINUE
C
C FORMAT STATEMENTS
C
110   FORMAT(I5,I5,I5)
120   FORMAT(16F5.0)
130   FORMAT(19A)
140   FORMAT(F5.0,I5)
150   FORMAT('TIME INTEGRATION FOR SCANLINES ',I3,' TO ',I3)
160   FORMAT(' WAVELENGTH (NM)      SUM OF DATA      SCANLINE #
     C BEST ROMBERG    % REL-ERROR')
170   FORMAT('      ')
175   FORMAT(5X,F7.2,5X,F12.2,4X,I12,6X,F12.2,5X,F6.3)
180   FORMAT(3X,F9.5,5X,F9.5)
      IF(FN.EQ.5)GOTO 190
      FN=5
      GOTO 200
190   STOP
      END
      DOUBLEPRECISIONFUNCTION SUM(X,J,K)
C
C CALCULATE APPROPRIATE SUM FOR THE ROMBERG TRIANGLE BASED ON
C CURRENT GRID SIZE PARAMETER L.
C
      REAL*8 X(512)
      INTEGER J,K,L,DELTAX,M
      L=2.0D0**(J-1)-1
      DELTAX= 128/(L+1)
      SUM=0.0D0
      DO 10 I=1,L
         M=I*DELTAX+(K-1)*128
10       SUM=SUM+X(M)
      RETURN
      END
      SUBROUTINE ROMBER(TRAP,L)
C
C  CALCULATE THE NEXT MEMBER OF THE ROMBERG TRIANGLE
C
      REAL*8 TRAP(8,8)
      INTEGER K,L,I
      I=9-L
      DO 10 K=1,I
10    TRAP(L,K)=DEXP(DLOG(4.0D0)*(L-1)+DLOG(TRAP(L-1,K+1))-
      CLOG(4.0D0**C(L-1)-1.0D0))-DEXP(DLOG(TRAP(L-1,K))-
      CDLOG(4.0D0**(L-1)-1.0D0))
      RETURN
      END
```

FILE: 0314 DATA A KANSAS STATE UNIVERSITY VM/SP CMS

FILE LPA314
TIME INTEGRATION FOR SCANLINES 10 TO 139

WAVELENGTH (NM)	SUM OF DATA	SCANLINE #	BEST ROMBERG	% REL-ERROR
371.50	33009.00	10	33014.54	0.017
371.14	34037.00	11	34058.09	0.061
370.78	36609.00	12	36712.60	0.283
370.41	38515.00	13	38543.71	0.064
370.05	42196.00	14	42116.98	0.188
369.69	45255.00	15	45243.33	0.026
369.33	49298.00	16	49355.01	0.116
368.97	53091.00	17	53189.16	0.185
368.61	58384.00	18	58393.26	0.057
368.25	62389.00	19	62454.48	0.105
367.89	66306.00	20	66382.54	0.115
367.53	68826.00	21	68763.42	0.091
367.17	73109.00	22	73192.41	0.114
366.80	75670.00	23	75660.04	0.013
366.44	78758.00	24	78766.21	0.010
366.08	79905.00	25	79862.85	0.053
365.72	83042.00	26	83214.43	0.207
365.36	85009.00	27	85069.23	0.071
365.00	87706.00	28	87655.43	0.058
364.64	88012.00	29	87981.09	0.035
364.28	89526.00	30	89586.62	0.068
363.92	89946.00	31	89923.31	0.020
363.56	91626.00	32	91571.45	0.060
363.19	93035.00	33	93229.43	0.230
362.83	93295.00	34	93180.71	0.111
362.47	95423.00	35	95520.91	0.105
362.11	97321.00	36	97297.72	0.024
361.75	96955.00	37	97023.51	0.153
361.39	98133.00	38	98114.21	0.019
361.03	97796.00	39	97955.63	0.156
360.67	97017.00	40	96984.70	0.033
360.31	94130.00	41	94253.83	0.131
359.95	92626.00	42	92719.32	0.089
359.59	91757.00	43	91698.33	0.064
359.22	91410.00	44	91348.54	0.151
358.86	91842.00	45	91900.49	0.064
358.50	92765.00	46	92724.17	0.044
358.14	92510.00	47	92723.34	0.187
357.78	92235.00	48	92065.44	0.184
357.42	91722.00	49	92242.68	0.343
357.06	92726.00	50	92678.95	0.051

Sample output from program "INOUT"

Program "TRANS" used to calculate the time integrations for the signal-ratio plots.

```
C ***********************************************************************
C   THIS PROGRAM CALCULATES THE INTEGRAL OVER A DEFINED TIME SEGMENT
C USING THE TRAPEZOIDAL ESTIMATE.  THE USER MUST DEFINE THE NUMBER
C OF INTEGRATING REGIONS, NIR, AND THE STARTING AND ENDING CHANNEL
C NUMBER FOR EACH OF THESE REGIONS.  SEE THE SAMPLE HEADER INPUT
C FILE IMMEDIATELY FOLLOWING THE PROGRAM.  RECALL THE SCANLINE
C NUMBERS DEFINE SPECIFIC WAVELENGTHS WHILE THE CHANNEL NUMBERS
C DEFINE SPECIFIC TIMES FOR THE SIGNAL INTENSITY DATA.  THE PROGRAM
C ALSO CALCULATES THE INTEGRAL OF THE SIGNAL LIGHT INTENSITY FOR
C DEFINED WAVELENGTHS IN THE SOFT (THE SIGNAL LIGHT INTENSITY AS
C FUNCTION OF TIME) CALCULATIONS. THE PROGRAM IS EXECUTED FROM AN
C EXEC FILE.
C ***********************************************************************
C
C BEGIN BY DEFINING THE PRECISION AND THE INPUT AND OUTPUT FILES,
C INPUT FN=4, OUTPUT FN=6, AND 10 TO 32.
C
      REAL*8 TOT(100),X1(16,32),X(512),SOFT(512),TOTAL,TIME,TSTART,
     $SWL,EWL,LAMDA
      INTEGER IR(100),START,FINI,I,J,K,L,M,N,II,FN,KK,NIR,
     $FLAG,FN2,NPAGE
      CHARACTER*30 STRING
      FN=4
C
C READ IN HEADER DATA AND TIME CALIBRATION INFORMATION (TIME &
C TSTART)
C
200   READ(FN,110)START,FINI,NIR,TIME,TSTART
      DO 10 I=1,512
10    SOFT(I)=0.0D0
      FLAG=0
      READ(FN,190)(IR(I),I=1,NIR+1)
      READ(FN,*)SWL,EWL
      WRITE(6,170)
      WRITE(6,150)START,FINI
      WRITE(6,170)
      WRITE(6,170)
      WRITE(6,160)
      WRITE(6,170)
      KK=0
C
C READ IN THE SIGNAL LIGHT INTENSITY DATA
C
      DO 100 II=START,FINI
         DO 15 I=I,NIR
15       TOT(I)=0.0D0
         TOTAL=0.0D0
         READ(FN,130)STRING
         READ(FN,130)STRING
```

```
          DO 1 I=1,32
1         READ(FN,120)(X1(J,I),J=1,16)
          DO 6 J=1,16
             DO 5 I=1,32
                M=(I-1)*16+J
                X(M)=X1(J,I)
5            TOTAL=TOTAL+X(M)
6         CONTINUE
          TOTAL=TOTAL-(X(1)+X(512))/2.0D0
C
C NOW, FOR EACH INTEGRATED TIME REGION, CALCULATE THE AREA USING
C THE TRAPEZOIDAL ESTIMATE.
C
          DO 50 J=1,NIR
             DO 40 I=IR(J),IR(J+1)
40           TOT(J)=TOT(J)+X(I)
          TOT(J)=TOT(J)-(X(IR(J))+X(IR(J+1)))/2.0D0
50        CONTINUE
C
C PERFORM A WAVLENGTH CALIBRATION.  IF THE WAVELENGTH IS OUTSIDE OF
C THE REGION DEFINED FOR THE WAVELENGTH INTEGRATION, DO NOT INCLUDE
C THE SIGNAL LIGHT INTENSITY DATA IN THE WAVELENGTH INTEGRATION
C ESTIMATE.
C
          LAMDA=-0.361D0*(II)+375.108D0
          IF(LAMDA.LT.SWL)GOTO 70
          IF(LAMDA.GT.EWL)GOTO 70
          FLAG=1
C
C PERFORM INTEGRATION OVER DEFINED WAVELENGTH BAND I.E.
C SWL<LAMDA<EWL.
C
C NEXT PRINT OUT THE RESULTS OF THE WAVELENGTH AND TIME INTEGRATIONS
C
          DO 60 I=1,512
60           SOFT(I)=X(I)+SOFT(I)
70        WRITE(6,175)LAMDA,TOTAL/1.0D04,TOT(1)/1.0D04,TOT(2)/1.0D04
          DO 80 I=1,NIR
          FN2=9+I
80        WRITE(FN2,180)LAMDA,TOT(I)/1.0D04
          IF(KK.NE.5)GOTO90
          WRITE(6,170)
          KK=0
90        KK=KK+1
100    CONTINUE
       WRITE(6,170)
109    IF(FLAG.EQ.0)GOTO 300
       WRITE(1,170)
       WRITE(1,170)
       WRITE(1,170)
```

```
      WRITE(1,171)SWL,EWL
      WRITE(1,170)
      WRITE(1,181)
      WRITE(1,170)
      WRITE(1,170)
C
C PERFORM TIME CALIBRATION FOR HARD COPY
C
      DO 108 I=1,512
108      WRITE(1,191)TSTART+TIME*(I-1),SOFT(I)
C
C FORMAT STATEMENTS
C
110   FORMAT(3I5,2E10.3)
120   FORMAT(16F5.0)
130   FORMAT(19A)
150   FORMAT('TIME INTEGRATION FOR SCANLINES ',I3,' TO ',I3)
160   FORMAT(' WAVELENGTH (NM)      TRAP INTEGRAL      TOT( 1)
     $TOT(2)')
170   FORMAT('  ')
171   FORMAT('WAVELENGTH INTEGRATION OVER ',F7.2,' TO ',F7.2)
175   FORMAT(2X,F7.2,14X,F7.2,7X,F7.2,9X,F7.2)
180   FORMAT(2F7.2)
181   FORMAT('  TIME(NS)        WAVELENGTH INTEGRAL')
190   FORMAT(11I5)
191   FORMAT(2F9.2)
300   END
C BELOW IS A SAMPLE HEADER FILE USED TO SUPPLY THE BASIC
C INFORMATION NECESSARY FOR PROGRAM EXECUTION.  IN THE FIRST LINE
C NUMBERS CORRESPOND TO :
C 1&2. STARTING AND ENDING SCNALINES FOR CURRENT INTEGRATION (10,
C      139)
C   3. THE NUMBER OF DEFINED TIME REGIONS (10)
C 4&5. THE TIME PER CHANNEL SLOPE AND THE STARTING TIME FOR THE TIME
C      CALIBRATION (0.67 AND 250)
C
C ON THE SECOND LINE THE ELEVEN NUMBERS ARE USED TO DEFINE THE
C CHANNEL NUMBERS WHERE ONE TIME REGION ENDS AND THE OTHER STARTS.
C THE NUMBER OF DATA POINTS ON THIS LINE ALWAYS EQUALS THE NUMBER OF
C.INTEGRATING REGIONS PLUS ONE.
C
C FINALLY, ON THE LAST LINE, THE STARTING AND ENDING WAVELENGTHS,
C SWL AND EWL, ARE GIVEN FOR INTEGRATION OF THE SIGNAL LIGHT
C INTENSITY OVER WAVELENGTH.
C
C NOTE THE PRECISION OF EACH DATA POINT IN THE HEADER AFFECTS PROPER
C EXECUTION.  DEFINE ALL VALUES ACCORDING TO PROPER PRECISION.
```

```
C  10  139   10     0.67D0    250.0D0
C   1   50  100  150  200  250  300  350  400  450  512
C  245.0D0    255.0D0
```

Appendix C: Transient Reflectivity Plots

Figures 13a to 13r, the transient relfectivity plots for dielectric mirror 14, irradiated in position A. The block-out mean beam current was 5 A while the pulse length was 20 ns.

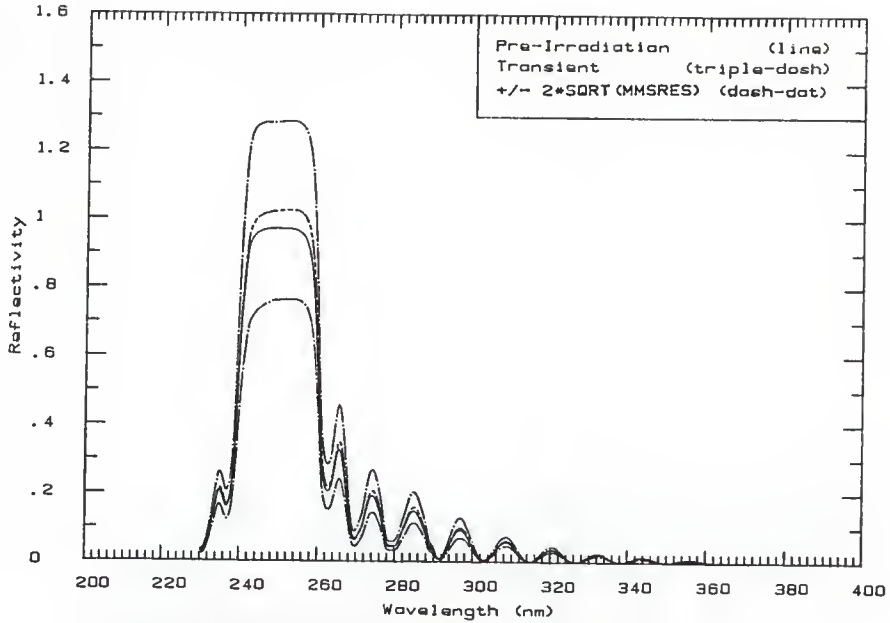

Fig. 13a The pre-irradiation reflectivity compared to the transient reflectivity based on Fig. 1a. (0.0-5.0 ns), for dielectric mirror 14.

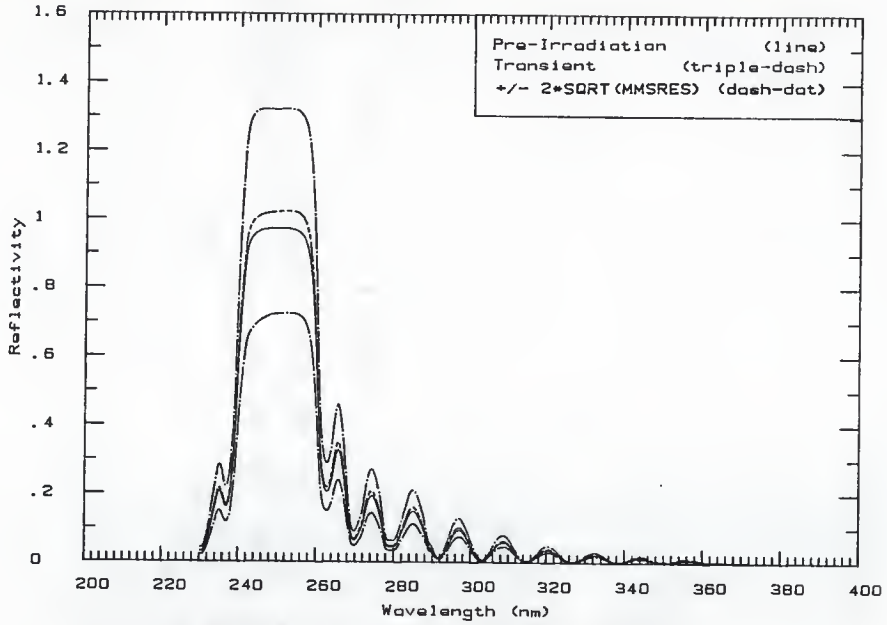

Fig. 13b The pre-irradiation reflectivity compared to the transient reflectivity based on Fig. 1b. (5.0-10.0 ns), for dielectric mirror 14.

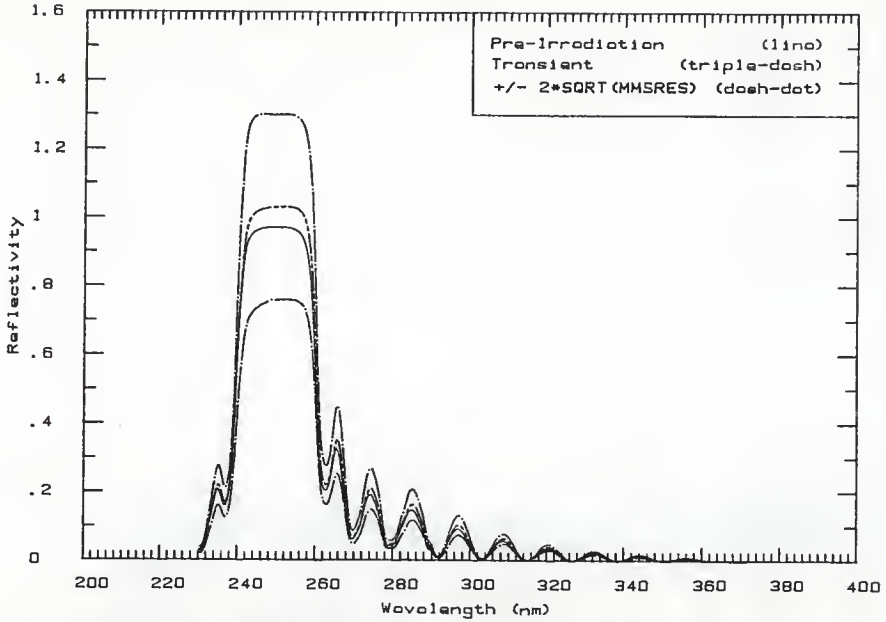

Fig. 13c The pre-irradiation reflectivity compared to the transient reflectivity based on Fig. 1c. (10.0-15.0 ns), for dielectric mirror 14.

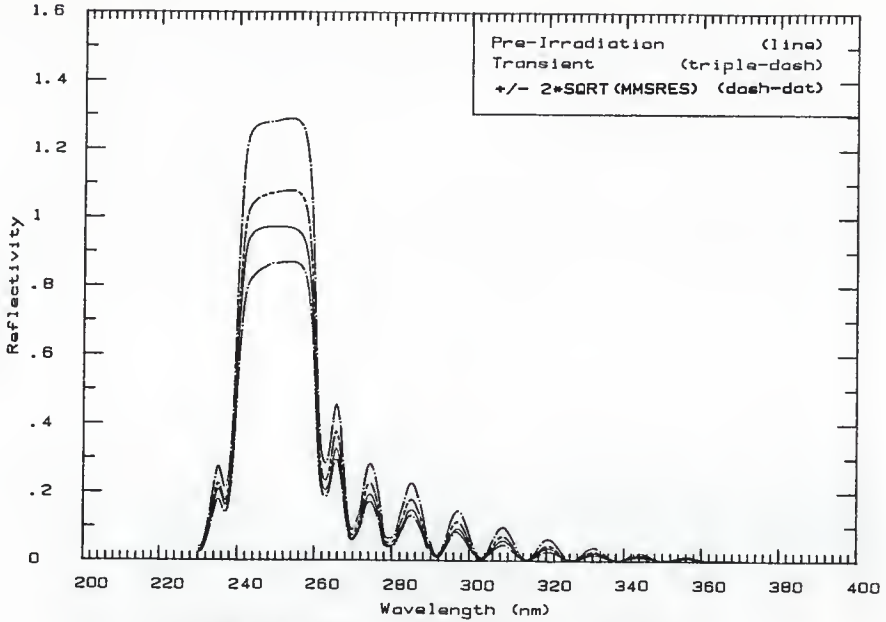

Fig. 13d The pre-irradiation reflectivity compared to the transient reflectivity based on Fig. 1d. (15.0-20.0 ns), for dielectric mirror 14.

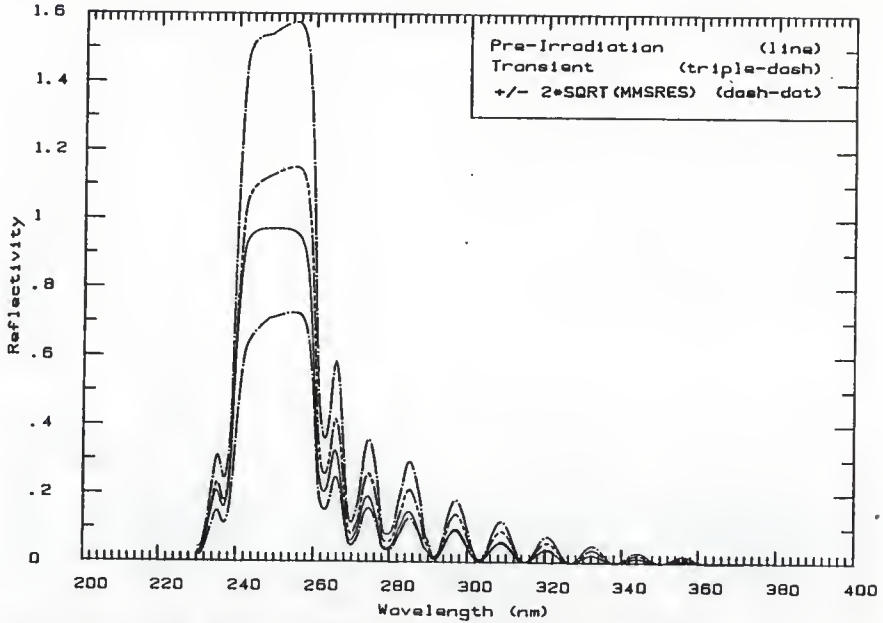

Fig. 13a The pre-irradiation reflectivity compared to the transient reflectivity based on Fig. 1e. (20.0-25.0 ns), for dielectric mirror 14.

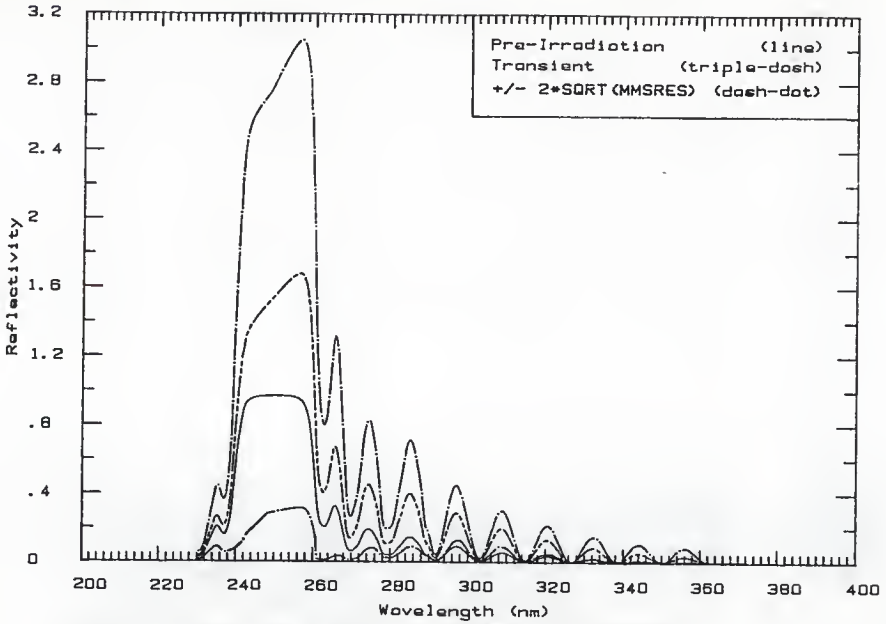

Fig. 13f The pre-irradiation reflectivity compared to the transient reflectivity based on Fig. 1f, (25.0-41.3 ns), for dielectric mirror 14.

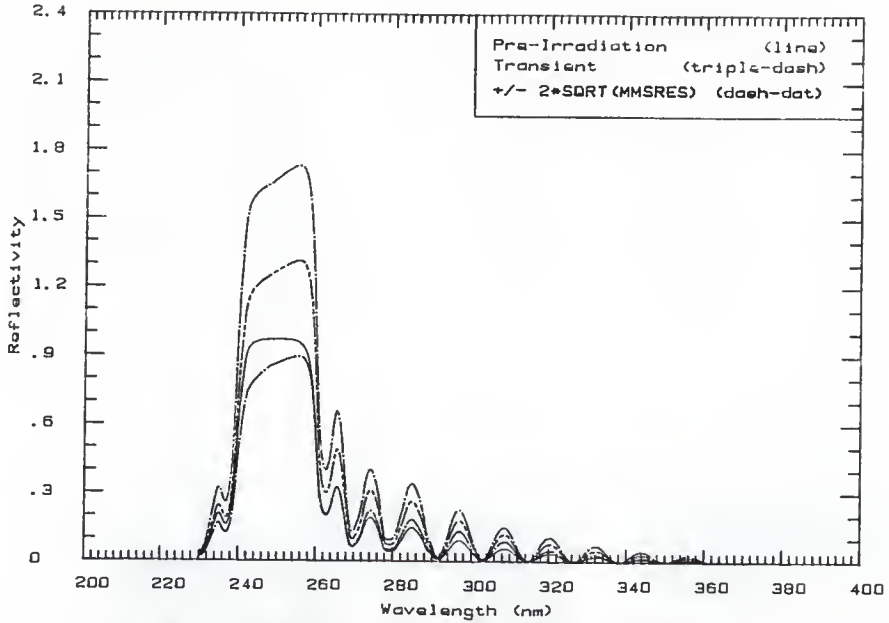

Fig. 13g The pre-irradiation reflectivity compared to the transient reflectivity based on Fig. 1g. (41.3-57.5 ns), for dielectric mirror 14.

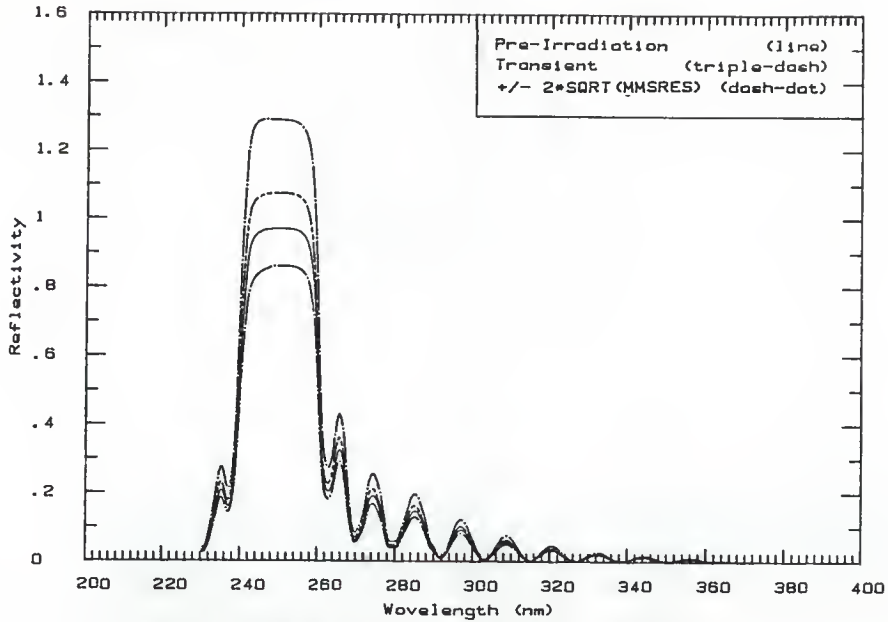

Fig. 13h The pre-irradiation reflectivity compared to the transient reflectivity based on Fig. 1h. (57.5-73.8 ns). for dielectric mirror 14.

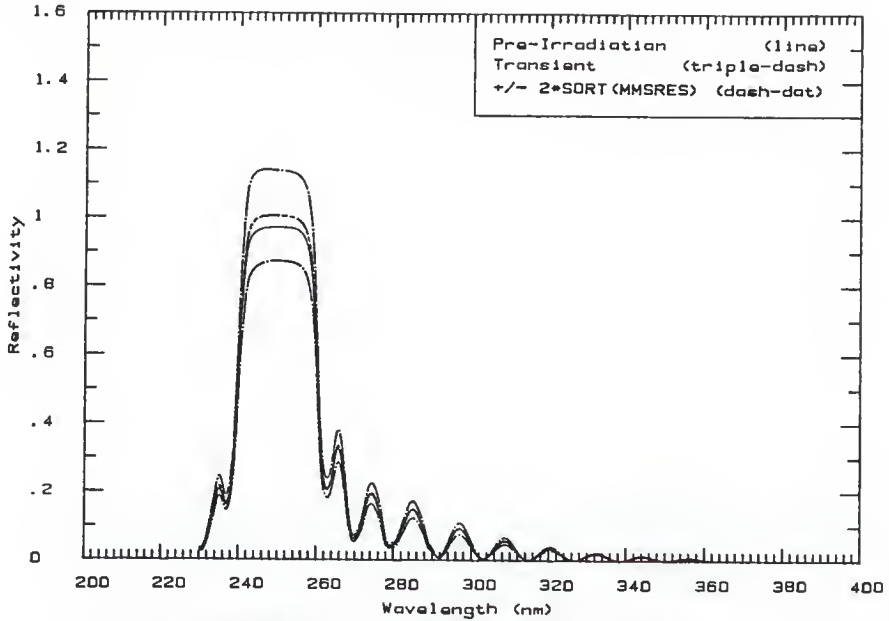

Fig. 13i The pre-irradiation reflectivity compared to the transient reflectivity based on Fig. 11. (73.8-88.0 ns), for dielectric mirror 14.

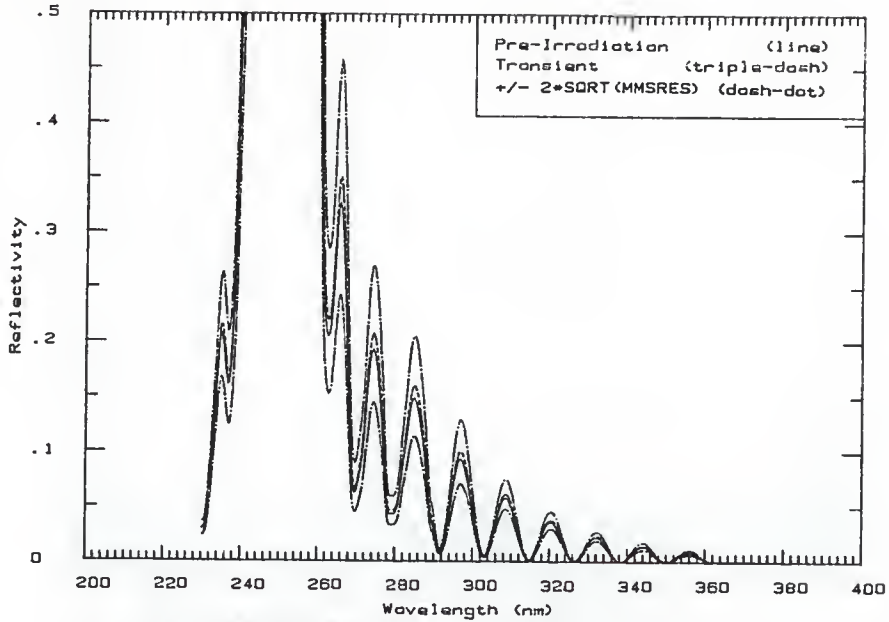

Fig. 13j The expanded view of the pre-irradiation and transient reflectivities of Fig. 13a for dielectric mirror 14.

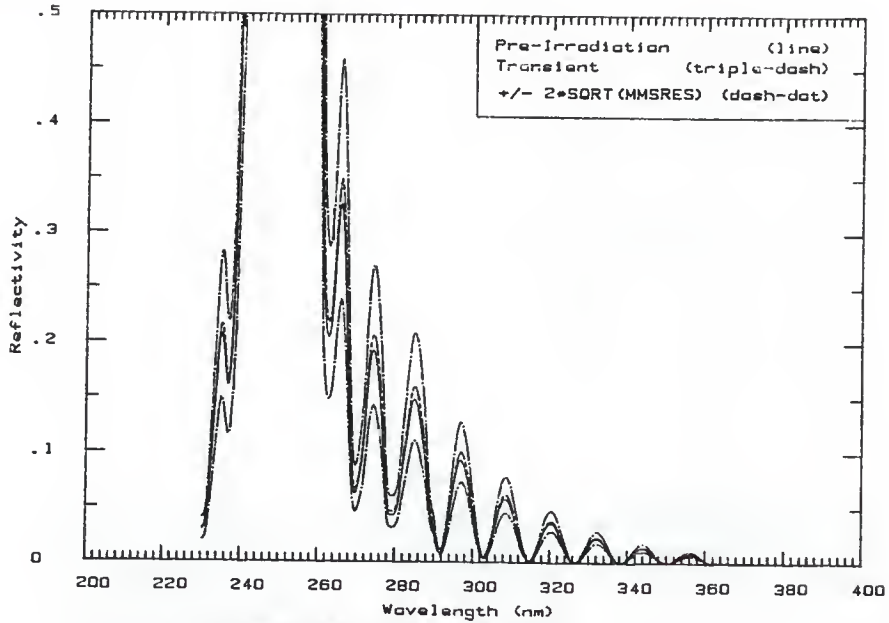

Fig. 13k The expanded view of the pre-irradiation and transient reflectivities of Fig. 13b for dielectric mirror 14.

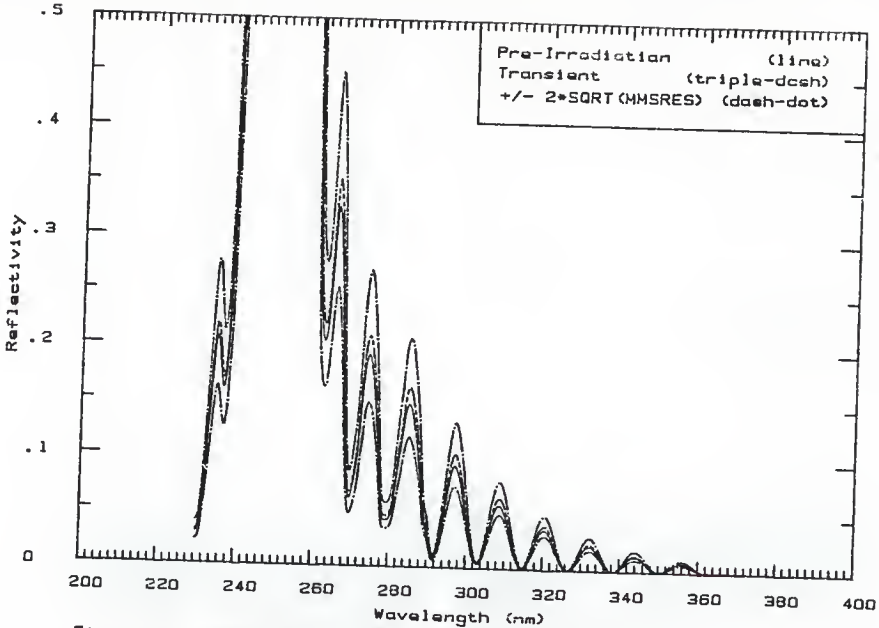

Fig. 131 The expanded view of the pre-irradiation and transient reflectivities of Fig. 13c for dielectric mirror 14.

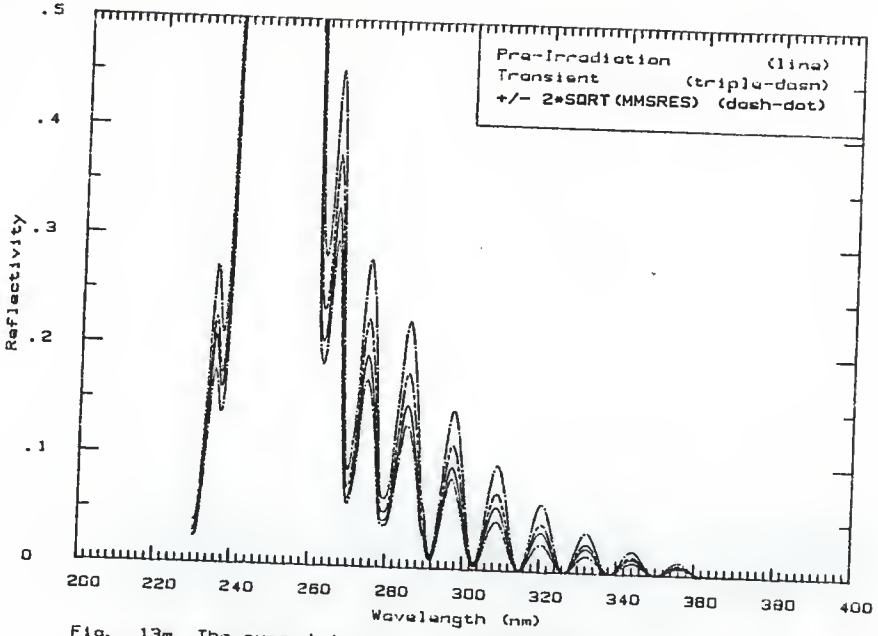

Fig. 13m The expanded view of the pre-irradiation and transient reflectivities of Fig. 13d for dielectric mirror 14.

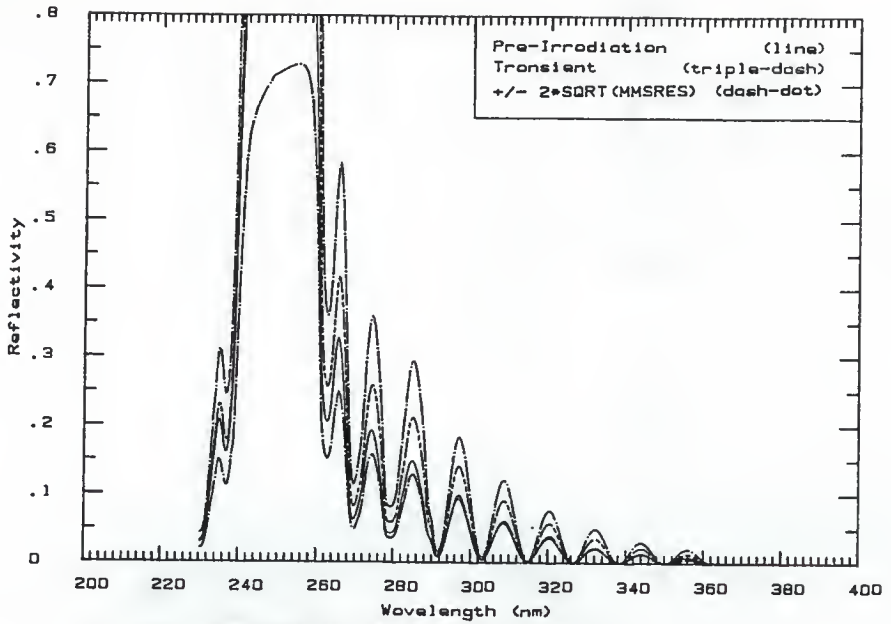

Fig. 13n The expanded view of the pre-irrodiotion and tronsient reflectivities of Fig. 13e for dielectric mirror 14.

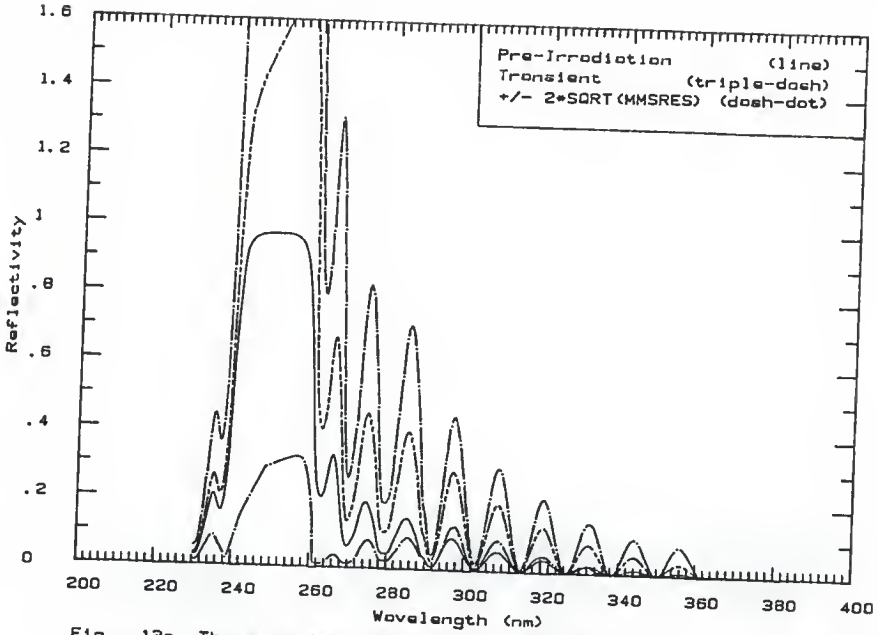

Fig. 13e The exponded view of the pre-irradiation and transient reflectivities of Fig. 13f. for dielectric mirror 14.

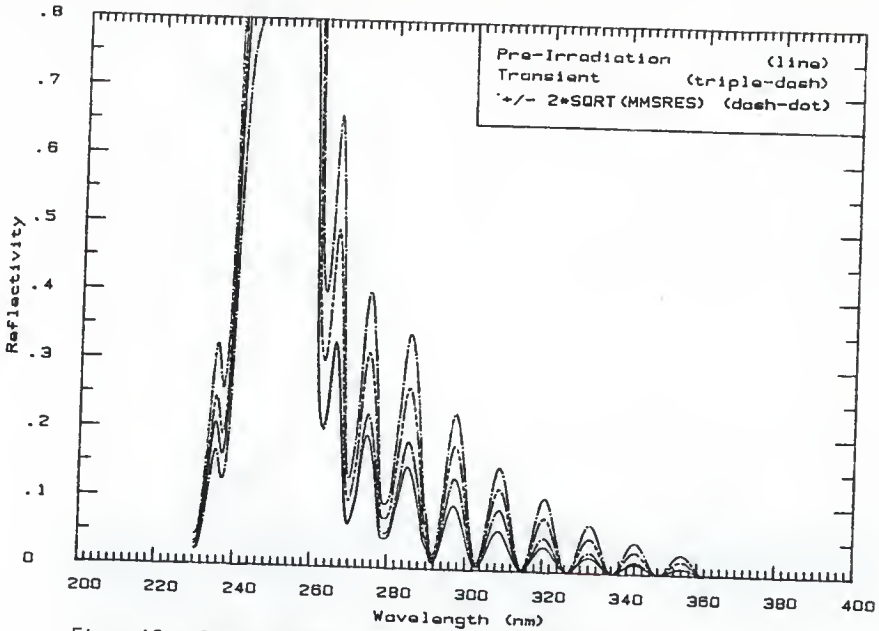

Fig. 13p The expanded view of the pre-irrodiotion and transient reflectivities of Fig. 13g for dielectric mirror 14.

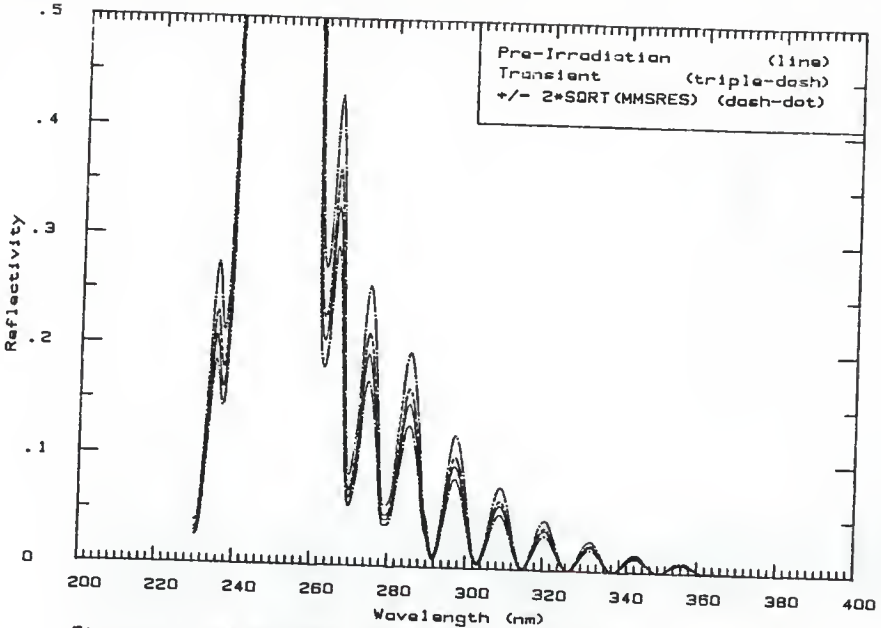

Fig. 13g The expanded view of the pre-irradiation and transient reflectivities of Fig. 13h for dielectric mirror 14.

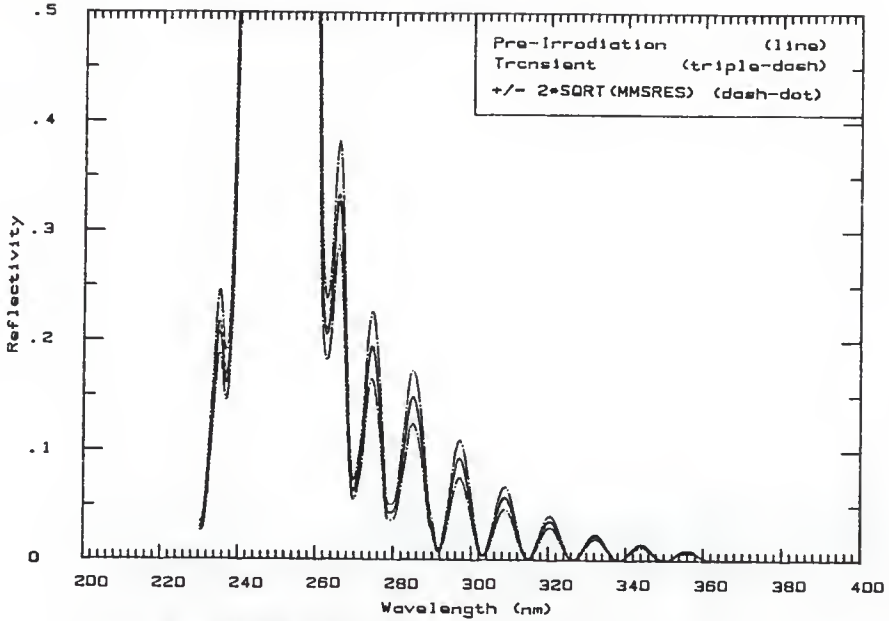

Fig. 13r The exponded view of the pre-irradiation and transient reflectivities of Fig. 13i for dielectric mirror 14.

Figures 14a to 14r, the transient reflectivity plots for dielectric mirror 12, irradiated in position A. The block-out mean beam current was 225 mA while the pulse length was 500 ns.

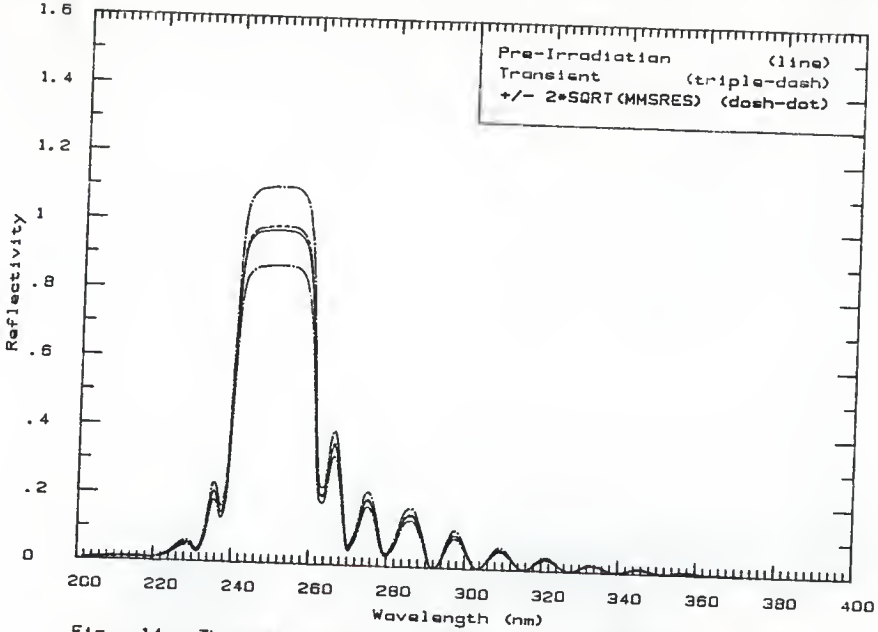

Fig. 14a The pre-irradiation reflectivity compared to the transient reflectivity based on Fig. 2a. (0.0-37.0 ns), for dielectric mirror 12 in position A.

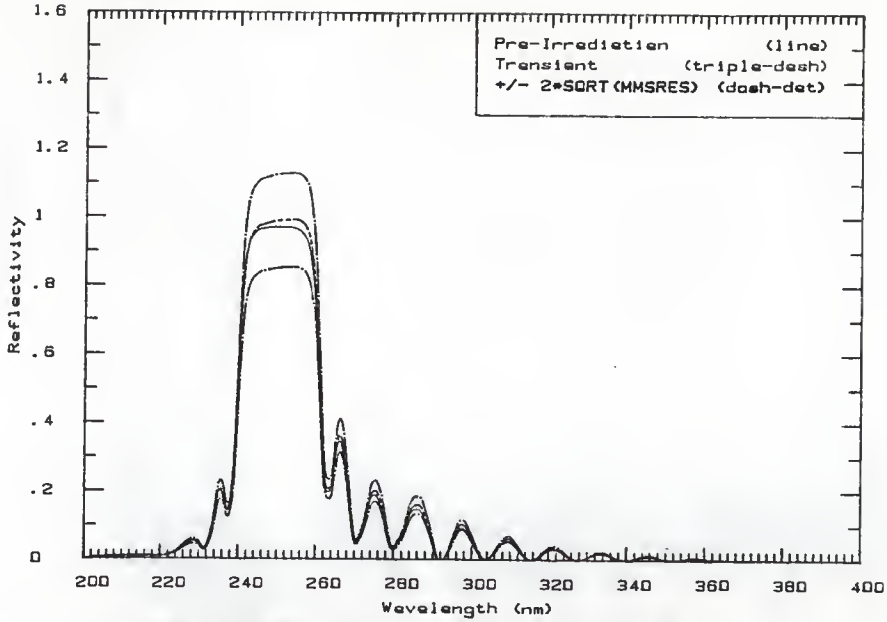

Fig. 14b The pre-irradiation reflectivity compared to the transient reflectivity based on Fig. 2b, (37.0 -70.5 ns), for dielectric mirror 12 in position A.

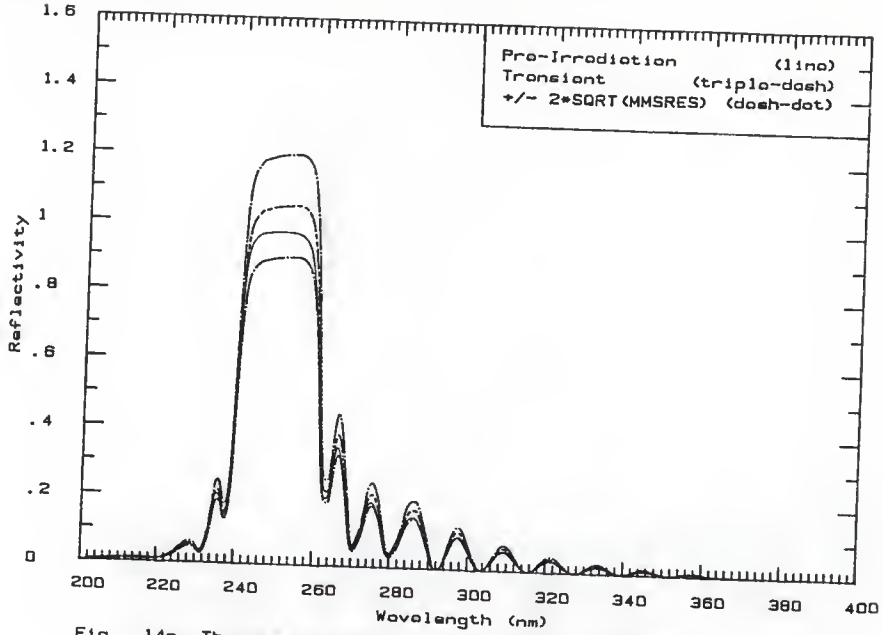

Fig. 14c The pre-irrodiotion reflectivity comporod to the tronsiont reflectivity bosod on Fig. 2c. (70.5 -104 ns). for dioloctric mirror 12 in position A.

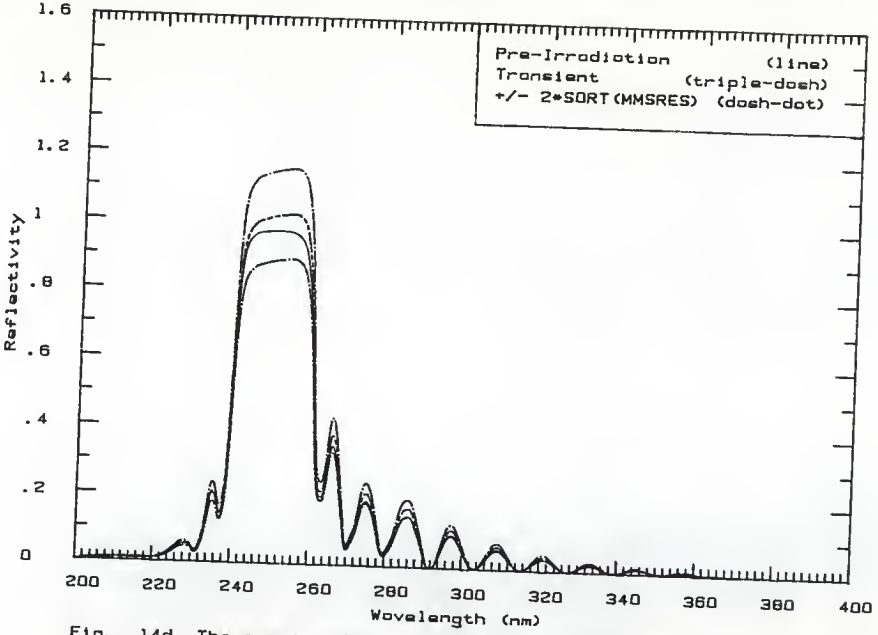

Fig. 14d The pre-irradiation reflectivity compared to the transient reflectivity based on Fig. 2d. (104-138 ns). for dielectric mirror 12 in position A.

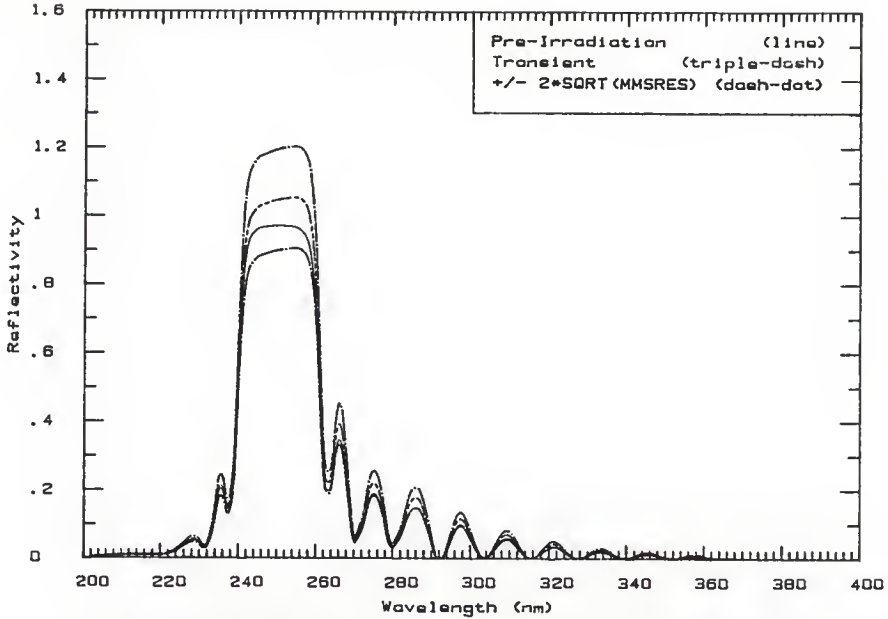

Fig. 14e The pre-irradiation reflectivity compared to the transient reflectivity based on Fig. 2e. (138-171 ns). for dielectric mirror 12 in position A.

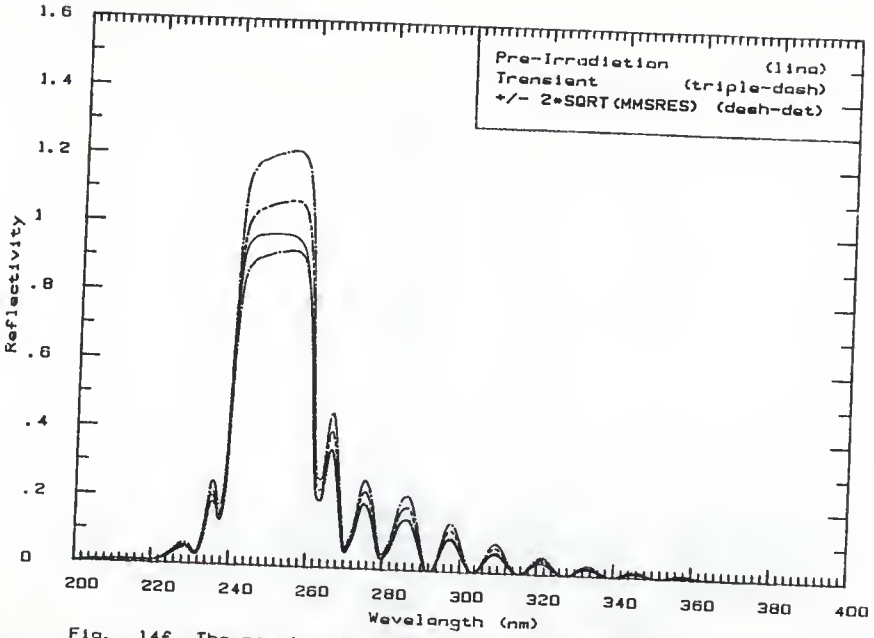

Fig. 14f The pre-irradiation reflectivity compared to the transient reflectivity based on Fig. 2f. (171-205 ns), for dielectric mirrer 12 in position A.

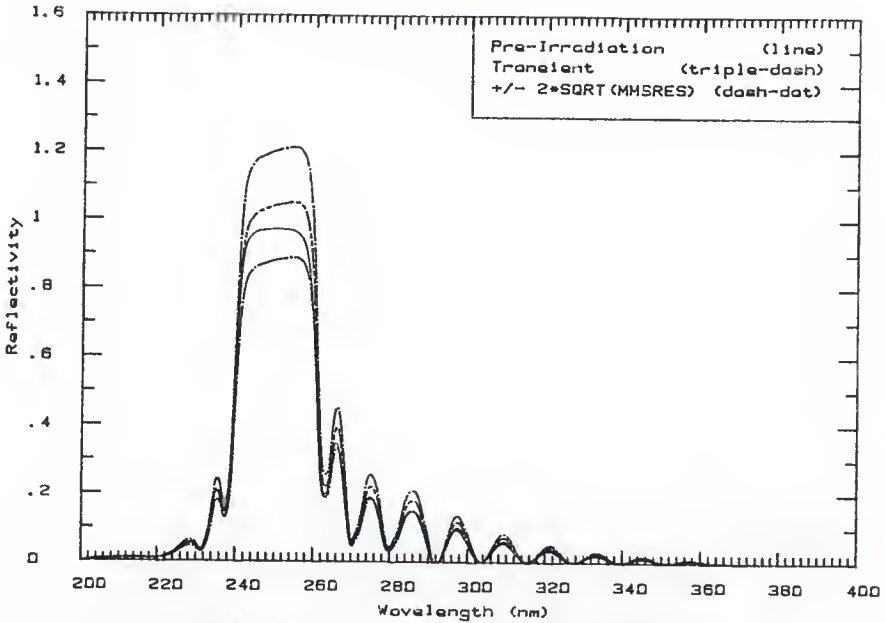

Fig. 14g The pre-irradiation reflectivity compared to the transient reflectivity based on Fig. 2g. (205-238 ns), for dielectric mirror 12 in position A.

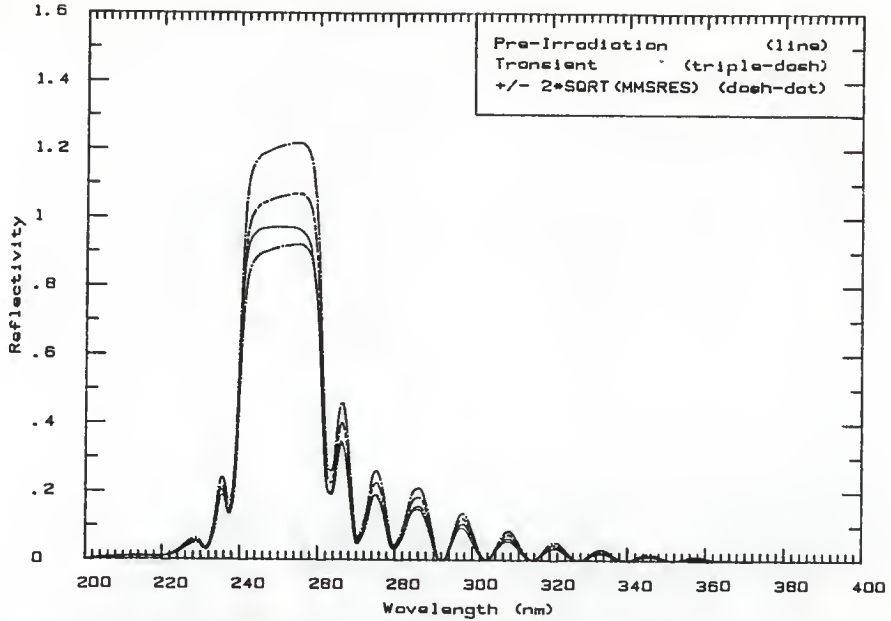

Fig. 14h The pre-irradiation reflectivity compared to the transient reflectivity based on Fig. 2h. (238-272 ns). for dielectric mirror 12 in position A.

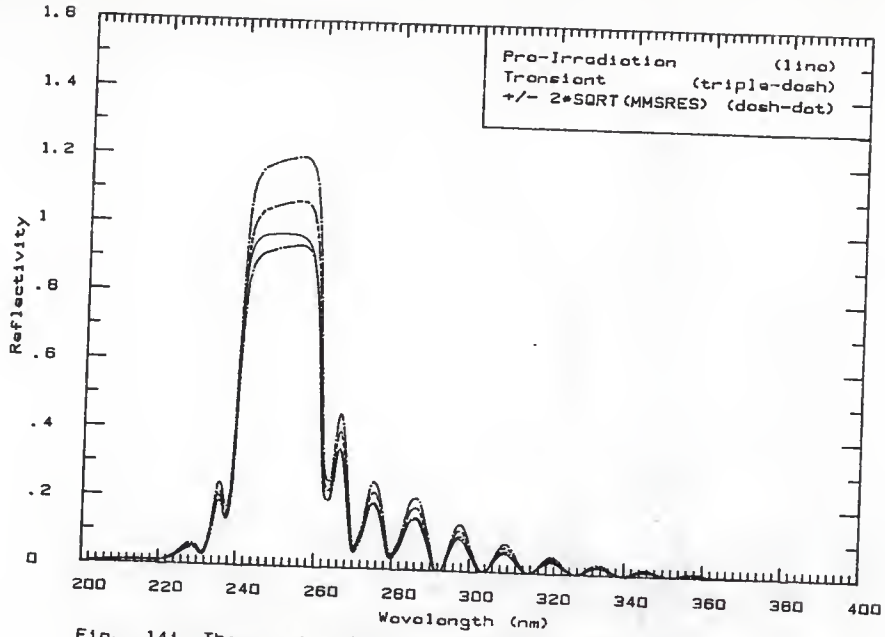

Fig. 141 The pre-irradiation reflectivity compared to the transient reflectivity based on Fig. 21. (272-313 ns). for dielectric mirror 12 in position A.

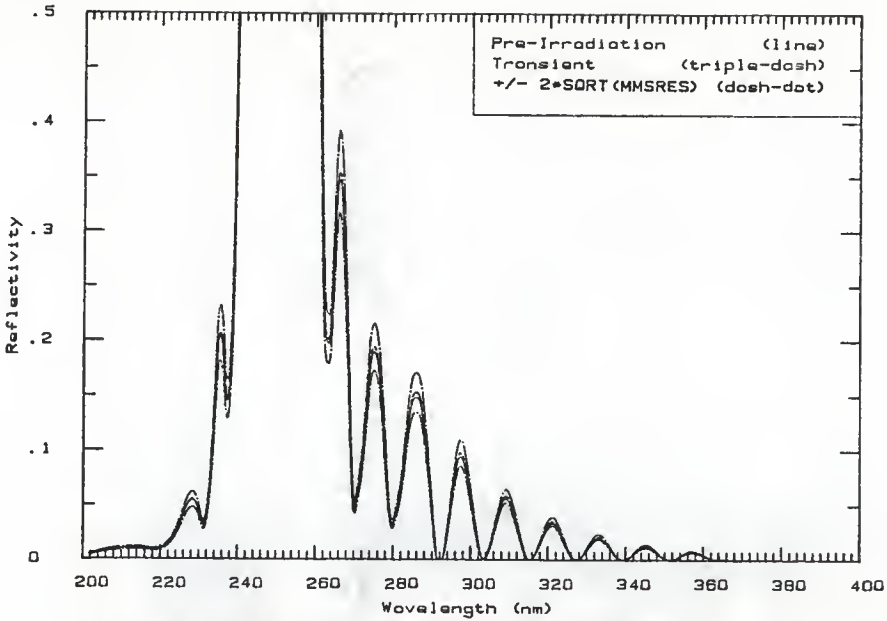

Fig. 14j The expanded view of the pre-irradiation and transient reflectivities of Fig. 14c for dielectric mirror 12 in position A.

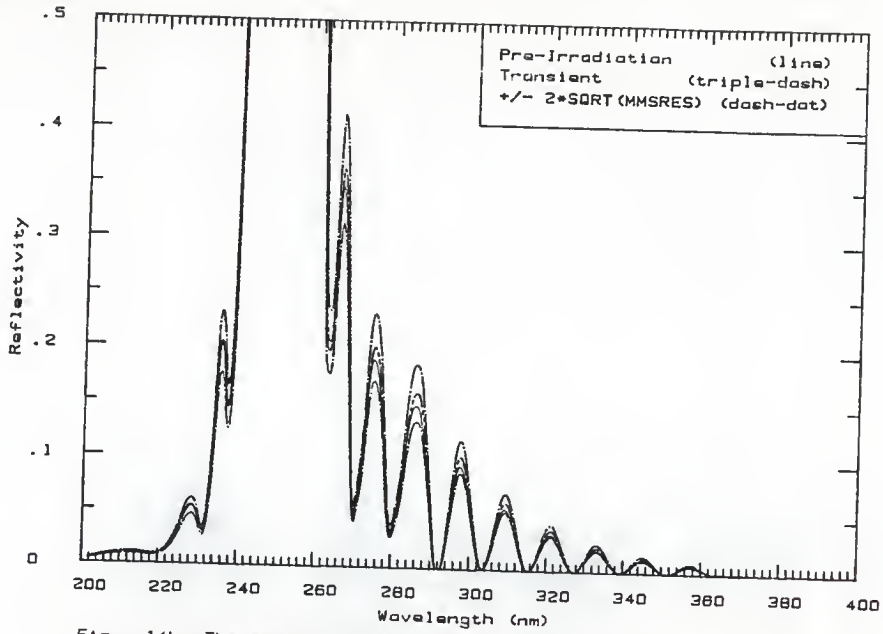

Fig. 14k The expanded view of the pre-irradiation and transient reflectivities of Fig. 14b for dielectric mirror 12 in position A.

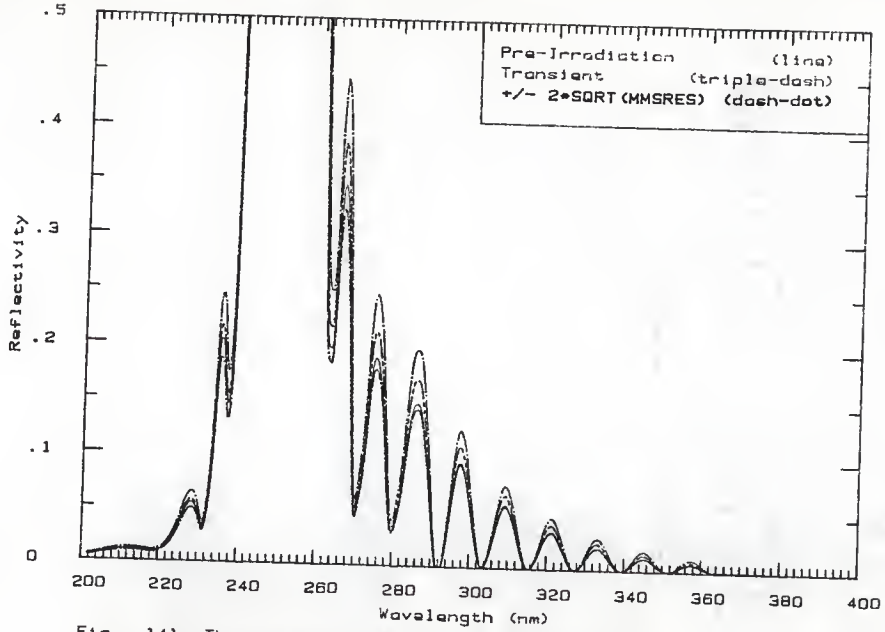

Fig. 141 The expanded view of the pre-irradiation and transient reflectivities of Fig. 14c for dielectric mirror 12 in position A.

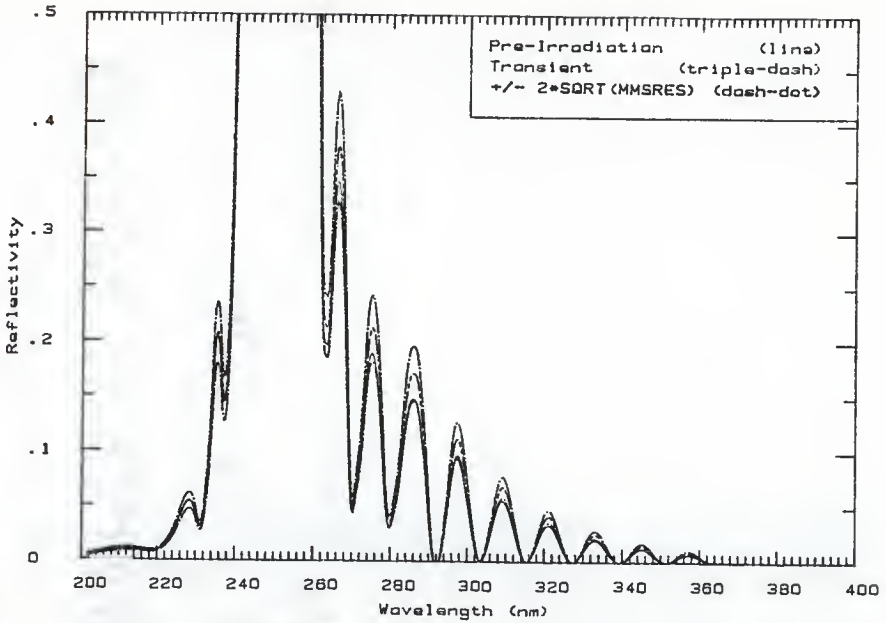

Fig. 14m The expanded view of the pre-irradiation and transient reflectivities of Fig. 14d for dielectric mirror 12 in position A.

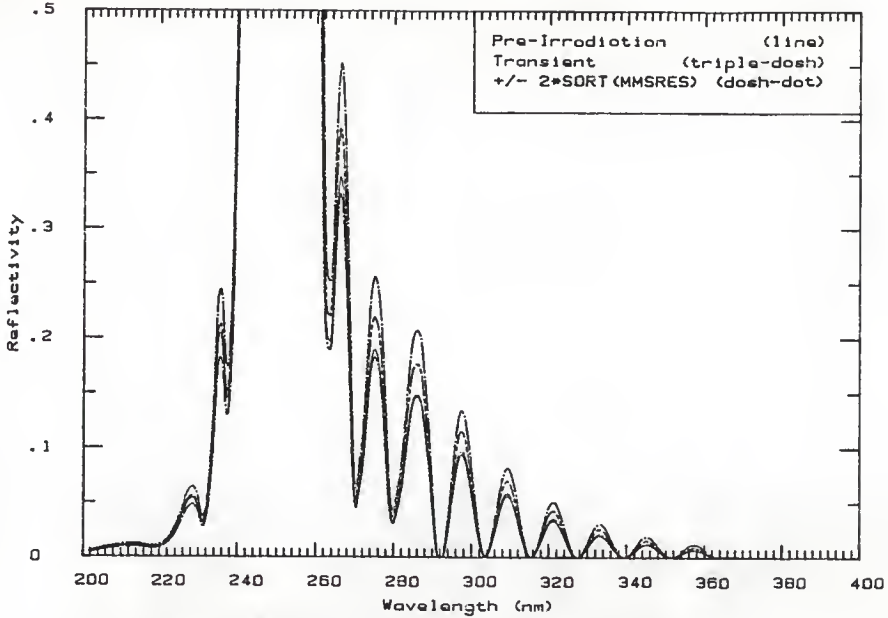

Fig. 14n The exponded view of the pre-irrodiotion and tronsient reflectivities of Fig. 14e for dielectric mirror 12 in position A.

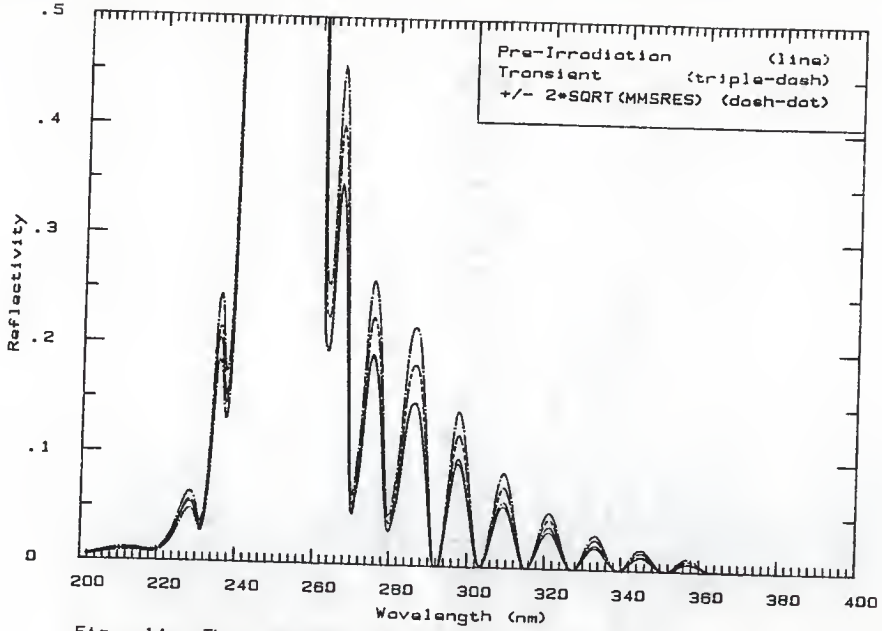

Fig. 14e The expanded view of the pre-irradiation and transient reflectivities of Fig. 14f for dielectric mirror 12 in position A.

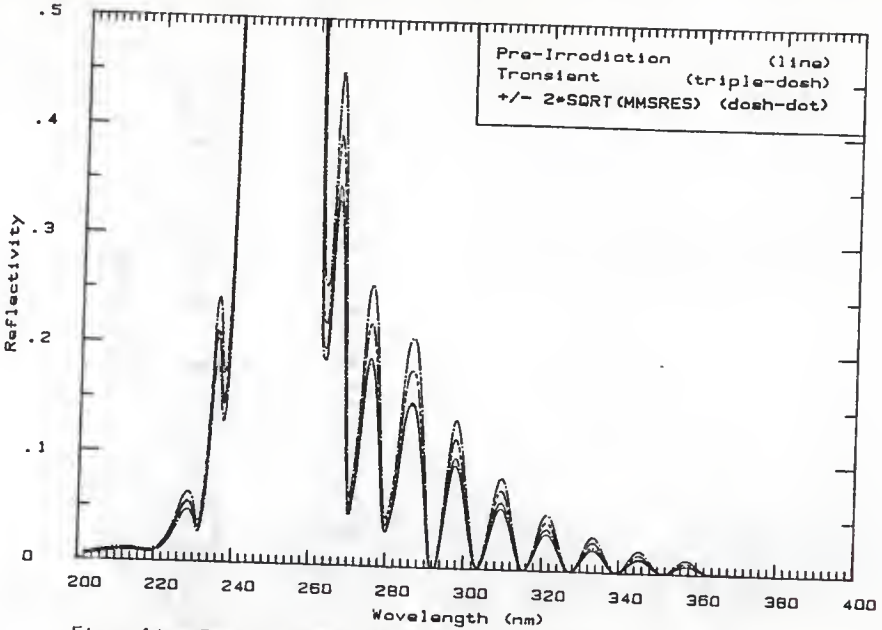

Fig. 14p The exponded view of the pre-irrodiotion and transient reflectivities of Fig. 14g for dielectric mirror 12 in position A.

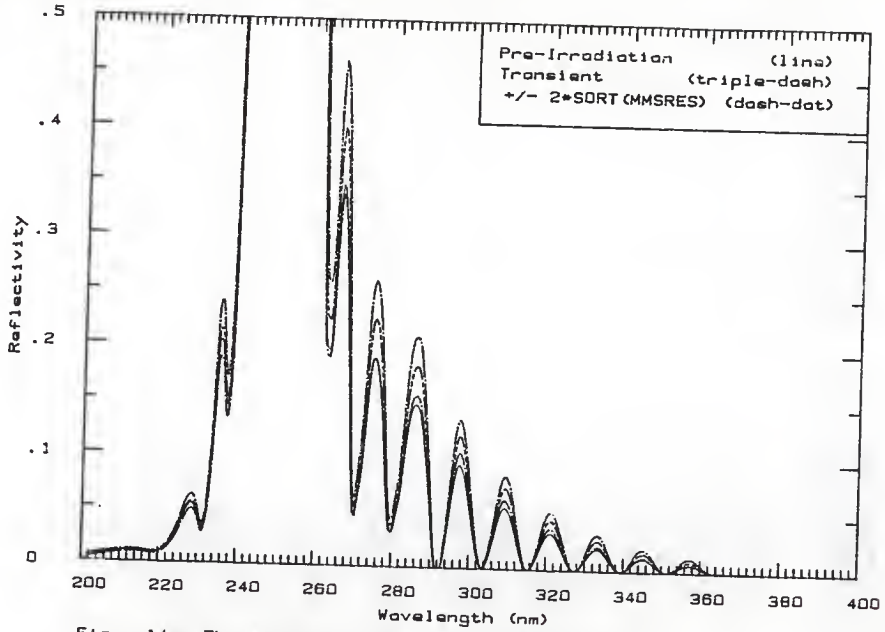

Fig. 14g The expanded view of the pre-irradiation and transient reflectivities of Fig. 14h for dielectric mirror 12 in position A.

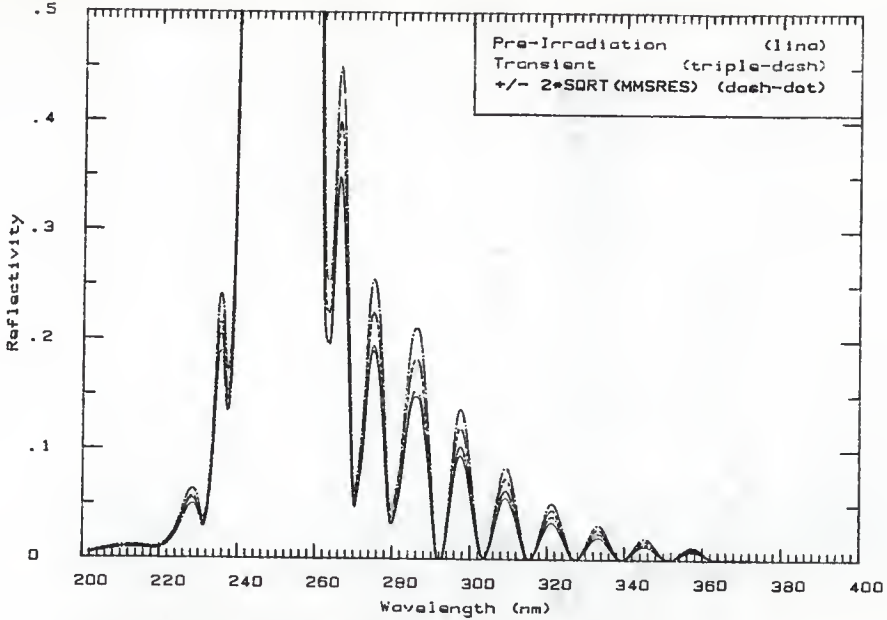

Fig. 14r The expanded view of the pre-irradiation and transient reflectivities of Fig. 14i for dielectric mirror 12 in position A.

Figures 15a to 15t, the transient reflectivity plots for dielectric mirror 13, irradiated in position B. The block-out mean beam current was 225 mA while the pulse length was 500 ns.

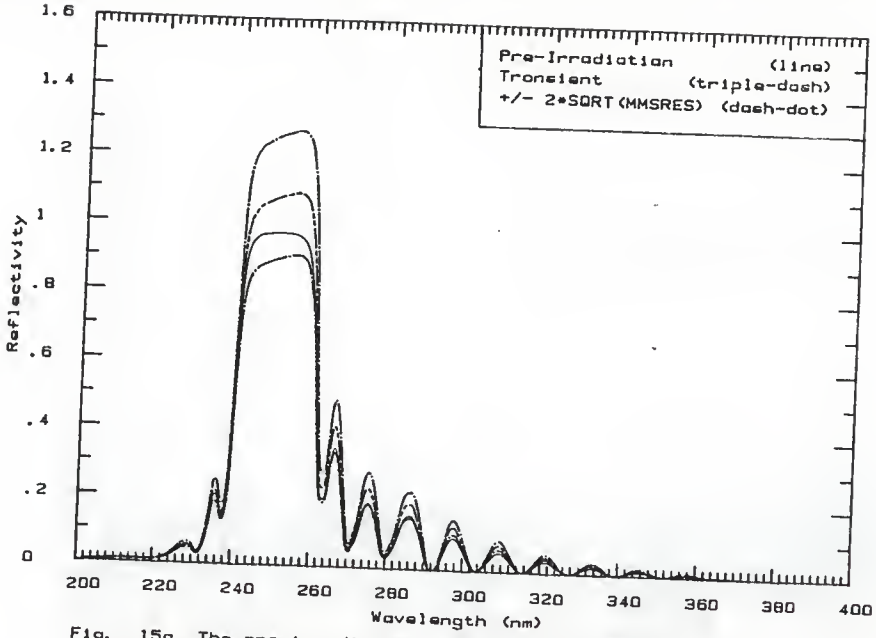

Fig. 15a The pre-irradiation reflectivity compared to the transient reflectivity based on Fig. 3a. (250 -284 ns). for dielectric mirror 12 in position B.

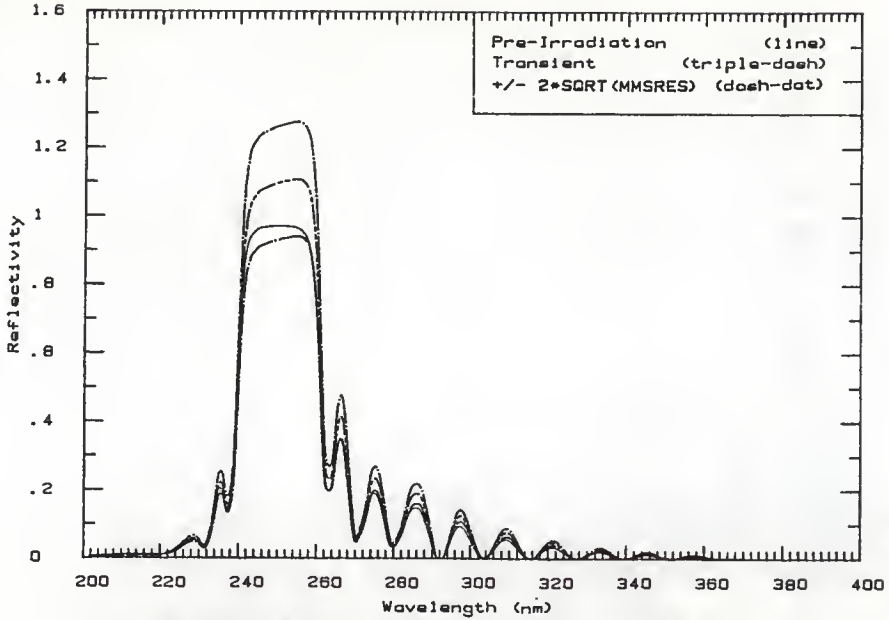

Fig. 15b The pre-irradiation reflectivity compared to the transient reflectivity based on Fig. 3b. (284 -317 ns), for dielectric mirror 12 in position 8.

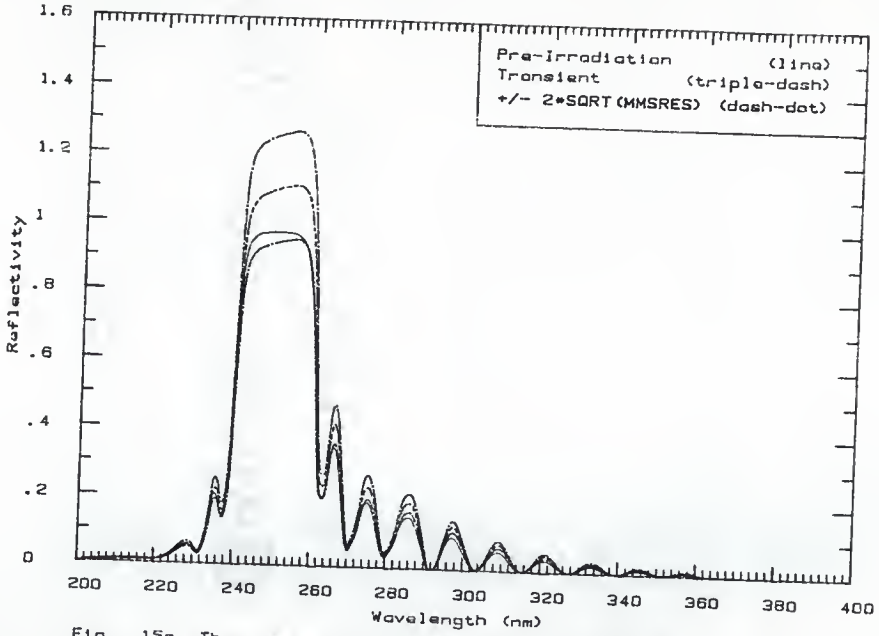

Fig. 15c The pre-irradiation reflectivity compared to the transient reflectivity based on Fig. 3c. (317 -351 ns). for dielectric mirror 12 in position 8.

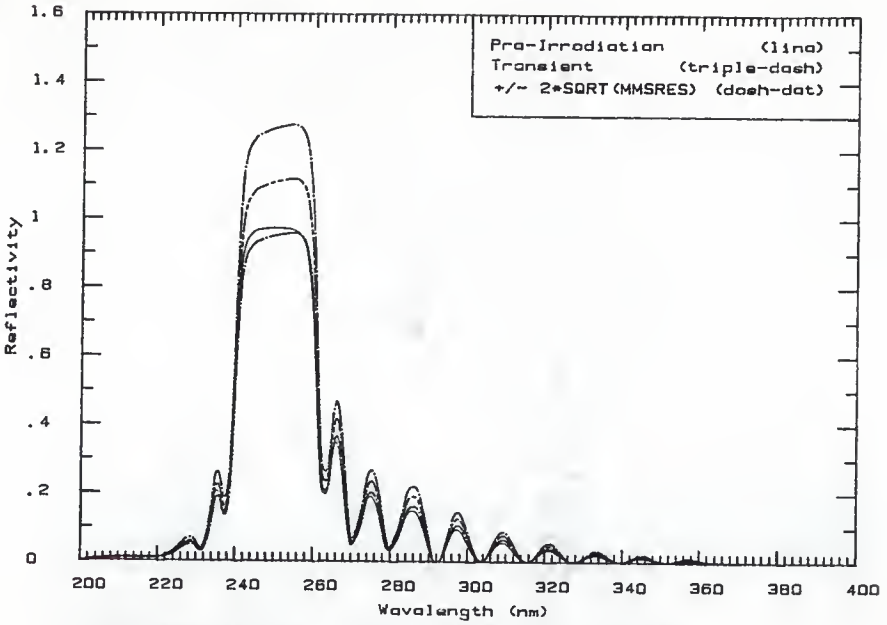

Fig. 15d The pre-irradiation reflectivity compared to the transient reflectivity based on Fig. 3d, (351 -384 ns), for dielectric mirror 12 in position 8.

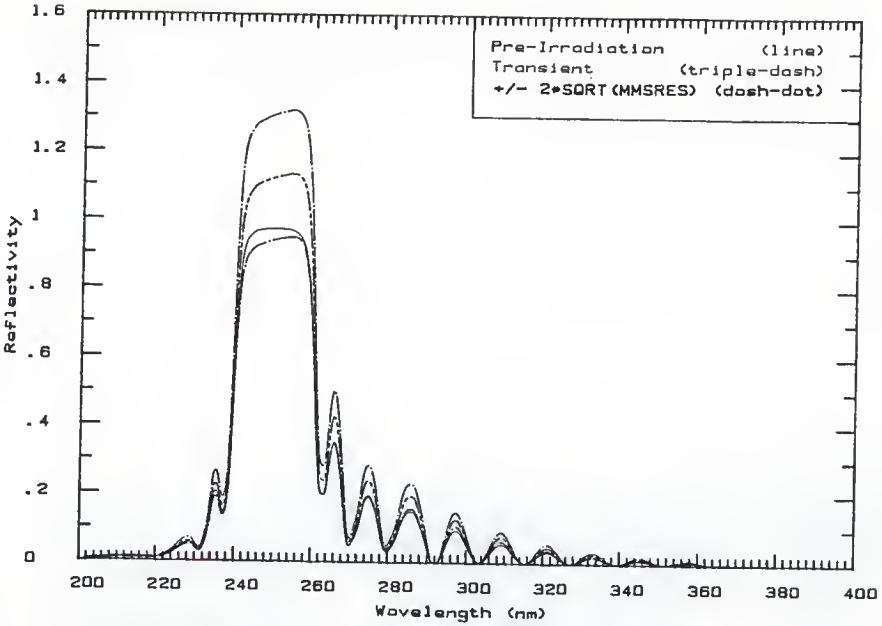

Fig. 15e The pre-irradiation reflectivity compared to the transient reflectivity based on Fig. 3e. (384 -418 ns), for dielectric mirror 12 in position 8.

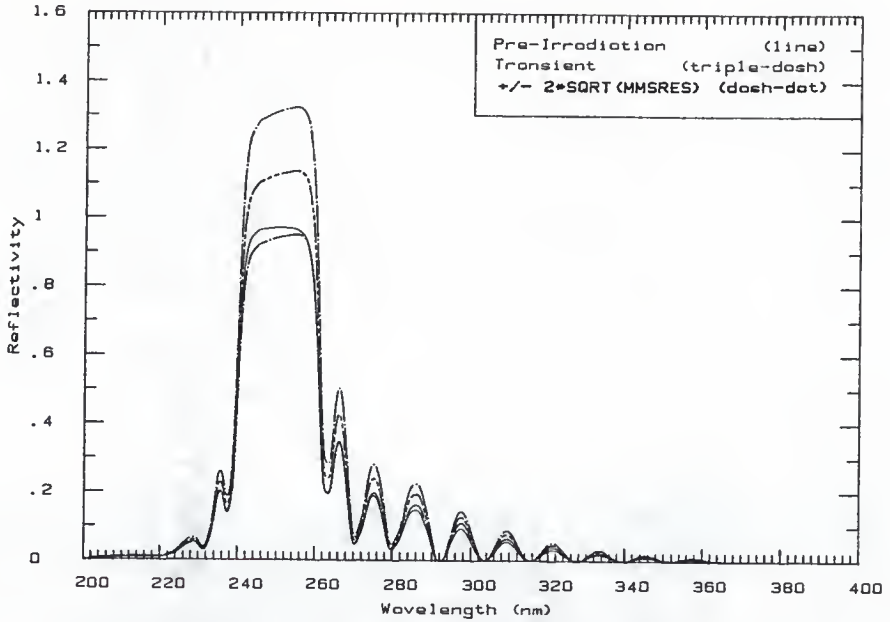

Fig. 15f The pre-irradiation reflectivity compared to the transient reflectivity based on Fig. 3f. (418 -451 ns), for dielectric mirror 12 in position 8.

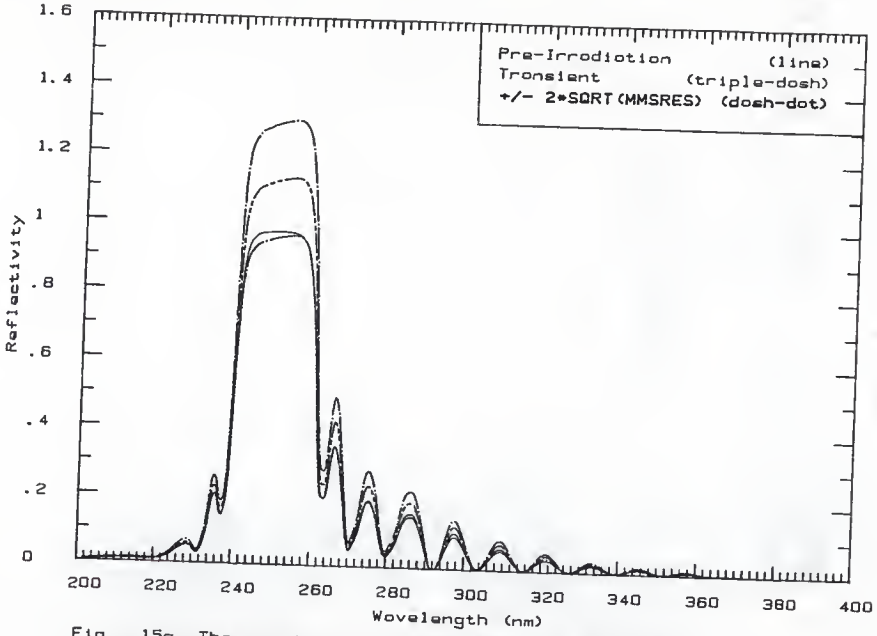

Fig. 15g The pre-irradiation reflectivity compared to the transient reflectivity based on Fig. 3g. (451 -485 ns), for dielectric mirror 12 in position 8.

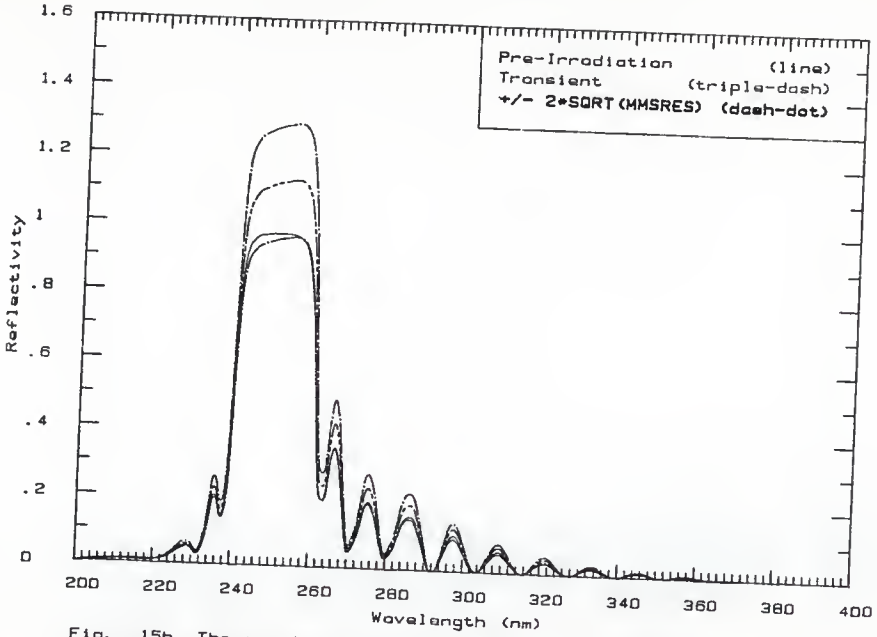

Fig. 15h The pre-irradiation reflectivity compared to the transient reflectivity based on Fig. 3h. (485 -518 ns). for dielectric mirror 12 in position 8.

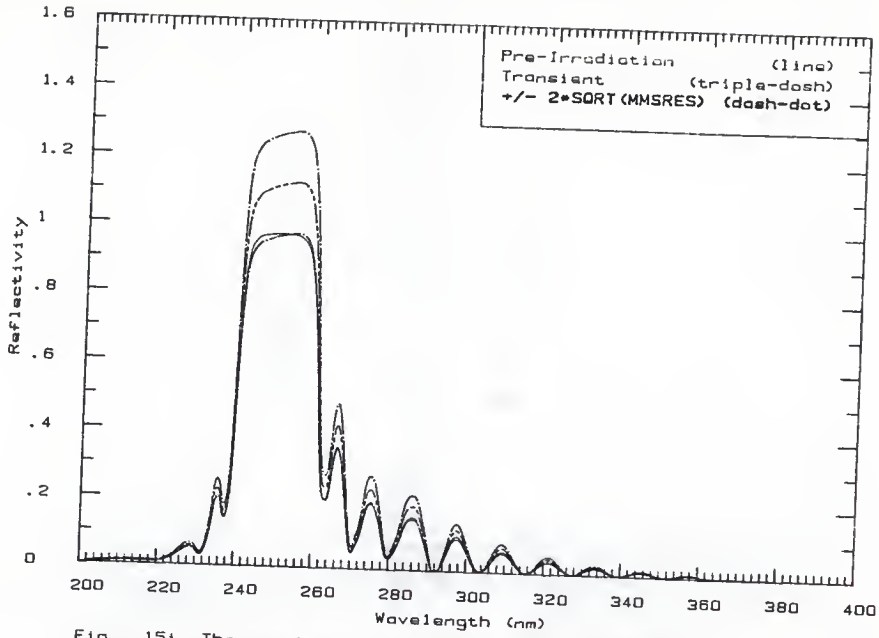

Fig. 15i The pre-irradiation reflectivity compared to the transient reflectivity based on Fig. 3i. (518 -552 ns), for dielectric mirror 12 in position 8.

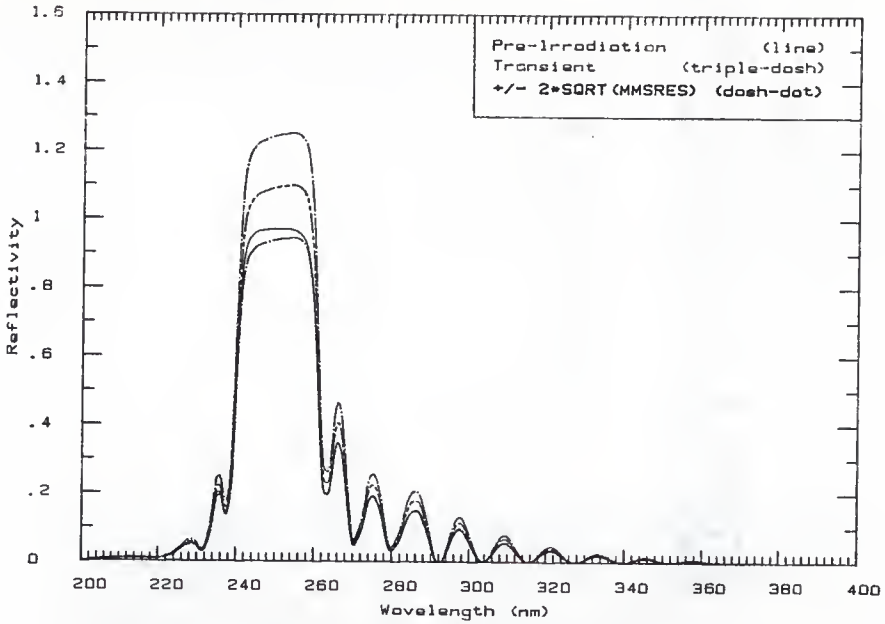

Fig. 15j The pre-irradiation reflectivity compared to the transient reflectivity based on Fig. 3j. (552 -593 ns), for dielectric mirror 12 in position 8.

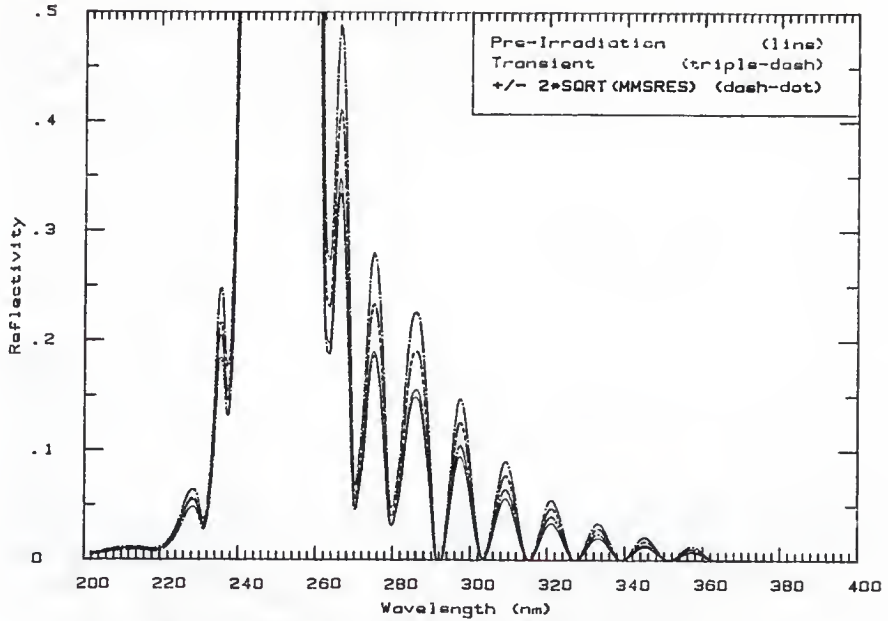

Fig. 15k The expanded view of the pre-irradiation and transient reflectivities of Fig. 15a for dielectric mirror 12 in position 8.

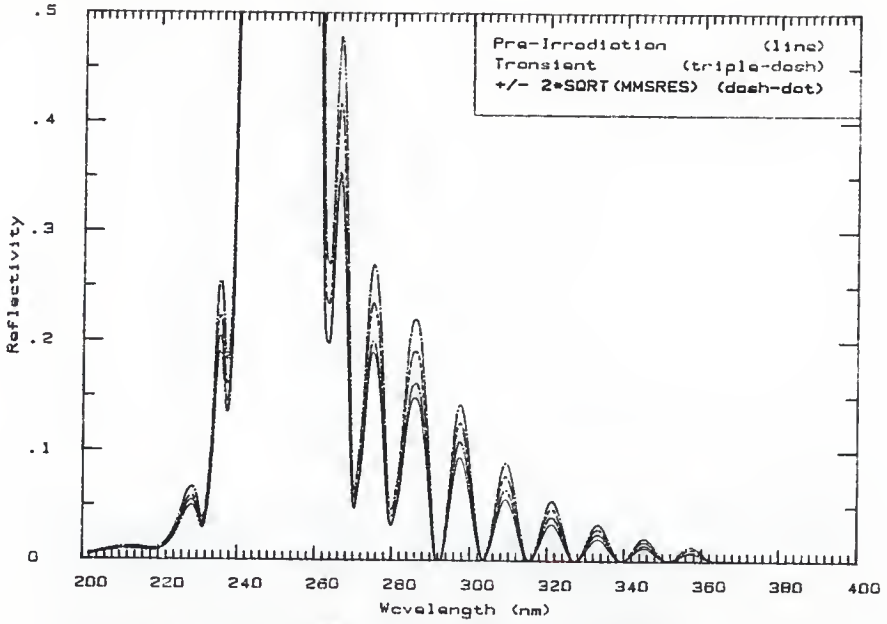

Fig. 15l The expanded view of the pre-irradiation and transient reflectivities of Fig. 15b for dielectric mirror 12 in position B.

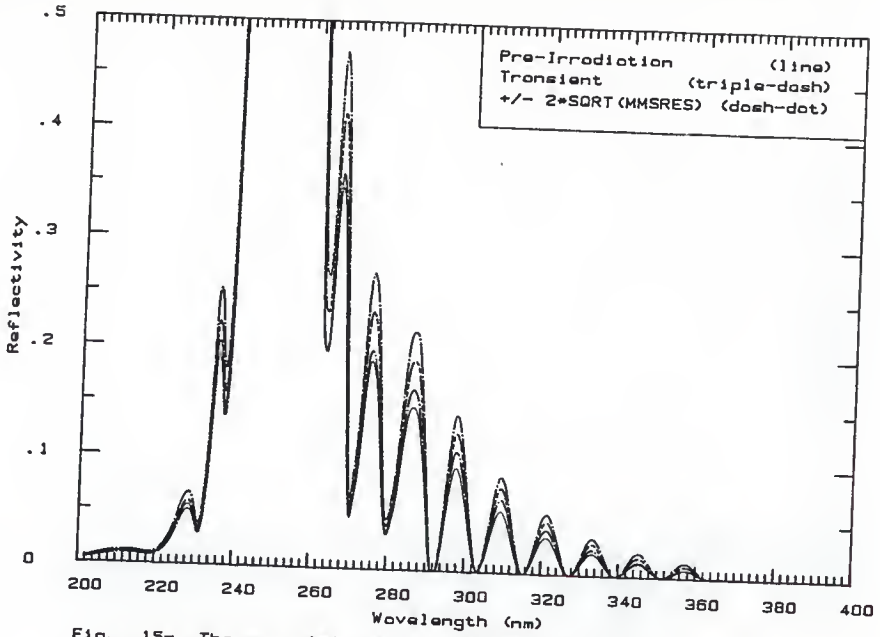

Fig. 15m The exponded view of the pre-irradiation and transient reflectivities of Fig. 15c for dielectric mirror 12 in position B.

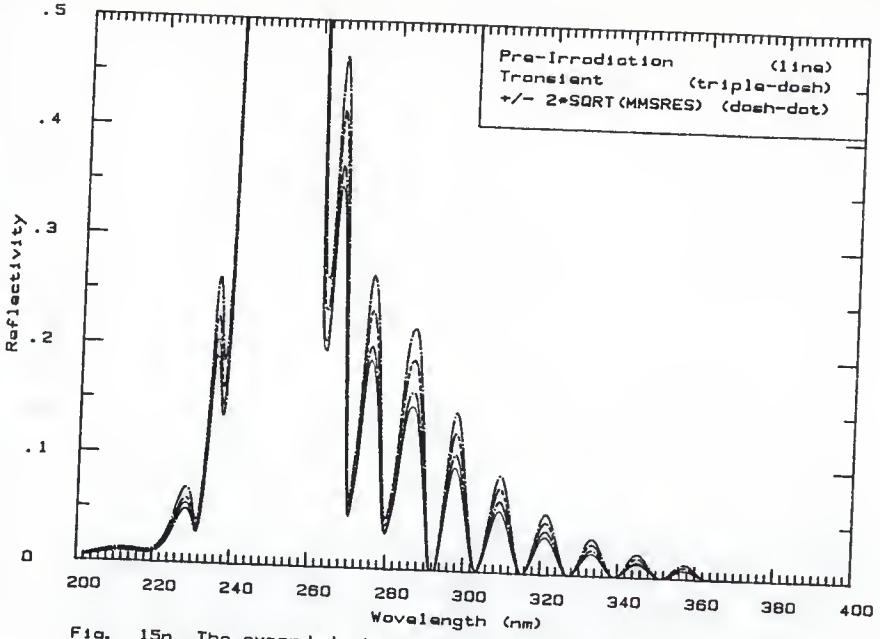

Fig. 15n The expanded view of the pre-irradiation and transient reflectivities of Fig. 15d for dielectric mirror 12 in position B.

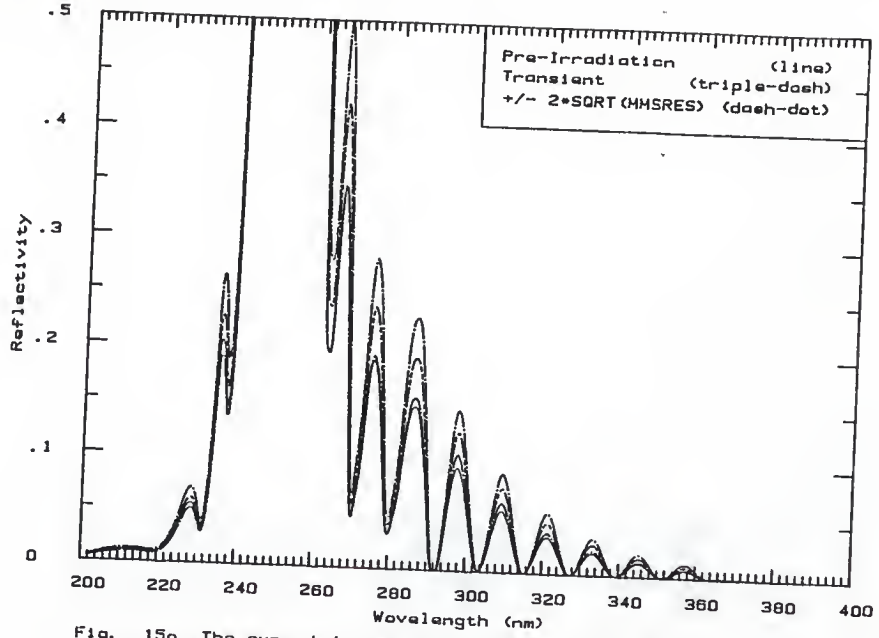

Fig. 15o The expanded view of the pre-irradiation and transient reflectivities of Fig. 15e for dielectric mirror 12 in position 8.

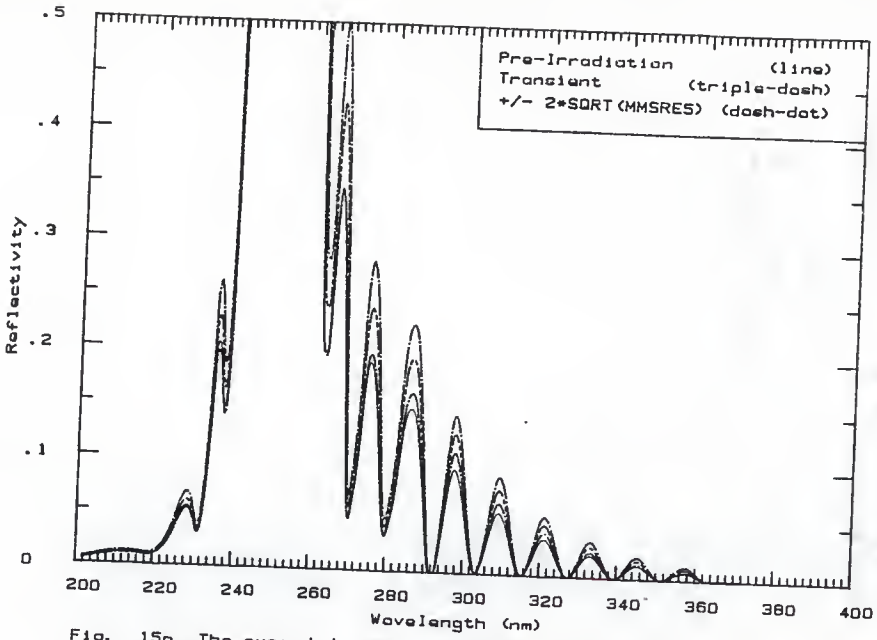

Fig. 15p The exponded view of the pre-irradiation and transient reflectivities of Fig. 15f for dielectric mirror 12 in position 8.

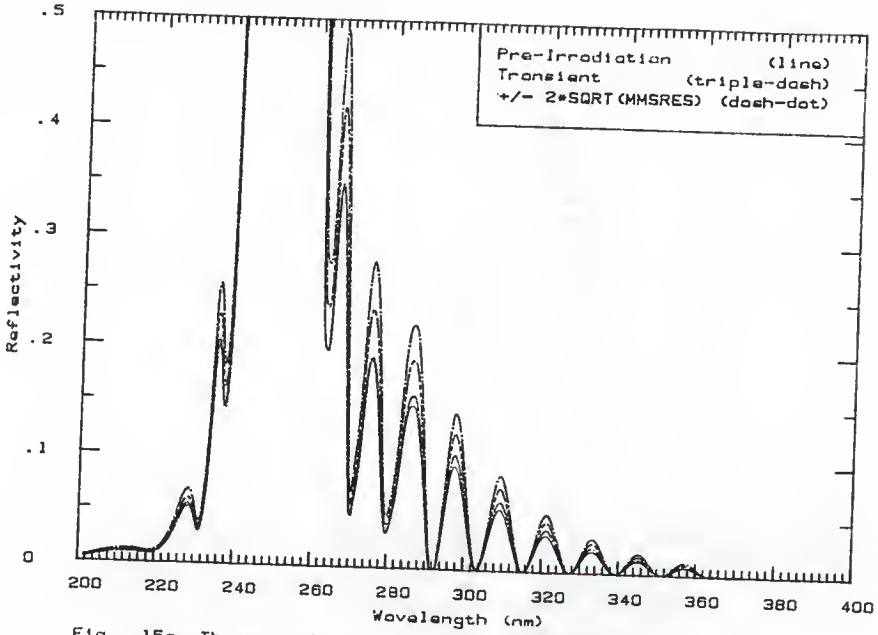

Fig. 15q The exponded view of the pre-irradiation and transient reflectivities of Fig. 15g for dielectric mirror 12 in position B.

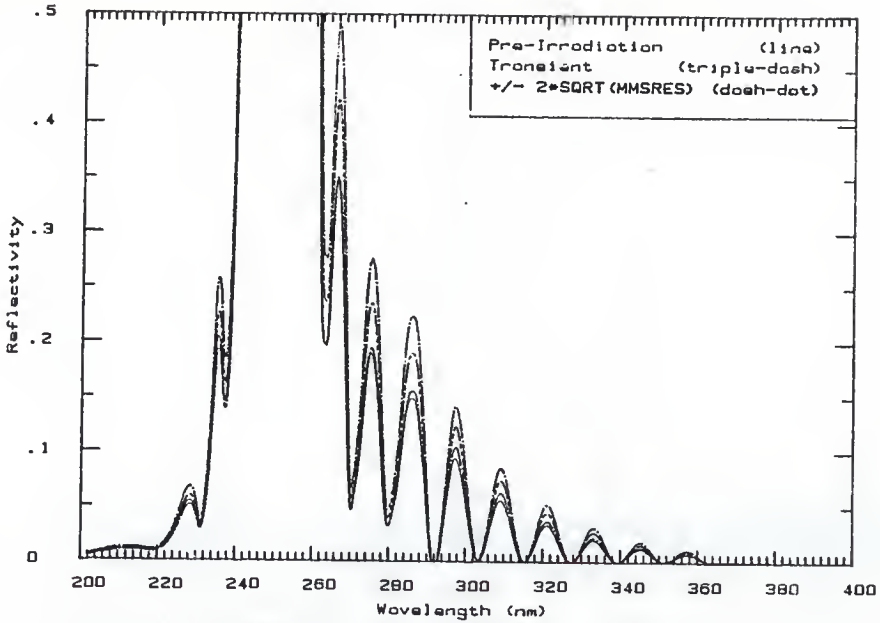

Fig. 15r The expanded view of the pre-irradiation and transient reflectivities of Fig. 15h for dielectric mirror 12 in position 8.

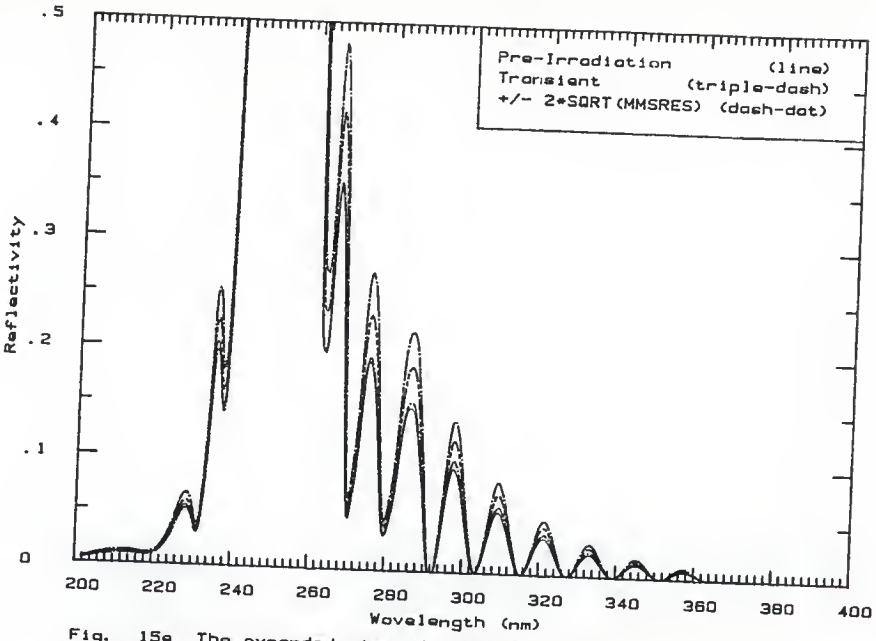

Fig. 15e The expanded view of the pre-irradiation and transient reflectivities of Fig. 15i for dielectric mirror 12 in position 8.

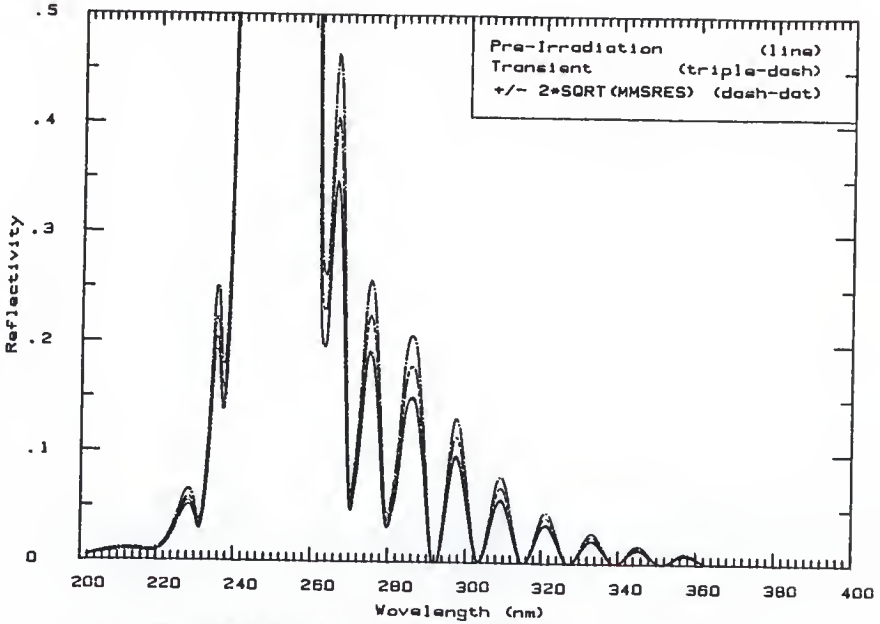

Fig. 15t The exponded view of the pre-irrodiation and transient reflectivities of Fig. 15j for dielectric mirror 12 in position 8.

Figures 16a to 16r, the transient reflectivity plots for dielectric mirror 13, irradiated in position A. The block-out mean beam current was 225 mA while the beam pulse length was 200 ns.

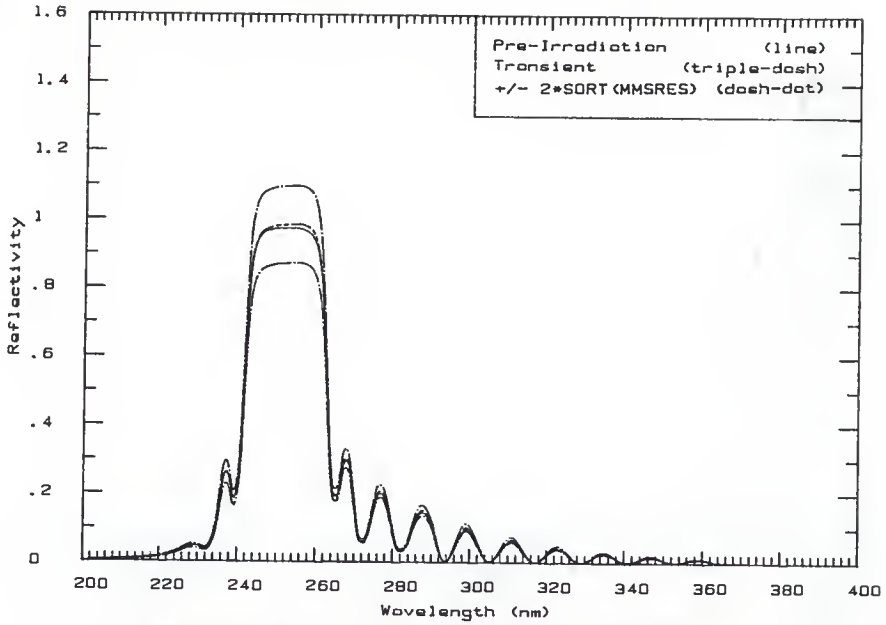

Fig. 16a The pre-irradiation reflectivity compared to the transient reflectivity based on Fig. 4a, (0.8 -20.9 ns), for dielectric mirror 13 in position A.

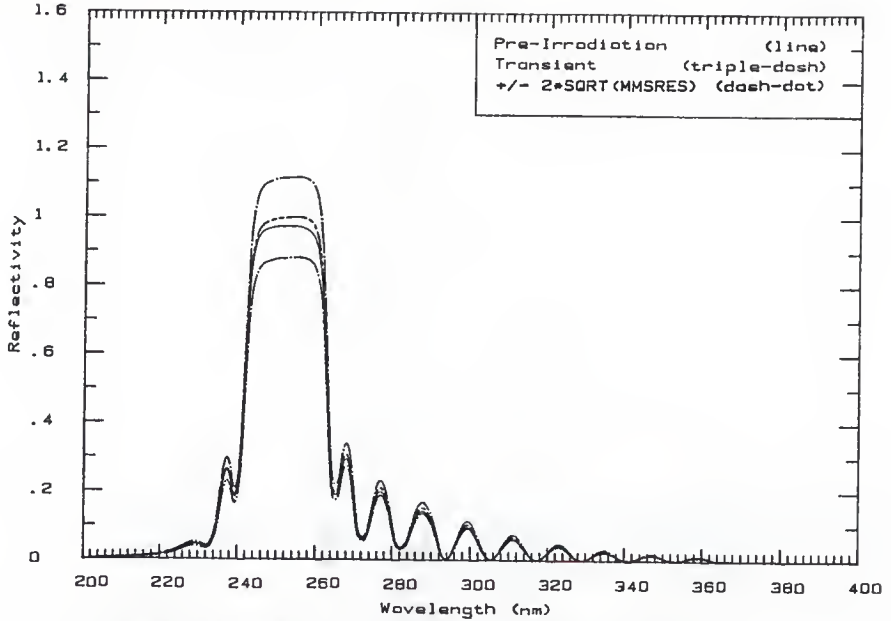

Fig. 16b The pre-irradiation reflectivity compared to the transient reflectivity based on Fig. 4b. (20.9 -41.0 ns), for dielectric mirror 13 in position A.

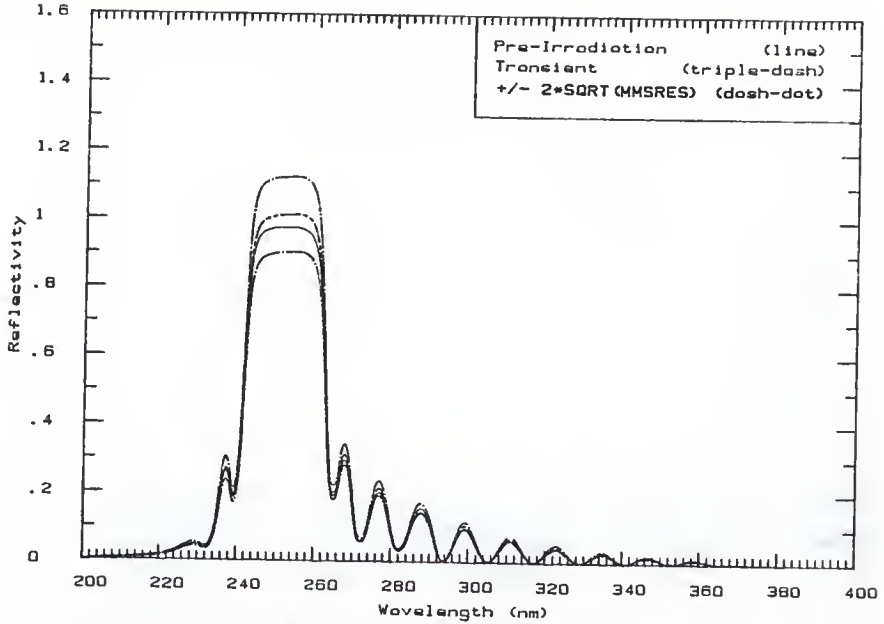

Fig. 16c The pre-irradiation reflectivity compared to the transient reflectivity based on Fig. 4c. (41.0 -61.1 ns), for dielectric mirror 13 in position A.

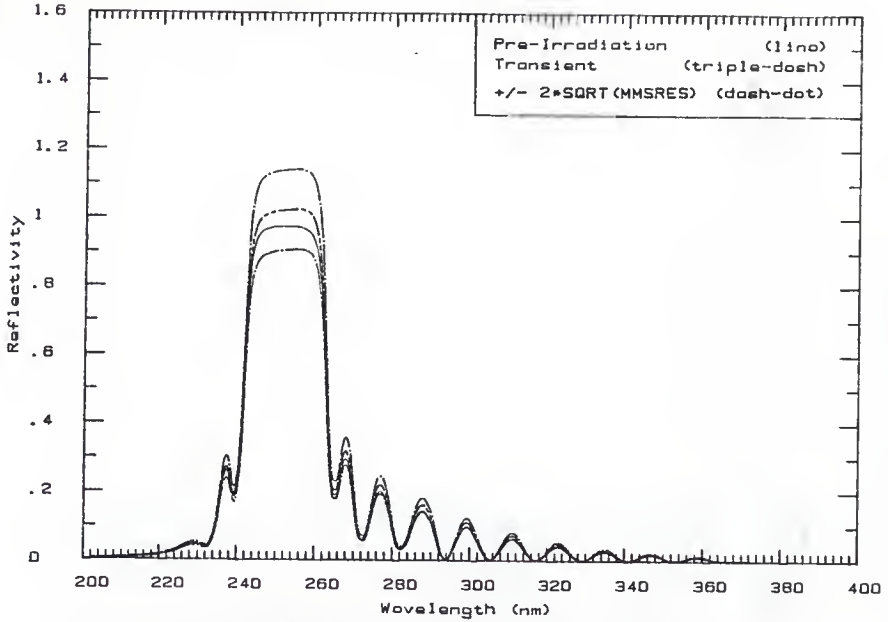

Fig. 16d The pre-irradiation reflectivity compared to the transient reflectivity based on Fig. 4d. (61.1 -81.2 ns), for dielectric mirror 13 in position A.

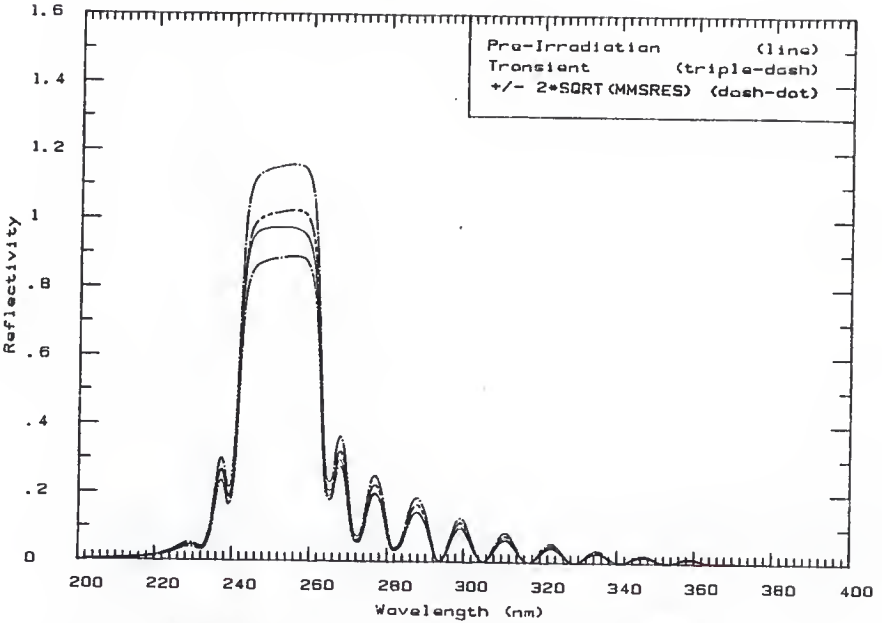

Fig. 16a The pre-irradiation reflectivity compared to the transient reflectivity based on Fig. 4a. (81.2 -101 ns), for dielectric mirror 13 in position A.

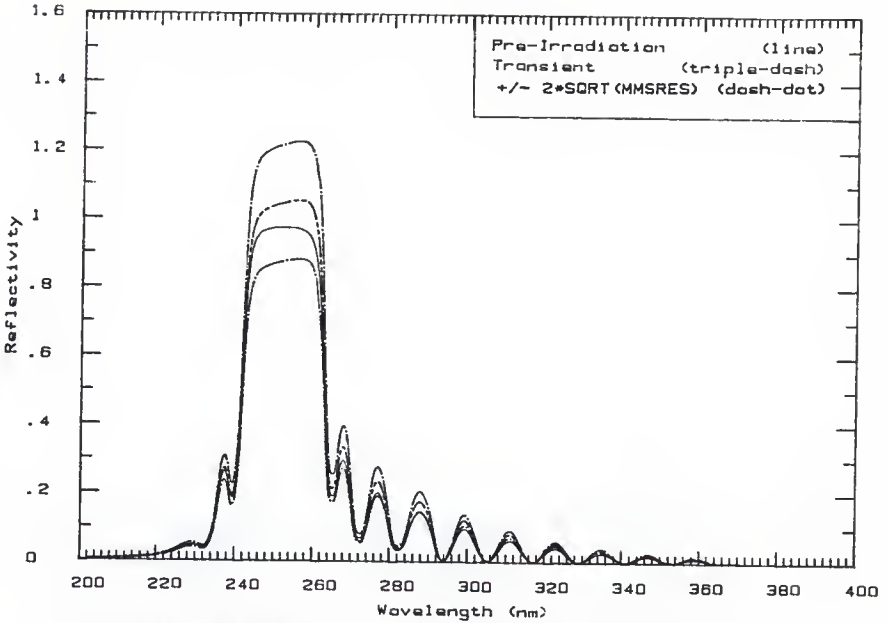

Fig. 16f The pre-irradiation reflectivity compared to the transient reflectivity based on Fig. 4f, (101 -121 ns), for dielectric mirror 13 in position A.

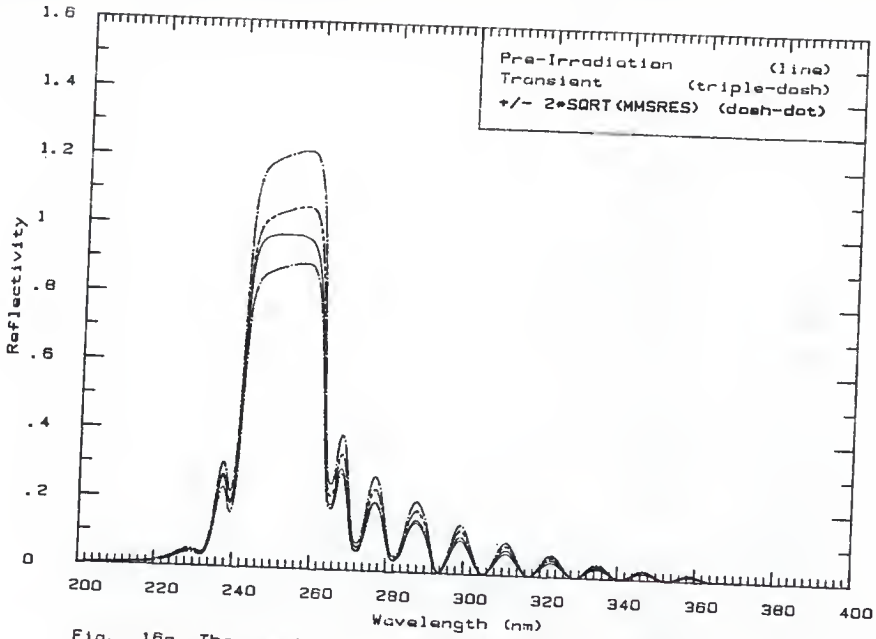

Fig. 16g The pre-irradiation reflectivity compared to the transient reflectivity based on Fig. 4g. (121 -142 ns), for dielectric mirror 13 in position A.

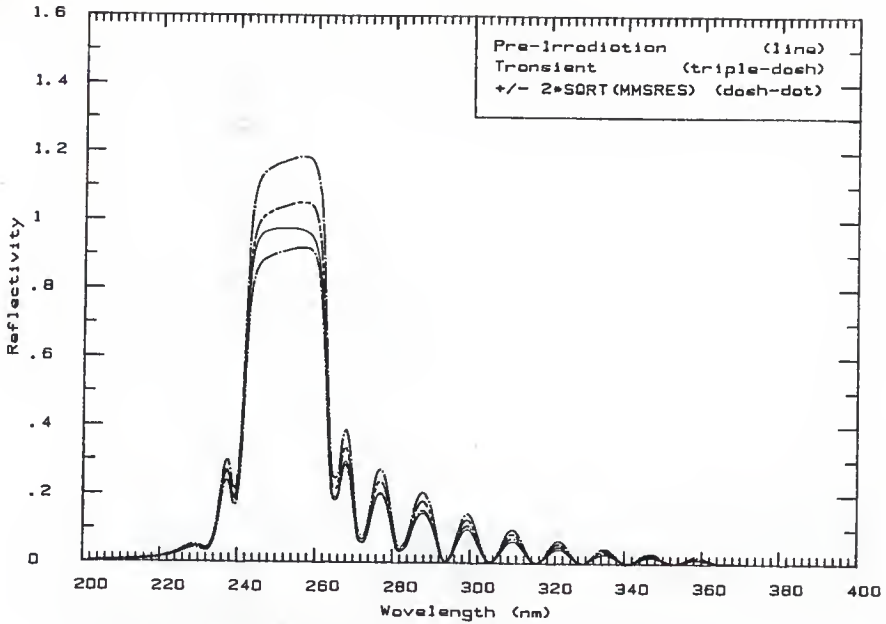

Fig. 16h The pre-irradiation reflectivity compared to the transient reflectivity based on Fig. 4h. (142 -162 ns). for dielectric mirror 13 in position A.

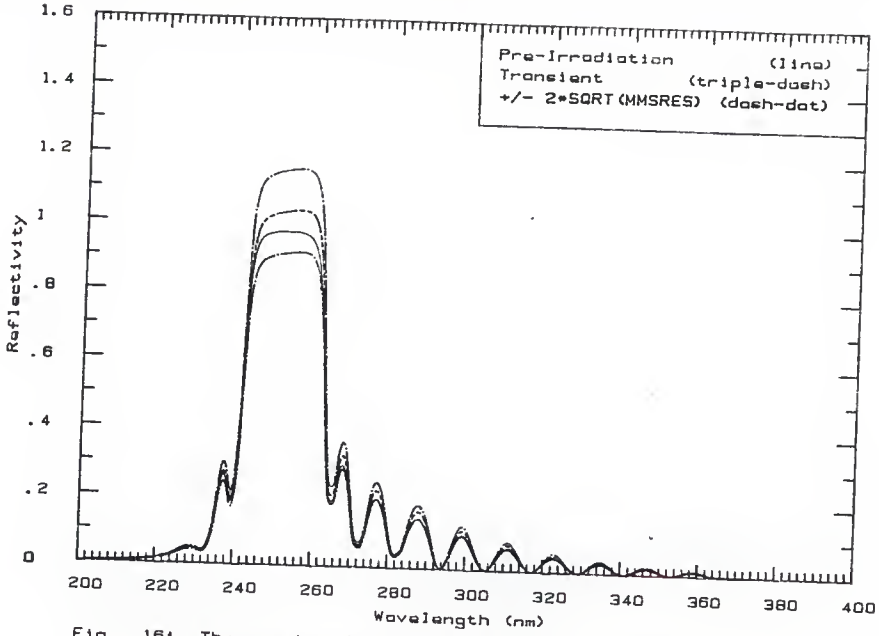

Fig. 161 The pre-irradiation reflectivity compared to the transient reflectivity based on Fig. 41. (162 -183 ns), for dielectric mirror 13 in position A.

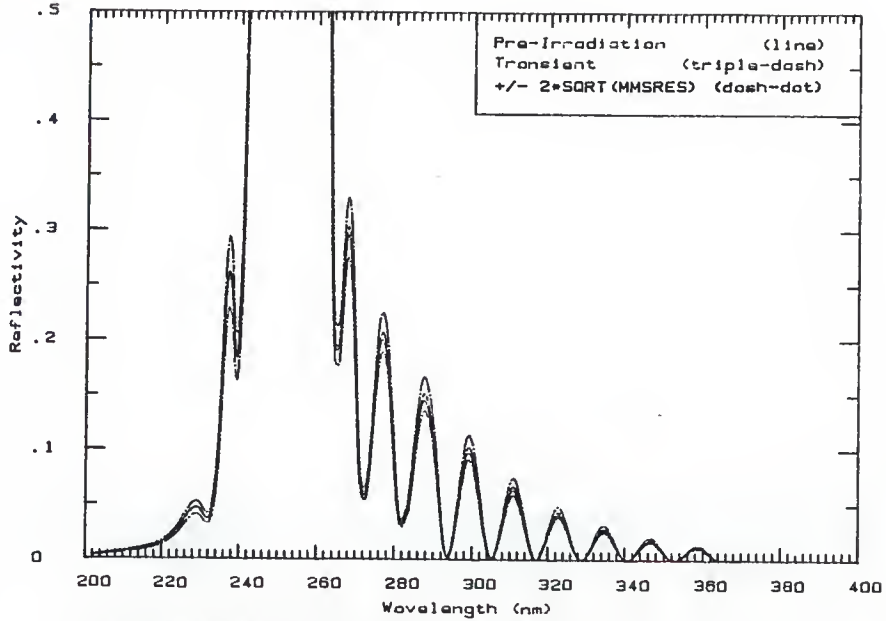

Fig. 18J The expanded view of the pre-irradiation and transient reflectivities of Fig. 16a for dielectric mirror 13 in position A.

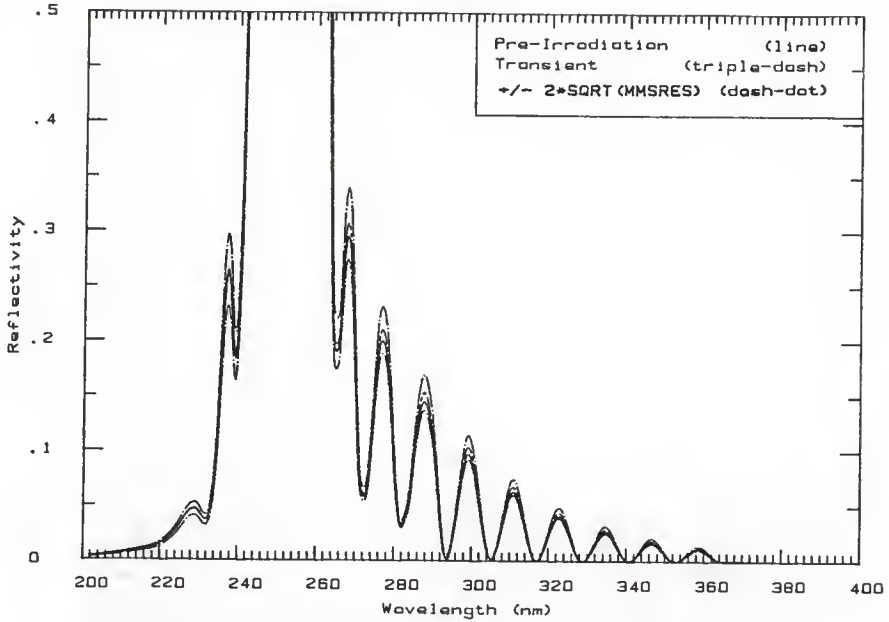

Fig. 16k The expanded view of the pre-irradiation and transient reflectivities of Fig. 16b for dielectric mirror 13 in position A.

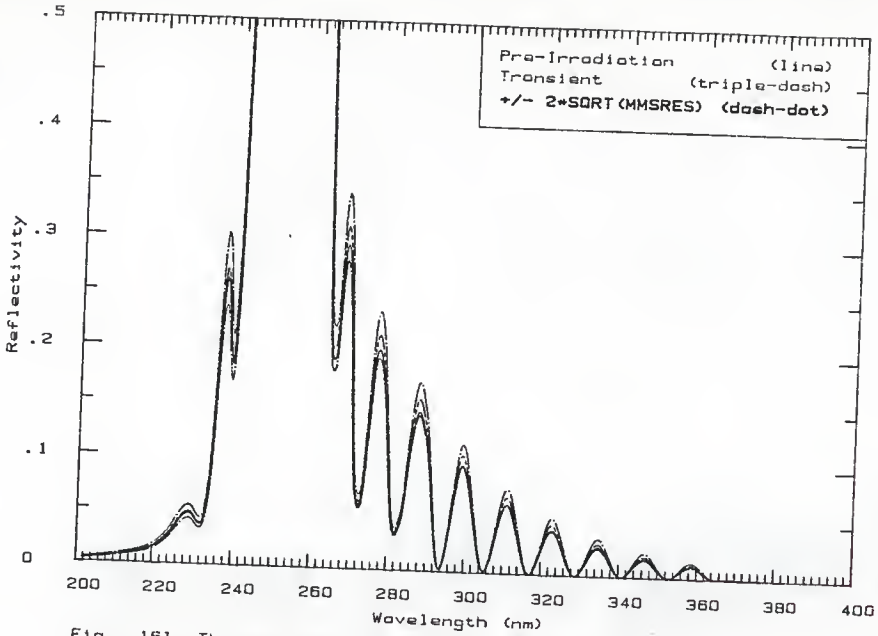

Fig. 16l The exponded view of the pre-irrodiation and transient reflectivities of Fig. 16c for dielectric mirror 13 in position A.

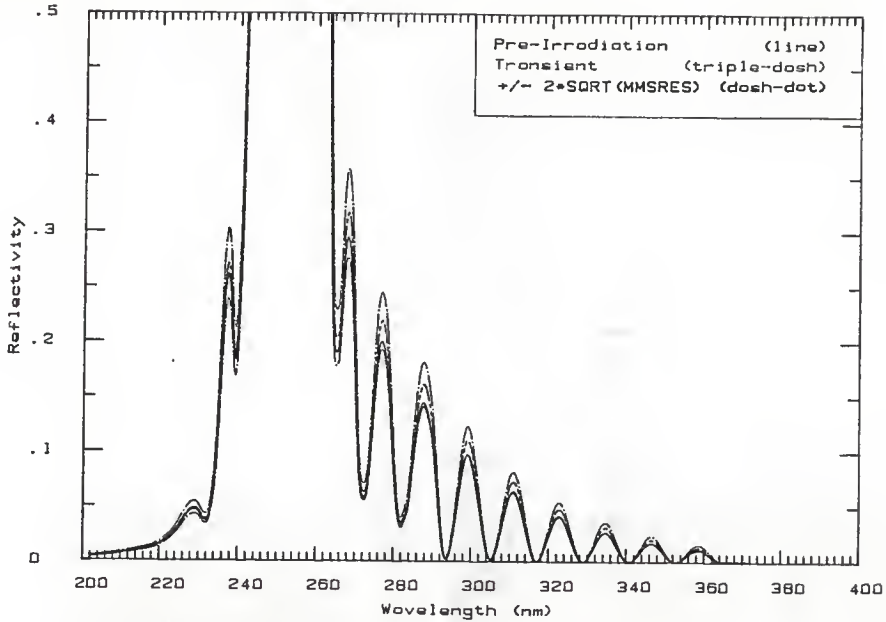

Fig. 16m The exponded view of the pre-irradiation and transient reflectivities of Fig. 16d for dielectric mirror 13 in position A.

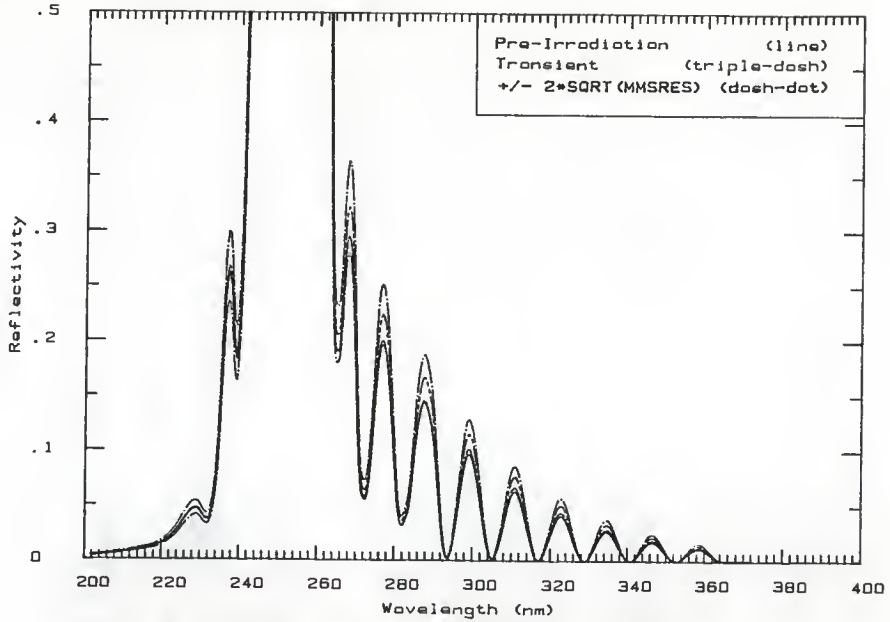

Fig. 16n The exponded view of the pre-irradiation and transient reflectivities of Fig. 16e for dielectric mirror 13 in position A.

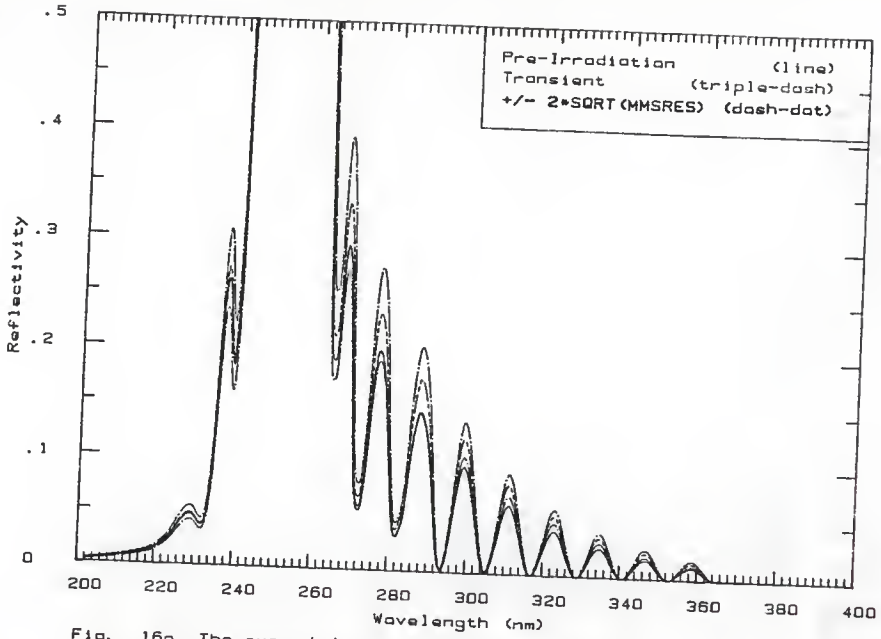

Fig. 16a The expanded view of the pre-irradiation and transient reflectivities of Fig. 16f for dielectric mirror 13 in position A.

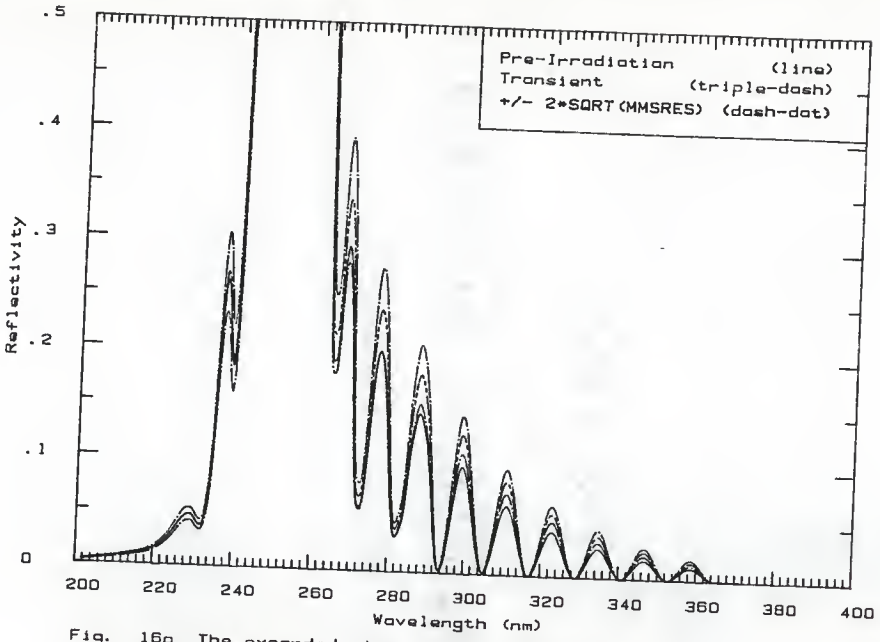

Fig. 16p The expanded view of the pre-irradiation and transient reflectivities of Fig. 16g for dielectric mirror 13 in position A.

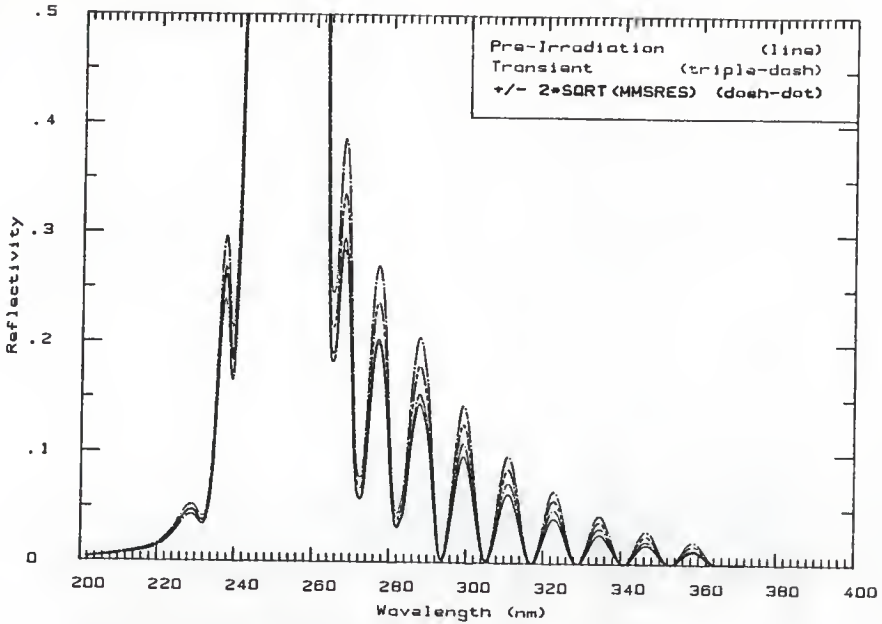

Fig. 16g The expanded view of the pre-irradiation and transient reflectivities of Fig. 16h for dielectric mirror 13 in position A.

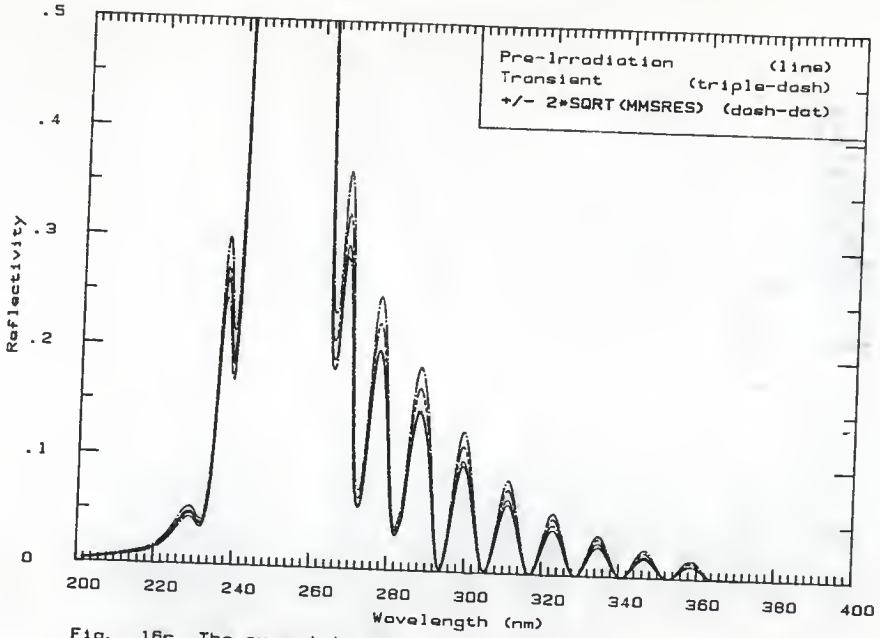

Fig. 16r The expanded view of the pre-irradiation and transient reflectivities of Fig. 16i for dielectric mirror 13 in position A.

Figures 17a to 17r, the transient reflectivity plots for dielectric mirror 13, irradiated in position B. The block-out irradiation mean beam current was 225 mA and the pulse length was 200 ns.

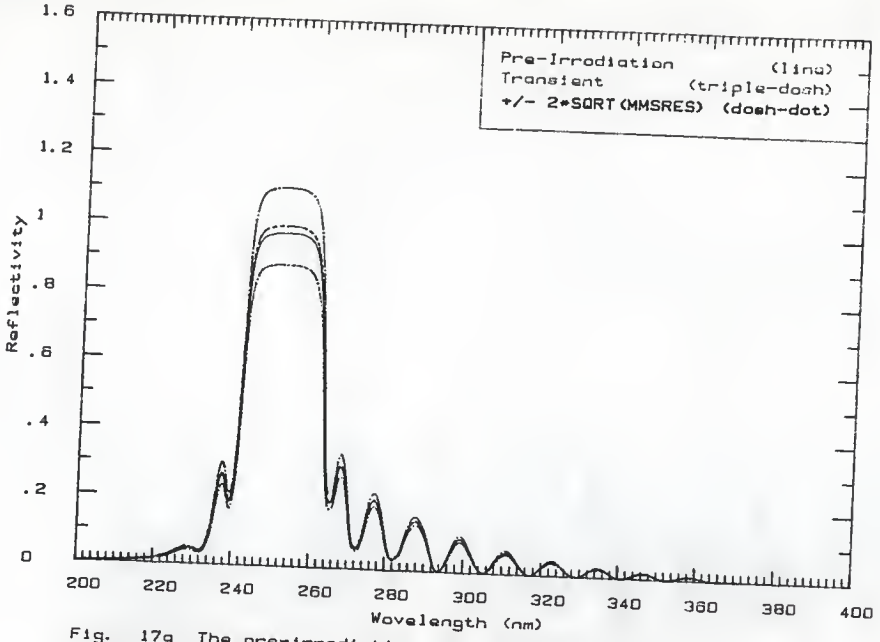

Fig. 17a The pre-irradiation reflectivity compared to the transient reflectivity based on Fig. 5a. (0.25 -33.8 ns), for dielectric mirror 13 in position 8.

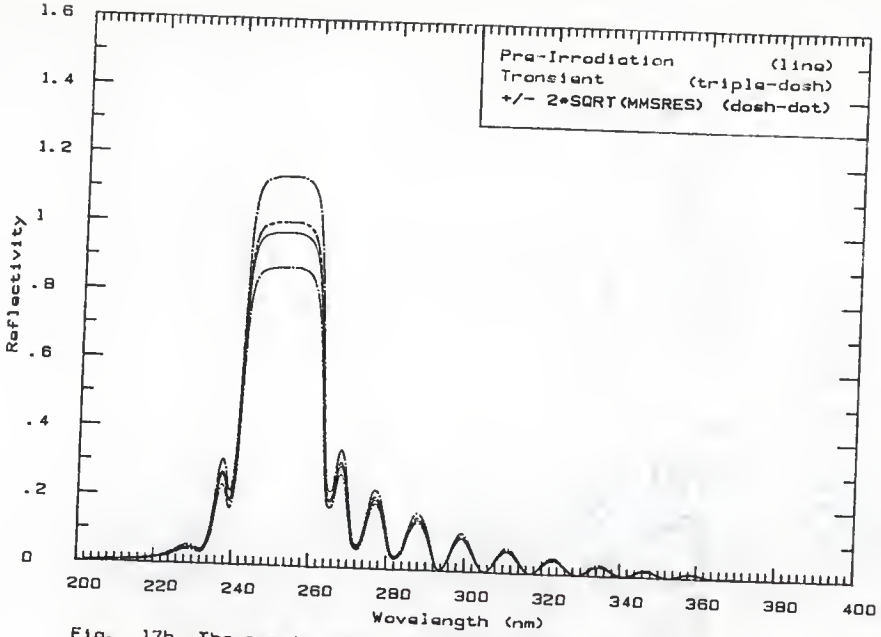

Fig. 17b The pre-irradiation reflectivity compared to the transient reflectivity based on Fig. 5b. (33.8 -87.3 ns), for dielectric mirror 13 in position 8.

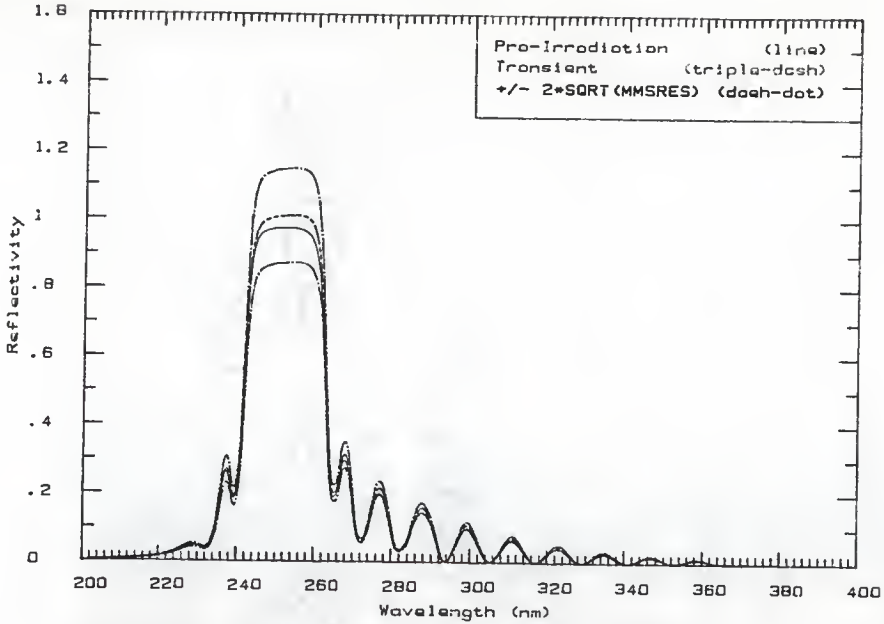

Fig. 17c The pre-irradiation reflectivity compared to the transient reflectivity based on Fig. 5c. (67.3 -101 ns). for dielectric mirror 13 in position B.

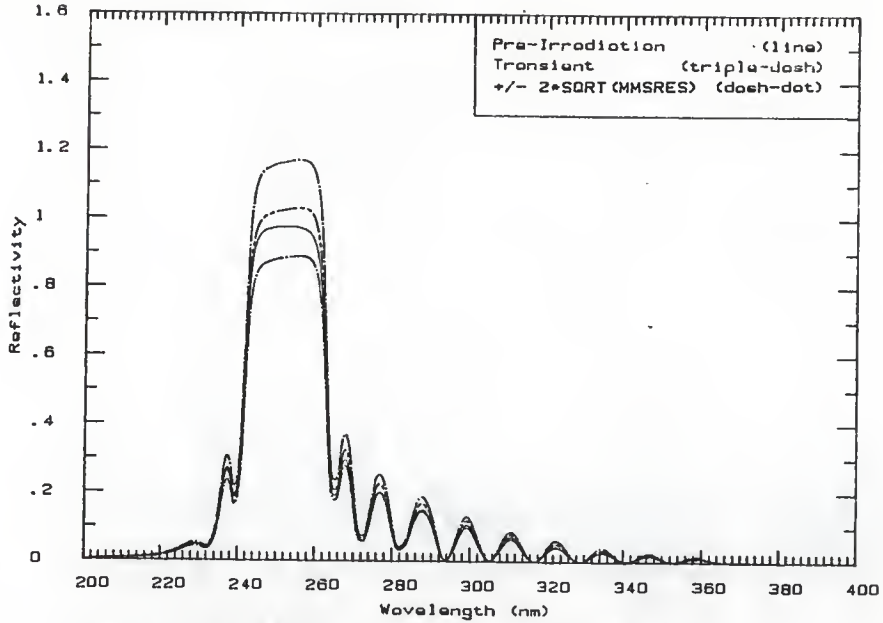

Fig. 17d The pre-irradiation reflectivity compared to the transient reflectivity based on Fig. 5d. (101 -134 ns). for dielectric mirror 13 in position 8.

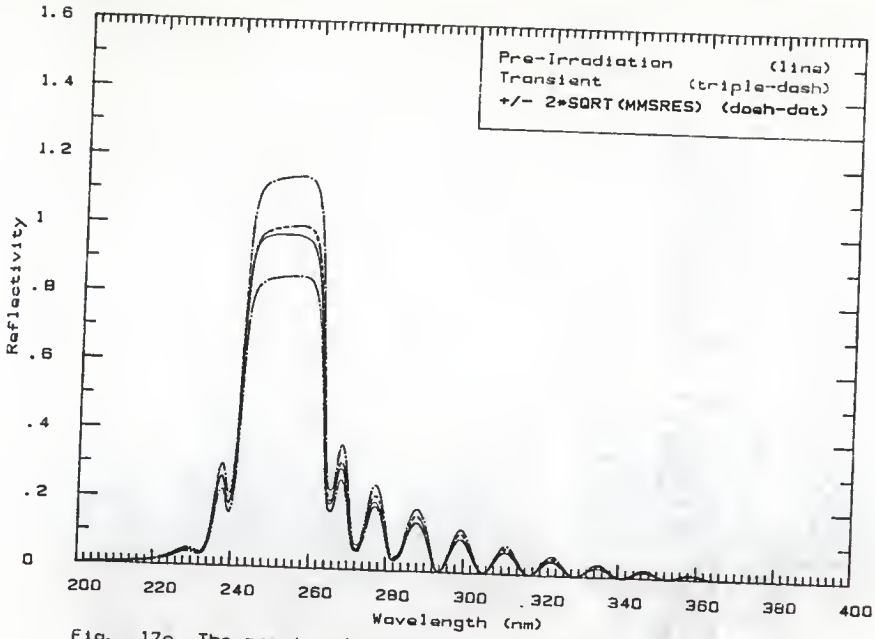

Fig. 17e The pre-irradiation reflectivity compared to the transient reflectivity based on Fig. 5e. (134 -168 ns), for dielectric mirror 13 in position B.

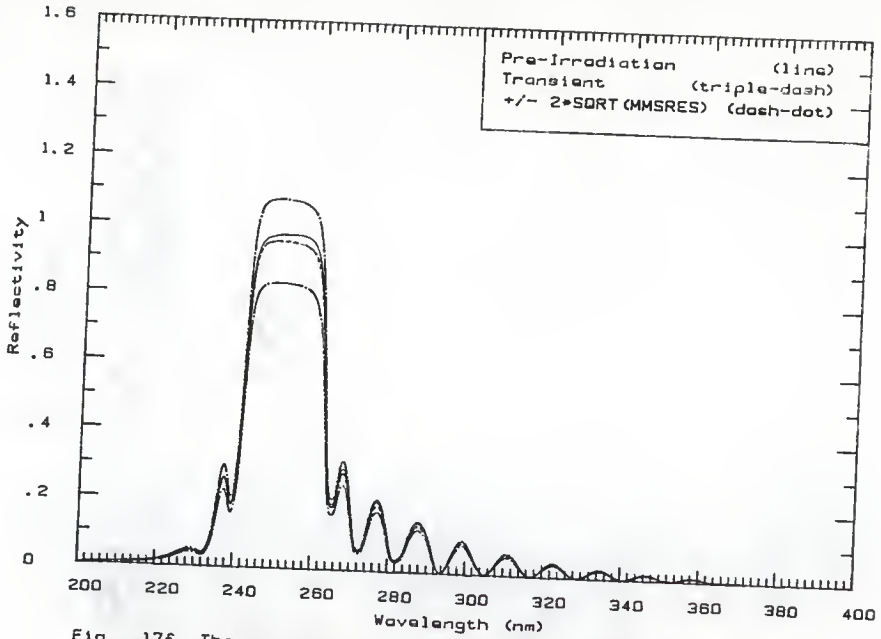

Fig. 17f The pre-irradiation reflectivity compared to the transient reflectivity based on Fig. 5f. (168 -201 ns), for dielectric mirror 13 in position 8.

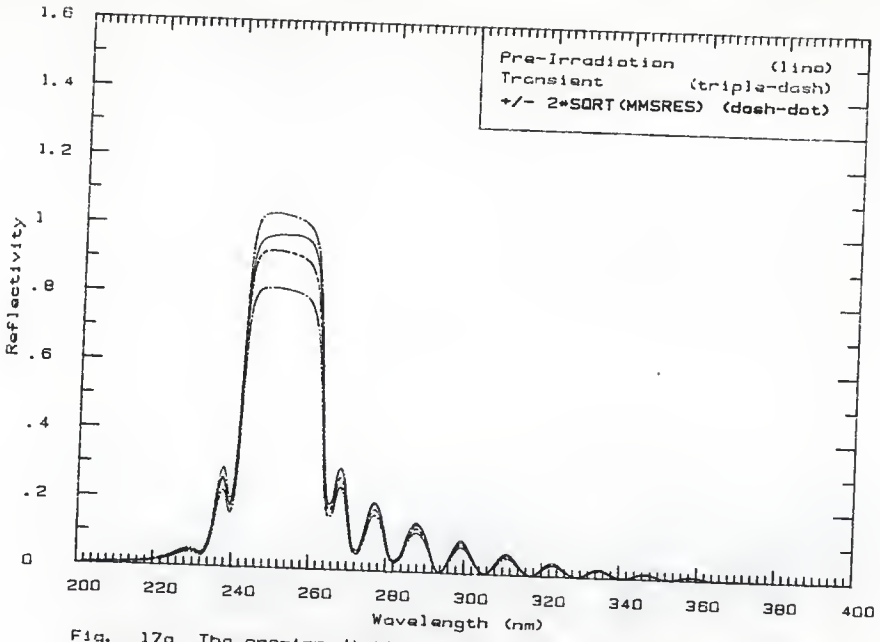

Fig. 17g The pre-irradiation reflectivity compared to the transient reflectivity based on Fig. 5g. (201 -235 ns), for dielectric mirror 13 in position 8.

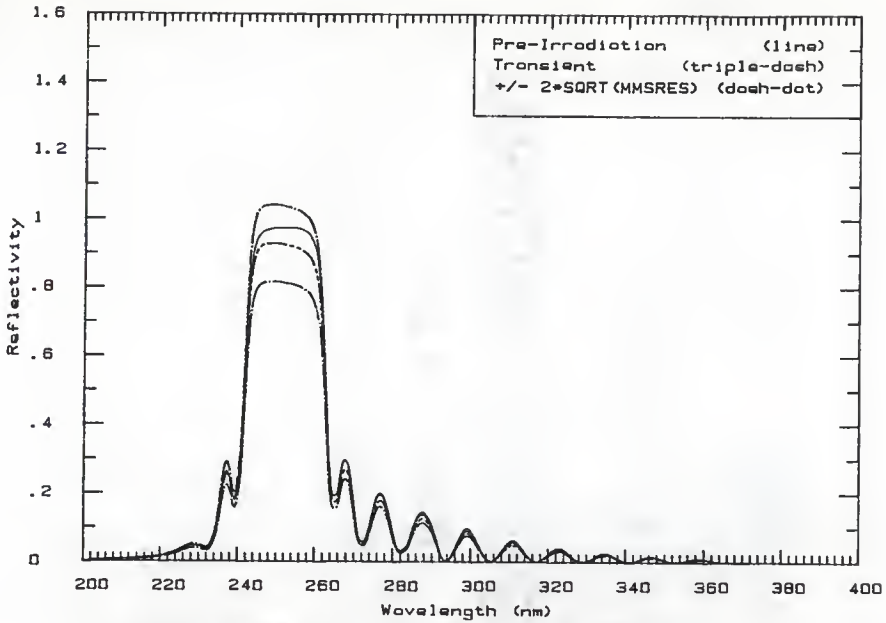

Fig. 17h The pre-irradiation reflectivity compared to the transient reflectivity based on Fig. 5h, (235 -268 ns). for dielectric mirror 13 in position B.

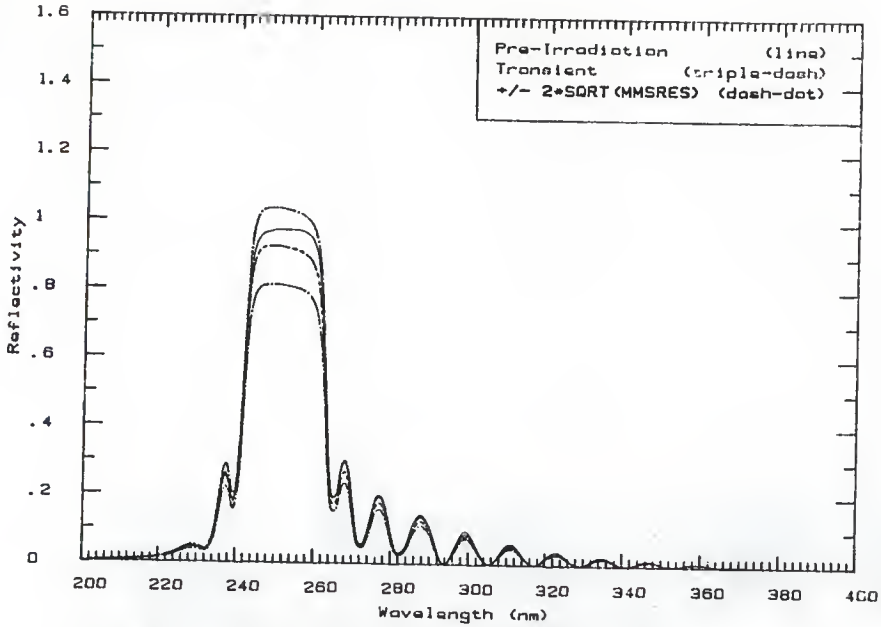

Fig. 171 The pre-irradiation reflectivity compared to the transient reflectivity based on Fig. 5i. (268 -293 ns), for dielectric mirror 13 in position B.

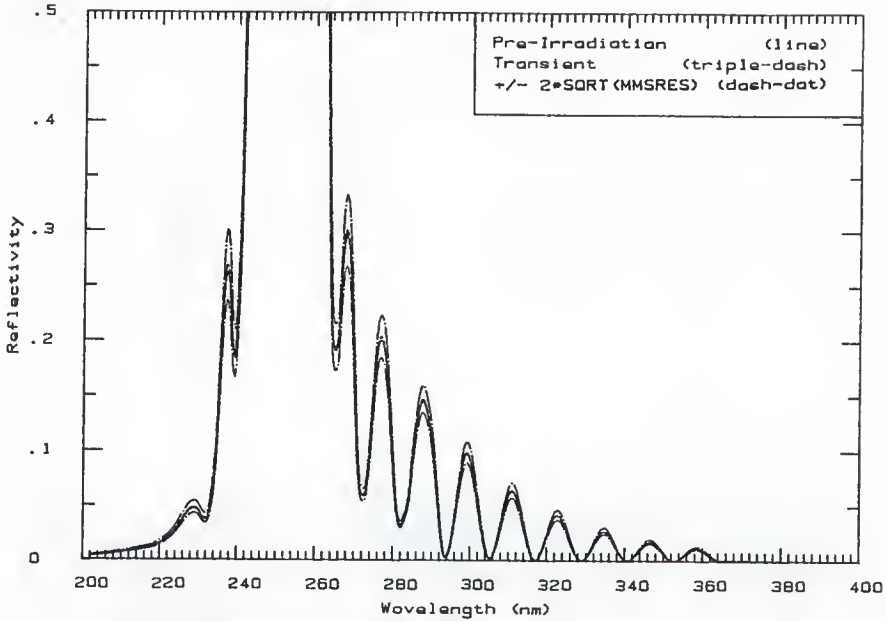

Fig. 17J The expanded view of the pre-irradiation and transient reflectivities of Fig. 17a for dielectric mirror 13 in position 8.

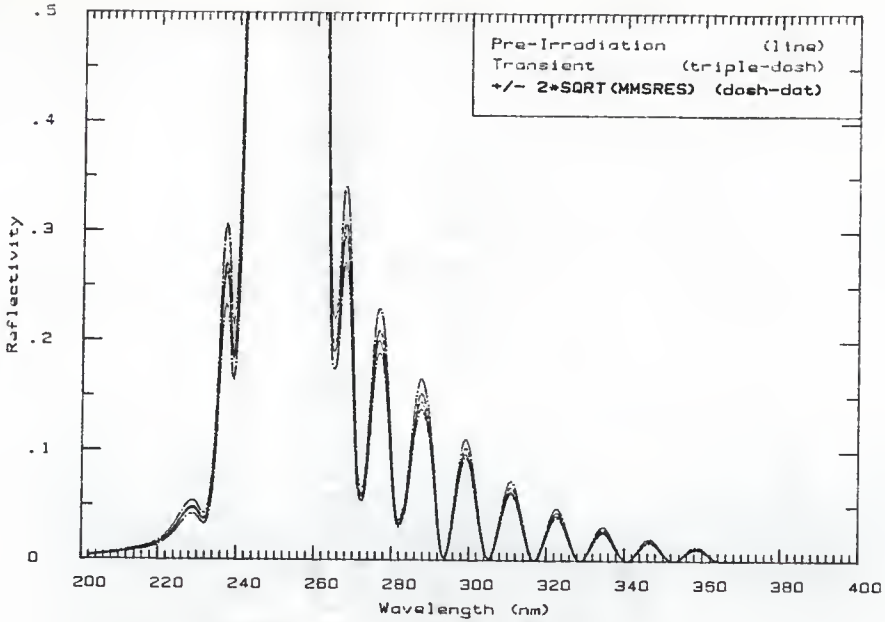

Fig. 17k The exponded view of the pre-irradiation and transient reflectivities of Fig. 17b for dielectric mirror 13 in position 8.

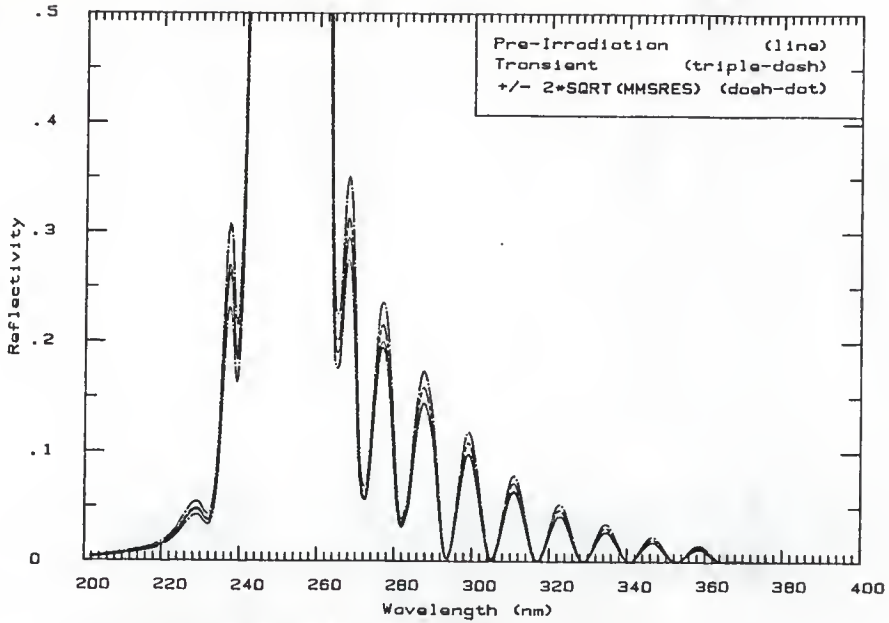

Fig. 171 The exponded view of the pre-irradiation and transient reflectivities of Fig. 17c for dielectric mirror 13 in position 8.

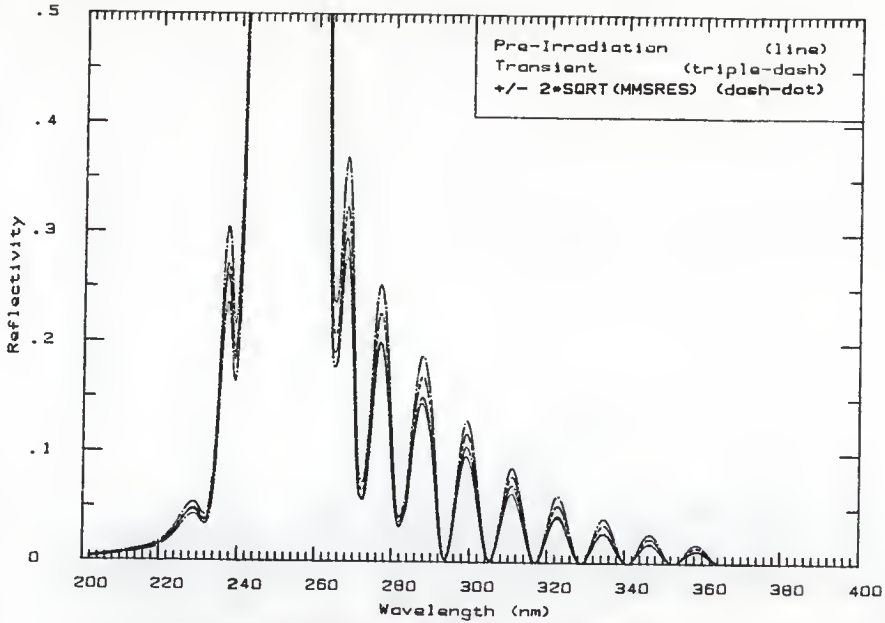

Fig. 17m The expanded view of the pre-irradiation and transient reflectivities of Fig. 17d for dielectric mirror 13 in position B.

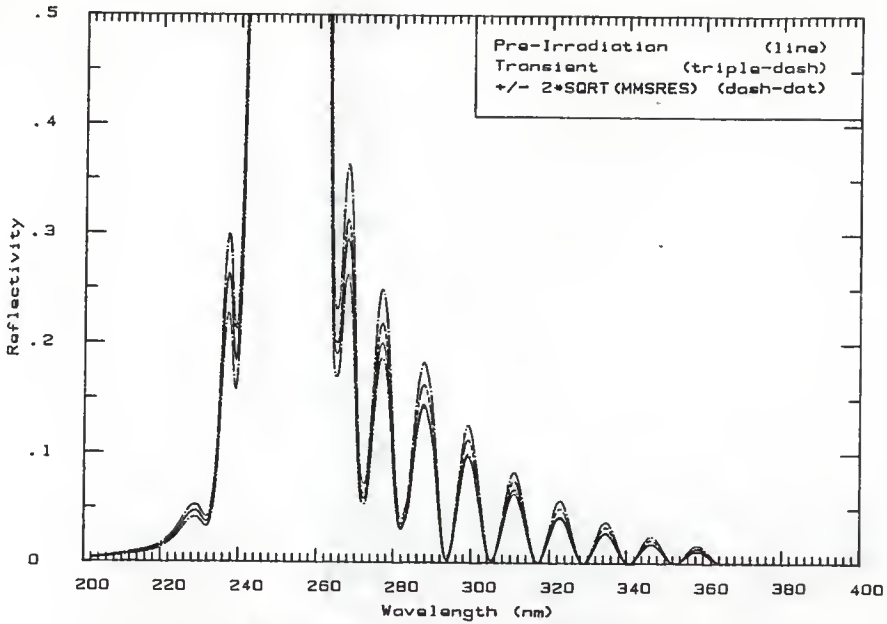

Fig. 17n The exponded view of the pre-irradiation and transient reflectivities of Fig. 17a for dielectric mirror 13 in position B.

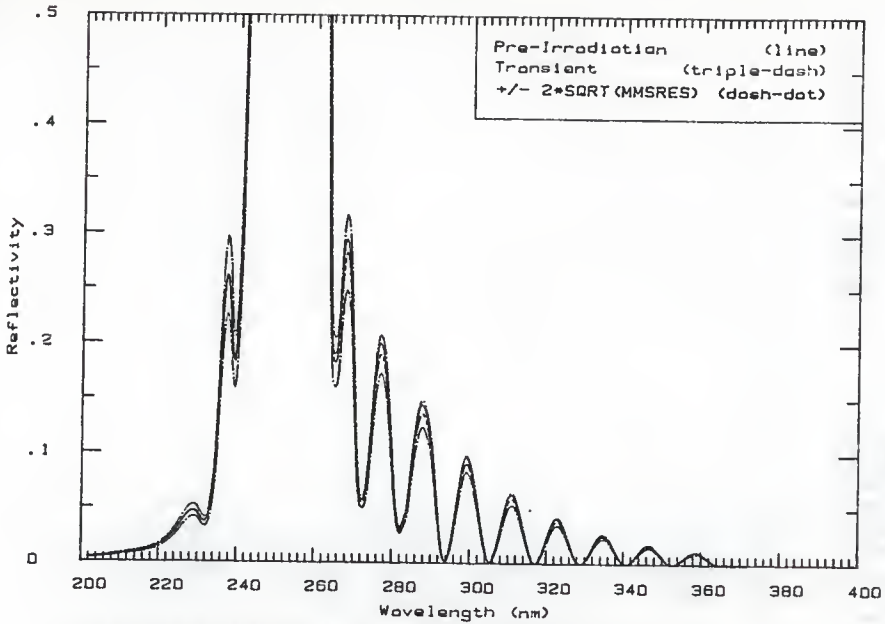

Fig. 17o The expanded view of the pre-irradiation and transient reflectivities of Fig. 17f for dielectric mirror 13 in position 8.

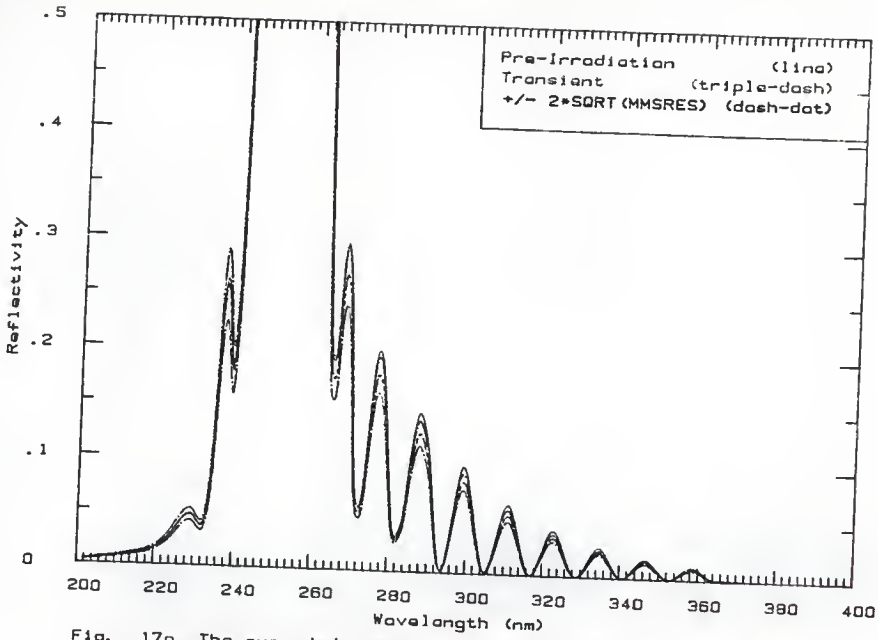

Fig. 17p The expanded view of the pre-irradiation and transient reflectivities of Fig. 17g for dielectric mirror 13 in position 8.

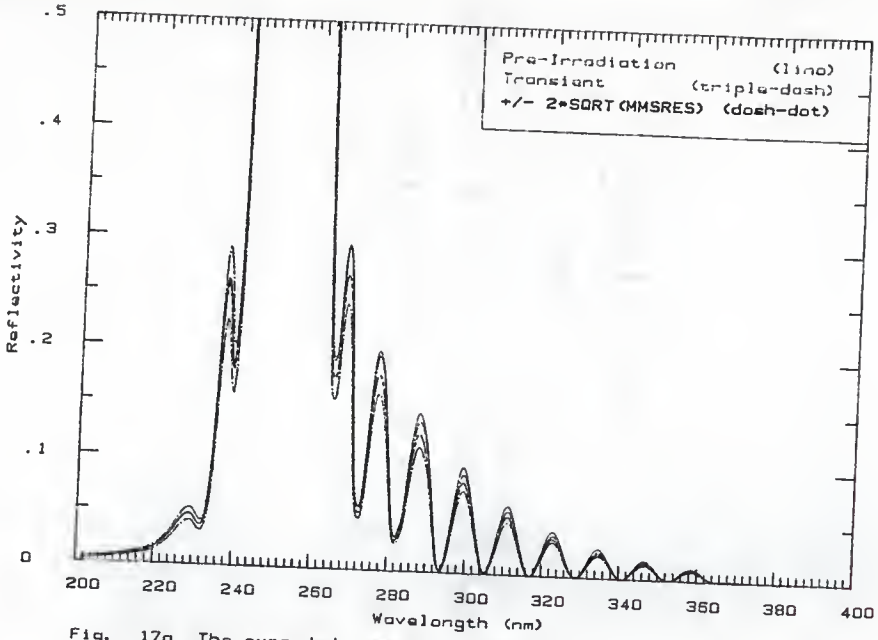

Fig. 17g The expanded view of the pre-irradiation and transient reflectivities of Fig. 17h for dielectric mirror 13 in position 8.

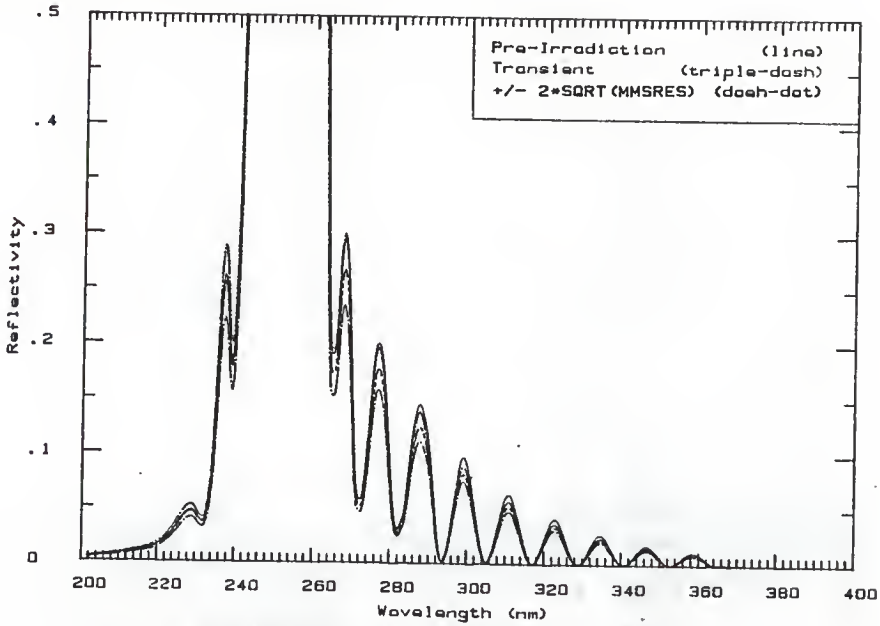

Fig. 17r The expanded view of the pre-irradiation and transient reflectivities of Fig. 17i for dielectric mirror 13 in position 8.

Figures 18a to 18r, the transient reflectivity plots for dielectric mirror 26, irradiated in position A. The block-out irradiation mean beam current was 225 mA and the pulse length was 500 ns.

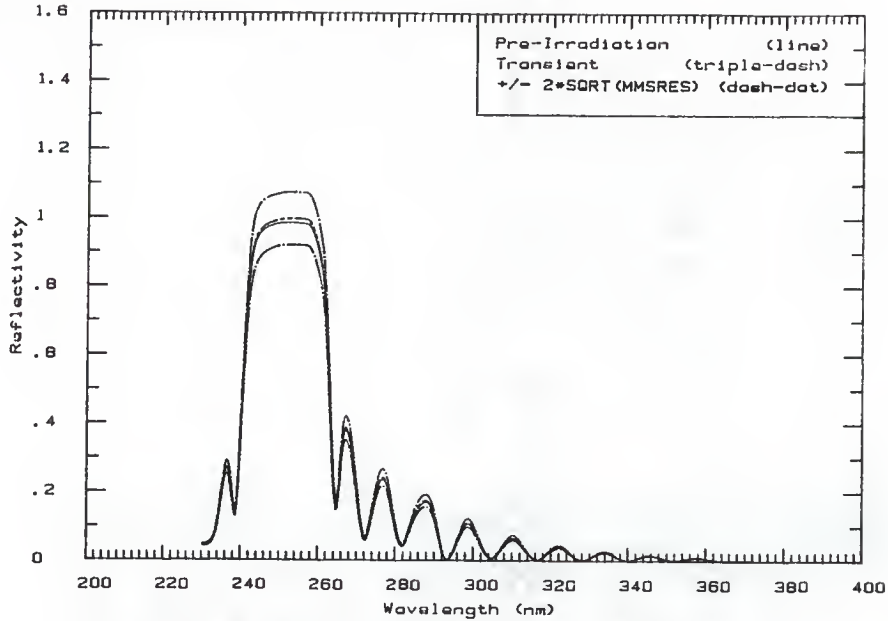

Fig. 18a The pre-irradiation reflectivity compared to the transient reflectivity based on Fig. 8a, (0.0 -37 ns), for dielectric mirror 26.

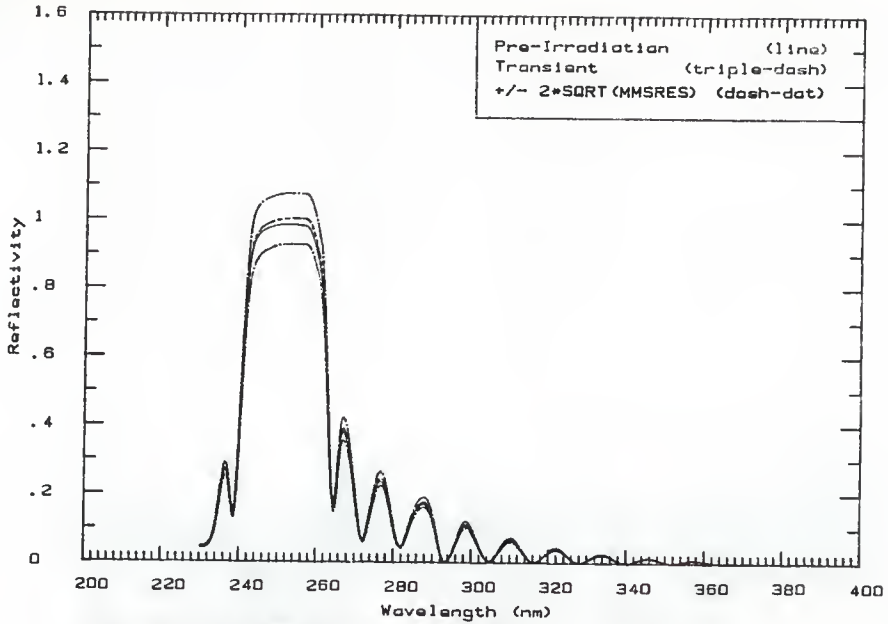

Fig. 18b The pre-irradiation reflectivity compared to the transient reflectivity based on Fig. 6b. (37.0 -70.5 ns), for dielectric mirror 26.

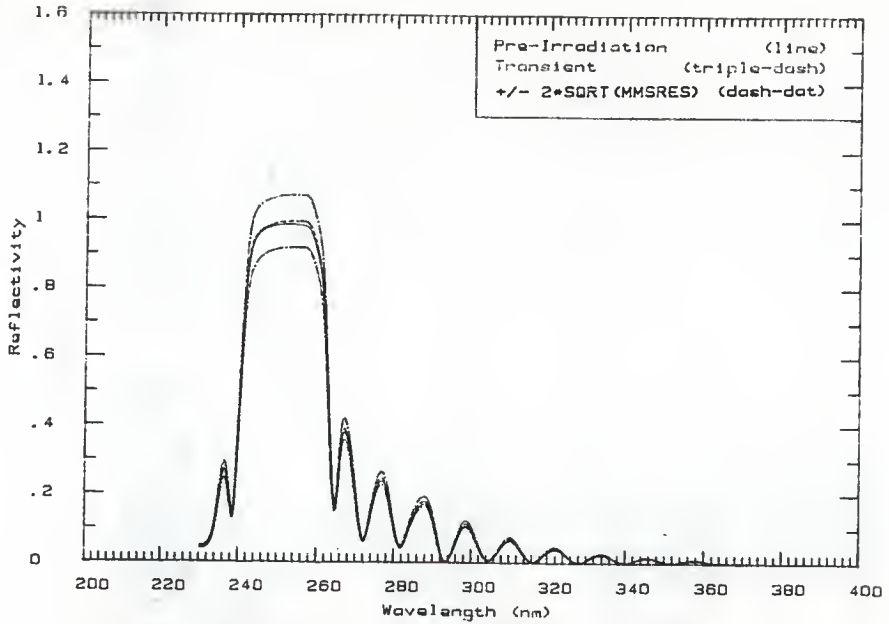

Fig. 18c The pre-irradiation reflectivity compared to the transient reflectivity based on Fig. 6c, (70.5 -104 ns), for dielectric mirror 28.

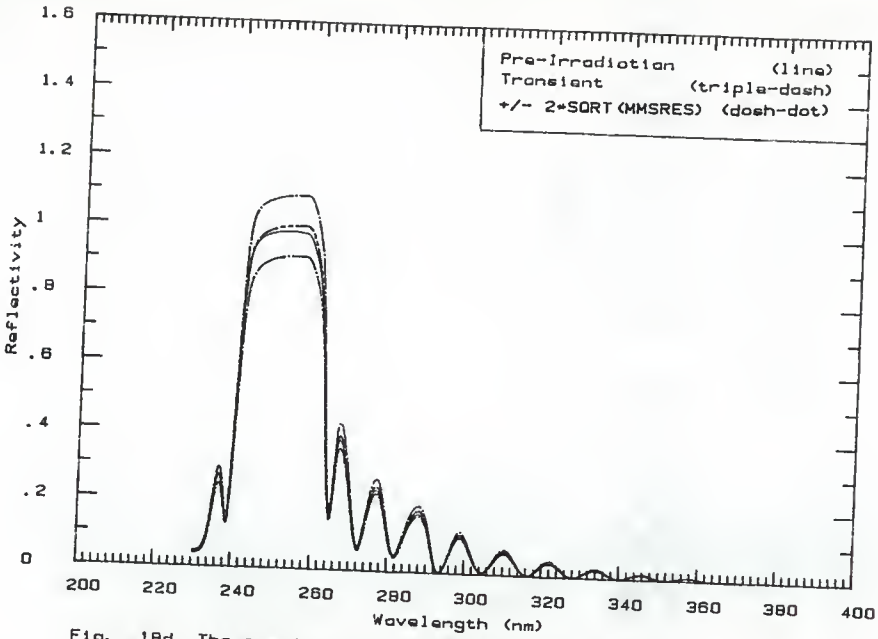

Fig. 18d The pre-irradiation reflectivity compared to the transient reflectivity based on Fig. 6d. (104 -138 ns). for dielectric mirror 26.

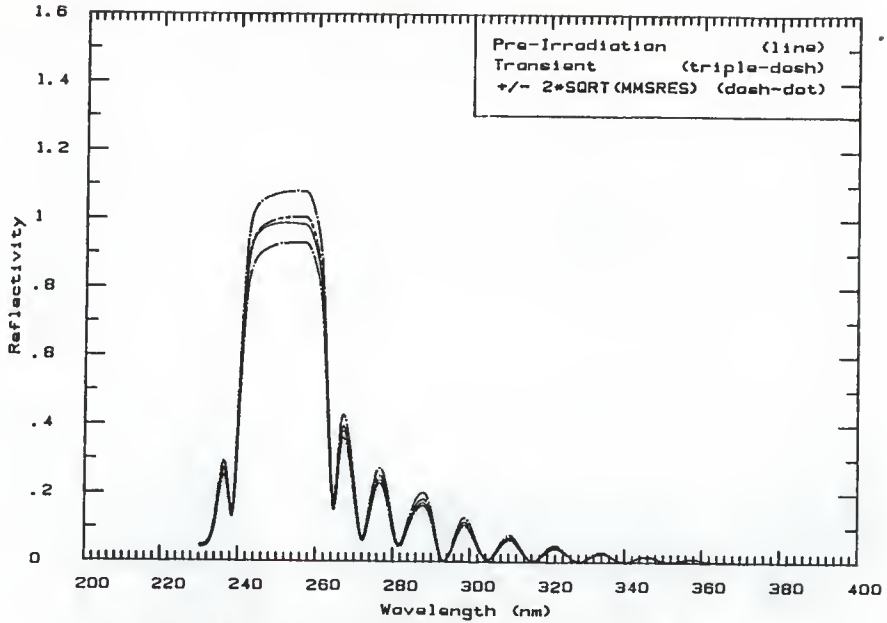

Fig. 18a The pre-irradiation reflectivity compared to the transient reflectivity based on Fig. 6a, (138 -171 ns), for dielectric mirror 26.

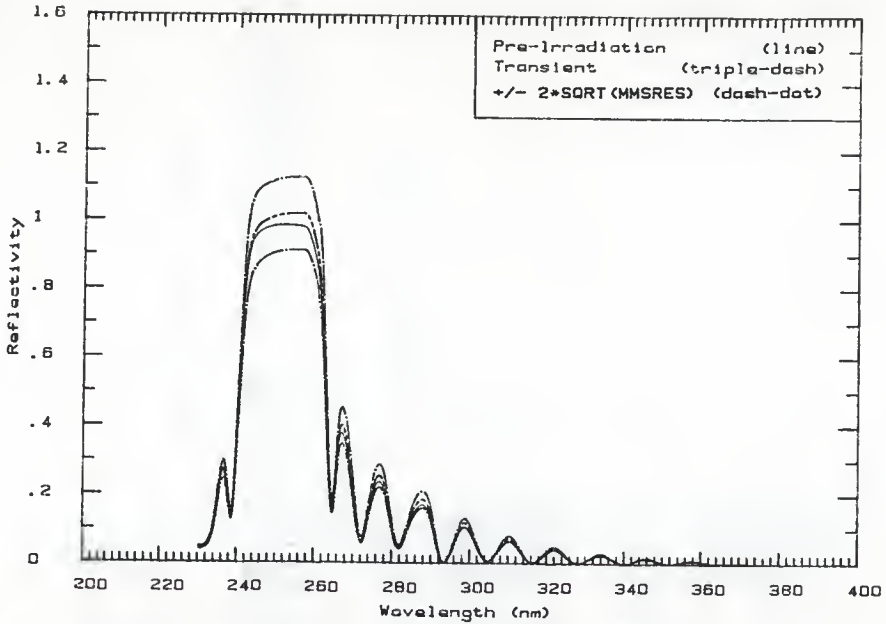

Fig. 18f The pre-irradiation reflectivity compared to the transient reflectivity based on Fig. 6f. (171 -205 ns), for dielectric mirror 26.

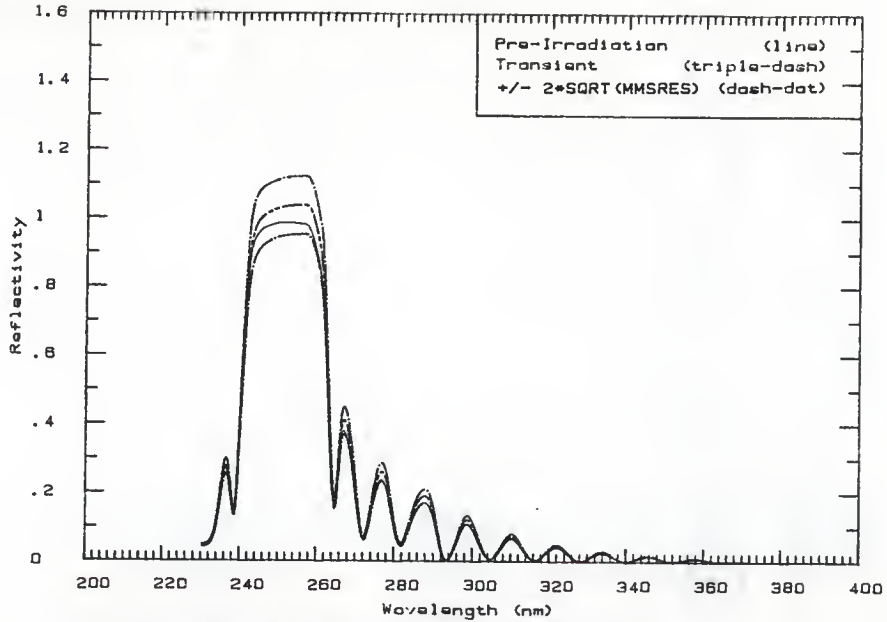

Fig. 18g The pre-irradiation reflectivity compared to the transient reflectivity based on Fig. 6g. (205 -238 ns), for dielectric mirror 26.

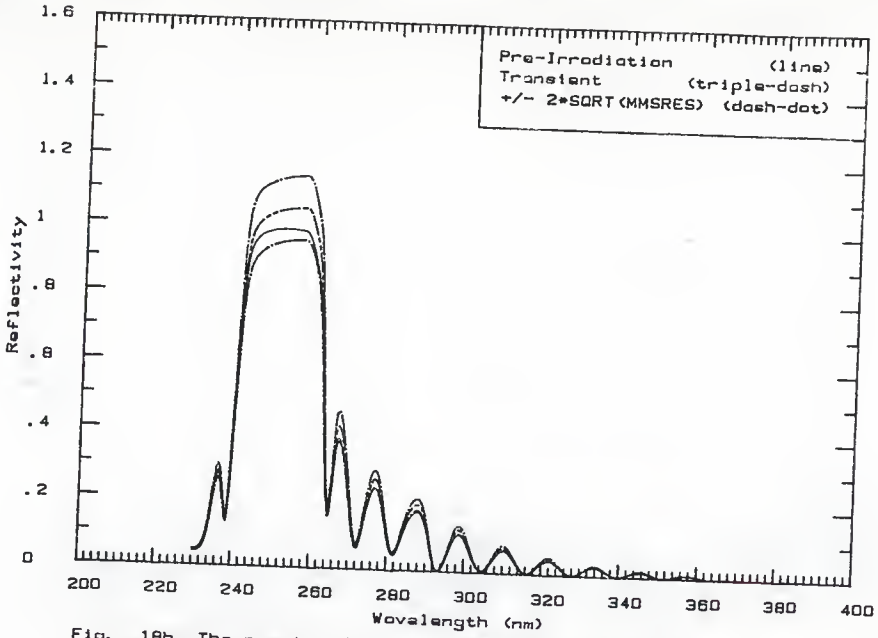

Fig. 18h The pre-irrodiation reflectivity compared to the transient reflectivity based on Fig. 6h. (238 -272 ns). for dielectric mirror 26.

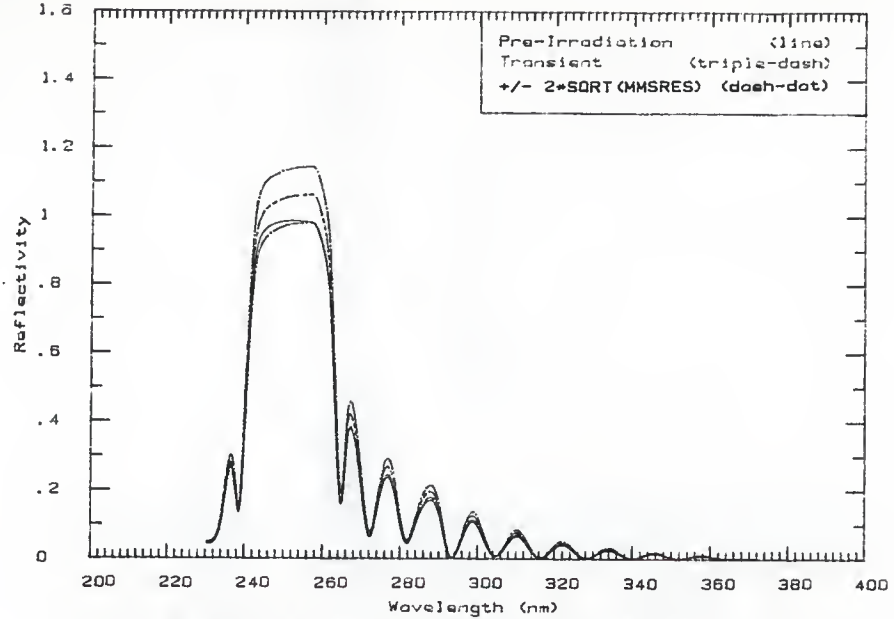

Fig. 181 The pre-irradiation reflectivity compared to the transient reflectivity based on Fig. 61. (272 -313 ns). for dielectric mirror 26.

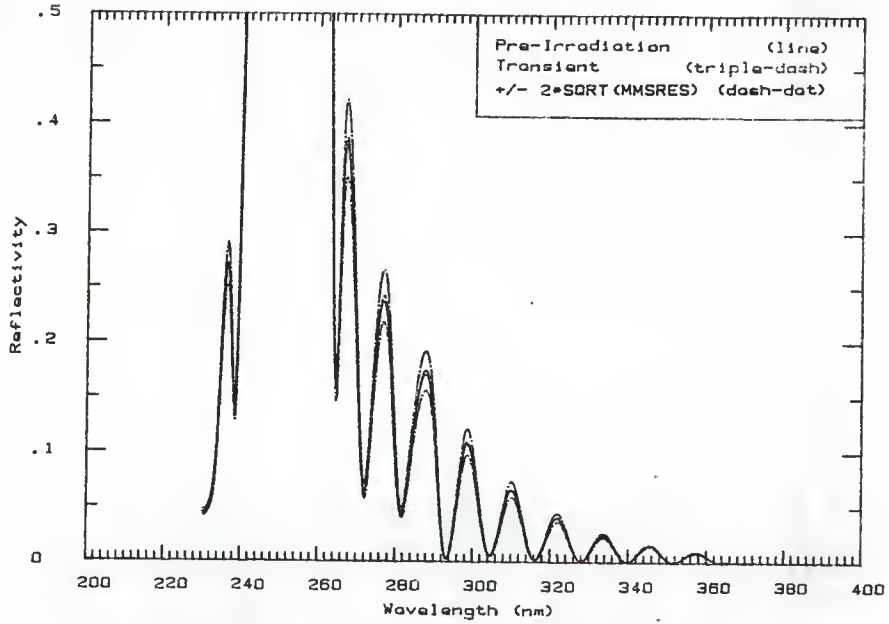

Fig. 18J The expanded view of the pre-irradiation and transient reflectivities of Fig. 18a for dielectric mirror 26.

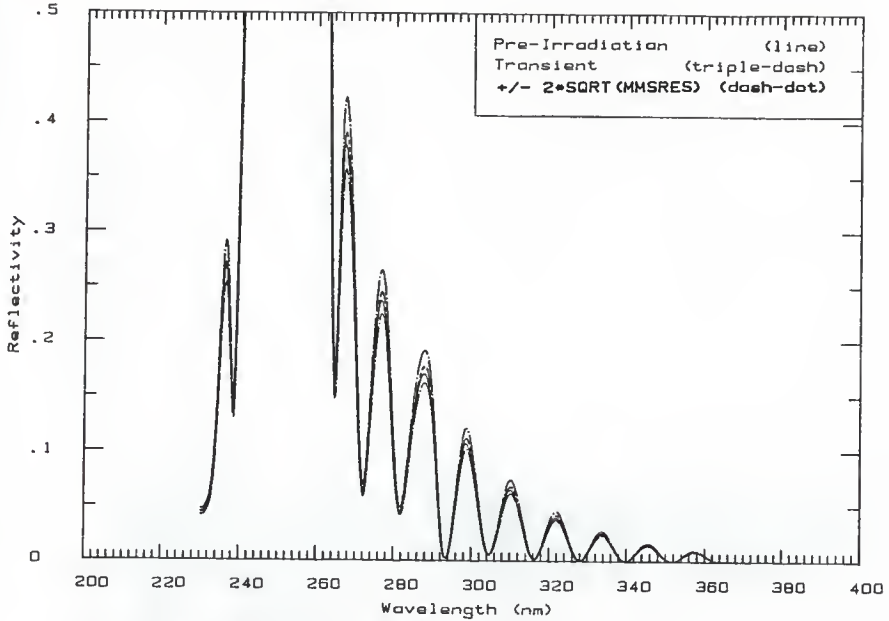

Fig. 18k The expanded view of the pre-irradiation and transient reflectivities of Fig. 18b for dielectric mirror 26.

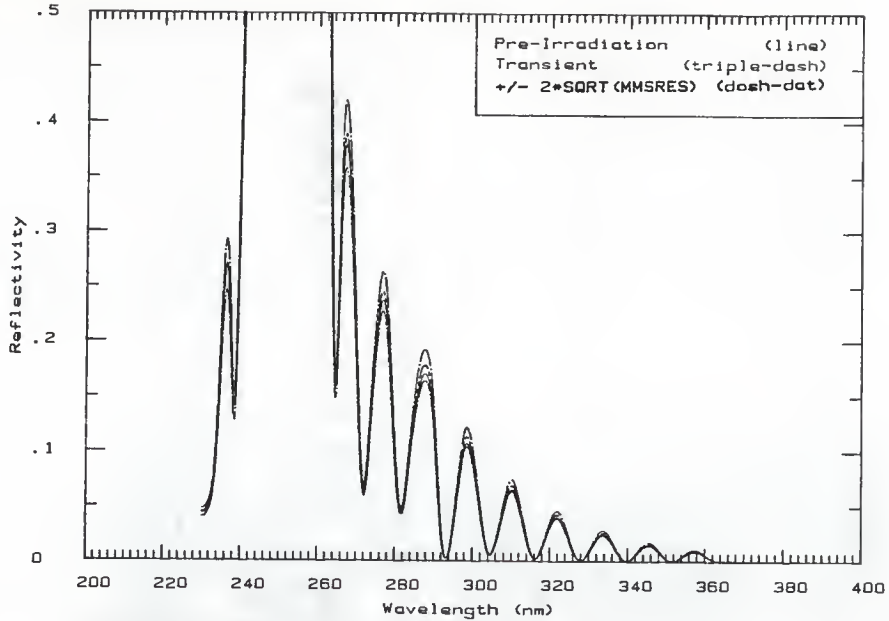

Fig. 181 The expanded view of the pre-irradiation and transient reflectivities of Fig. 18c for dielectric mirror 26.

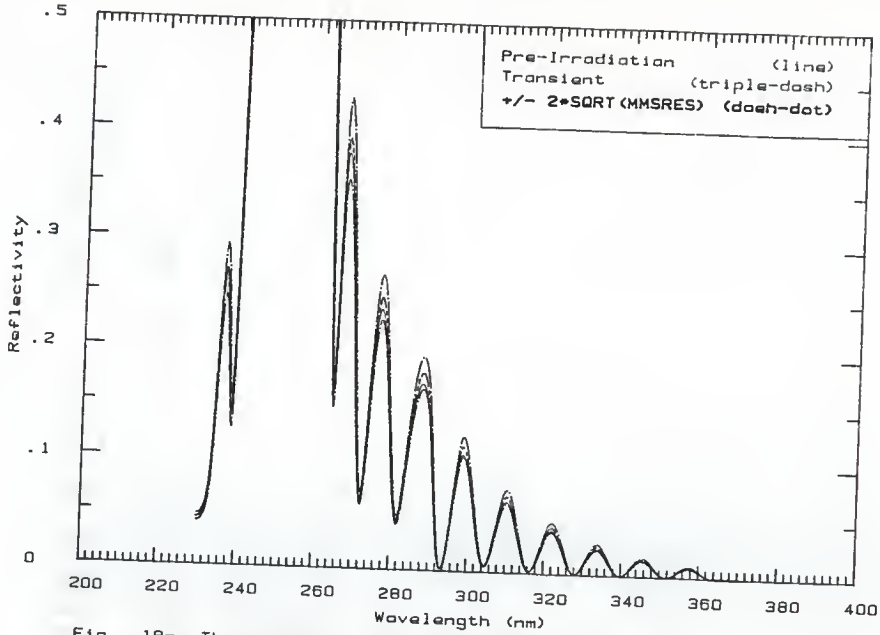

Fig. 18m The expanded view of the pre-irradiation and transient reflectivities of Fig. 18d for dielectric mirror 26.

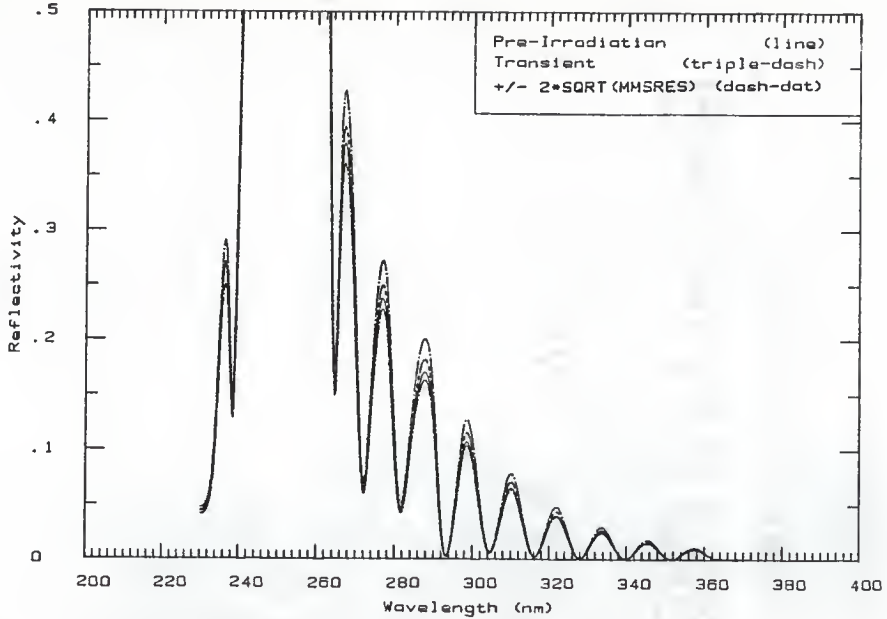

Fig. 18n The expanded view of the pre-irradiation and transient reflectivities of Fig. 18e for dielectric mirror 26.

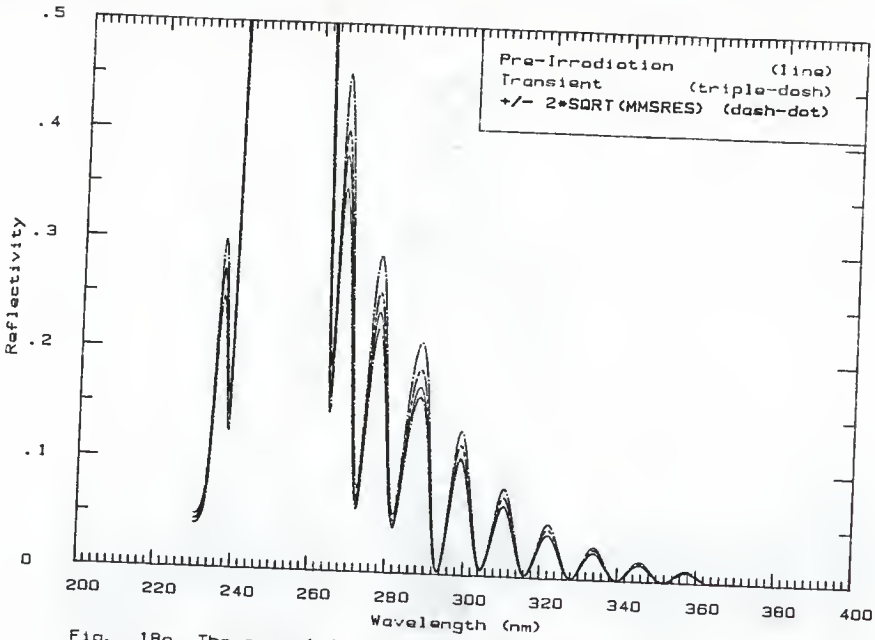

Fig. 18o The expanded view of the pre-irradiation and transient reflectivities of Fig. 18f for dielectric mirror 26.

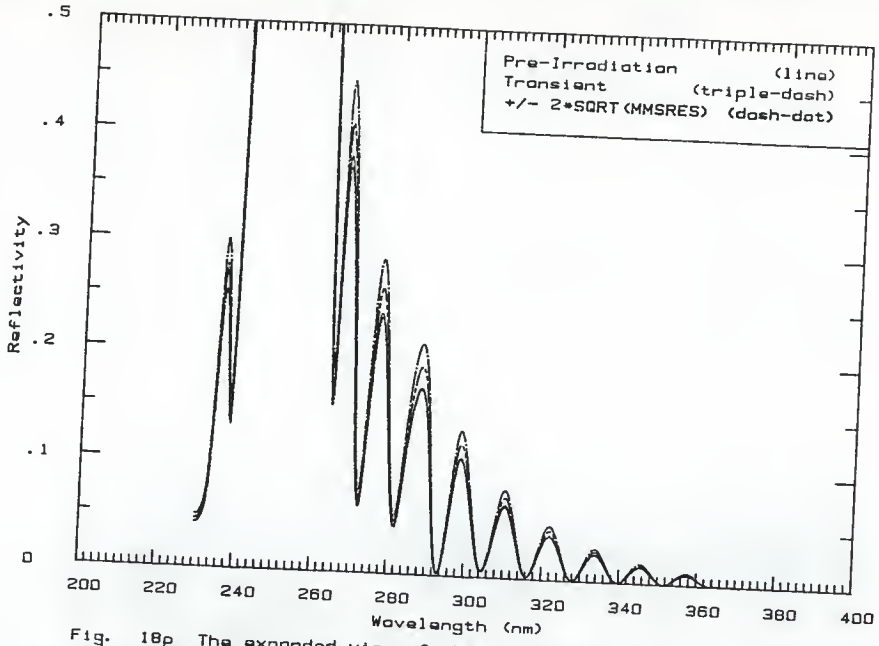

Fig. 18p The expanded view of the pre-irradiation and transient reflectivities of Fig. 18g for dielectric mirror 26.

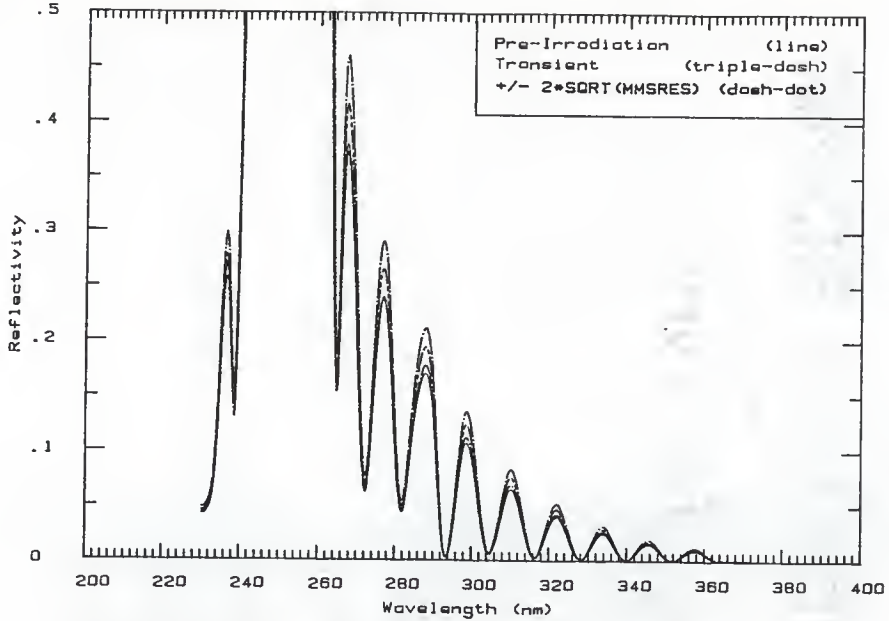

Fig. 18g The expanded view of the pre-irradiation and transient reflectivities of Fig. 18h for dielectric mirror 26.

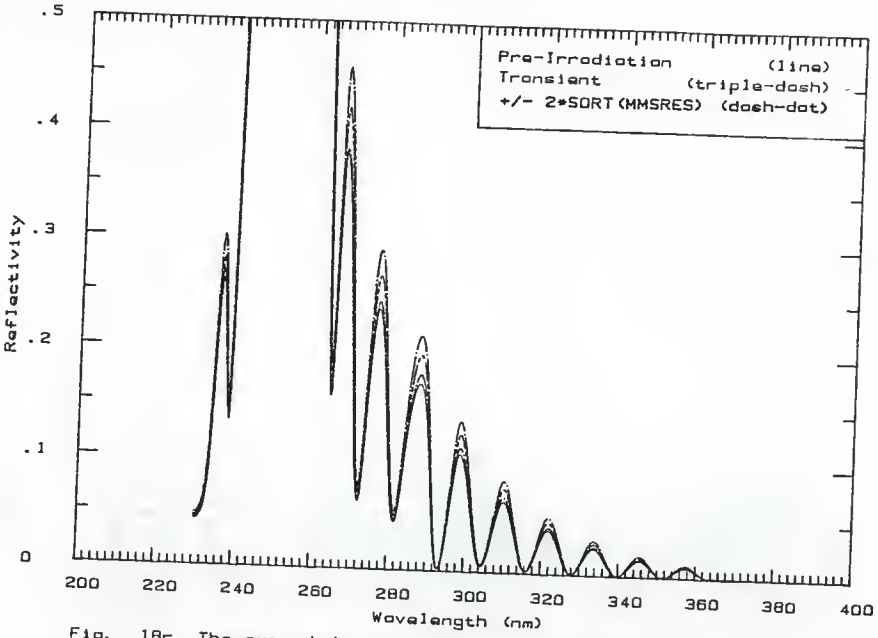

Fig. 18r The expanded view of the pre-irradiation and transient reflectivities of Fig. 18i for dielectric mirror 26.

Figures 19a to 19i, the transient reflectivity plots for metal-coated mirror 1L, irradiated in position A. The block-out irradiation mean beam current was 5 A and the pulse length was 20 ns.

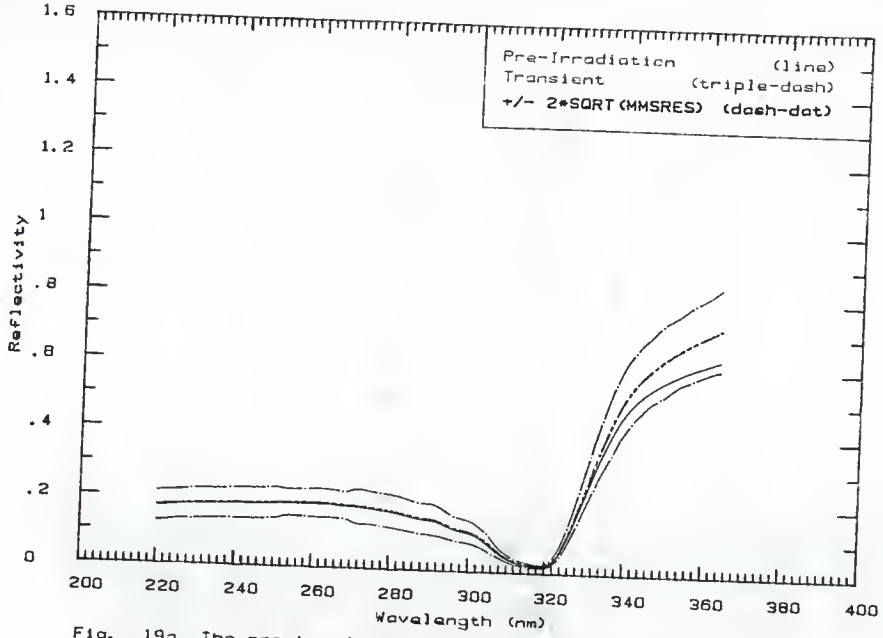

Fig. 19a The pre-irradiation reflectivity compared to the transient reflectivity based on Fig. 7a. (0.0-5.0 ns), for metal-coated mirror IL.

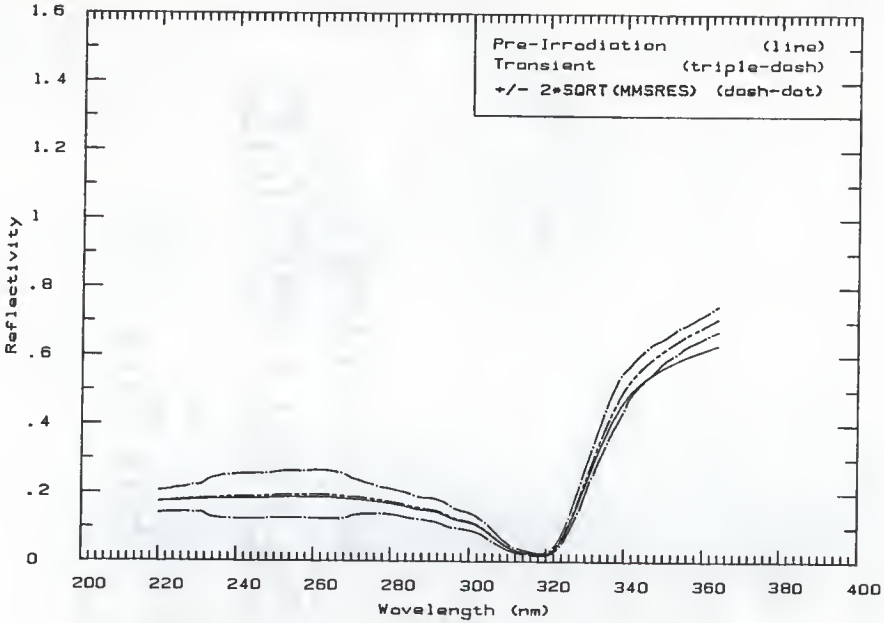

Fig. 19b The pre-irradiation reflectivity compared to the transient reflectivity based on Fig. 7b, (5.0-10.0 ns), for metal-coated mirror 1L.

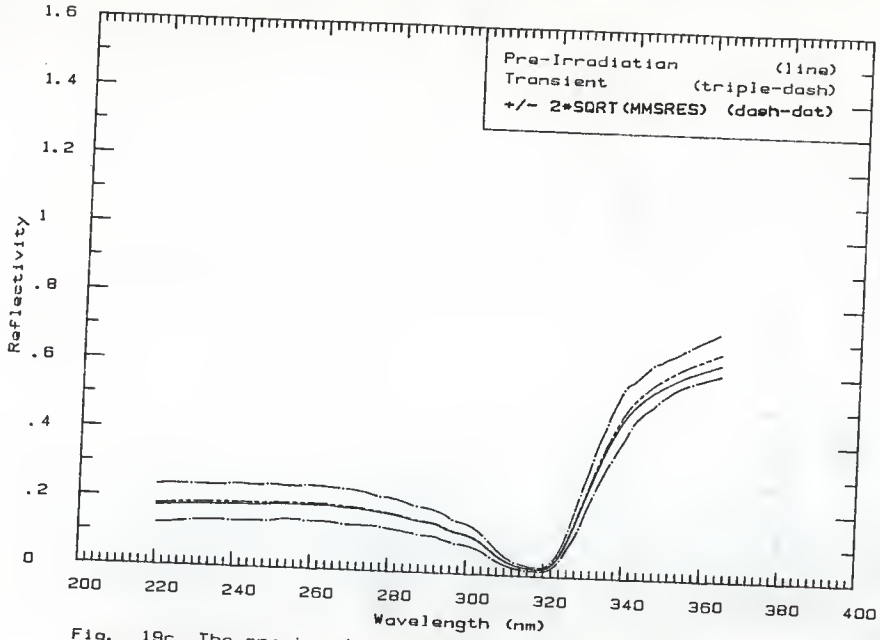

Fig. 19c The pre-irradiation reflectivity compared to the transient reflectivity based on Fig. 7c. (10.0 -15.0 ns), for metal-coated mirror 1L.

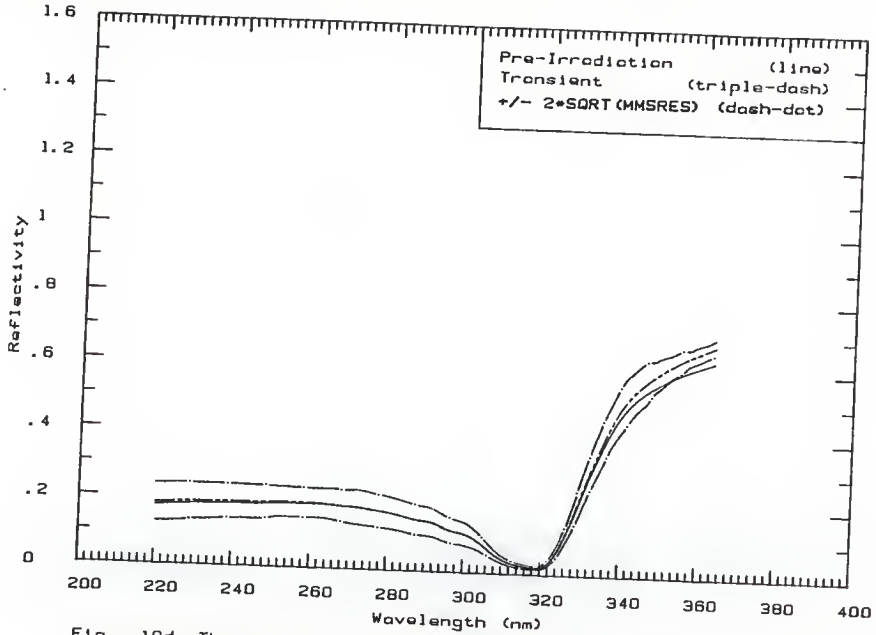

Fig. 19d The pre-irradiation reflectivity compared to the transient reflectivity based on Fig. 7d. (15.0 -20.0 ns), for metal-coated mirror 1L.

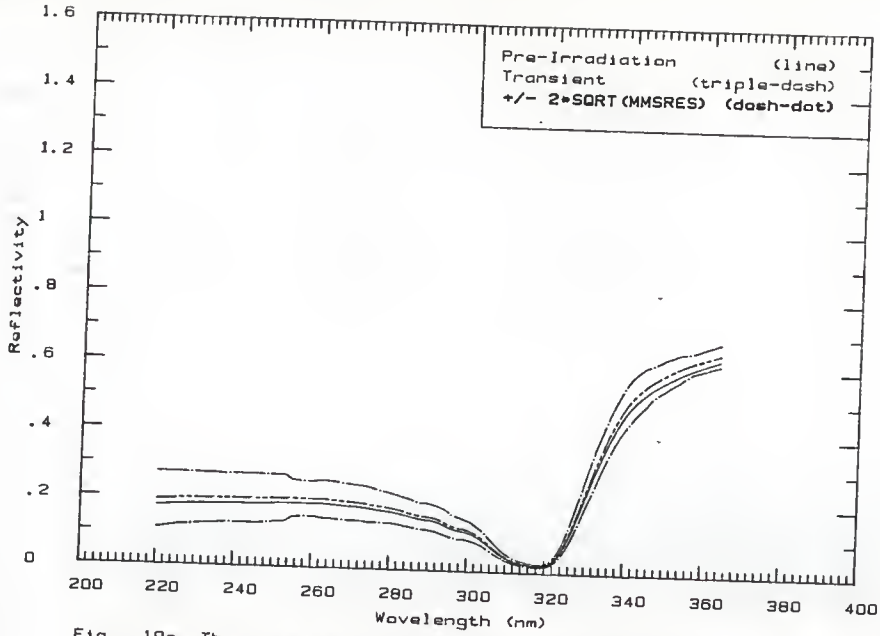

Fig. 19a The pre-irradiation reflectivity compared to the transient reflectivity based on Fig. 7a, (20.0 -25.0 ns), for metal-coated mirror 1L.

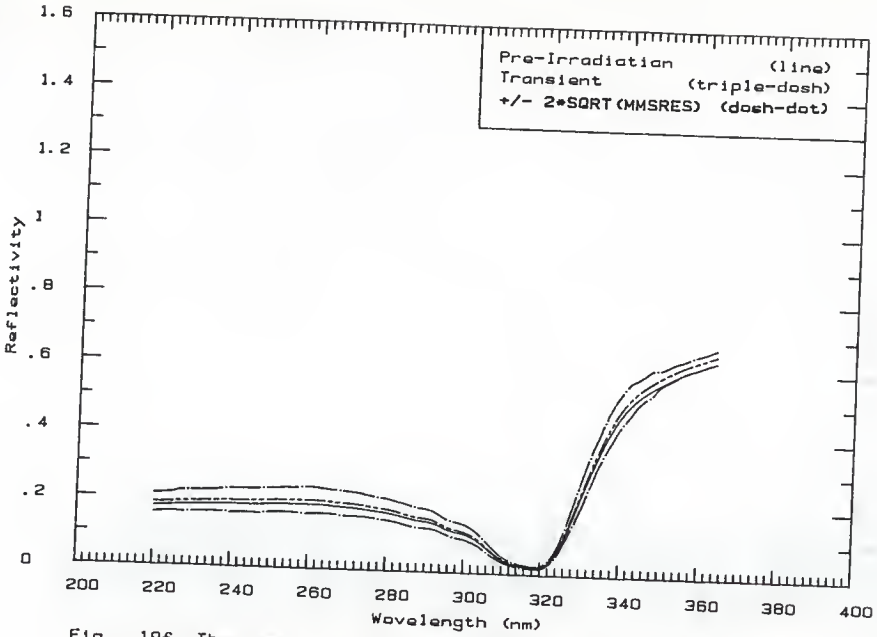

Fig. 19f The pre-irradiation reflectivity compared to the transient reflectivity based on Fig. 7f. (25.0 -41.3 ns), for metal-coated mirror 1L.

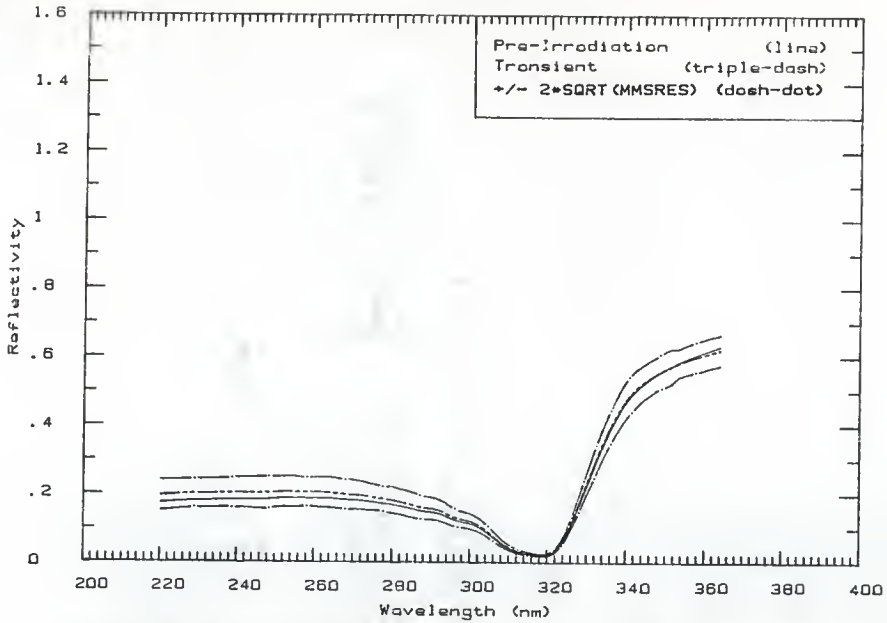

Fig. 19g The pre-irradiation reflectivity compared to the transient reflectivity based on Fig. 7g. (41.3 -57.5 ns). for metal-coated mirror 1L.

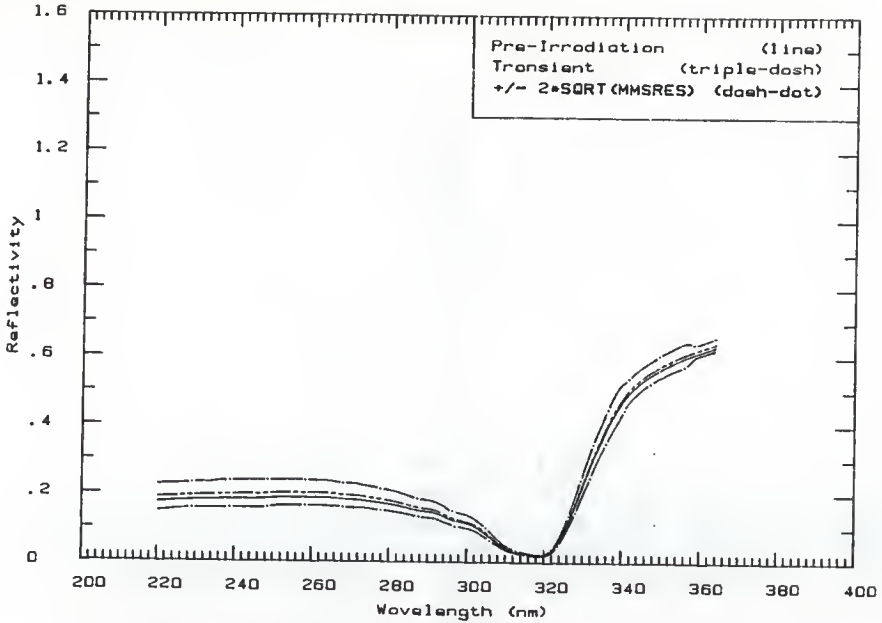

Fig. 19h The pre-irradiation reflectivity compared to the transient reflectivity based on Fig. 7h, (57.5 -73.8 ns), for metal-coated mirror 1L.

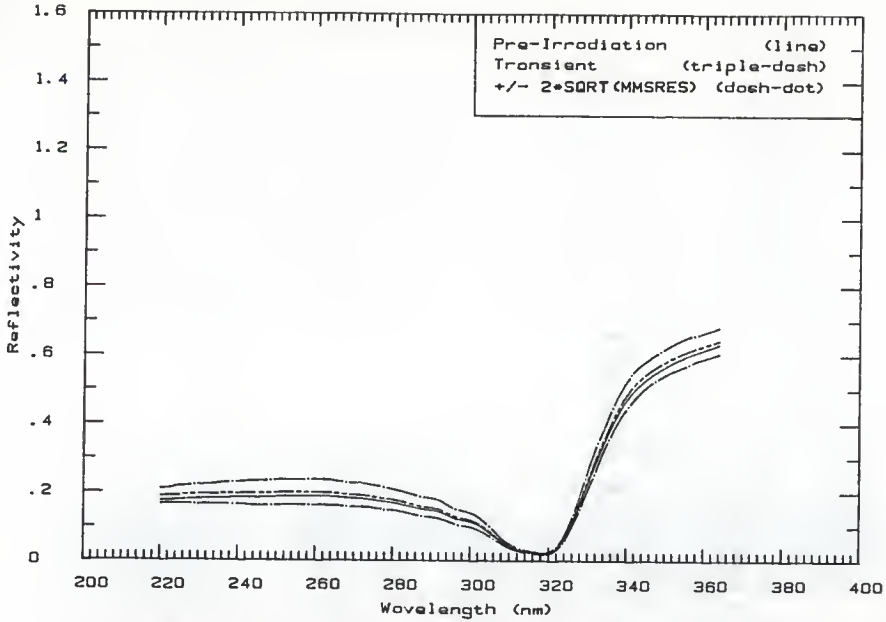

Fig. 19i The pre-irradiation reflectivity compared to the transient reflectivity based on Fig. 7i, (73.8 -88.0 ns), for metal-coated mirror 1L.

Figures 20a to 20 i, the transient reflectivity plots for metal-coated mirror 2L, irradiated in position A. The block-out irradiation mean beam current was 225 mA and the pulse length was 200 ns.

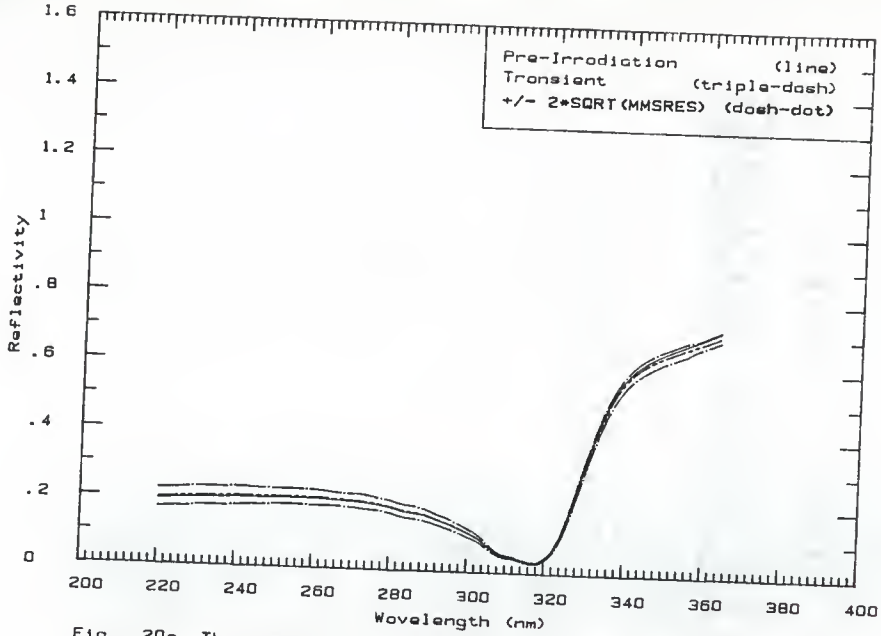

Fig. 20o The pre-irrodiation reflectivity compared to the transient reflectivity based on Fig. 8o. (0.8 -20.9 ns), for metal-coated mirror 2L, in position A.

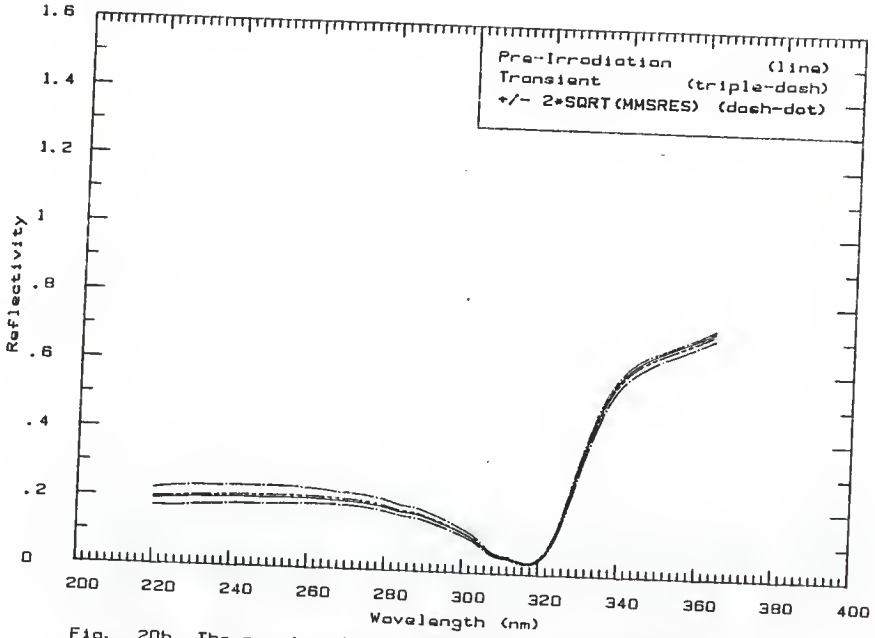

Fig. 20b The pre-irradiation reflectivity compared to the transient reflectivity based on Fig. 8b. (20.9 -41.0 ns), for metal-coated mirror 2L, in position A.

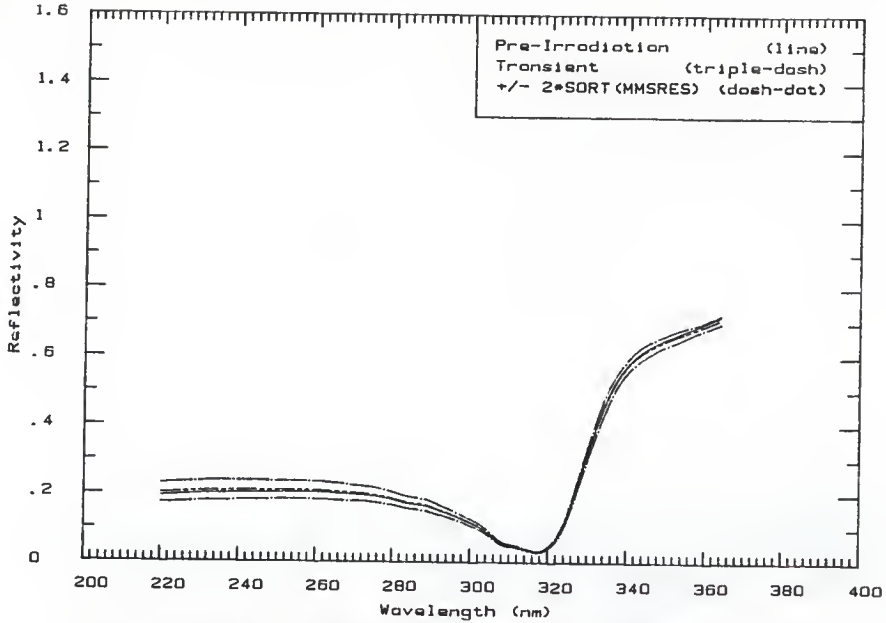

Fig. 20c The pre-irradiation reflectivity compared to the transient reflectivity based on Fig. 8c. (41.0 -61.1 ns), for metal-coated mirror 2L, in position A.

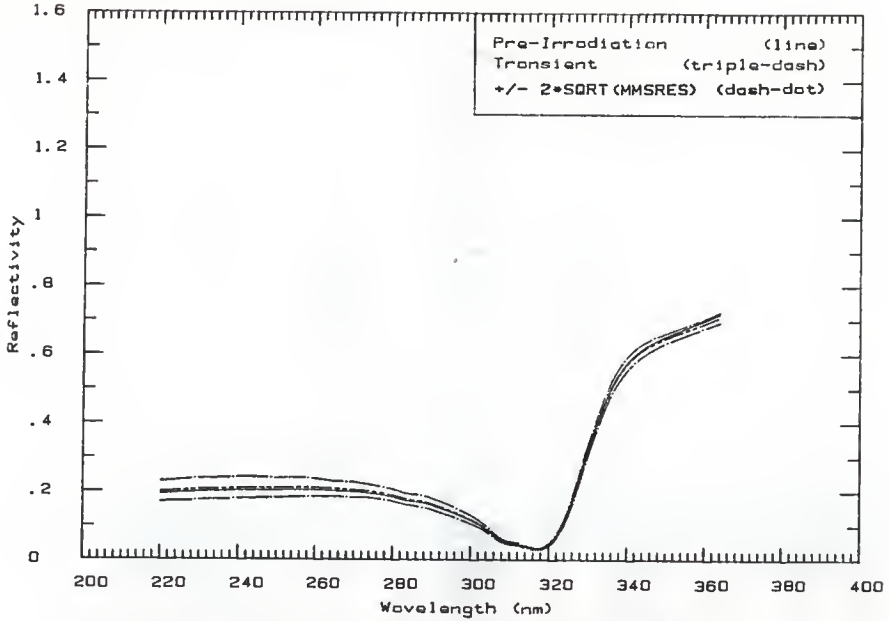

Fig. 20d The pre-irradiation reflectivity compared to the transient reflectivity based on Fig. 8d. (61.1 -81.2 ns), for metal-coated mirror 2L, in position A.

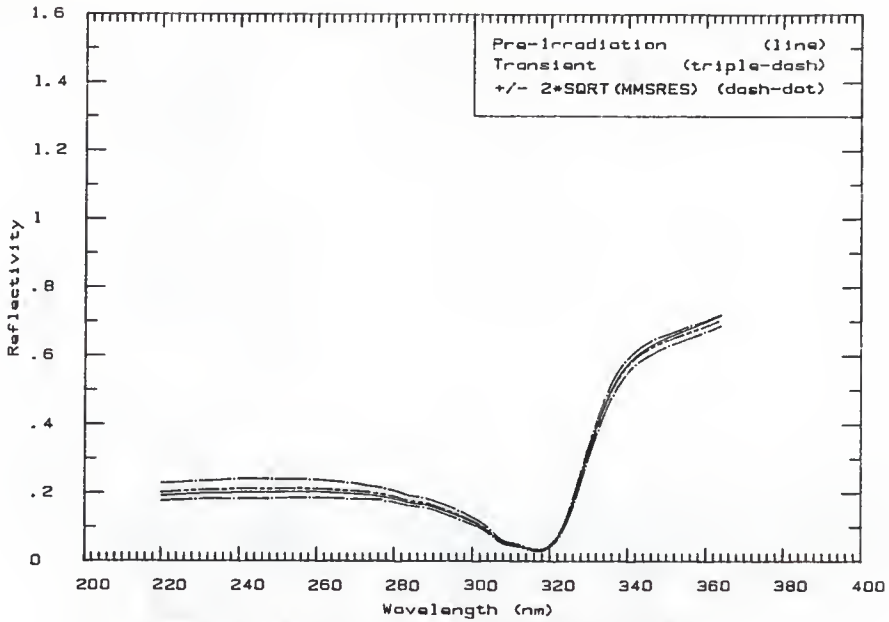

Fig. 20a The pre-irradiation reflectivity compared to the transient reflectivity based on Fig. 8a. (81.2 -101 ns), for metal-coated mirror 2L, in position A.

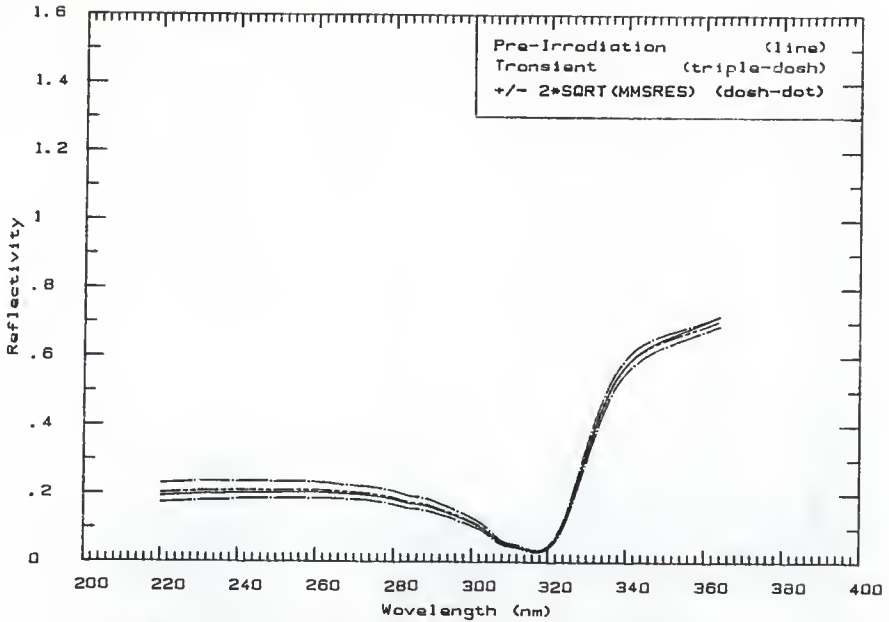

Fig. 20f The pre-irrodiation reflectivity compared to the transient reflectivity based on Fig. 8f. (101 -121 ns), for metal-coated mirror 2L, in position A.

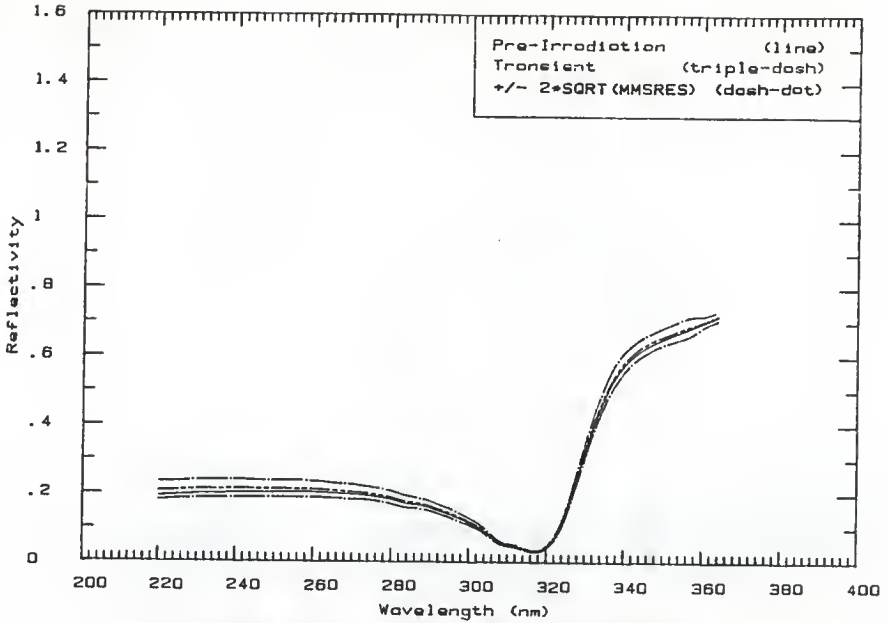

Fig. 20g The pre-irradiation reflectivity compared to the transient reflectivity based on Fig. 8g. (121 -142 ns), for metal-coated mirror 2L, in position A.

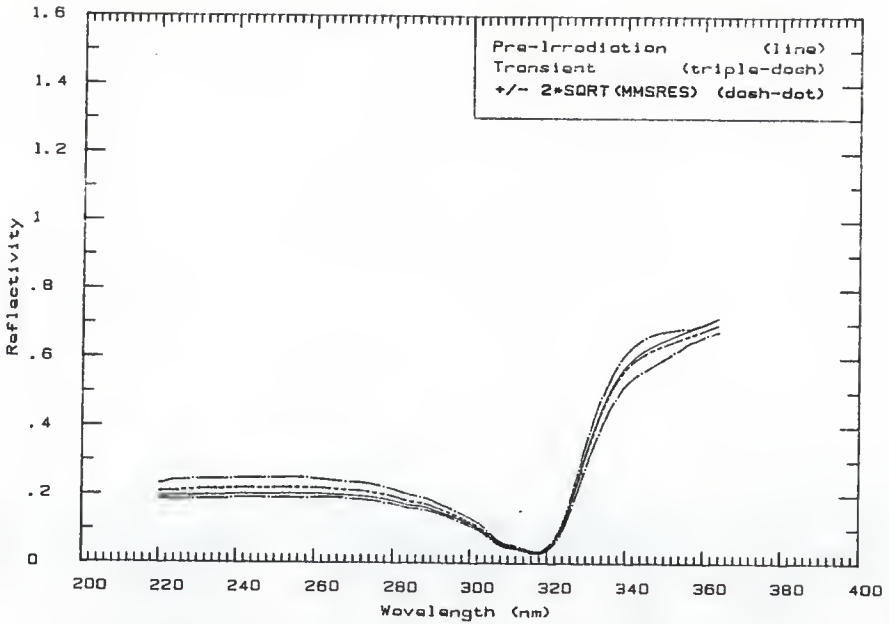

Fig. 20h The pre-irradiation reflectivity compared to the transient reflectivity based on Fig. 8h. (142 -162 ns), for metal-coated mirror 2L, in position A.

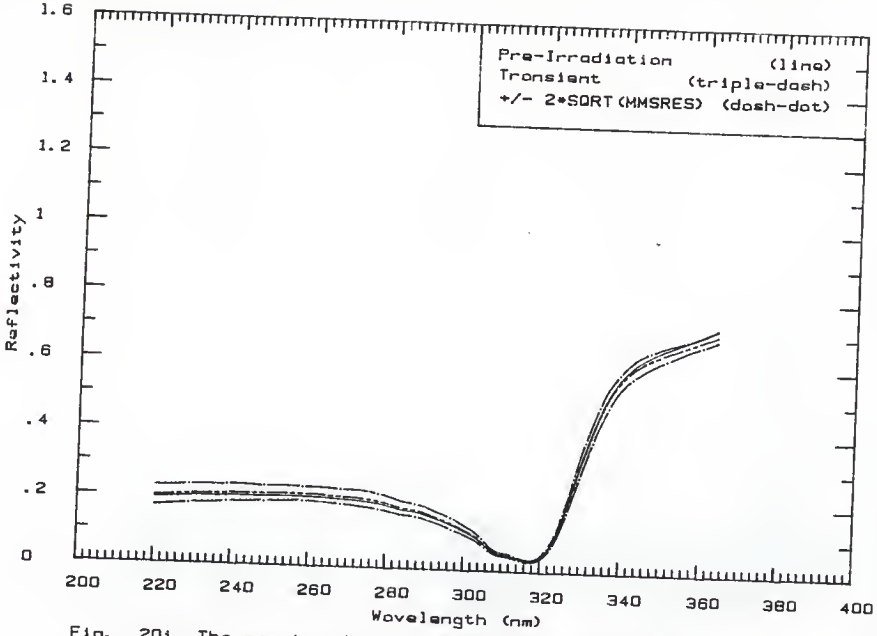

Fig. 20i The pre-irradiation reflectivity compared to the transient reflectivity based on Fig. 8i. (162 -183 ns), for metal-coated mirror 2L, in position A.

Figures 21a to 21i, the transient reflectivity plots for metal-coated mirror 2L, irradiated in position B. The block-out mean beam current was 225 mA while the pulse length was 200 ns.

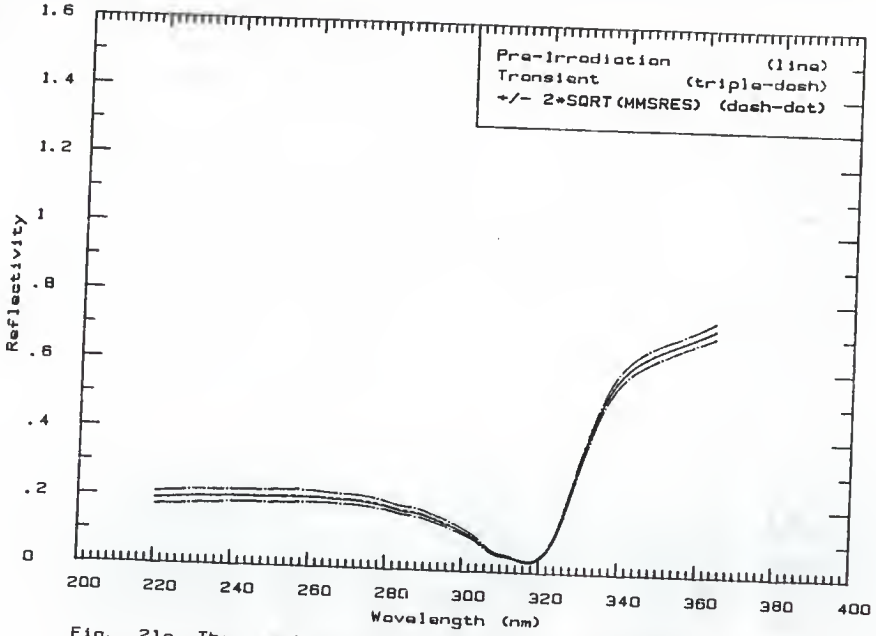

Fig. 21a The pre-irradiation reflectivity compared to the transient reflectivity based on Fig. 9a. (0.25 -33.8 ns), for metal-coated mirror 2L, in position B.

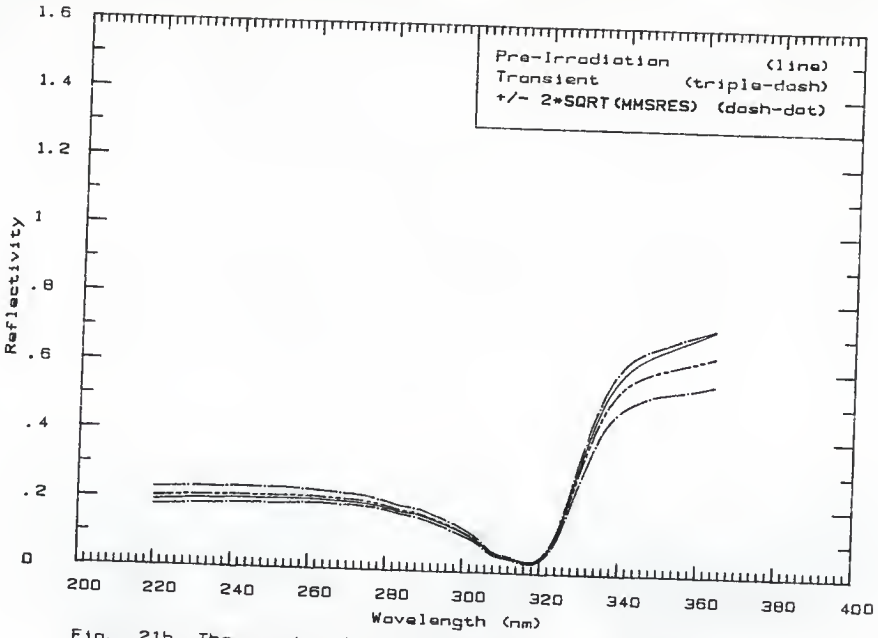

Fig. 21b The pre-irradiation reflectivity compared to the transient reflectivity based on Fig. 9b. (33.8 -67.3 ns). for metal-coated mirror 2L. in position 8.

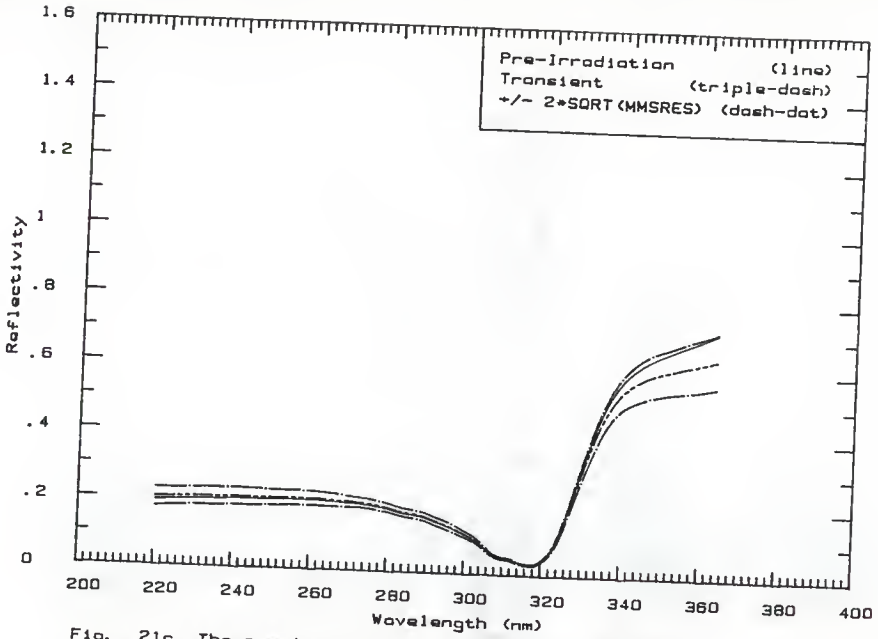

Fig. 21c The pre-irradiation reflectivity compared to the transient reflectivity based on Fig. 9c. (67.3 -101 ns), for metal-coated mirror 2L, in position B.

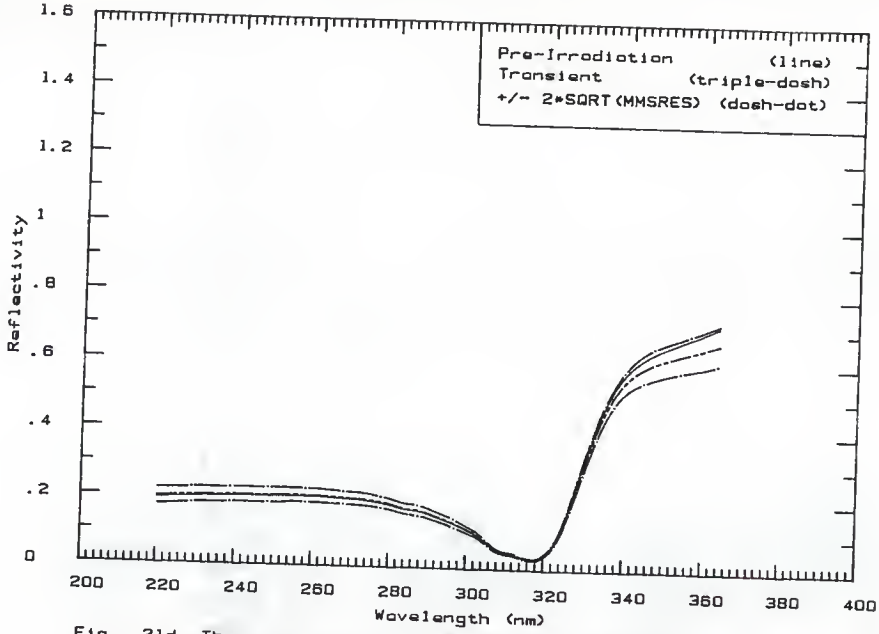

Fig. 21d The pre-irrodiotion reflectivity compored to the transient reflectivity bosed on Fig. 9d. (101 -134 ns), for metal-cooted mirror 2L, in position 8.

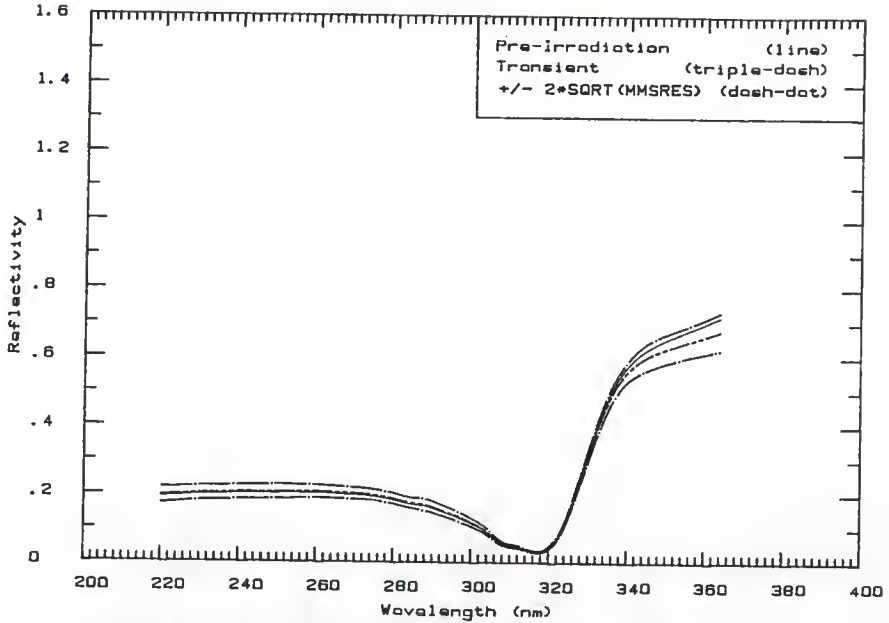

Fig. 21e The pre-irradiation reflectivity compared to the transient reflectivity based on Fig. 9e. (134 -168 ns). for metal-coated mirror 2L. in position 8.

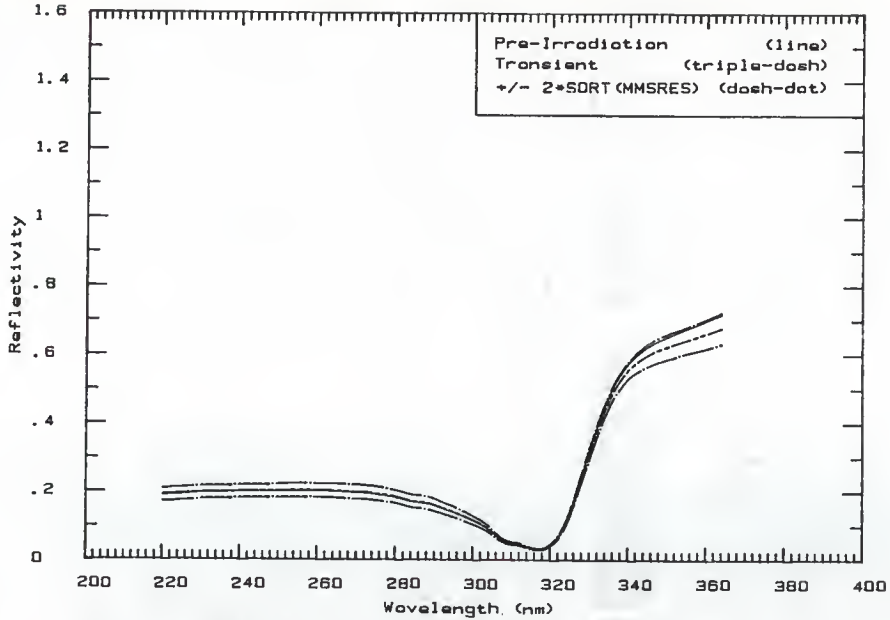

Fig. 21f The pre-irradiation reflectivity compared to the transient reflectivity based on Fig. 9f. (168 -201 ns), for metal-coated mirror 2L, in position 8.

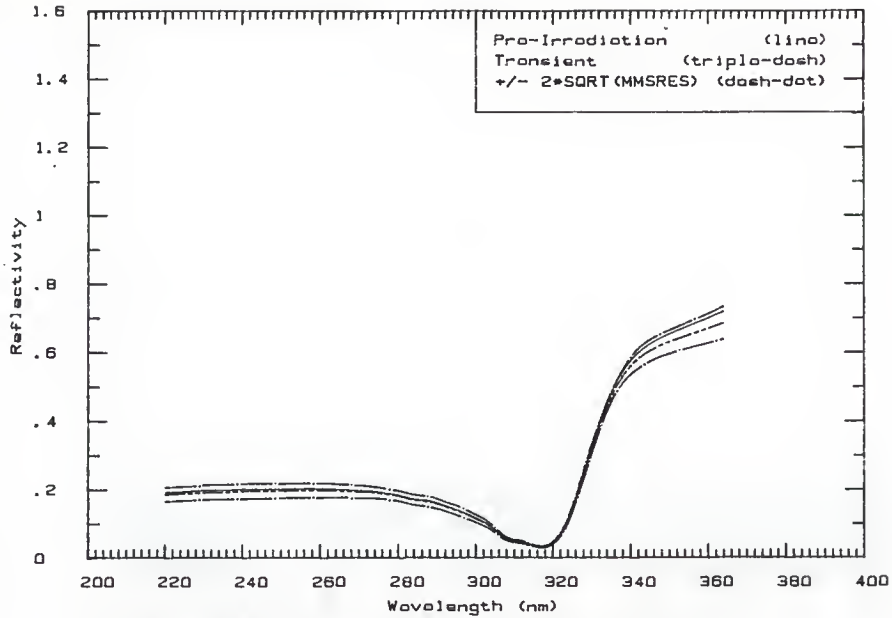

Fig. 21g The pre-irradiation reflectivity compared to the transient reflectivity based on Fig. 9g. (20) -235 ns), for metal-coated mirror 2L, in position 8.

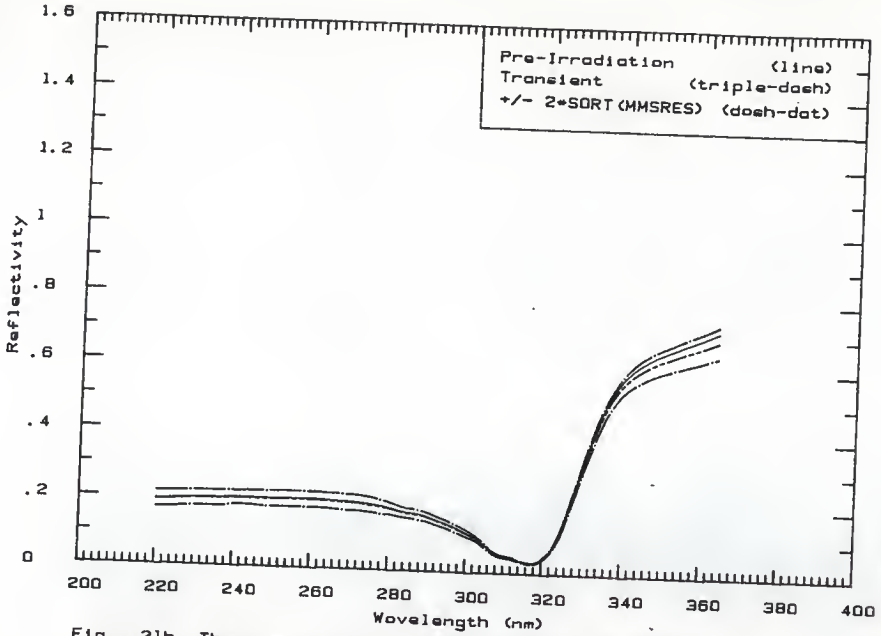

Fig. 21h The pre-irradiation reflectivity compared to the transient reflectivity based on Fig. 9h. (235 -268 ns), for metal-coated mirror 2L, in position B.

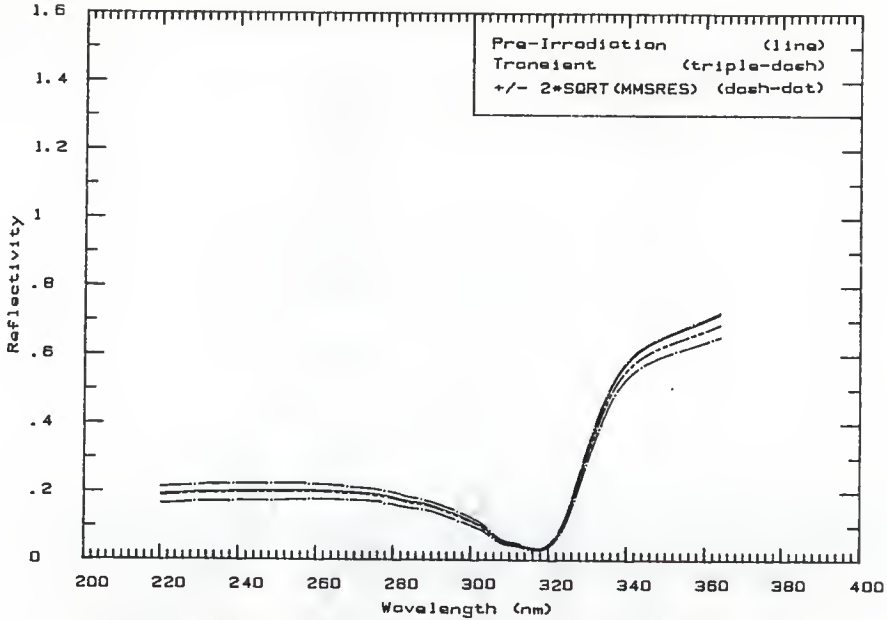

Fig. 211 The pre-irradiation reflectivity compared to the transient reflectivity based on Fig. 91. (268 -293 ns). for metal-coated mirror 2L. in position B.

Figures 22a to 22i, the transient reflectivity plots for metal-coated mirror 6L, irradiated in position A. The block-out mean beam current was 5 A while the pulse length was 20 ns.

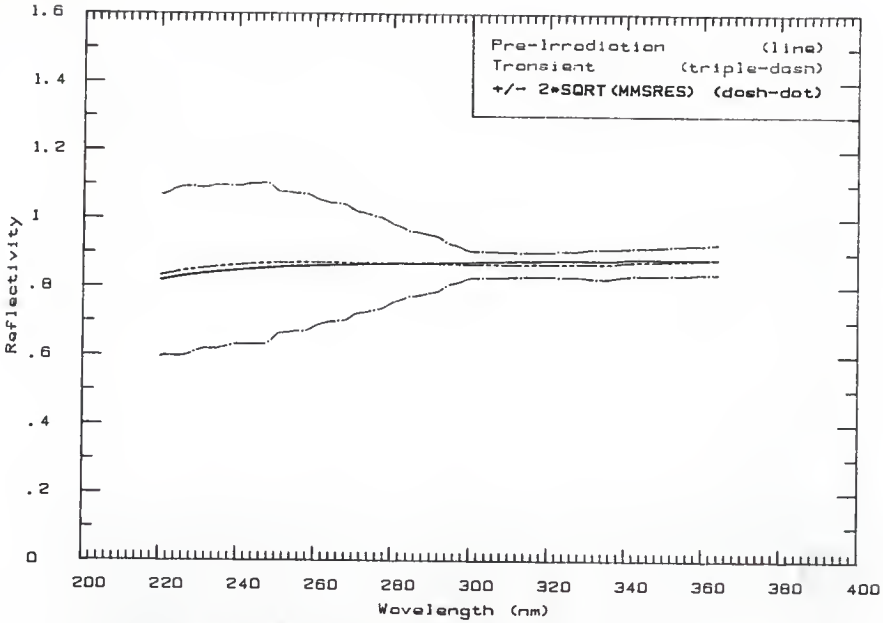

Fig. 22a The pre-irradiation reflectivity compared to the transient reflectivity based on Fig. 10a. (0.0-5.0 ns), for metal-coated mirror 6L.

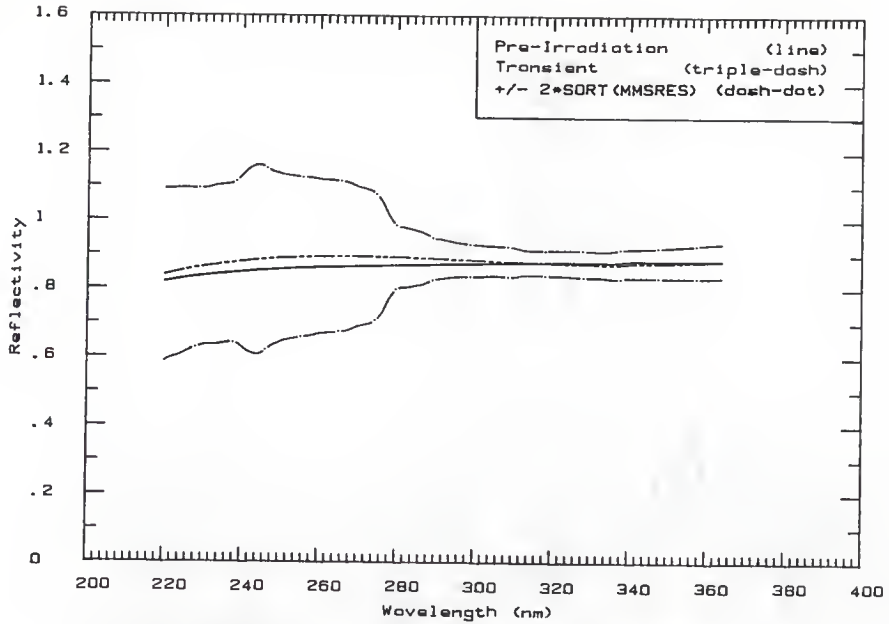

Fig. 22b The pre-irradiation reflectivity compared to the transient reflectivity based on Fig. 10b. (5.0-10.0 ns), for metal-coated mirror 6L.

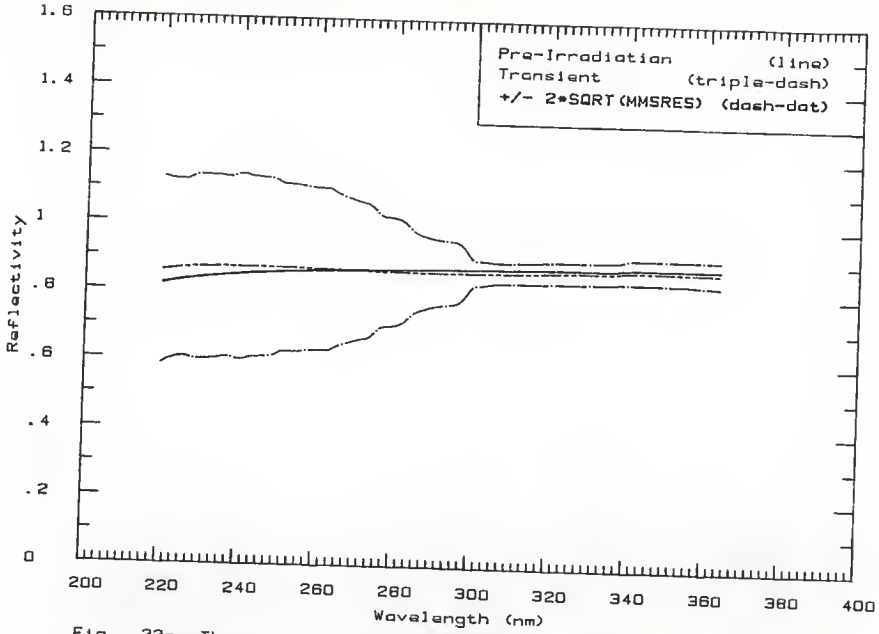

Fig. 22c The pre-irradiation reflectivity compared to the transient reflectivity based on Fig. 10c, (10.0-15.0 ns), for metal-coated mirror 6L.

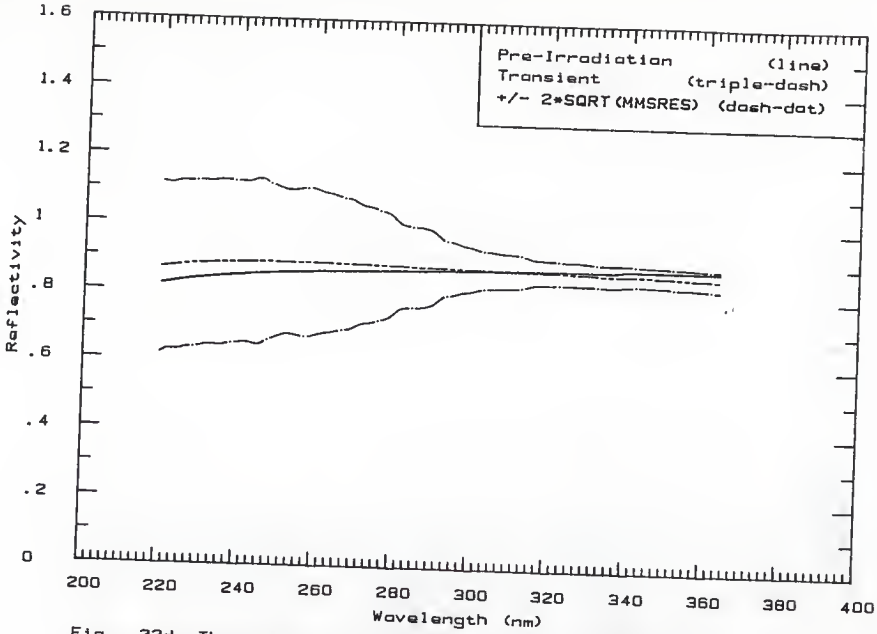

Fig. 22d The pre-irradiation reflectivity compared to the transient reflectivity based on Fig. 10d. (15.0-20.0 ns), for metal-coated mirror 6C.

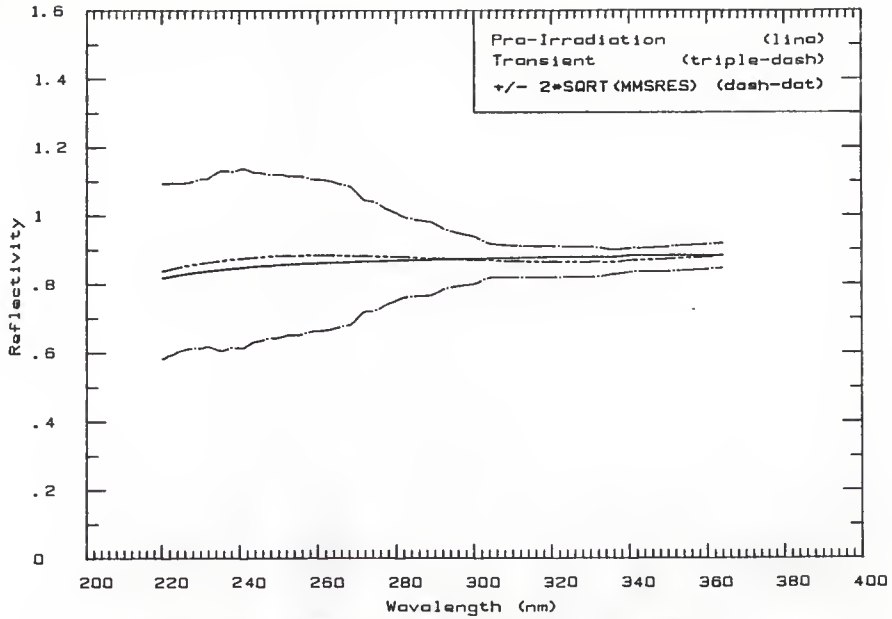

Fig. 22e The pre-irradiation reflectivity compared to the transient reflectivity based on Fig. 10e, (20.0-25.0 ns), for metal-coated mirror 6C.

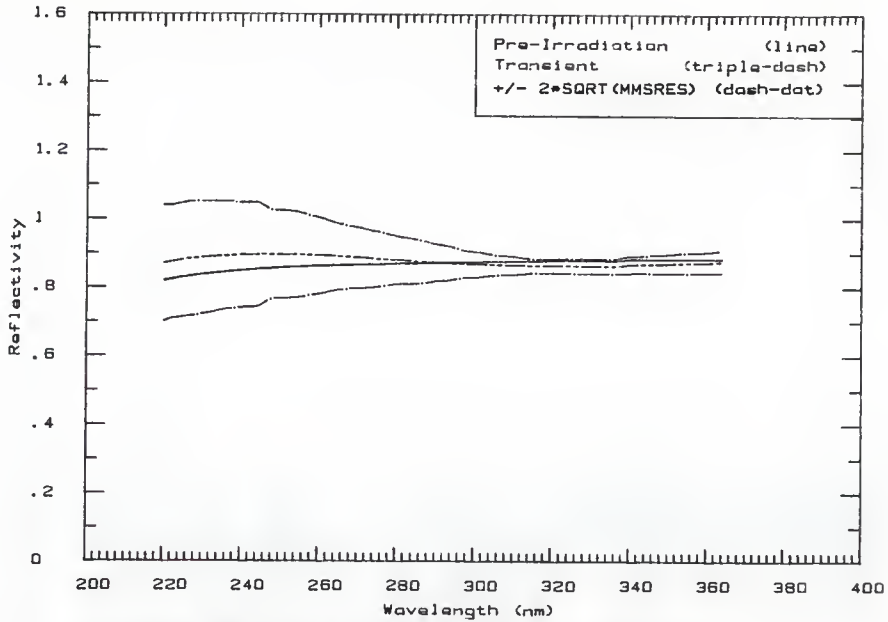

Fig. 22f The pre-irradiation reflectivity compared to the transient reflectivity based on Fig. 10f, (25.0-41.3 ns), for metal-coated mirror 6C.

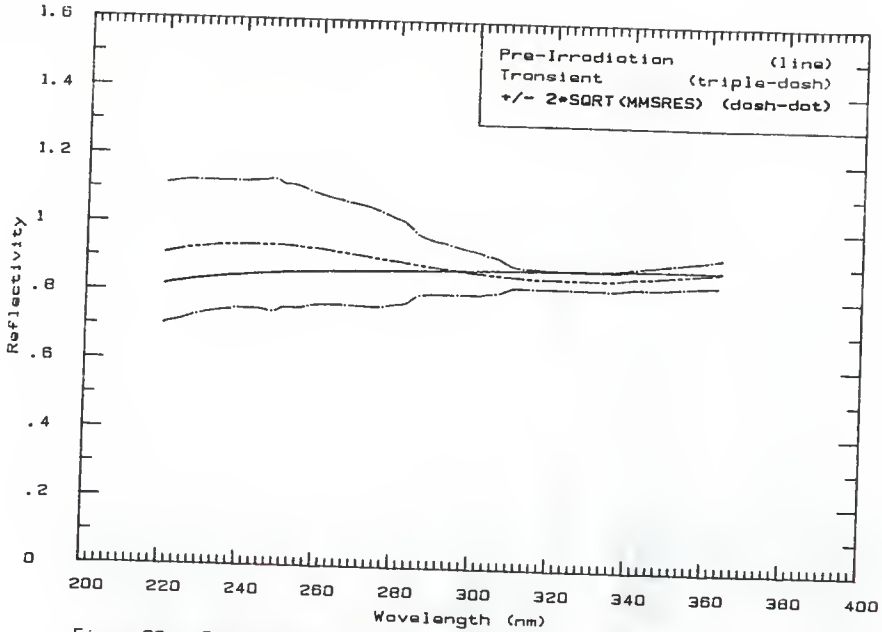

Fig. 22g The pre-irradiation reflectivity compared to the transient reflectivity based on Fig. 10g. (41.3-57.5 ns), for metal-coated mirror 6C.

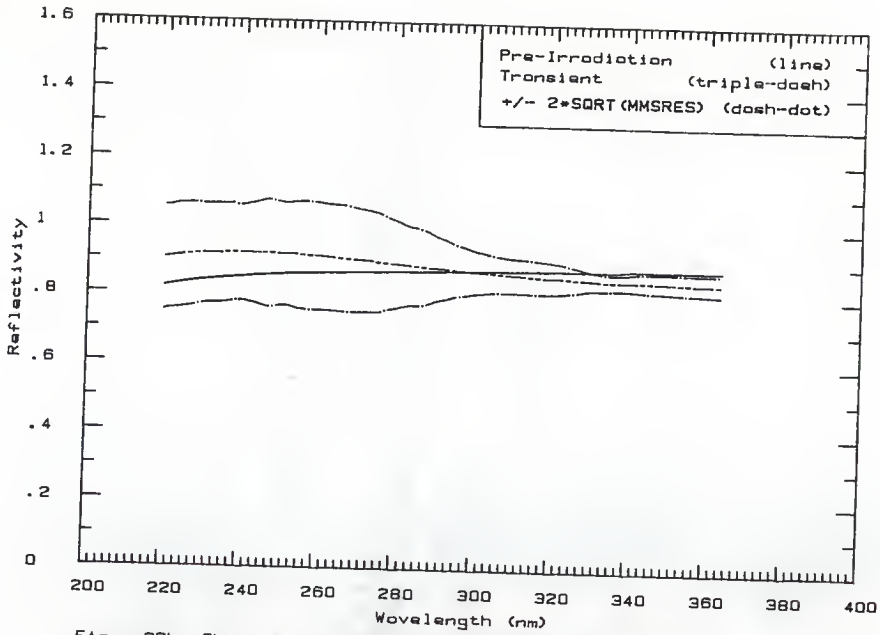

Fig. 22h The pre-irrodiotion reflectivity compared to the transient reflectivity based on Fig. 10h. (57.5-73.8 ns), for metal-coated mirror 6C.

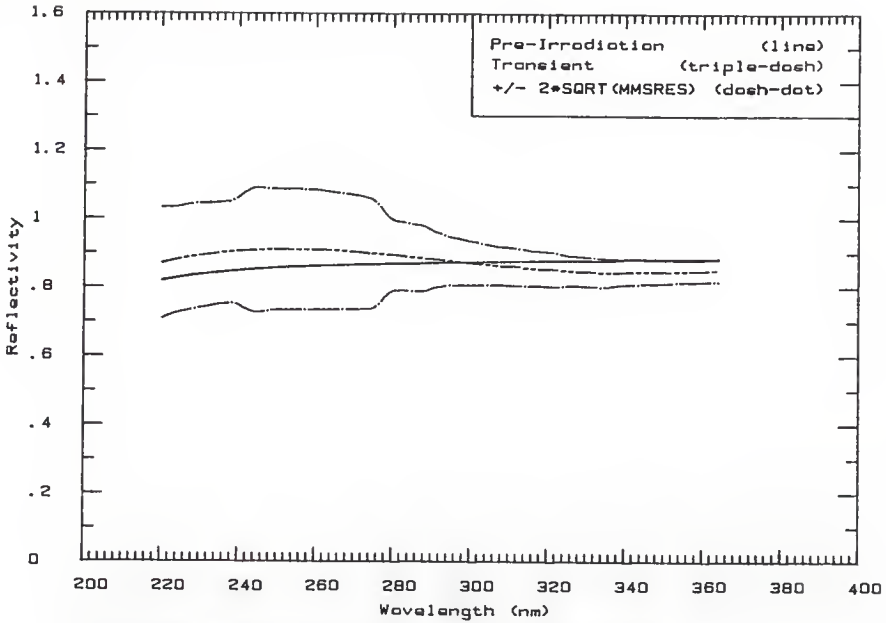

Fig. 22i The pre-irradiation reflectivity compared to the transient reflectivity based on Fig. 10i, (73.8-88.0 ns), for metal-coated mirror 6C.

Figures 23a to 23i, the transient reflectivity plots for metal-coated mirror 7L, irradiated in position A. The block-out mean beam current was 225 mA while the pulse length was 500 ns.

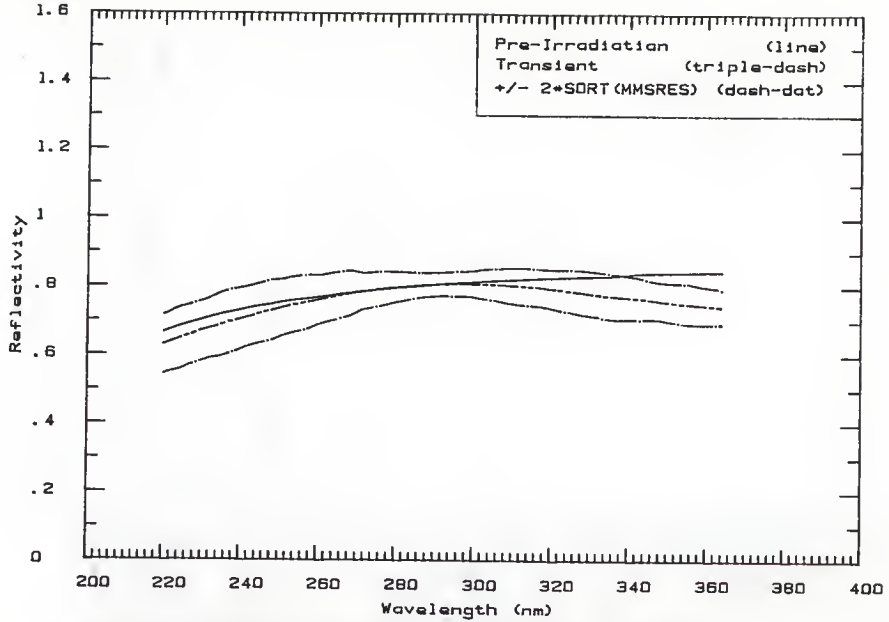

Fig. 23a The pre-irradiation reflectivity compared to the transient reflectivity based on Fig. 11a. (0.0 -37.0 ns), for metal-coated mirror 7L in position A.

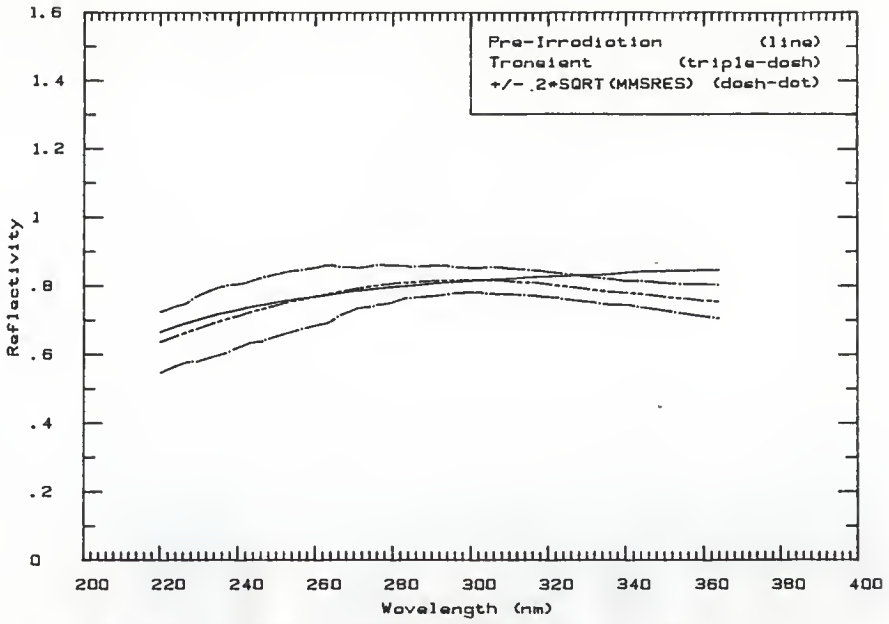

Fig. 23b The pre-irrodiotion reflectivity compored to the tronsient reflectivity bosed on Fig. 11b, (37.0 -70.5 ns), for metol-cooted mirror 7L in position A.

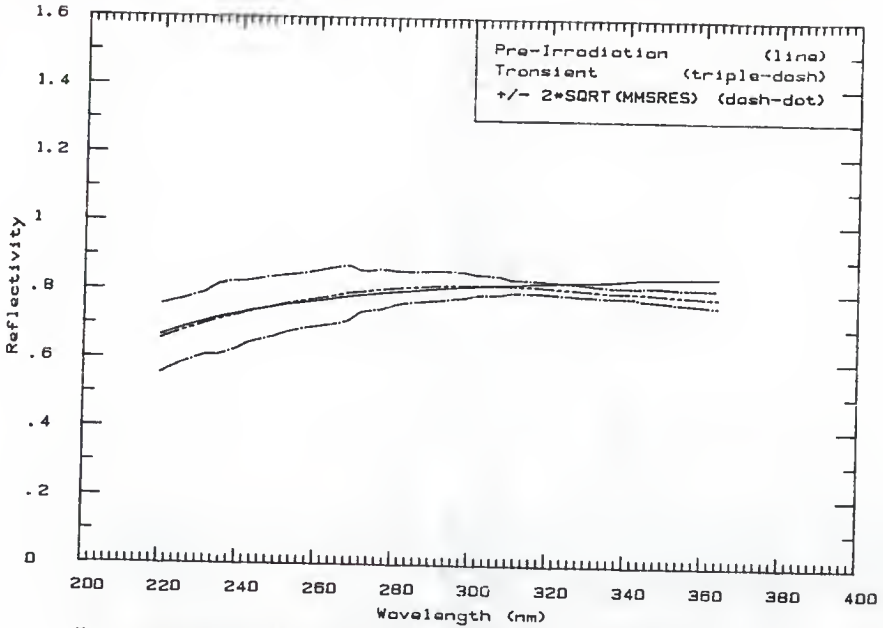

Fig. 23c The pre-irradiation reflectivity compared to the transient reflectivity based on Fig. 11c. (70.5 -104 ns). for metal-coated mirror 7L in position A.

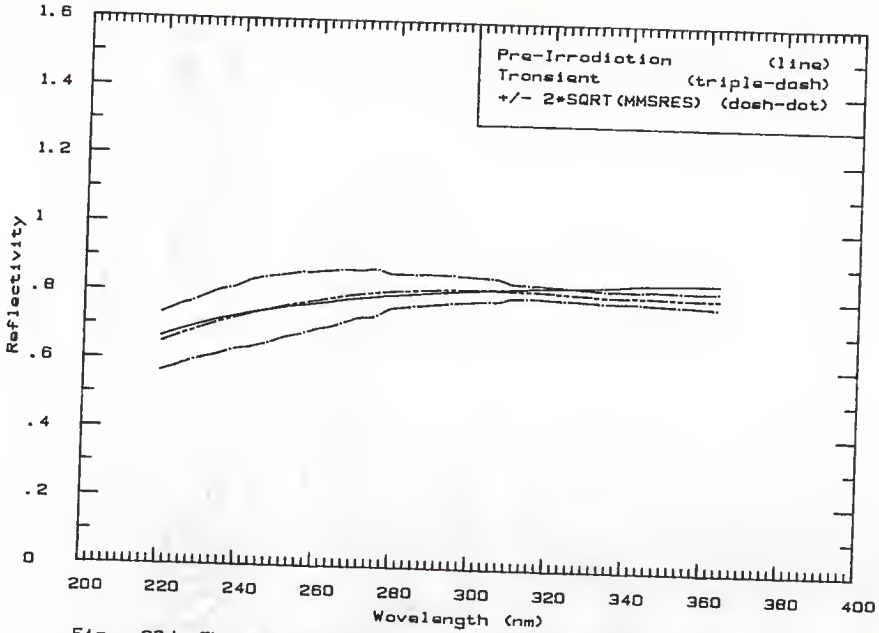

Fig. 23d The pre-irrodiotion reflectivity compared to the tronsient reflectivity based on Fig. 11d. (104 -138 ns), for metal-coated mirror 7L in position A.

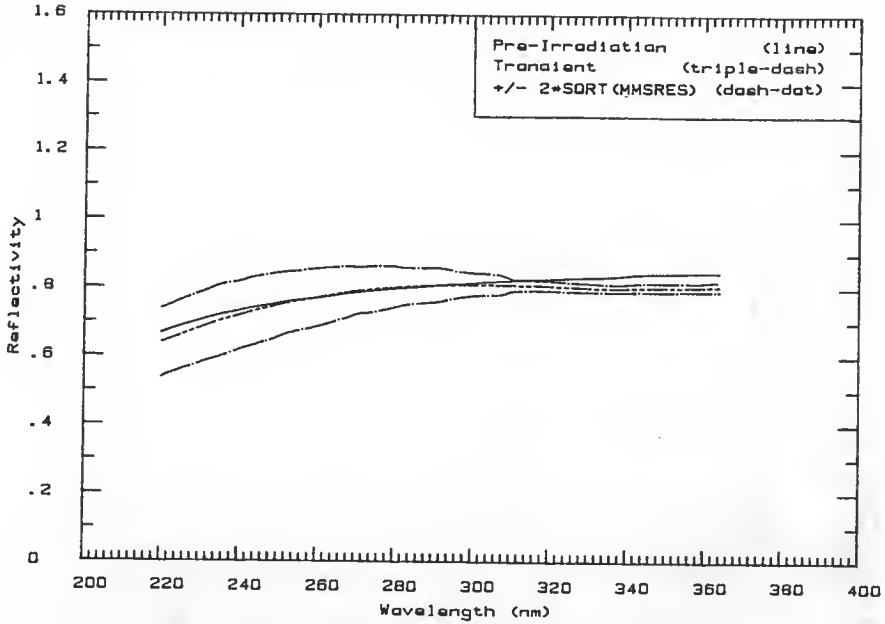

Fig. 23e The pre-irradiation reflectivity compared to the transient reflectivity based on Fig. 11e. (138 -171 ns), for metal-coated mirror 7L in position A.

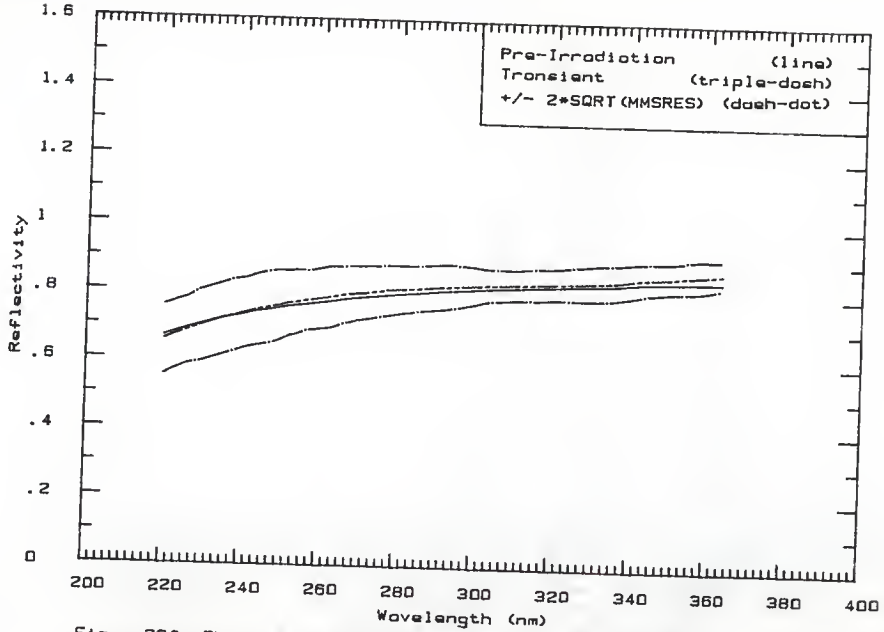

Fig. 23f The pre-irradiation reflectivity compared to the transient reflectivity based on Fig. 11f. (171 -205 ns), for metal-coated mirror 7L in position A.

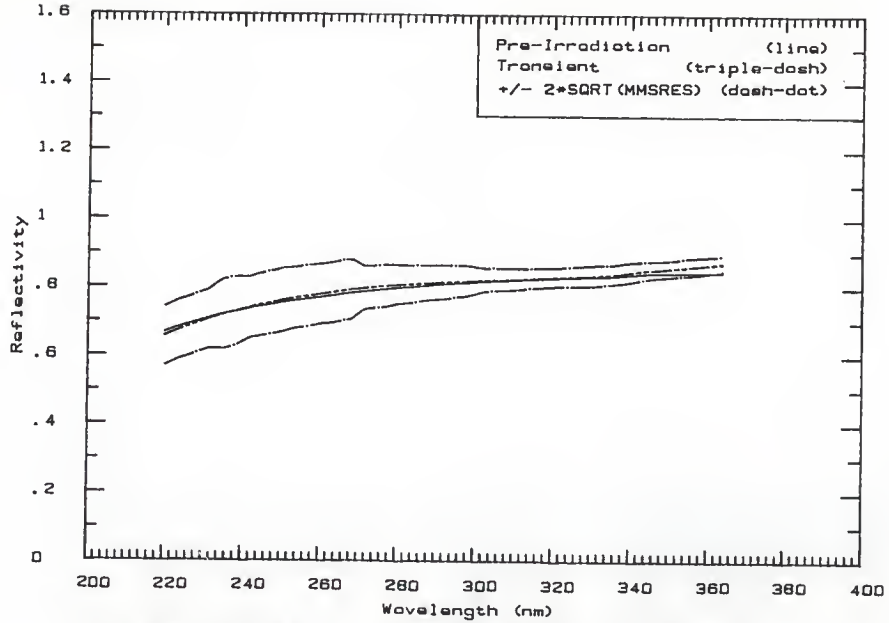

Fig. 23g The pre-irradiation reflectivity compared to the transient reflectivity based on Fig. 11g. (205 -238 ns), for metal-coated mirror 7L in position A.

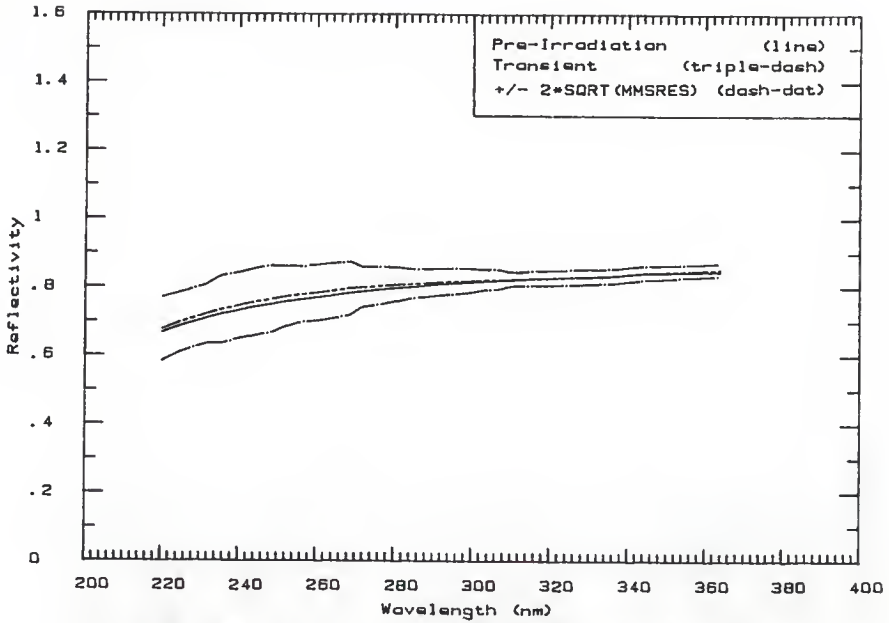

Fig. 23h The pre-irradiation reflectivity compared to the transient reflectivity based on Fig. 11h, (238 -272 ns), for metal-coated mirror 7L in position A.

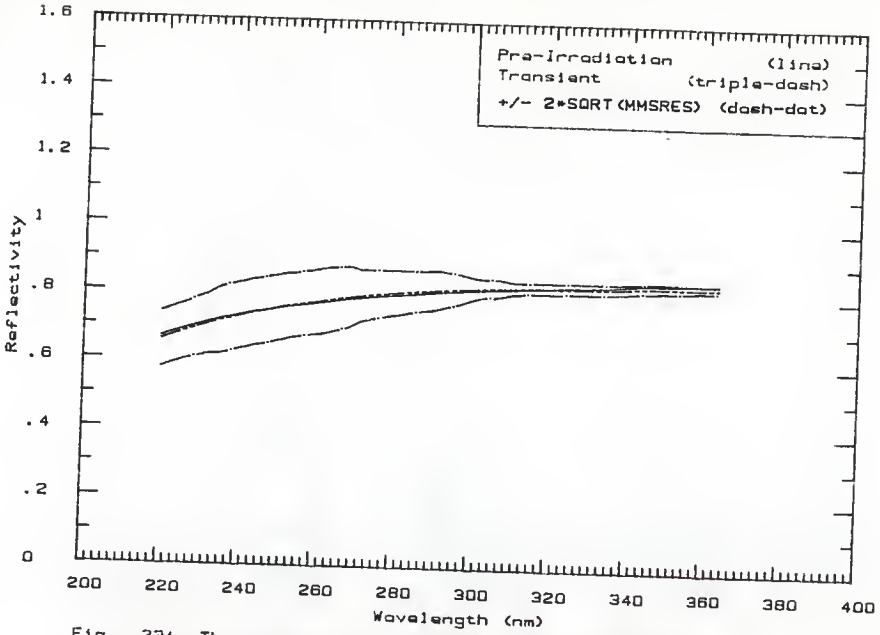

Fig. 23i The pre-irradiation reflectivity compared to the transient reflectivity based on Fig. 11i. (272 -313 ns). for metal-coated mirror 7L in position A.

Figures 24a to 24j, the transient reflectivity plots for metal-coated mirror 7L, irradiated in position B. The block-out beam mean current was 225 mA while the pulse length was 500 ns.

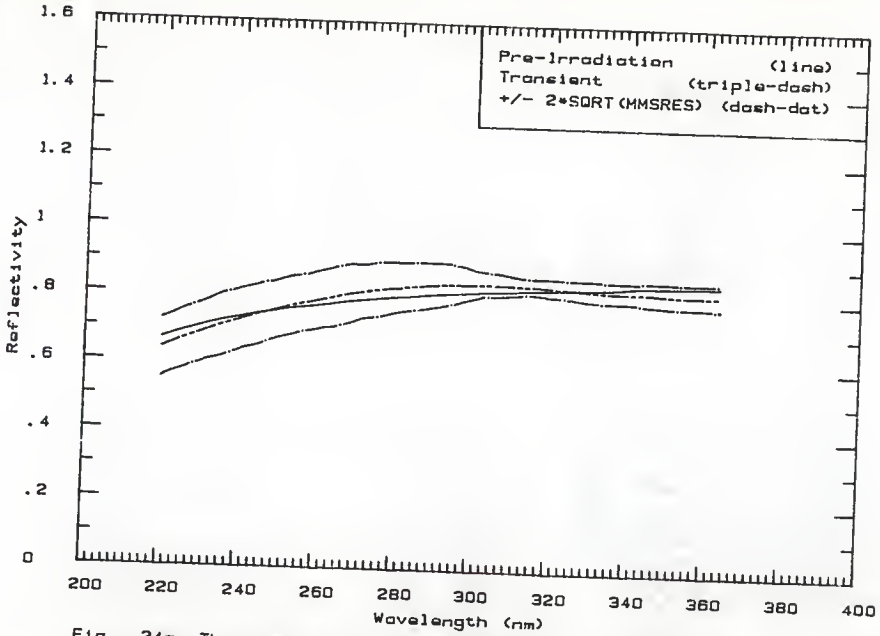

Fig. 24a The pre-irradiation reflectivity compared to the transient reflectivity based on Fig. 12a. (250 -284 ns), for metal-coated mirror 7L in position B.

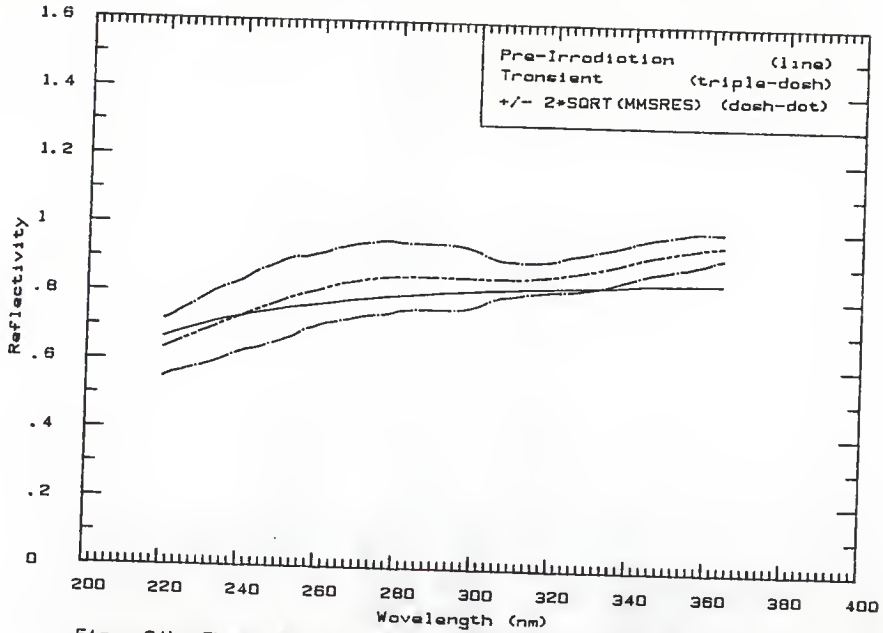

Fig. 24b The pre-irradiation reflectivity compared to the transient reflectivity based on Fig. 12b. (284 -317 ns), for metal-coated mirror 7L in position 8.

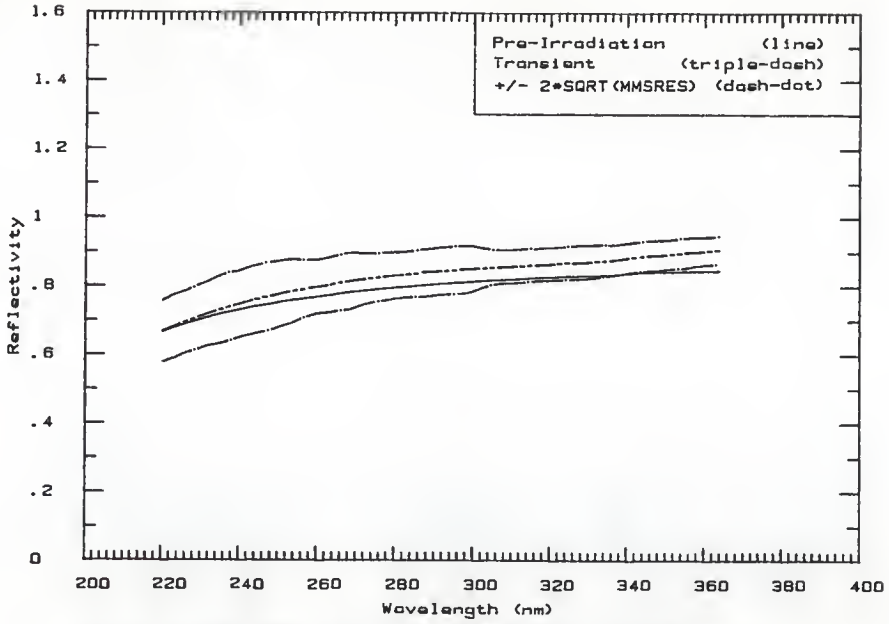

Fig. 24c The pre-irradiation reflectivity compared to the transient reflectivity based on Fig. 12c. (317 -351 ns), for metal-coated mirror 7L in position 8.

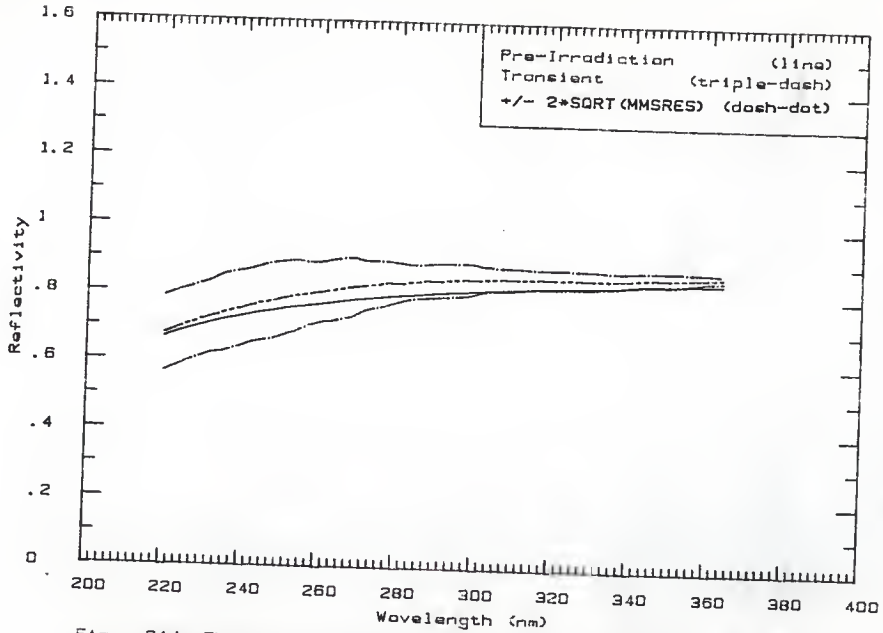

Fig. 24d The pre-irradiation reflectivity compared to the transient reflectivity based on Fig. 12d. (35] -384 ns). for metal-coated mirror 7L in position B.

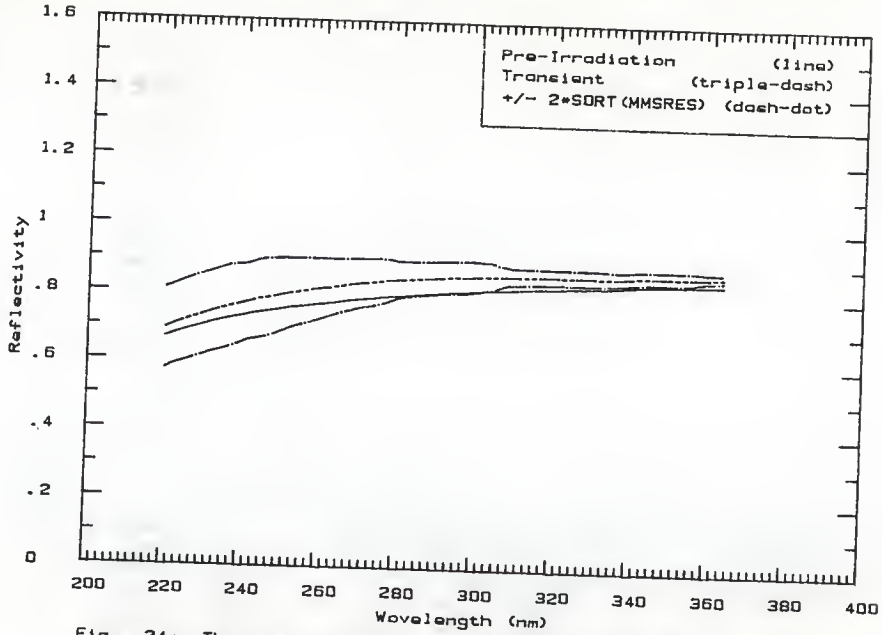

Fig. 24a The pre-irradiation reflectivity compared to the transient reflectivity based on Fig. 12a, (384 -418 ns), for metal-coated mirror 7L in position B.

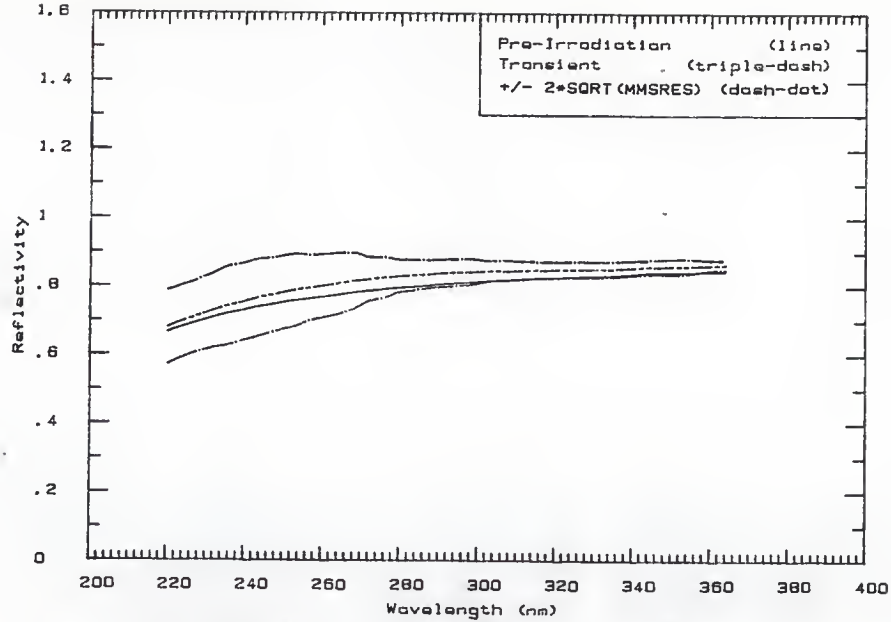

Fig. 24f The pre-irradiation reflectivity compared to the transient reflectivity based on Fig. 12f. (418 -451 ns), for metal-coated mirror 7L in position 8.

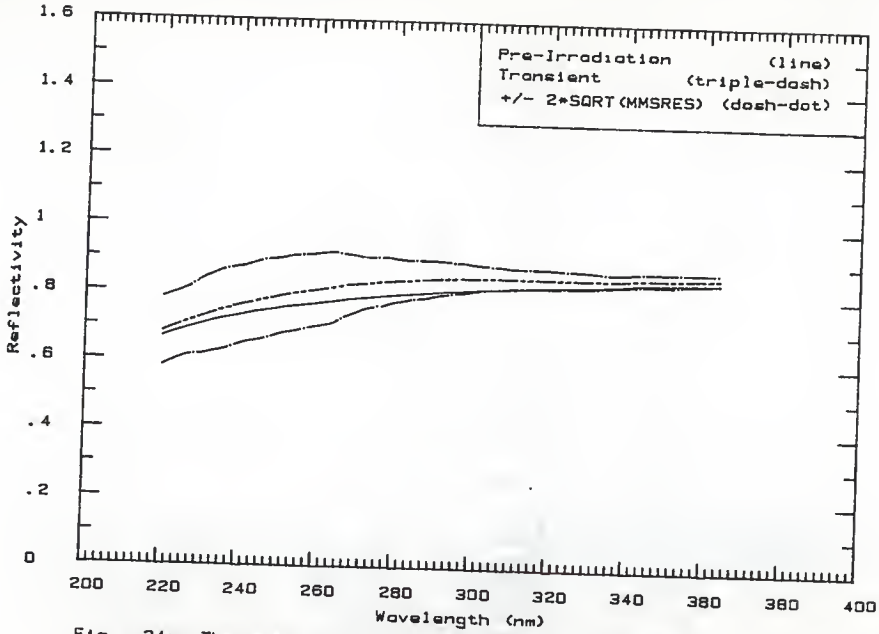

Fig. 24g The pre-irradiation reflectivity compared to the transient reflectivity based on Fig. 12g. (451 -485 ns), for metal-coated mirror 7L in position B.

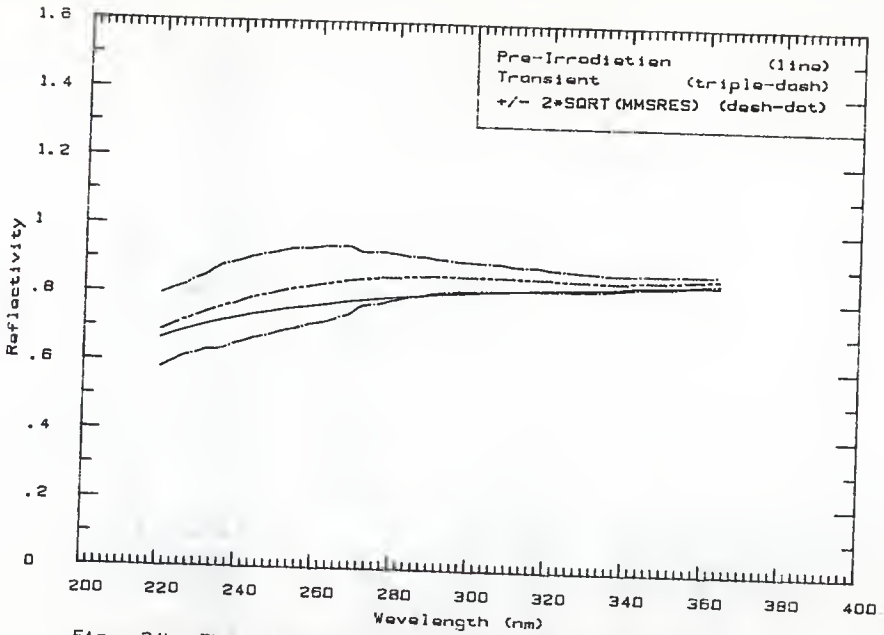

Fig. 24h The pre-irradiation reflectivity compared to the transient reflectivity based on Fig. 12h. (485 -518 ns). for metal-coated mirror 7L in position B.

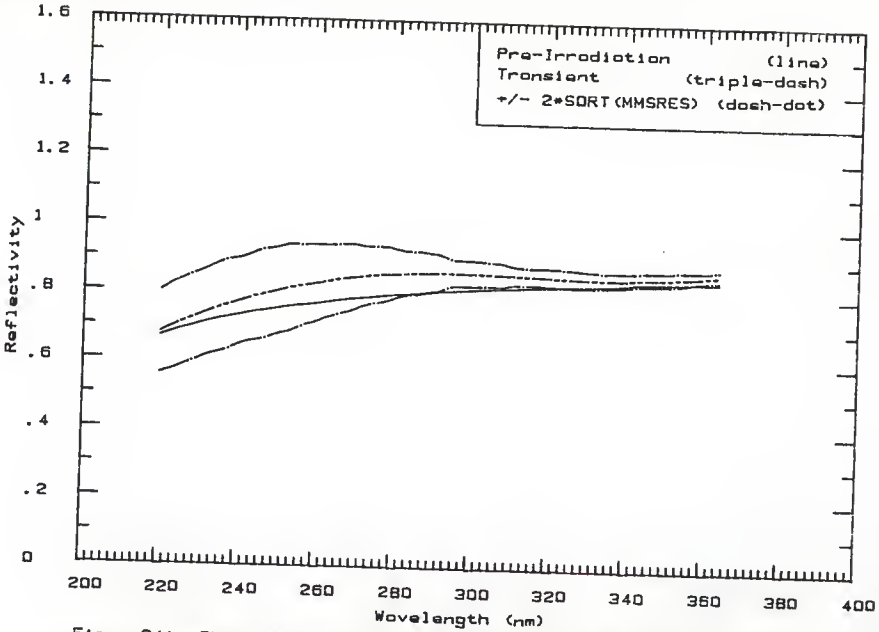

Fig. 241 The pre-irradiation reflectivity compared to the transient reflectivity based on Fig. 121. (518 -552 ns), for metal-coated mirror 7L in position 8.

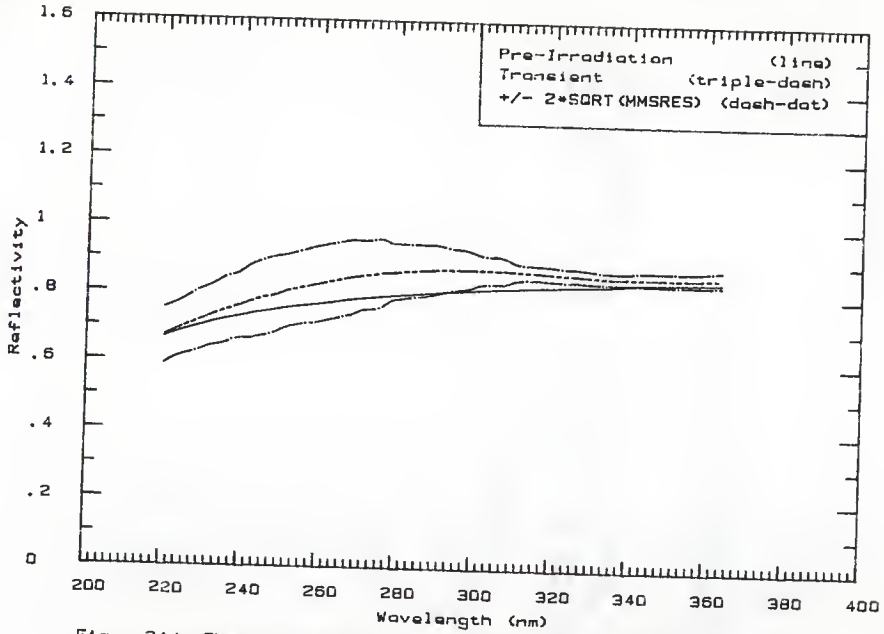

Fig. 24j The pre-irradiation reflectivity compared to the transient reflectivity based on Fig. 12j. (552 -593 ns), for metal-coated mirror 7L in position 8.

Appendix D: Pre-irradiation reflectivity curves for all mirrors listed in Table 3.1.

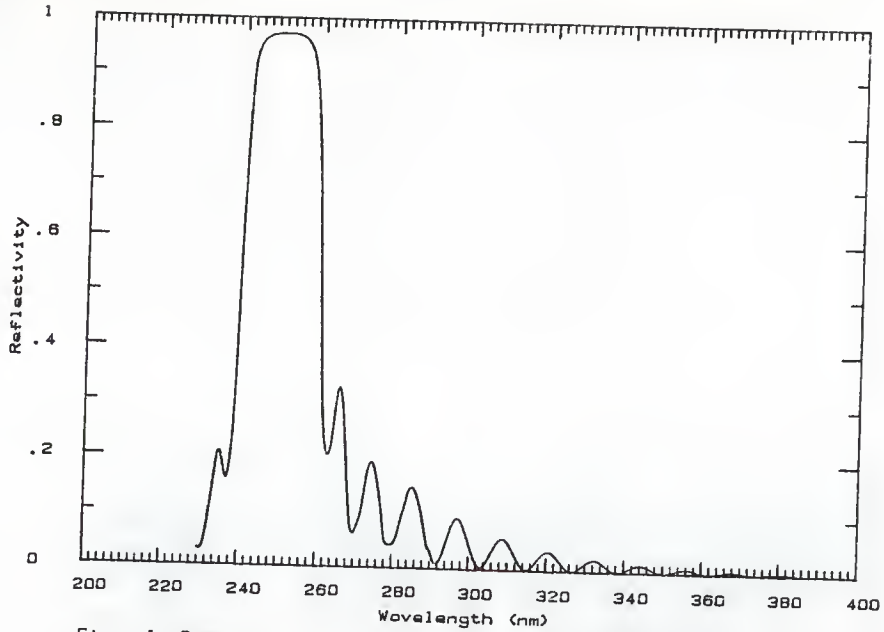

Fig. 1 Pre-irrodiation reflectivity for dielectric mirror number 14.

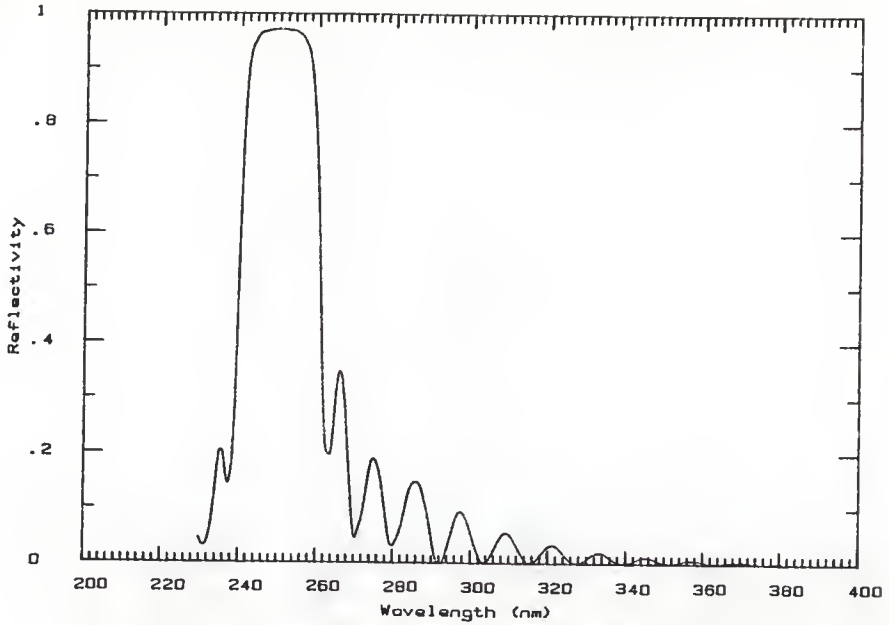

Fig. 2 Pre-irrodiotion reflectivity for dielectric mirror number 12.

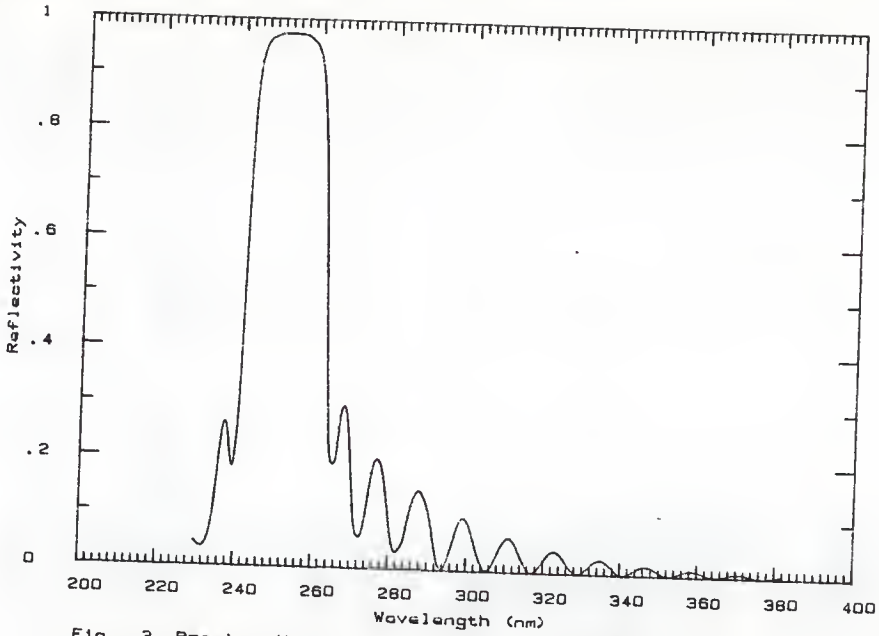

Fig. 3 Pre-irradiation reflectivity for dielectric mirror number 13.

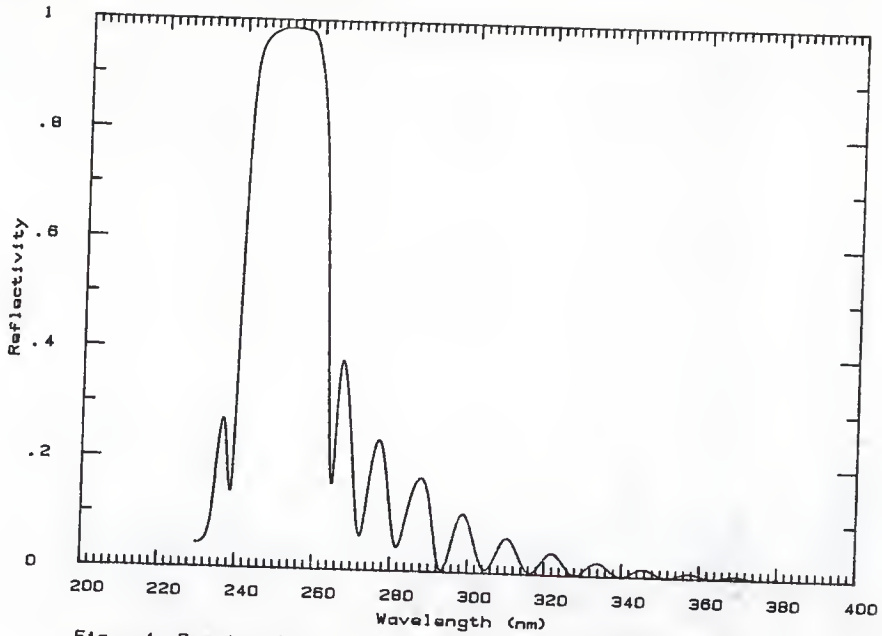

Fig. 4 Pre-irradiation reflectivity for dielectric mirror number 26.

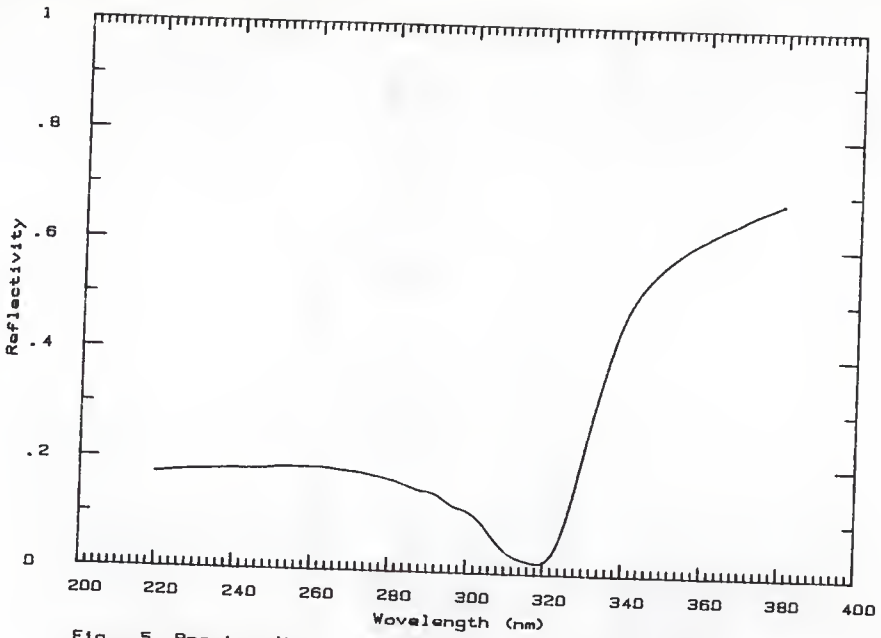

Fig. 5 Pre-irrodiotion reflectivity for metal-coated mirror number 1L.

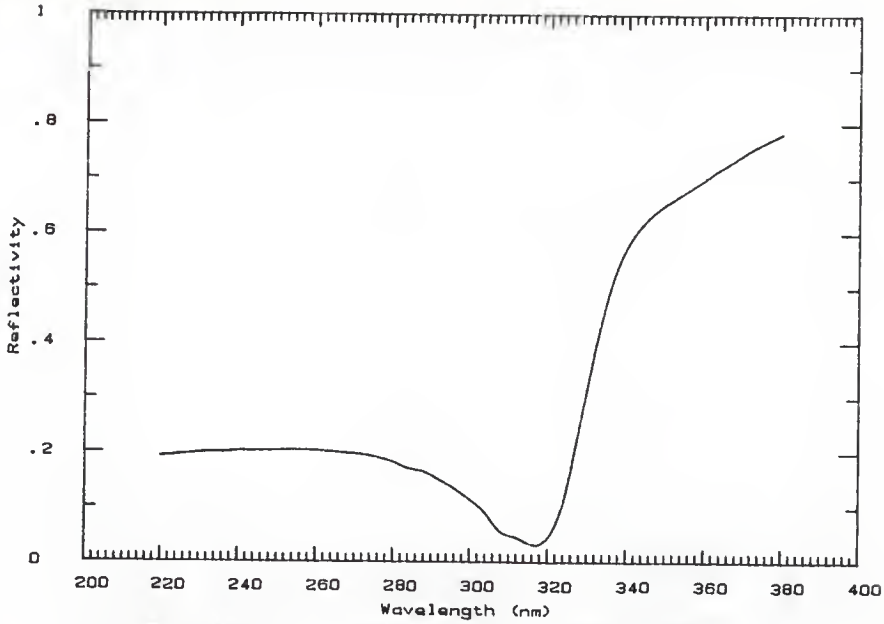

Fig. 6 Pre-irradiation reflectivity for metal-coated mirror number 2L.

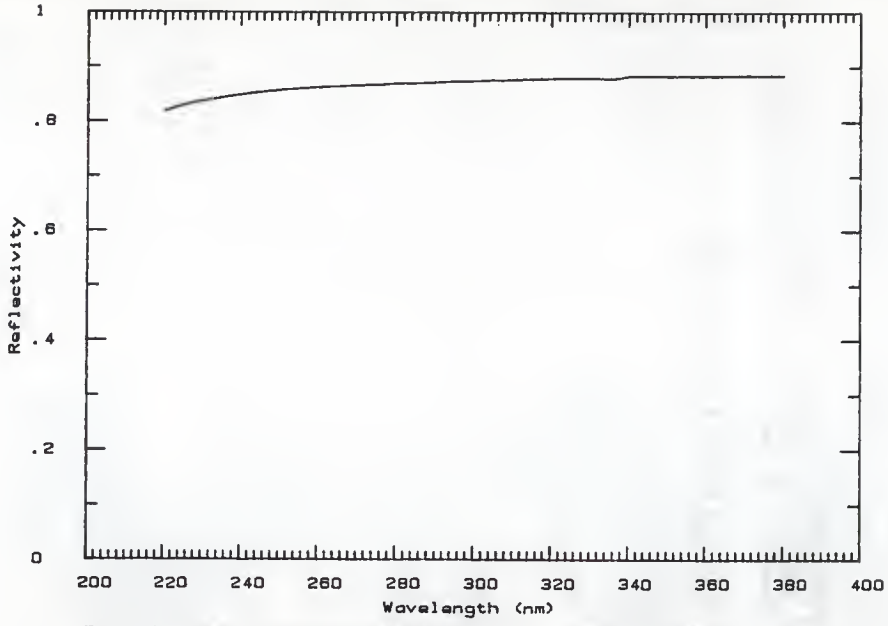

Fig. 7 Pre-irradiation reflectivity for metal-coated mirror number 6L.

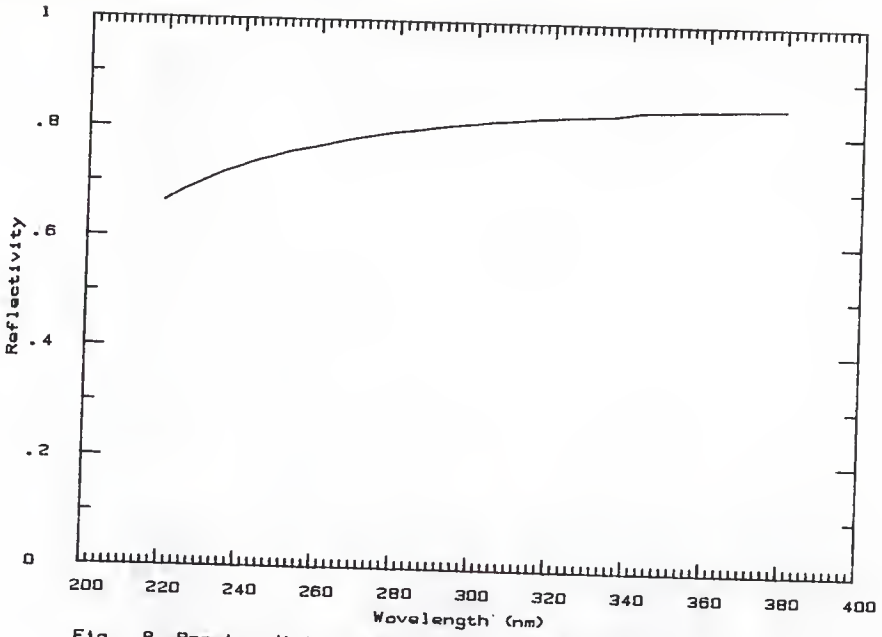

Fig. 8 Pre-irradiation reflectivity for metal-coated mirror number 7L.

Appendix E: Block-in and Block-out Irradiation Picture Data

Each picture in Appendix E is identified by a three-digit file number following the letters "LPA" appearing on the lower right-hand corner of each picture just above the color-intensity scale. Use the information in Table E1 to identify a specific irradiation.

The color levels on the photographs represent the signal light intensity seen at the video camera as a function of time and wavelength. The origin of each data set is found in the lower right-hand corner of each photograph. The wavelength and time scales are the abscissa and ordinate, respectively. The third dimension, color level, represents the signal light intensity.

Table E1 The LPA file numbers for the block-in and block-out irradiations and their corresponding page numbers.

Mirror Number	Block Position	Irradition Position	LPA File Number	Page Number
14	in	A	313	E7
	out	A	314	
12	in	A	210	E3
	out	A	211	
	in	B	212	E4
	out	B	213	
13	in	A	303	E5
	out	A	304	
	in	B	305	E6
	out	B	306	
26	in	A	100	E3
	out	A	102	
1L	in	A	317	E8
	out	A	318	
2L	in	A	307	E6
	out	A	308	
	in	B	309	E7
	out	B	310	
6L	in	A	315	E8
	out	A	316	
7L	in	A	214	E4
	out	A	215	
	in	B	216	E5
	out	B	217	

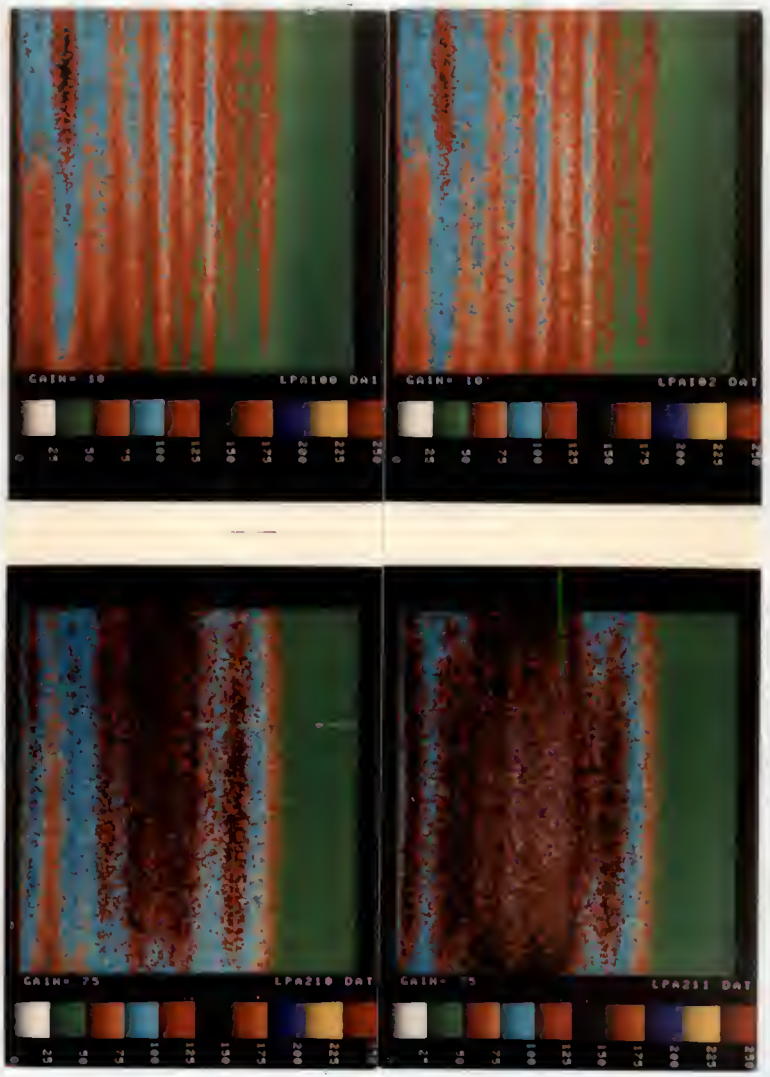
GAIN= 10
LPA100 DAT
GAIN= 10
LPA102 DAT
GAIN= 75
LPA210 DAT
GAIN= 75
LPA211 DAT

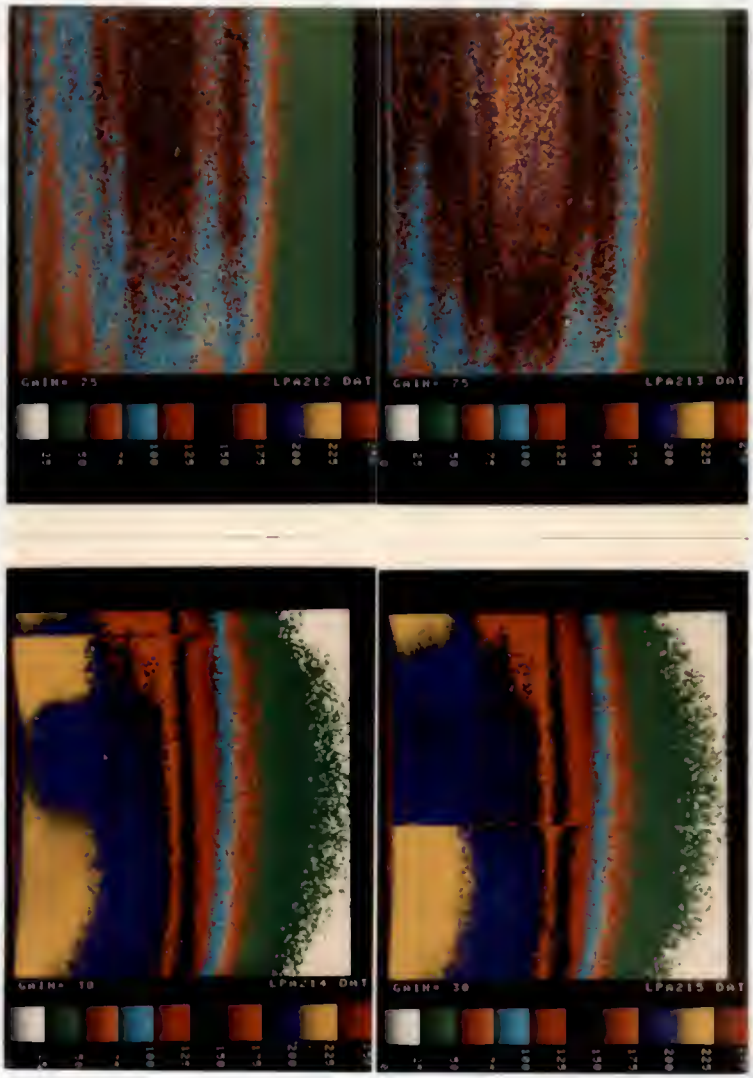
GAIN= 25
LPA212 DAT
GAIN= 25
LPA213 DAT
GAIN= 30
LPA214 DAT
GAIN= 30
LPA215 DAT

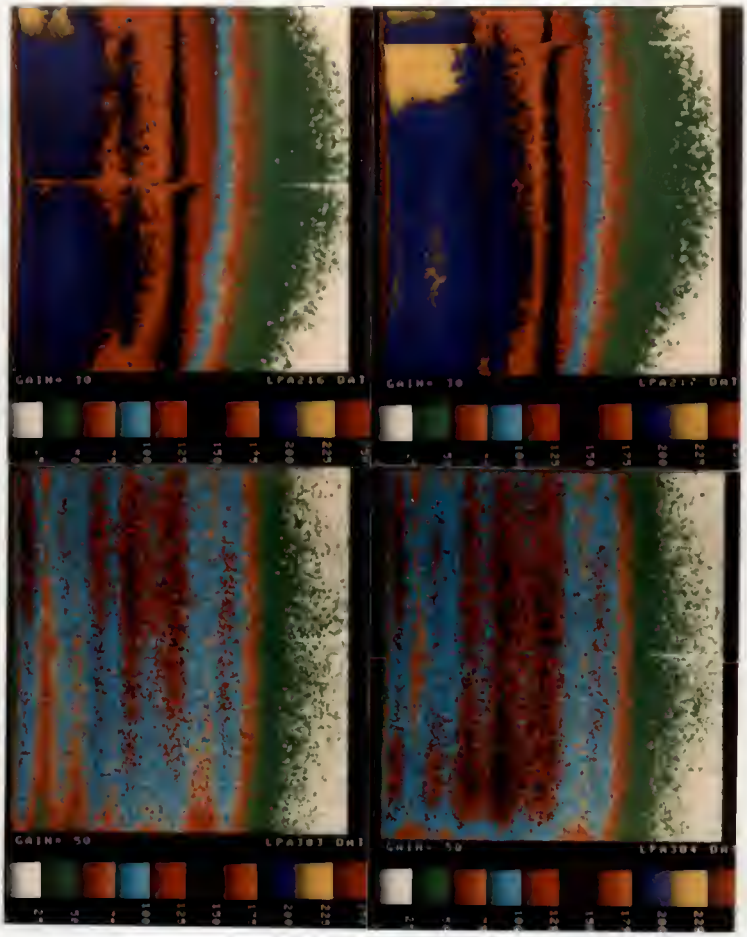
GAIN= 30
GAIN= 30
GAIN= 50
GAIN= 50

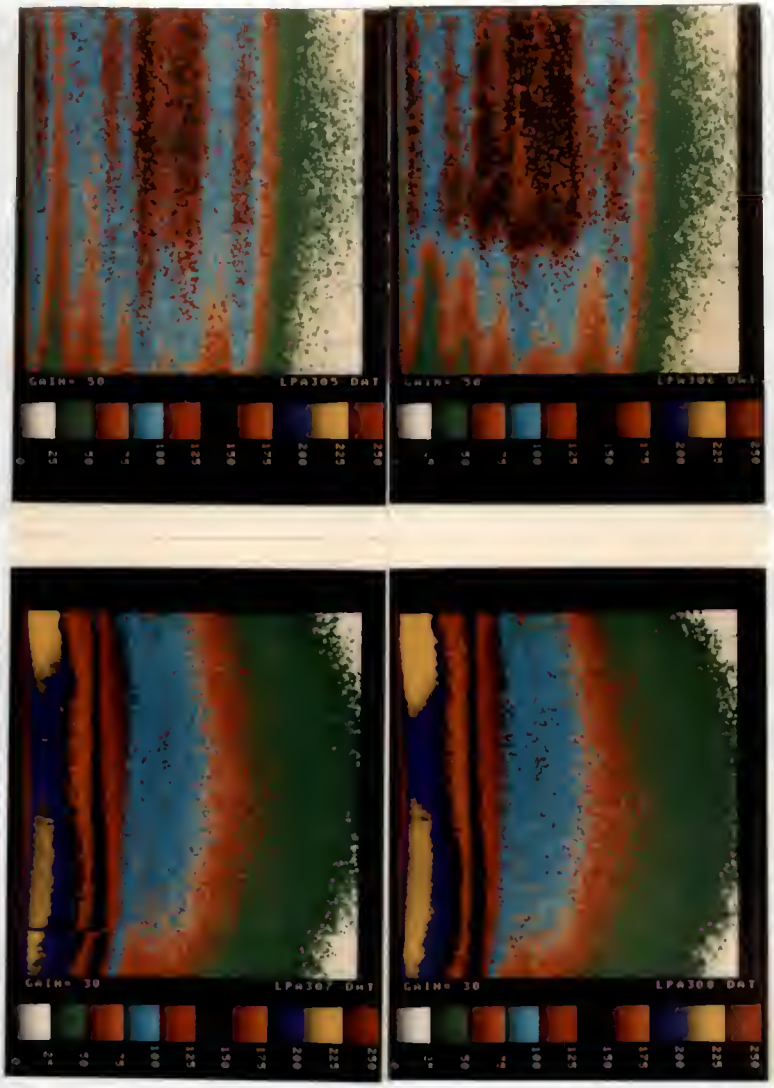
GAIN= 30
LPA305.DAT
GAIN= 30
LPA306.DAT
GAIN= 30
LPA307.DAT
GAIN= 30
LPA308.DAT

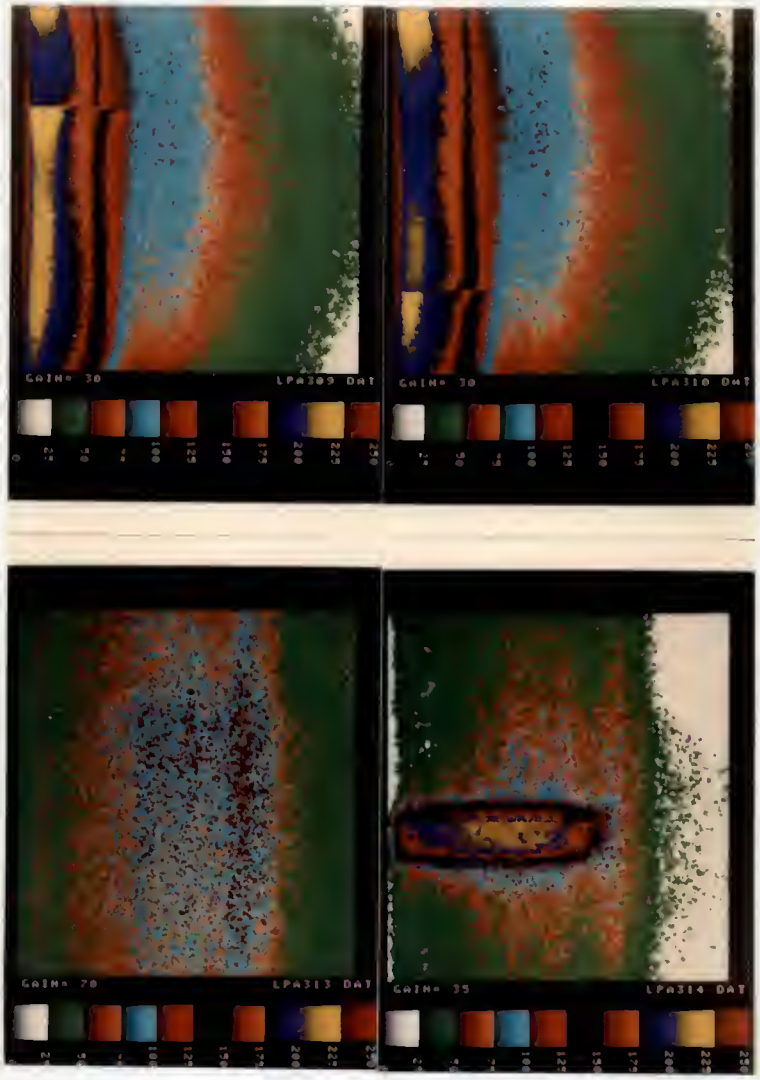
GAIN= 30
LPA309 DAT
GAIN= 30
LPA310 DAT
GAIN= 20
LPA313 DAT
GAIN= 35
LPA314 DAT

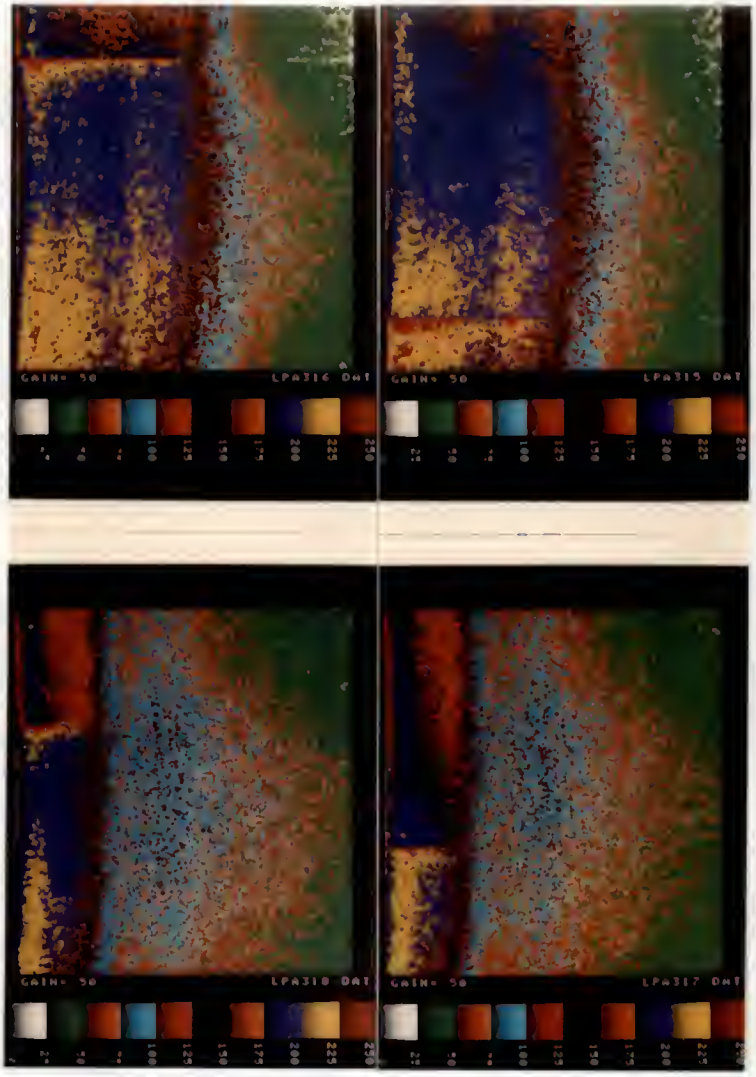
GAIN= 50
LPA316 DAT
GAIN= 50
LPA315 DAT
GAIN= 50
LPA318 DAT
GAIN= 50
LPA317 DAT

TRANSIENT REFLECTIVITY RESPONSE OF LASER MIRRORS TO ELECTRON BEAM IRRADIATION

by

Kevin A. Stroh

B.S., Kansas State University, 1984

AN ABSTRACT OF A MASTER'S THESIS

submitted in partial fulfillment of the

requirements for the degree

MASTER OF SCIENCE

Department of Nuclear Engineering

KANSAS STATE UNIVERSITY
Manhattan, Kansas

1987

ABSTRACT

The transient effects of electron radiation on dielectric and metal-coated mirrors was studied to estimate transient mirror reflectivity. The electron radiation came from single short-time (20 ns to 500 ns) pulses with mean currents from 225 mA for the longer pulses to 5 A for the shorter pulses. High fluences of 15 MeV electrons were used to simulate the effects of a high fluence gamma-rays and the secondary electron effects caused by gamma-rays. The goal of the irradiations was to measure the transient reflectivity of the dielectric, aluminum, and silver-on-copper coated mirrors, determine statistically significant deviations from pre-irradiation reflectivities, and note if any differences occured at important wavelengths. The dielectric mirrors were designed to operate in a KrF excimer laser system at 248 nm. The results of the investigation suggest the electron beam had a significant transient effect on the aluminum and dielectric mirrors. Estimates of the transient reflectivity versus wavelength were plotted. The estimates were based on ratios of pre-irradiation and transient light intensities measured at a streak camera detector.